INVESTIGATING FERROPTOSIS AS AN APPROACH TO TREATING MULTIPLE MYELOMA

By

Rachel Mynott
BMedSci (Hons)

Thesis
Submitted to Flinders University
for the degree of

Doctor of Philosophy

College of Medicine and Public Health
22nd July 2025

TABLE OF CONTENTS

ABSTRACT

Multiple myeloma (MM) is an incurable haematological malignancy and while novel therapies have improved the survival of people with MM, drug resistance is inevitable. Ferroptosis is an iron-dependent form of cell death and since its first characterisation in 2012, an exponential amount of research has been undertaken showing that cancer cells are vulnerable to ferroptosis. Whilst ferroptosis has been demonstrated in MM in the literature, these cells are generally less sensitive to ferroptosis-inducing agents compared to solid tumours and other blood cancers. In this thesis we aimed to investigate the mechanisms behind ferroptosis sensitivity in MM to uncover ways in which to make them more susceptible to this unique form of cell death. We found that compared to another B-cell malignancy, diffuse large B-cell lymphoma (DLBCL), MM cell lines were generally less sensitive to the ferroptosis-inducing agent, RSL3. However, one MM cell line (OPM2) was markedly sensitive to ferroptosis. Investigating the OPM2 MM cell line further, we found that it had differential expression of ferroptosis-related genes compared to the most resistant MM cell line, KMS-11. We found that both exogenous arachidonic acid (AA) and iron could sensitise both OPM2 and KMS-11 cells to RSL3. Moreover, we discovered that inhibiting ferroptosis suppressor protein 1 (FSP1), which is not expressed in ferroptosis-sensitive OPM2 cells, was a robust way in which to sensitise KMS-11 cells to RSL3. Next, we translated our research into an *ex vivo* model whereby patient-derived MM cells were co-cultured with other autologous bone marrow mononuclear and stromal cells. We found that patient-derived MM cells were much more susceptible to RSL3 compared to lymphocytes and this difference in sensitivity was even more apparent when cells were supplemented with AA. We identified key genes of which expression correlated with ferroptosis sensitivity in patient-derived MM cells, as well as a higher proportion of monounsaturated fatty acid-containing phospholipids conferring resistance to cell death induced by RSL3 combined with AA. A wider range of patient-derived samples should be tested to support these conclusions, however, our findings demonstrate that MM cell lines and patient-derived MM cells can be sensitised to ferroptosis by supplementation with ferroptosis substrates such as AA. Taken together, we conclude that developing ferroptosis-inducing therapies may be a promising future strategy for treating MM.

DECLARATION

I certify that this thesis:

1. does not incorporate without acknowledgment any material previously submitted for a degree or diploma in any university

2. and the research within will not be submitted for any other future degree or diploma without the permission of Flinders University; and

3. to the best of my knowledge and belief, does not contain any material previously published or written by another person except where due reference is made in the text.

Signed.....Rachel Mynott.....

Date 25/02/2025

ACKNOWLEDGEMENTS

I have so many people to thank for their support and guidance throughout my PhD, whether that be people that were there for me every step of the way, people that provided assistance for a few weeks or months or even the people who I met once at a conference or PhD coffee catch up that inspired me or made me smile on a day when I needed it most.

Firstly, I want to acknowledge that this research is supported by an Australian Government Research Training Program (RTP) Scholarship. In the last few years obtaining financial support to complete a PhD has become increasingly difficult. I am so grateful to have received this support, as well as a scholarship top up from the Margaret Fay Fuller Foundation in my final year. I also want to acknowledge the Flinders Foundation who not only supported me with a 6-month scholarship to enable me to start my PhD earlier, but who also supported me throughout my candidature financially for conference travel, as well as always showing an interest in my work and allowing me to connect with donors and patients who made my work possible.

I want to thank all our external collaborators who provided mentorship, encouragement and also assisted me with a number of assays and reagents throughout my project. I thank Professor Scott Ayton, Dr Adam Southon and Celeste Mawal for their ferroptosis insights and performing assays at the Florey Institute. I want to acknowledge our colleagues at the CCB who also provided me with a lot of support through our regular virtual meetings, as well as setting up our shRNA work: Professor Claudine Bonder, Professor Stuart Pitson, Dr Manjun Li and Paul Moretti. I also acknowledge the SAGC team, in particular Letitia Clark, who performed the RNA sequencing and Dr Shashi Marri and Dr Daniel Thomson for performing the bioinformatics magic to get the data into a digestible form for me. I must also acknowledge my lab colleague, the lipidomics whizz Ali Habib, who ran the majority of my lipidomic samples, with assistance from Associate Professor Marten Snel and Dr Paul Trim to get our experimental and analytic methodologies set up.

I particularly want to acknowledge and pay my respects to all the patients and their families who donated samples to our biobanking project, as well Flinders Medical Centre haematology staff that assisted with patient identification, consenting and sample collection. The final aim of my project would not have been possible without the generosity of all these people.

As to our Flinders University colleagues, I am thankful to Dr Nick Eyre at the Flinders Microscopy Facility for teaching me how to use the various microscopes, as well as Professor Luke Selth and Professor Michael

Michael for lending their expertise and providing constructive feedback from an outside perspective. I also want to thank Professor Michael Michael and Professor Janni Petersen and their incredible teams for creating such a warm, welcoming and supportive environment to work in. Having started honours with minimal lab experience, these guys were always willing to answer any of my silly questions and let me borrow various reagents over the last 5+ years. Also, a special shout out to all the level 4 lab girlies who kept me sane and whose lunchtime company and quiz night chaos made it bearable to go into uni on the days when my PhD got the better of me. And a huge thanks to Alana and Demi, without our virtual writing sessions I genuinely wonder if this thesis would have ever been completed.

Now to the haem team. What started as just myself, Pamela Kassais and Professor Craig Wallington-Gates on the first day of my honours degree has turned into a wonderful group of researchers. To my previous colleagues, Dr Ben Weimann and Joanna Cole, I thank them for their friendship and lending an ear to my never-ending complaints. I want to thank Ali for putting up with my poor teaching abilities when he first started in our lab and thank both him and Dr Charlotte Downes for being incredible lab colleagues. They were always willing to help me out, provide feedback, problem solve, pick up my slack in the shared lab duties when needed, and answer my various random questions as I've been writing my thesis. I am so thankful to Dr Giles Best on my supervisory team for all his support over the last 5+ years. He has always been a very calm presence and excellent sounding board, withstanding my word vomits as I try to interpret confusing data, and providing insightful thoughts and ideas that have helped guide my project and thesis writing. Last but not least, my primary supervisor, Professor Craig Wallington-Gates. Craig took me on as an honours student without any experience in an academic research laboratory and taught me everything I needed to know to get me started. I am eternally grateful for his trust in me and my ideas, I have learnt so much from him and am thankful for his unwavering support, especially when things got tough. I have so much respect for every person in the haem team and am so grateful to each of them for contributing to my immense growth, both as a scientist and human being during my PhD.

And of course, my family and friends; they have all shown so much interest and support during my PhD, even when they had no clue what I was talking about. Whilst everyone listed above helped with the generation/analysis of data, production of my thesis and/or my growth as a scientist, my family and friends truly kept me sane and happy, and I know for a fact without such a strong support system I would have given up long ago. I thank Alex and Anne for sticking by me and my antics for over 10 years, and my partner Jono for being my rock through this rollercoaster journey. I want to thank my close-knit, beautiful family and especially my mum, Jodie and dad, Craig who have supported me through every life decision and encouraged me to continue growing and learning. I know I have made them proud because they never fail to remind me.

PUBLICATIONS

Featured in thesis:

Mynott, RL, Habib, A, Best, OG & Wallington-Gates, CT 2023. Ferroptosis in haematological malignancies and associated therapeutic nanotechnologies. International Journal of Molecular Sciences, 24, 7661. https://doi.org/10.3390/ijms24087661

Habib, A, **Mynott, RL,** Best, OG, Revesz IA, Prestidge CA & Wallington-Gates, CT 2025. Novel (1S,3R)-RSL3-encapsulated polyunsaturated fatty acid rich liposomes sensitise multiple myeloma cells to ferroptosis-mediated cell death. Internation Journal of Molecular Sciences, 26(14), 6579. https://doi.org/10.3390/ijms26146579 (includes figures from Chapter 3)

Other publications during candidature:

Mynott, RL & Wallington-Beddoe, CT 2021. Inhibition of p-glycoprotein does not increase the efficacy of proteasome inhibitors in multiple myeloma cells. ACS Pharmacology & Translational Science, 4(2): p. 713-729. https://doi.org/10.1021/acsptsci.0c00200

Mynott, RL & Wallington-Beddoe, CT 2021. Drug and solute transporters in mediating resistance to novel therapeutics in multiple myeloma. ACS Pharmacology & Translational Science, 4(3): p. 1050-1065. https://doi.org/10.1021/acsptsci.1c00074

Wallington-Beddoe, CT. & **Mynott, RL** 2021. Prognostic and predictive biomarker developments in multiple myeloma. Journal of Hematology & Oncology, 14(1): p. 151. https://doi.org/10.1186/s13045-021-01162-7

CONFERENCES AND MEETINGS

Mynott, RL, Habib, A, Best, OG & Wallington-Gates, CT 2023. Multiple myeloma cells can be sensitised to RSL3-induced ferroptosis using arachidonic acid, ferric ammonium citrate or by inhibiting FSP1 (oral presentation). FerrOZtosis. Melbourne, Victoria.

Mynott, RL, Habib, A, Best, OG & Wallington-Gates, CT 2023. Multiple myeloma cells can be sensitised to RSL3-induced ferroptosis using arachidonic acid, ferric ammonium citrate or by inhibiting FSP1 (oral presentation). Japan and Australia Meeting on Cell Death. Melbourne, Victoria.

Mynott, RL, Habib, A, Best, OG & Wallington-Gates, CT 2023. Multiple myeloma cells can be sensitised to RSL3-induced ferroptosis using arachidonic acid, ferric ammonium citrate or by inhibiting FSP1 (poster). Ferroptosis: When Metabolism Meets Cell Death EMBO Workshop. Seeon, Germany.

Mynott, RL, Habib, A, Best, OG & Wallington-Gates, CT 2022. Multiple myeloma cells can be sensitised to a new form of regulated cell death termed ferroptosis (poster). Blood Meeting. Sydney, Australia.

Mynott, RL, Habib, A, Best, OG & Wallington-Gates, CT 2022. Investigating ferroptosis as an approach to treating multiple myeloma and other aggressive B cell malignancies (oral presentation). ASMR Medical Research Week, South Australian Scientific Meeting. Adelaide, Australia.

Mynott, RL, Habib, A, Best, OG & Wallington-Gates, CT 2021. Investigating ferroptosis as an approach to treating multiple myeloma and other aggressive B cell malignancies (poster). Emerging Leaders Showcase, Flinders University. Adelaide, Australia.

FUNDING

2021-2023

Australian Government Research Training Program Scholarship

2023

Margaret Fay Fuller Top-Up Scholarship

Flinders Foundation Jane Ramsey conference travel support

2022

Flinders University Research Student Conference Travel Grant

Flinders Foundation conference travel support

2021

FHMRI Higher Degree by Research (HDR) Student Small Grant

2020

Flinders Foundation 6-month PhD Scholarship

LIST OF FIGURES

LIST OF SUPPLEMENTARY FIGURES

LIST OF TABLES

ABBREVIATIONS

ALL	Acute lymphoblastic leukaemia
AA	Arachidonic acid
ACSL	Acyl-CoA synthetase long-chain family
ALOX	Arachidonate lipoxygenase
AML	Acute myeloid leukaemia
BMSC	Bone marrow stromal cells
C11-BODIPY	BODIPY 581/591 C11 (lipid peroxidation sensor)
CAR-T	Chimeric antigen receptor T-cell
CLL	Chronic lymphocytic leukaemia
CML	Chronic myeloid leukaemia
CRISPR	Clustered regularly interspaced short palindromic repeats
CTRP	Cancer Therapeutics Response Portal
DEG	Differentially expressed genes
DLBCL	Diffuse large B-cell lymphoma
DMEM	Dulbecco's Modified Eagle Medium
DMSO	Dimethyl sulfoxide
DNA	Deoxyribonucleic acid
EC_{50}	Half-maximal effective concentration
ER	Endoplasmic reticulum
FAC	Ferric ammonium citrate
FACS	Fluorescence-activated cell sorting
FBS	Foetal bovine serum
FDA	Food and Drug Administration
Fe	Iron
Fer-1	Ferrostatin-1
FP	Fractional product
FSP1	Ferroptosis suppressor protein 1
FTH1	Ferritin heavy chain 1
FTL	Ferritin light chain
GPX4	Glutathione peroxidase 4
GSH	Glutathione
GSSG	Glutathione disulfide
HMOX1	Heme oxygenase 1 gene
HO-1	Heme oxygenase 1 protein
IC_{50}	Half maximal inhibitory concentration

KO	Knockout
LIP	Labile iron pool
Lip-1	Liproxstatin-1
LOX	Lipoxygenase
MM	Multiple myeloma
MNC	Mononuclear cell
MUFA	Monounsaturated fatty acid
NCOA4	Nuclear receptor coactivator 4
Nec-1s	Necrostatin-1s
NHL	Non-Hodgkin lymphoma
Nrf2	Nuclear factor erythroid 2-related factor 2
NSCLC	Non-small cell lung cancer
nTPM	Normalized transcript per million
OD	Optical density
PE	Phosphatidylethanolamine
PBS	Phosphate-buffered saline
PS	Phosphatidylserine
PUFA	Polyunsaturated fatty acid
p53	Tumour protein 53 (protein)
REN	Renilla luciferase
RFP	Red fluorescent protein
RNA	Ribonucleic acid
ROS	Reactive oxygen species
RPMI	Roswell Park Memorial Institute
RSD	Relative standard deviation
RSL3	(1S,3R) RAS-selective lethal 3
SD	Standard deviation
SFA	Saturated fatty acids
shRNA	Short hairpin RNA
siRNA	Small interfering RNA
SLC	Solute carrier family
TP53	Tumour protein p53 (gene)
xCT	SLC7A11

CHAPTER 1. INTRODUCTION AND LITERATURE REVIEW

A version of this chapter has been published and can be found at:

Mynott, RL, Habib, A, Best, OG & Wallington-Gates, CT 2023. Ferroptosis in Haematological Malignancies and Associated Therapeutic Nanotechnologies. International Journal of Molecular Sciences, 24, 7661. Doi: 10.3390/ijms24087661

R.L.M. and A.H reviewed the literature, and all authors contributed to the writing of the manuscript (RLM: 50%, AH: 30%, OGB: 10%, & CTW-G 10%).

The published literature review investigates ferroptosis in haematological malignancies, with a focus on moving towards nanotechnologies as methods for the delivery of ferroptosis-inducing therapies into cells. In the review we describe the major haematological cancers, ferroptosis and clinical applications thereof before providing an in-depth discourse on the use of ferroptosis-inducing nanotechnologies in cancer, focusing on those of haematological origin. We provide examples of dendritic mesoporous silica nanoparticles, iron oxide nanoparticles, micelles and liposomes employing tumour-targeting or precision approaches. Throughout, we highlight the significance of liposome-based nanotechnologies given their importance, as not only drug carriers but also ferroptosis-inducing therapeutics by supplying relevant phospholipids to the cancer cell. These nanotechnology sections have been condensed for the purpose of this thesis as while they relate to the overall future directions of this work, the details extend beyond the scope of the work generated during this project and are unnecessary in the context of the subsequent chapters. The full manuscript is available online at **https://doi.org/10.3390/ijms24087661**.

1.1 Introduction

Haematological malignancies comprise a large group of heterogeneous tumours that originate in blood-forming tissue, such as the bone marrow, or in the cells of the immune system. Broadly speaking, these tumours are grouped into those of myeloid or lymphoid origin and can be acute or chronic with regard to their natural history. Examples of bone marrow-derived malignancies include acute myeloid leukaemia, acute lymphoblastic leukaemia and chronic myeloid leukaemia, whilst chronic lymphocytic leukaemia, lymphomas and multiple myeloma (MM) are lymphoid malignancies originating outside the bone marrow in blood or lymphatic tissue. Given their biological heterogeneity, there are consequential differences in diagnostic, prognostic and therapeutic algorithms with many being treatable but not curable.

The term ferroptosis was coined in 2012 to describe a new form of regulated cell death characterised by the iron-dependent accumulation of lipid reactive oxygen species to lethal levels (Dixon et al., 2012). The sensitivity to ferroptosis is tightly linked to numerous biological processes, including the metabolism of amino acids, iron and polyunsaturated fatty acids (PUFA), and the biosynthesis of glutathione (GSH) and phospholipids. Ferroptosis has been implicated in the pathological cell death associated with degenerative diseases (e.g. Alzheimer's disease), stroke and traumatic brain injury, however, ferroptosis may also have a tumour-suppressor function that could be harnessed for cancer therapy (Stockwell et al., 2017). Importantly, lipid metabolism is intimately involved in determining cellular sensitivity to ferroptosis with certain polyunsaturated phospholipids being susceptible to the iron-dependent lipid peroxidation necessary for its execution (Yang et al., 2016). It is this dependence on certain phospholipids that paves the way for development of potential ferroptosis-inducing nanotechnologies, in particular those based on liposomes.

Cancer therapeutics have advanced tremendously over the past few decades with firstly a shift towards tumour-targeting mechanisms and more recently patient-individualised or precision strategies (Wallington-Beddoe and Mynott, 2021, Ebert et al., 2022). An example of the former is the monoclonal antibody daratumumab which targets CD38 on the surface of MM plasma cells whilst venetoclax represents a precision therapeutic in MM patients whose plasma cells harbour a translocation of chromosomes 11 and 14, (t(11;14)), which upregulates Bcl-2, the target of venetoclax (Palumbo et al., 2016, Kumar et al., 2020). Thus, cancer drug classes have expanded to include traditional chemotherapeutics such as DNA damaging agents and mitotic spindle inhibitors, tumour-targeting small molecule inhibitors, tumour-targeting immunological agents (monoclonal antibodies, bi-specific antibodies, antibody-drug conjugates, chimeric antigen receptor T-cells (CAR-T cells)) and precision therapeutics which may incorporate any one or more of the other therapeutic classes (Wallington-Beddoe and Mynott, 2021). Nanotechnologies, on the other hand, are often seen as vehicles for existing cancer drugs which aim to maximise cancer cell cytotoxicity through improved drug pharmacokinetics and pharmacodynamics (Liu et al., 2023a). This approach aims to not only increased tumour killing but also minimise both on-target and off-target related drug toxicities, particularly when incorporating tumour-targeting and precision principles.

1.2 Multiple Myeloma

Multiple myeloma (MM) is a malignancy of antibody-producing plasma cells of the bone marrow (Rajkumar and Kumar, 2016). In Australia in 2020, 2,220 people were diagnosed with MM at a median age of 72.4 years with an overall survival at 5 years of 59.5% (Australian Institute of Health and Welfare, 2024). A diagnosis of MM is defined as the presence of more than 10% clonal plasma cells in the bone marrow, as well as one or more of the "CRAB" criteria: hypercalcaemia, renal insufficiency, anaemia, or bone lytic lesions. Other

diagnostic criteria have been recently introduced including at least 60% clonal plasma cells in the bone marrow, one or more focal bone marrow lesion on magnetic resonance imaging (MRI) imaging (indicating bone marrow involvement), or an involved to uninvolved free immunoglobulin light chain ratio > 100 (Rajkumar and Kumar, 2016).

The median survival of patients with MM has significantly improved since the 1990s, predominantly due to the introduction of new therapeutic agents (Kumar et al., 2008, Kazandjian and Landgren, 2021). These novel therapies include the proteasome inhibitors (e.g. bortezomib and carfilzomib), immunomodulatory drugs (e.g. lenalidomide and pomalidomide) and monoclonal antibodies (e.g. daratumumab and elotuzumab, which target the CD38 and SLAMF7 proteins, respectively) (Mynott and Wallington-Beddoe, 2021, Kumar et al., 2008). In practice, these drugs are not used alone but rather in combination; however, despite significant improvements in quality of life and overall survival in the last few decades, disease relapse is inevitable.

1.3 Lymphomas

Lymphomas are a diverse group of haematopoietic malignancies that arise from the clonal proliferation of lymphocytes, usually in lymph nodes. Characterization of lymphomas morphologically, immunophenotypically and genetically allows for the identification of many different subtypes with varying prognostic and treatment algorithms, however they are generally classified as either Hodgkin lymphomas (HL) or non-Hodgkin lymphoma (NHL) (Lewis et al., 2020). HLs can be identified in lymph nodes by the presence of Reed-Sternberg cells admixed with variable numbers of B-cells, T cells and other haematopoietic lineages. These lymphomas tend to be highly chemo-sensitive with a 5-year survival rate exceeding 80% (Shanbhag and Ambinder, 2018). NHLs constitute a large group of diverse lymphoid tumours of either B or T cell origin with B-cell NHLs being more common than T cell NHLs.

Diffuse large B-cell lymphoma (DLBCL) is the most common non-Hodgkin lymphoma (NHL), accounting for 30-40% of all NHL cases, and approximately one third of all newly diagnosed lymphoma cases worldwide (Sehn and Salles, 2021, Li et al., 2018). A treatment regimen consisting of cyclophosphamide, doxorubicin, vincristine, and prednisone (CHOP) combined with the monoclonal antibody, rituximab (R-CHOP) is the current frontline treatment for DLBCL (Sehn and Salles, 2021). While over 60% of patients can be cured with R-CHOP, those with either primary refractory disease or who relapse after a period of remission have poorer outcomes (Sehn and Salles, 2021). DLBCL can be further classified into two main molecular subtypes, activated B-cell (ABC) and germinal centre B-cell (GCB); the former being associated with a significantly worse prognosis and complete remission (CR) rates of 30% and 70%, respectively (Li et al., 2018). In approximately 10% of cases, translocations involving *MYC* and *Bcl-2* and/or *Bcl-6* (double and triple hit DLBCL) are identified,

which are also associated with less favourable clinical outcomes (Kim et al., 2020, Petrich et al., 2014). Furthermore, overexpression of Bcl-2 and MYC ('double-expressor') can occur through mechanisms that do not involve chromosomal translocations (Kim et al., 2020, Riedell and Smith, 2018). It is for these patients with poorer clinical outcomes that novel therapeutics are urgently required.

1.4 Leukaemias

Leukaemias are a heterogenous group of diseases that arise from the clonal proliferation of immature or mature leukocytes (Chennamadhavuni et al., 2022). It is estimated that 5,202 people will be diagnosed with leukaemia in 2022 in Australia, with a 5-year survival rate of 64.4% (Australian Institute of Health and Welfare, 2024). Leukaemias can be characterised by the cell of origin (lymphoid or myeloid) and by the rate of proliferation (acute or chronic) (Chennamadhavuni et al., 2022). The predominant subtypes of leukaemia and their prevalence in Australia are outlined in Table 1-1.

Table 1-1: Leukaemia statistics from 2020 Cancer data in Australia.

Leukaemia subtype	Median age at diagnosis (years)	Number of cases diagnosed	Number of deaths	5-year survival rate in 2016-2020 (%)
Acute lymphoblastic leukaemia (ALL)	15.5	431	90	75.1
Acute myeloid leukaemia (AML)	70.9	1165	1161	27.2
Chronic lymphocytic leukaemia (CLL)	72.1	1861	327	87.2
Chronic myeloid leukaemia (CML)	59.2	398	82	84.9

Data extracted from 2020 Cancer data in Australia (Australian Institute of Health and Welfare, 2024)

Chemotherapy, chemoimmunotherapy and stem cell transplantation are common treatment options for leukaemia but with a better understanding of the mechanisms that drive these diseases, novel targeted agents are becoming more widely used. Response and outcome rates vary significantly between the different forms of leukaemia but invariably a proportion of patients will relapse with refractory disease. Whilst survival rates among patients diagnosed with acute leukaemia have improved markedly in the last few decades, particularly for patients under the age of 50, 5-year survival rates for patients with acute lymphoblastic

leukaemia (ALL) or acute myeloid leukaemia (AML) remain as low as 12% and 4%, respectively, for patients over the age of 80 at diagnosis (Beckmann et al., 2022).

Unlike patients with acute leukaemia who generally require intensive treatment, patients with chronic leukaemia are often initially managed with a 'watch and wait' approach with minimal to no treatment required for many years (Chennamadhavuni et al., 2022). Approximately 30% of patients diagnosed with chronic lymphocytic leukaemia (CLL) never require treatment, whereas many CLL patients will have or will rapidly develop symptomatic disease after diagnosis, requiring early intervention (Gong et al., 2022). Chronic myeloid leukaemia (CML) is a slow growing malignancy characterised by the Philadelphia chromosome formed by a reciprocal translocation of chromosomes 22 and 9 (Granatowicz et al., 2015). The resulting fusion oncogene (BCR-ABL) is effectively targeted by tyrosine kinase inhibitors such as imatinib, which have significantly improved survival rates among CML patients (Granatowicz et al., 2015).

1.5 Ferroptosis

Regulated cell death is a fundamental physiological process that ensures cell integrity and homeostasis. While apoptosis is arguably the most well studied form of cell death, a relatively recent study by Dixon *et al*., described an iron-dependent form of cell death associated with an accumulation of lipid peroxides, which they termed ferroptosis (Dixon et al., 2012). Ferroptosis is morphologically, genetically and biochemically distinct from other forms of cell death, including apoptosis, as it can be inhibited by iron chelation and lipophilic antioxidants (Yang and Stockwell, 2016). Cells undergoing ferroptosis have a characteristic "ballooning phenotype" with an enlarged, empty cytoplasm, in contrast to the small, shrunken appearance of apoptotic cells with distinct membrane blebbing that precedes apoptotic body formation (Battaglia et al., 2020, Tang and Tang, 2019). Ferroptotic cells also lack key morphological changes associated with other forms of programmed cell death, such as apoptotic bodies or the autophagosomes associated with apoptosis and autophagy, respectively (Battaglia et al., 2020). Other features of ferroptosis, including reduced mitochondrial volume, increased mitochondrial membrane density and the absence of mitochondrial cristae can also be observed using transmission microscopy (Dixon et al., 2012).

Since its discovery, ferroptosis has been associated with many biological processes involved in cellular homeostasis, iron and amino acid regulation, and metabolism of PUFAs (Stockwell et al., 2017). In the context of cancer, induction of ferroptosis has the potential to be a novel treatment strategy, particularly for patients who relapse with drug resistant disease following treatment with standard therapies. As cancer cells generally have higher levels of reactive oxygen species (ROS) due to increased metabolic and growth rates, cell death mechanisms such as ferroptosis that further elevate ROS levels may be a particularly effective and

specific approach for the treatment of a range of cancers (Chiang et al., 2018). In addition to the aforementioned morphological changes, ferroptosis can be distinguished from other forms of cell death by monitoring accumulation of lipid peroxides, using fluorescently-labelled fatty acid analogues (i.e., C11-BODIPY), and through inhibition of cell death by either iron chelation (i.e., deferoxamine, DFO) or lipophilic antioxidants (liproxstatin-1 (Lip-1), ferrostatin-1 or vitamin E) (Cao and Dixon, 2016). Furthermore, ferroptosis cannot be prevented by inhibitors of apoptosis, necroptosis, or autophagy (i.e., Z-VAD-FMK, necrostatin-1s and chloroquine, respectively) (Dixon et al., 2012).

1.5.1 The Role of Iron in Ferroptosis

Iron is essential for cellular homeostasis (Dev and Babitt, 2017), with key roles in oxygen transport, oxidative phosphorylation and DNA biosynthesis (MacKenzie et al., 2008). As iron chelation inhibits ferroptosis, this form of cell death is also clearly an iron-dependent process (Dixon et al., 2012). Intracellular iron levels are primarily regulated by the iron-storage protein ferritin, and the transferrin receptor (TfR) which shuttles transferrin-bound iron into the cell through receptor- mediated endocytosis. The level of non-protein bound iron (labile iron pool) has implications in ferroptosis as labile iron reacts with hydrogen peroxide inside cells, yielding highly reactive hydroxyl radicals in a process known as the Fenton reaction (Ayala et al., 2014). These radicals indiscriminately damage all surrounding organic material within a range of a few nanometres, resulting in cellular damage (Ayala et al., 2014). Iron also plays a role in ferroptosis through its actions on a group of iron-containing enzymes that mediate lipid peroxidation, known as lipoxygenases (LOXs) (Stockwell et al., 2017, Shintoku et al., 2017). The key role of these enzymes is demonstrated by the LOX inhibitor, zileuton, which confers resistance to ferroptotic cell death in HT22 neuronal cells (Liu et al., 2020). Furthermore, genetic knockdown or pharmacological inhibition of arachidonate lipoxygenases (ALOXs) protects cells against ferroptosis induced by erastin (Yang et al., 2016).

1.5.2 Lipid Peroxidation

Lipid peroxidation is a characteristic feature of ferroptosis, distinguishing it from other forms of programmed cell death. Phospholipid peroxidation results in the oxidative degradation of lipids, formation of peroxyl radicals and damage to the plasma membrane (Gaschler and Stockwell, 2017, Conrad et al., 2018). Sensitivity to ferroptosis is associated with the degree of lipid saturation, the cellular location of the phospholipids and the number of phospholipids containing PUFA relative to those containing monounsaturated fatty acids (MUFA) (Stockwell et al., 2017). Phospholipids containing PUFAs are more readily oxidised and therefore supplementation with PUFAs such as arachidonic acid (AA) and linoleic acid (LA) increase the sensitivity of cancer cells to ferroptosis (Beatty et al., 2021, Kagan et al., 2017, Yang et al., 2016). Other studies support this notion that cellular sensitivity to ferroptosis is associated with their lipidomic profile, demonstrating that

incorporation of MUFAs into phospholipids reduces the generation of lipid ROS in membranes and therefore protects against ferroptosis (Yang et al., 2016, Magtanong et al., 2019). MUFAs can also displace PUFAs from intracellular phospholipids, including in the plasma membrane, reducing the potential for lipid ROS accumulation (Magtanong et al., 2019).

1.5.3 System Xc^- and GPX4

xCT, encoded by the *SLC7A11* gene, is a major part of the system Xc^- cystine/glutamate antiporter. The regulatory component, SLC3A2, is involved in many other solute transporter systems and so xCT has been the focus of much of the work into system Xc^-. Glutamate is pumped out of the cell in exchange for cystine, which is rapidly reduced to cysteine (Koppula et al., 2018). Cysteine is a rate limiting factor in the production of GSH, an important antioxidant due to its role as a cofactor of glutathione peroxidase 4 (GPX4) (Jiang et al., 2021). GPX4 is the primary enzyme that reduces phospholipid hydroperoxides into their corresponding alcohols, inhibiting lipid peroxidation and subsequent ferroptosis (Stockwell et al., 2017, Seibt et al., 2019). When the activity of GPX4 is inhibited, either directly or through GSH depletion, and lipid peroxidation exceeds tolerable levels, ferroptotic cell death is initiated (Figure 1-1) (Yang et al., 2014, Stockwell et al., 2017).

Class 1 ferroptosis inducers deplete cellular GSH by inhibiting xCT and therefore preventing cystine uptake (e.g. erastin) or interfering with GSH synthesis (e.g. buthionine sulfoximine; BSO). In vivo studies of erastin have been limited by its pharmacokinetics and poor solubility but its more soluble analogue, imidazole ketone erastin (IKE), is metabolically stable and 100x more effective than erastin in some cell lines (Zhang et al., 2019, Sato et al., 2018). (1S,3R)-RSL3 (hereafter referred to as RSL3) was first described as a ferroptosis inducer in 2008 and shown to induce a similar phenotype to erastin via GSH-independent mechanisms (Yang and Stockwell, 2008). In addition to RSL3, another frequently described class 2 ferroptosis inducer is ML162 (Feng and Stockwell, 2018, Yu et al., 2017). Both RSL3 and ML162 are covalent inhibitors of GPX4 that bind and inhibit the protein directly (Moosmayer et al., 2021).

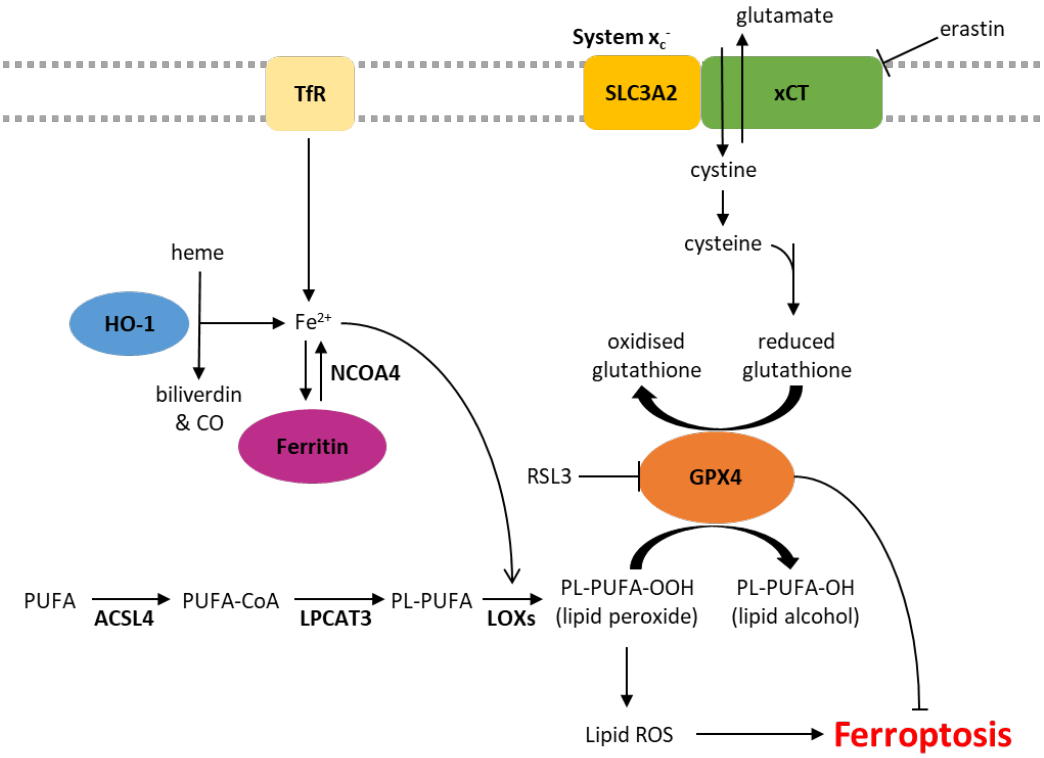

Figure 1-1: Biochemical pathways involved in the regulation of ferroptosis.

ACSL4, acyl-CoA synthetase long-chain family member 4; CO, carbon monoxide; Fe2+, ferrous iron; GPX4, glutathione peroxidase 4; HO-1, heme oxygenase 1; LOXs, lipoxygenases; LPCAT3, lysophosphatidylcholine acyltransferase 3; NCOA4, nuclear receptor coactivator 4; PL, phospholipid; PUFA, polyunsaturated fatty acid; ROS, reactive oxygen species; TfR, transferrin receptor.

1.5.4 Ferroptosis Suppressor Protein 1 and the Mevalonate Pathway

Ferroptosis has also been observed independent of GPX4 inhibition, likely due to the presence of other intracellular antioxidant systems. Recently, apoptosis-inducting factor mitochondrial 2 (AIFM2), which has since been renamed ferroptosis suppressor protein 1 (FSP1), has been implicated in resistance to ferroptosis (Bersuker et al., 2019, Doll et al., 2019). A study by Doll *et al*., demonstrated that knockout of FSP1 increased the sensitivity of melanoma (MDA-MD-435S), colorectal cancer (SW620), glioblastoma (U-373), lung cancer (A549 and NCI-H1437), and breast cancer (MDA-MB-436) cells to RSL3 (Doll et al., 2019). Furthermore, resistance to RSL3 could be restored by re-expression of mouse FSP1 in MDA-MB-436 breast cancer cells (Doll et al., 2019). FSP1 knockout in an osteosarcoma cell line (U-2 OS) did not affect GSH levels, suggesting its mechanisms of action are independent of xCT or GSH synthesis (Bersuker et al., 2019). The mechanism by which FSP1 mediates resistance to ferroptosis is thought to involve coenzyme Q_{10} (CoQ_{10}, also known as ubiquinone), generated by the mevalonate pathway. The mevalonate pathway is a multifaceted biological pathway that leads to the production of isopentenyl pyrophosphate (IPP) as well as ubiquinone (Figure 1-2). IPP is involved in the maturation of selenocysteine, an amino acid required for GPX4 translation (Warner et al., 2000, Yang and Stockwell, 2016). IPP can also be converted to farnesyl pyrophosphate, which is an

important upstream substrate in the generation of ubiquinone (Turunen et al., 2004). ubiquinone is a naturally occurring quinone that is vital to cell and tissue health in most aerobic organisms (Saini, 2011). Studies have shown that FSP1 reduces ubiquinone to CoQ_{10}-H_2 (ubiquinol), which is a radical-trapping antioxidant that prevents the accumulation of lipid peroxides associated with ferroptosis (Figure 1-2) (Doll et al., 2019, Bersuker et al., 2019).

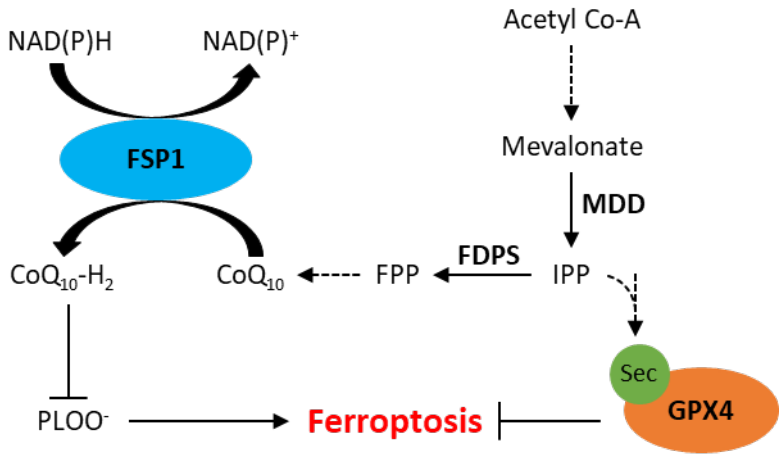

Figure 1-2: Schematic representation of the mevalonate pathway and its role in inhibition of ferroptosis.

CoQ_{10}, ubiquinone; CoQ_{10}-H_2, ubiquinol; FDPS, farnesyl diphosphate synthase; FPP, farnesyl phosphate; FSP1, ferroptosis suppressor protein 1; GPX4, glutathione peroxidase 4; IPP, isopentenyl phosphate; MDD, mevalonate diphosphate decarboxylase; $PLOO^{\cdot}$, lipid peroxyl radicals; Sec, selenocysteine. Dotted arrows represent multiple steps within a pathway.

1.6 Clinical Applications of Ferroptosis

1.6.1 Ferroptosis in Multiple Myeloma

Studies have already shown that treating MM cells with high concentrations of iron induces cell death, and this can be prevented by the ferroptosis inhibitor, ferrostatin-1 (Bordini et al., 2020). Despite this, MM cells were shown to be more resistant to erastin-induced ferroptosis compared to diffuse large B-cell lymphoma (DLBCL) cells (Yang et al., 2014). A recent study also demonstrated that levels of GPX4 and xCT are higher in MM plasma cells than in their healthy counterparts, suggesting MM plasma cells may be utilising this antioxidant pathway to withstand elevations in ROS levels (Zhong et al., 2020). Increased expression of these two proteins and their crucial roles in ferroptosis, suggests they may represent drug targets for the treatment of MM. Furthermore, high expression of ferroptosis suppressor genes correlate with reduced progression-free and overall survival in MM patients (Su et al., 2022). A number of groups have recently developed ferroptosis-related gene signatures that can be used to predict MM patient prognosis (Fu et al., 2022) and identify high-risk (Qin et al., 2022) and/or drug resistant patients (Gao et al., 2023). Fu *et al.* went on to show that erastin and doxorubicin synergistically reduce the viability of NCI-H929 and RPMI-8226 MM cells, via a mechanism that involves GPX4 degradation and subsequent ROS generation (Fu et al., 2022). Similarly, the

GPX4 inhibitors RSL3 and ML162 acted in synergy with bortezomib and lenalidomide, decreasing the proliferation of RPMI-8226 MM cells (Gao et al., 2023). Taken together, the aforementioned studies suggest that genes involved in ferroptosis may be useful to determine prognosis in MM, while ferroptosis-inducing drugs may enhance the efficacy of agents that are routinely used in the clinic.

The synthetic amino acid BSO has been found to reduce GSH levels in MM cells by inhibiting glutamate-cysteine ligase (GCL), the first enzyme in the GSH synthesis pathway, and increase the efficacy of bortezomib (Nerini-Molteni et al., 2008). In bladder carcinoma cells, expression of xCT was found to be upregulated following bortezomib treatment in an nuclear factor erythroid 2-related factor 2 (Nrf2)- and activating transcription factor (ATF)-dependent manner (Ye et al., 2014). Since expression of both Nrf2 and ATF4 transcription factors is associated with poor prognosis and drug resistance in patients with bladder cancers, inhibition of xCT may represent an effective treatment to increase the efficacy of proteasome inhibitors (Ye et al., 2014). Further supporting this, GSH degradation by omega-3 fatty acids increased the effects of bortezomib in OPM2 MM cells and transcriptomic pathway analyses of the treated cells revealed changes in several gene pathways including those with known roles in ferroptosis (Chen et al., 2021a). High-dose iron (600 μM ferric ammonium citrate) has also been shown to induce MM cell death and increase the efficacy of bortezomib in vitro and the bortezomib, melphalan and prednisone regimen, in a MM mouse model (Bordini et al., 2020). These effects were again shown to involve ferroptosis, with increased production of the lipid oxidation by-product malondialdehyde (MDA), and inhibition of cell death by ferrostatin-1 (Bordini et al., 2020).

Lipidomic analyses have shown that AA levels are decreased in plasma cells from patients with preclinical and early-stage MM (Panaroni et al., 2018). This was confirmed in another analysis showing that although MM patients had higher levels of n-6 PUFAs compared to healthy controls, overall AA levels were reduced (Jurczyszyn et al., 2015). An earlier study, which utilised fluorescently-tagged AA, demonstrated that this fatty acid is readily taken up by MM cells and is primarily incorporated into triglycerides and phospholipids, but that this uptake had no effect on proliferation (Desplat et al., 1999). The mode of transport has since been described to involve fatty acid transporters (FATPs) (Panaroni et al., 2022). More recently, addition of exogenous AA was associated with dose- and caspase-dependent apoptotic cell death in three MM lines, but not healthy human peripheral blood mononuclear cells (Abdi et al., 2014). Culturing cells in the presence of AA has also been shown to induce ferroptosis which could be reversed by ferrostatin-1; addition of physiological concentrations of AA was shown to decrease the proliferation and viability of primary MM cells and cell lines, with a concomitant decrease in GPX4 expression (Panaroni et al., 2019). It is important to note that while high concentrations of AA can induce death in MM cells, low concentrations have been shown to

promote their proliferation; in fact, MM cells induce lipolysis in bone marrow adipocytes and upregulate FATPs in the presence of free fatty acids (Panaroni et al., 2022). This highlights the need to better understand the physiological concentrations of AA that are required to induce cell death and improve delivery systems to ensure levels do not drop below the threshold at which cancer cell proliferation is promoted.

With the advent of large scale, high throughput drug screening technologies, there has been a rapid increase in the number of drugs that are now known to induce ferroptosis. FTY720 was first developed by structurally modifying the antibiotic myriocin and is now approved by the FDA for the treatment of multiple sclerosis (Zhong et al., 2020). Initial studies of FTY720 in MM suggested that this compound induces apoptosis and autophagy (Liao et al., 2012), however a more recent study showed that cell death in MM cells following treatment with FTY720 is associated with an accumulation of ROS and can, at least partially, be inhibited by ferrostatin-1 (Zhong et al., 2020). Furthermore, the study showed that FTY720 reduces expression of GPX4 and xCT *in vitro*, both at the mRNA and protein level and concluded that the drug likely induces ferroptosis and autophagy, mediated by the protein phosphatase 2A/AMP-activated protein kinase pathway (Zhong et al., 2020). The naturally occurring flavone, apigenin, and extracts from the plants *Thymus vulgaris, Arctium lappa, Fumaria officinalis L.* and *Lithospermum erythrorhizon* were also shown to induce cell death in a range of MM cell lines (N. Adham et al., 2020, Adham et al., 2021a, Adham et al., 2021b, Li et al., 2022b). Cell death could, at least partially, be inhibited with ferrostatin-1, Lip-1 or deferoxamine in all cases, suggesting ferroptosis was involved in the observed response and indicating that naturally derived plant extracts may be useful tools to induce ferroptosis in MM cells.

Recent research in MM has also uncovered a link between ferroptosis and subsequent DNA changes (Logie et al., 2021). Induction of ferroptosis in MM results in upregulation of a multitude of key genes involved in cellular stress, cell death, inflammation, and fatty acid metabolism, including the ferritin heavy chain 1 (*FTH1*), ferritin light chain (*FTL*), heme oxygenase 1 (*HMOX1*) and *SLC7A11* genes (Logie et al., 2021). Of 616 differentially expressed genes identified in MM cells undergoing ferroptosis, upregulation of 95 genes was inhibited by pre-treating cells with ferrostatin-1 (Logie et al., 2021). The 95 genes identified included those that encode zinc finger proteins and genes with roles in metal binding, nuclear receptor signalling and chromatin remodelling (Logie et al., 2021).

Taken together, these findings demonstrate that MM cells have the capacity to undergo ferroptosis, however, further studies are required to identify combinations and concentrations of ferroptosis-inducing agents that are achievable in vivo to harness the potential of ferroptosis clinically.

1.6.2 Ferroptosis in Lymphoma

DLBCL cells have been shown to be significantly more sensitive to erastin-induced growth inhibition, compared to MM and AML cells (Yang et al., 2014). This may be explained by the dependence of DLBCL cells on xCT for cysteine uptake as they are unable to synthesise cysteine from methionine via the transsulfuration pathway (Zhang et al., 2019). Furthermore, a number of ferroptosis gene signatures including genes such as *FTH1, GPX4,* six-transmembrane epithelial antigen of prostate 3 (*STEAP3*)*,* lysophosphatidylcholine acyltransferase 3 (*LPCAT3*) and others, have been developed to predict prognosis and overall survival in patients with DLBCL (Weng et al., 2022, Chen et al., 2023, Wu et al., 2023a). Specifically, expression of GPX4 was shown to be an independent marker of poor prognosis in DLBCL (Kinowaki et al., 2018). Immunohistochemistry was used to examine GPX4 expression in samples from 93 DLBCL patients, and the GPX4 positive group (35%) had significantly lower overall and progression free survival rates (Kinowaki et al., 2018). Interestingly, no significant changes in *GPX4* mRNA were observed, suggesting that GPX4 protein expression is regulated by post-transcriptional modification (Kinowaki et al., 2018). These findings support the idea that GPX4 may confer a survival advantage on DLBCL cells, possibly through oxidant tolerance and decreased sensitivity to ferroptosis, and that inhibition of GPX4 may represent a potential therapeutic target for patients with high risk DLBCL disease. A recent study found that treatment of DLBCL cells with dimethyl fumarate depletes the cells of GSH and retards their proliferation and that these effects were potentiated by inhibition of FSP1 (Schmitt et al., 2021). However, significantly higher levels of lipid peroxidation were observed in DLBCL cells classified as GBC than ABC following treatment with dimethyl fumarate, which may be due to elevated levels of 5-lipoxygenase in the GCB sub-type (Schmitt et al., 2021).

Propolis, a resinous product from Western honeybees has been shown to have anti-tumour properties in a range of cancer types. Recently, extracts from Chinese propolis were shown to induce cell death in the SU-DHL-2 DLBCL cell line, which were associated with significant changes in expression of proteins involved in ferroptosis-related signalling pathways (Liu et al., 2023b). Analysis by ultra-performance liquid chromatography electrospray ionization mass spectrometry (UPLC-ESI-MS) showed the extracts contain a variety of flavonoids, phenolic compounds, acylated glycerol and fatty acids. Included in the list of compounds was apigenin, which has previously been shown to induce ferroptosis on its own or as a compound in other plant extracts in MM and leukaemic cell lines (Adham et al., 2021a, Adham et al., 2021b, N. Adham et al., 2020). Another natural compound kayadiol, which is extracted from the pulp of a Japanese tree (*Torreya nucifera*), induced ferroptosis-mediated death of extranodal natural killer/T-cell lymphoma (NKTCL) cell lines and peripheral blood lymphocytes (PBLs) extracted from NKTCL patients but not healthy donor PBLs (He et al., 2022).

Sensitivity to ferroptosis varies between different DLBCL cell lines, with the IC50 of the erastin analogue, IKE, ranging from 1 nM to almost 100 µM (Zhang et al., 2019). Consistent with ferroptosis, cell death induced by IKE was associated with a significant increase in levels of lipid peroxidation and MDA and could be inhibited by pre-treating cells with ferrostatin-1 (Zhang et al., 2019). Similar effects were also observed in a mouse lymphoma model and were associated with a decrease in GSH levels from as early as 4 hours after IKE dosing (Zhang et al., 2019). Decreased tumour volume in mice treated with IKE, was consistent with increased MDA levels, which is indicative of lipid peroxidation and suggestive of ferroptosis as a mechanism of cell death. As single agents, the PUFAs AA, eicosapentaenoic acid (EPA) and γ-linolenic acid all caused a decrease in cell viability in the ferroptosis-sensitive DLBCL cell line SU-DHL-6 at relatively high concentrations (approaching 100 µM), whereas 10 µM was sufficient to sensitise the cells to IKE (Zhang et al., 2019). Conversely, addition of the MUFAs, oleic acid or palmitoleic acid, protected the cells from ferroptosis, which is consistent with earlier reports demonstrating that addition of oleic acid to the ferroptosis-sensitive BJeLR (human skin tissue), HT-1080 (fibrosarcoma), and G-401 (rhabdoid kidney tumour) cell lines can prevent RSL3-induced ferroptosis (Yang et al., 2016, Zhang et al., 2019).

As discussed earlier, iron homeostasis plays a critical role in ferroptosis and therefore targeting pathways that regulate iron levels may represent an effective treatment approach. A recent study in DLBCL with the small lysosomal iron-targeting molecule, ironomycin, demonstrated that the drug sequesters iron within lysosomes, which leads to the generation of lysosomal ROS, dysfunction of lysosomes and cell death (Devin et al., 2022). The observed mechanism of cell death was suspected to be ferroptosis, as levels of cellular GSH were depleted and the cell death was partially prevented by ferrostatin-1, but not by the necroptosis or apoptosis inhibitors, necrostatin-1 and Z-VAD-FMK, respectively (Devin et al., 2022, Mai et al., 2017), respectively.

Recent studies demonstrate that the cytotoxicity of APR-246 (eprenetapopt), a prodrug that binds mutant tumour protein p53 (p53), is iron dependent and can be prevented by iron chelators or inhibitors of lipid peroxidation, but not necroptosis, pyroptosis or apoptosis inhibitors, in DLBCL cells (Hong et al., 2022). Interestingly, the autophagy inhibitor chloroquine was able to prevent APR-246 induced death in OCI-Ly7 cells that harbor a missense mutation in exon 7 of the p53-encoding gene, *TP53*, but not any other DLBCL cell lines. The binding of APR-246 to mutant p53 restores the ability of the transcription factor to interact with target genes and as a result, induces ferritinophagy. APR-246 is also effective at inducing ferroptosis in cells with wild type *TP53*, through mechanisms that are thought to be independent of mutations in this gene (Hong et al., 2022). In Eμ-Myc mouse lymphoma cells, APR-246 induced apoptosis regardless of *TP53* status but was, however, more effective in wild type cells. Ferroptosis was not observed in these cells following APR-

246 treatment but Fer-1 could partially prevent cell death in histiocytic lymphoma cells (BAX/BAK/MLKL knockout U937 cells) (Wang et al., 2023). Other cancer cell lines and cell death mechanisms were investigated in this study leading to the conclusion that APR-246 can induce cell death via multiple mechanisms, including ferroptosis, regardless of *TP53* status (Wang et al., 2023).

Using computational and experimental approaches, altretamine, an FDA-approved anti-cancer drug used to treat ovarian cancer, was shown to have a similar mechanism of action as the drug sulfasalazine (Woo et al., 2015). Unlike sulfasalazine, however, altretamine did not deplete GSH levels in the U2932 DLBCL cell line but did induce a significant increase in oxidised phospholipids, implicating GPX4 as a target of this drug (Woo et al., 2015). Artesunate, a derivate of the plant extract artemisinin, is approved by the FDA for malaria treatment, but a recent study showed the compound also has anticancer effects that are mediated by ferroptosis. In Burkitt's lymphoma cells, only inhibitors of ferroptosis and not necroptosis or apoptosis could prevent artesunate-induced cytotoxicity. Furthermore, artesunate activity was associated with an increase in general ROS and lipid peroxidation and was revealed to involve the ATF4-CHOP-CHAC1 pathway (Wang et al., 2019a). Similarly, artesunate induced ferroptosis, as well as caspase-dependent apoptosis and cell cycle arrest, in adult T-cell leukaemia/lymphoma (ATLL) cells *in vitro* and a mouse xenograft model (Ishikawa et al., 2020). In a panel of DLBCL cell lines and a xenograft mouse model artesunate induced apoptosis, autophagy and ferroptosis through inhibition of STAT3 signalling, an important pro-survival pathway in cancer cells (Chen et al., 2021b). Further investigation of FDA-approved drugs, such as altretamine and artesunate, are warranted given the growing evidence that their effects are at least partially mediated by ferroptosis, and because their safety and pharmacokinetic profiles are already documented.

1.6.3 Ferroptosis in Leukaemia

Acute Lymphoblastic Leukaemia

T-cell acute lymphoblastic leukaemia (T-ALL) cells were shown to undergo ferroptosis following treatment with RSL3 or erastin in combination with the Smac mimetic, BV6, which binds proteins that inhibit apoptosis (Dächert et al., 2016). It has also been shown that lipoxygenases play an important role in ferroptosis in ALL cells, as the lipoxygenase inhibitors, Baicalein, NDGA, Zileuton or PD146176, prevent RSL3-induced cell death (Probst et al., 2017). The sensitivity of ALL cells to ferroptosis may be explained by hypermethylation of *FSP1* and downregulation of FSP1 expression at both the mRNA and protein level, which has been shown in several ALL cell lines and patient samples (Pontel et al., 2022). Furthermore, elevated FSP1 expression was correlated with a significantly worse overall survival in AML patients, but this has not yet been demonstrated in ALL (Pontel et al., 2022). Recent studies have shown that ferroptosis may also be involved in the efficacy of a number of natural plant extracts against ALL cells that are resistant to standard therapeutic agents and cells

from difficult-to-treat T-ALL patients (Mbaveng et al., 2018a, Mbaveng et al., 2018b, Lou et al., 2021, Wu et al., 2023b).

Acute Myeloid Leukaemia

An extensive number of studies have focused on the potential role of ferroptosis in the treatment of acute myeloid leukaemia (AML). These include investigations into the effects of combining erastin with chemotherapy drugs (Yu et al., 2015) or the ferroptotic effects of other agents such as the antimalarial drug dihydroartemisinin (Du et al., 2019, Grignano et al., 2023), a novel all-trans retinoic acid derivative (Du et al., 2020) and the circRNAs circKDM4C, which upregulates ferroptosis (Dong et al., 2021) and circZBTB46 which prevents ferroptosis (Long et al., 2023). Natural derivatives with ferroptosis-inducing potential in AML have also been identified including a pollen flavonoid extract, typhaneoside (Zhu et al., 2019), a monoterpenoid plant extract, perillaldehyde (Catanzaro et al., 2022), and the diterpenoid epoxide plant extract, triptolide, which induces ferroptosis and sensitises AML and chronic myeloid leukaemia (CML) cells to doxorubicin (Wu et al., 2023b). Inhibitors of aldehyde dehydrogenase 3a2 and GPX4 have also been shown to synergise and induce cell death via ferroptosis in AML cells, both in vitro and in vivo (Yusuf et al., 2020).

As discussed earlier, APR-246 induces ferroptosis in DLBCL cells, effects that have also been demonstrated in AML cells, independent of *TP53* mutational status (Hong et al., 2022, Birsen et al., 2021). Through several methods, using various cell death inhibitors and by measuring markers of necroptosis (MLKL phosphorylation) and apoptosis (caspase cleavage), it was determined that APR-246 only induced ferroptosis and not other forms of cell death in AML cells (Birsen et al., 2021). Furthermore, APR-246 synergised with other ferroptosis inducers in vitro and while it was ineffective as a single agent against wild-type AML cells *in vivo*, it effectively reduced tumour burden in mice engrafted with SLC7A11 knockdown AML cells (Birsen et al., 2021). A number of phase II and III clinical trials have investigated APR-246 in combination with azacitidine for patients with AML or myelodysplastic syndromes (MDS) and mutated *TP53* (Phase Ib/II Clinical Trials Identifiers: NCT03072043 & NCT03588078, Phase III Clinical Trials identifier: NCT03745716). While ferroptosis was not specifically investigated in these clinical trials, the drugs were well tolerated and the resulting data suggested APR-246 enhanced the anti-tumour effects of azacytidine (Sallman et al., 2021, Cluzeau et al., 2021, Mishra et al., 2022).

A study by Akiyama *et al*., demonstrated that high expression of the *SLC7A11* or *GPX4* genes is associated with significantly shorter overall survival rates in AML patients (Akiyama et al., 2021). Zhong *et al*., also found that along with other ferroptosis-related genes that were differentially expressed in AML patients, *GPX4* overexpression was associated with poor prognosis in other publicly available cohorts (Zhong et al., 2022).

Overexpression of *GPX4* in AML patients highlights this as a potentially efficacious drug target in this cancer; this is supported by both studies which found that inhibition of GPX4 with ML210 or RSL3 induced death of AML cells *in vitro* (Akiyama et al., 2021, Zhong et al., 2022). This is also supported by other studies, which have shown that higher expression of *SLC7A11*, *GPX4* and *LPCAT3* is associated with a worse prognosis in AML, while overexpression of *TFRC*, which encodes the transferrin receptor, was found to protect cells against ferroptosis (Wei et al., 2020, Wei et al., 2021). In paediatric patients with non-M3 AML, *FTH1* expression was associated with a poor prognosis, and is upregulated during proliferation of AML cell lines (Zhang et al., 2023a). Numerous publications have identified other ferroptosis-related gene signatures, eluding to the relevance of ferroptosis in AML but also indicating that the dataset used and other factors may determine what genes are predictive of both prognosis and ferroptosis-sensitivity in AML (Zhu et al., 2022, Shao et al., 2021, Huang et al., 2022, Zhou and Chen, 2021, Ke et al., 2022, Guo and Zhou, 2022).

Chronic Lymphocytic Leukaemia

Primary chronic lymphocytic leukaemia (CLL) cells have been shown to express low levels of xCT and rely on cysteine produced by bone marrow stromal cells to reduce levels of intracellular ROS (Zhang et al., 2012). The cysteine taken up by CLL cells fuels production of GSH, which protects the cells from the cytotoxic effects of fludarabine and oxaliplatin. Inhibitors of xCT or depletion of GSH significantly increased the sensitivity of CLL cells to both fludarabine and oxaliplatin (Zhang et al., 2012). Although the study by Zhang *et al.* was conducted prior to the description of ferroptosis, the effects of the xCT inhibitor and GSH depletion on cell viability strongly suggest that the cytotoxic effects observed involved ferroptosis. More recently, a study on primary CLL cells and cell lines also showed that treating cells with iron in combination with the Bruton's tyrosine kinase (Btk) inhibitor, ibrutinib, or the BCL-2 inhibitor, venetoclax, led to a significant accumulation of MDA and death of leukemic B-cells, but not their healthy counterpart (Bordini et al., 2022). Although apoptosis is understood to be the predominant mechanism of action of both ibrutinib and venetoclax, ferroptosis may also play an important role and potentiate the efficacy of these drugs. A study of a relatively small cohort of 36 CLL patients identified a ferroptosis-related prognostic score, whereby nine genes were associated with worse overall and treatment-free survival (Pan et al., 2022). Further mechanistic studies are required to understand whether these genes have a ferroptosis-related function in CLL patients in addition to their prognostic value.

Chronic Myeloid Leukaemia

Cysteine depletion in an imatinib-resistant chronic myeloid leukaemia (CML) cell line (K562/G01), but not wild type parental cells (K562) induced ferroptosis through upregulation of the gene encoding thioredoxin reductase 1 (TXNRD1) (Liu et al., 2021b). TXNRD1 is a member of the thioredoxin system, an important

antioxidant and redox regulator (Liu et al., 2021b). Despite the increase in gene expression, the activity of TXNRD1 was decreased which was thought to be as a result of negative feedback regulation (Liu et al., 2021b). These findings led the researchers to investigate the effects of shRNA-mediated knockdown of TXNRD1 in wild type K562 cells. In these knockdown cells, cysteine depletion caused a decrease in viability which could be prevented by Fer-1, as well as increased ROS and MDA levels, and morphological changes consistent with ferroptotic cell death (Liu et al., 2021b). The effect of TXNRD1 knockdown on the sensitivity of CML cells to cysteine depletion suggests the thioredoxin system may play a role in regulating ferroptosis. The drug tetrandrine citrate kills CML cells *in vitro* and reduces tumour growth in an imatinib-resistant mouse xenograft model (Xu et al., 2012); while ferroptosis was not investigated in this study, subsequent findings have shown that tetrandrine citrate does induce ferroptosis in breast cancer cells through GPX4 degradation and upregulation of ferritinophagy (Yin et al., 2022).

1.7 Potential Nanotechnologies for Induction of Ferroptosis

Emerging nanotechnologies have the potential to significantly improve the targeted delivery and pharmacokinetic behaviour of drugs, leading to a reduction in toxicities (Onoue et al., 2014). Drug delivery is an important determinant of efficacy in the treatment of cancer and has been a limiting factor in the development of therapeutic options, including those that target ferroptosis signalling pathways. Large molecules pose many issues in drug delivery, including poor solubility, poor absorption, off target binding and *in vivo* instability. In the context of ferroptosis, primarily *in vitro* studies of erastin and RSL3 have been conducted due to poor solubility and toxicities *in vivo* (Zhao et al., 2020, Jiang et al., 2021). This is because, despite the fact cancer cells are generally more sensitive to ferroptosis, these compounds also have significant effects against healthy tissues. To harness ferroptosis as an approach for cancer therapy, new means of specifically targeting the tumour cells must be developed (Pei et al., 2021). Ferroptosis-inducing nanotechnologies have been investigated in cancers of the breast, colon, lung and for neuroblastoma and hepatocellular carcinoma (Yang et al., 2019, Liang et al., 2021, Liu et al., 2021a, Zhang et al., 2021a, Han et al., 2022, Ji et al., 2022, Wu et al., 2022a, Yu et al., 2022, Zhang et al., 2022a).

1.8 Ferroptosis Nanotechnologies in Haematological Malignancies

While there are a limited number of studies that have examined the potential of nanotechnologies as a means of inducing ferroptosis in haematological malignancies, there are however, numerous studies reporting the efficacy of non-ferroptosis related nanotechnologies in these cancers, suggesting their utility in this area. One example is pegylated liposomal doxorubicin, or DOXIL, which was the first FDA approved nanotherapeutic drug for cancer therapy (Barenholz, 2012). DOXIL outperformed conventional doxorubicin in terms of clinical efficacy, pharmacokinetics, biodistribution, toxicity and overall improvement to patient

quality of life (Barenholz, 2012). While no studies to date have examined ferroptosis-targeting nanotechnologies in MM, other nanotechnologies, such as DOXIL have shown promise in this malignancy, for example, liposomes containing bortezomib (Braham et al., 2018, Deshantri et al., 2020, Federico et al., 2020, Barenholz, 2012).

A number of studies have investigated ferroptosis-inducing nanotherapies in lymphoma. Zhang *et al.* showed variable effects of the erastin analogue, IKE, on the viability of DLBCL cell lines, with IC50s ranging from 1 nM to 100 μM, and that cell death and lipid oxidation following treatment of SU-DHL-6 cells with IKE could be prevented with ferrostatin-1 (Zhang et al., 2019). IKE was then encapsulated in polyethylene glycol-poly (lactic-co-glycolic acid) (PEG-PLGA) nanoparticles and used to treat mice bearing an SU-DHL-6 xenograft (Zhang et al., 2019). Although similar effects of free IKE and IKE-containing nanoparticles were observed on tumour size, only mice treated with free IKE and not IKE nanoparticles showed signs of toxicity, which was evident as a loss in weight. This toxicity was thought to be due to precipitation of the drug in the peritoneal cavity, while IKE nanoparticles appeared to accumulate mainly in the tumour tissue rather than in the plasma (Zhang et al., 2019).

Nanoparticles may also have the capacity to aid in the induction of ferroptosis by mechanisms other than through drug delivery. For example, a recent study demonstrated that high-density lipoprotein (HDL)-like nanoparticles resulted in cell death of cell lines and primary Burkitt's lymphoma B-cells,, DLBCL and T cell–rich B-cell lymphoma through mechanisms consistent with ferroptosis (Rink et al., 2021). These HDL-like nanoparticles were manufactured to specifically target scavenger receptor type B1 (SCARDB1), which regulates cholesterol uptake. As result of their binding to SCARDB1, these nanoparticles were found to induce a compensatory increase in *de novo* cholesterol synthesis, which led to a depletion of GPX4 and initiation of ferroptosis confirmed using C11-BODIPY as a sensor of lipid ROS and the ferroptosis inhibitor, ferrostatin-1 (Rink et al., 2021).

Ferumoxytol is an FDA approved polyglucose sorbitol carboxymethyl ether-coated ION, which is used for iron replacement therapy and has recently been reported to have antitumour activity. Ferumoxytol inhibited cell proliferation of DLBCL cell lines while also inducing a dose dependent reduction in cell viability, that was originally described as apoptosis. Upon further research it was determined that ferumoxytol treatment induced an increase in phospholipid ROS, by LiperFluo staining, suggesting that ferroptosis contributed to the observed cell death (Huang et al., 2023). The mechanism of action of ferumoxytol involves the release of ferrous and ferric iron once the IONs are within macrophages in the liver, spleen and bone marrow, triggering the Fenton reaction and production of ROS (Pai and Garba, 2012). Ferumoxytol treatment in DLBCL mice

models inhibited the growth of tumours by inducing ferroptosis in a dose independent manner, with no significant differences in mice bodyweight between treatments. Electron microscopy analysis of in vivo samples revealed mitochondrial membrane rupture and reduced mitochondrial cristae, suggestive of ferroptosis (Huang et al., 2023). Similar to DLBCL, ferumoxytol induces oxidative stress and cell death in AML cells in vitro (Trujillo-Alonso et al., 2019). While ferumoxytol has only been approved by the FDA for the treatment of patients with chronic kidney disease and anaemia, the results of this study highlight the potential of ferroptosis-inducing IONs as a treatment for haematological malignancies.

Recently, nanoparticles loaded with a drug that targets N6-methyl-adenosine (m6a) RNA methylation were shown to be effective against AML cells both in vitro and in vivo (Cao et al., 2022). These nanoparticles were modified to deplete AML cells of GSH and to target the leukaemic cells by conjugation to a peptide that recognises C-type lectin-like molecule-1 (CLL-1), which is overexpressed on AML blasts and stem cells. Cell death was associated with reduced GPX4 activity and increased levels of lipid peroxidation, suggesting ferroptosis was a key mechanism of action of these nanoparticles (Cao et al., 2022). A similar approach was taken by Yu *et al.,* who found that AML cells had higher GSH levels and GSH/GSSG ratio than normal haematopoietic cells in a mouse model (Yu et al., 2023). They developed a GSH-responsive cysteine polymer-based ferroptosis-inducing nanomedicine (GCFN) and found that the nanomedicine caused GSH depletion through oxidation of GSH through the disulphide group in the cysteine polymer. An increase in MDA, C11-BODIPY staining and the ability of Fer-1 to prevent death and cell proliferation inhibition indicated the involvement of ferroptosis. Furthermore, GCFN specifically targeted the bone marrow and spleen of an AML mouse model where leukemic cells are most abundant, while uptake in wild type mice was mostly localised to the liver. In the bone marrow specifically, 97.6% of the leukaemic stem cells and 84.6% of the AML cells took up fluorescently labelled GCFN while of the haematopoietic stem and progenitor cells (HSPCs) and other immune cell populations, took up less than 15% of the nanomedicine. While this nanomedicine was not specifically generated to target leukaemic cells, it was thought that their proclivity for cysteine uptake was the underlying reason for their cancer-targeting quality (Yu et al., 2023).

1.9 Conclusions

Haematological malignancies affect thousands of people worldwide every year, and despite many therapeutic advances, a significant proportion of patients will relapse with drug refractory disease. Ferroptosis represents a potential approach for treating a range of cancers, particularly those that do not respond to standard chemotherapies, which generally rely on induction of apoptosis. The ever-growing number of studies on ferroptosis since first being described in 2012 have greatly increased our understanding of this mechanism of cell death. However, further work is required to define how ferroptosis is regulated and

determine why there is such variability in sensitivity between different cancers and sometimes even within the same cancer. This is crucial for the development of novel treatment approaches that harness the potential of ferroptosis.

The main factors limiting pre-clinical and clinical trials of ferroptosis-mediated therapies are the poor pharmacokinetics and toxicities associated with bona fide ferroptosis inducers. Nanotechnologies designed to specifically target and precisely deliver drugs to tumour cells may be one approach towards improving specificity and increasing bioavailability. We have discussed many of the studies to date that have described different nanotechnologies that may be applicable in this context, including liposomes, which enable the targeted delivery of relevant lipids and encapsulated ferroptosis-inducing compounds to tumour cells. Combinations of ferroptosis-inducing compounds with current chemotherapies that are predominantly inducers of apoptosis, have also been shown to have potent antitumour effects. This suggests that low doses of ferroptosis-inducing compounds may be effective when used in conjunction with existing chemotherapeutic regimens, possibly reducing toxicities and the development of drug resistance. It is envisaged that with further research, a class of ferroptosis-inducing, anti-cancer nanotherapeutics will find its place alongside other novel cancer drug classes, including monoclonal antibodies, antibody-drug conjugates and CAR-T cells.

1.10 Hypothesis and Aims

The review of the literature highlighted a gap in our understanding of ferroptosis in the context of MM, and the specific mechanisms behind the variable susceptibility of different haematological malignancies to ferroptosis. Many groups have identified key cellular features which might play a role in ferroptosis sensitivity in other cell types, and thus the aim of this project is to determine their relevance in MM. To this end, the following hypothesis was developed together with specific aims designed to enable its testing.

Hypothesis: Multiple myeloma (MM) can be forced to undergo ferroptosis by increasing cellular labile iron or lipid peroxidation.

Aim 1: Investigate the susceptibility of MM and DLBCL cells to ferroptosis **(Chapters 3 & 4)**.

Aim 2: Determine mechanisms that render MM cells sensitive to ferroptosis by investigating key genes, proteins and lipids involved in ferroptosis. **(Chapter 5)**.

Aim 3: Investigate the sensitivity of primary patient myeloma cells to ferroptosis **(Chapter 6)**.

CHAPTER 2. MATERIALS AND METHODS

2.1 Materials

2.1.1 Cell lines

RPMI-8226 (ATC CCL-155) human MM cell line was obtained from the American Type Culture Collection (Manassas, VA). LP-1 (ACC 41) and OPM2 (ACC 50) human MM cell lines were purchased from the Leibniz Institute DSMZ-German Collection of Microorganisms and Cell Cultures GmbH (Braunschweig, Germany). KMS-11 (JCRB1179) human MM cell line was purchased from Cell Bank Australia (Sydney, Australia). NCI-H929 (referred to as H929) were kindly provided by Prof. Andrew Spencer (Monash University, Vic, Australia) and KMS-18 cells kindly provided by Prof. Junia Melo (SA Pathology, Australia). Farage, HBL-1, Riva, SU-DHL-8 and U-2932 DLBCL cells were a kind gift from Dr Giles Best (Flinders University). Hek-293t cells were a kind gift from A/Prof Michael Michael (Flinders University).

2.1.2 Cell culture

All MM and DLBCL cells were cultured in RPMI 1640 (Gibco) supplemented with 10% foetal bovine serum, 50 units/mL penicillin, 0.25 mg/mL streptomycin, 2 mM L-glutamine, and 15 mM Hepes buffer (all Gibco). Hek293t cells were cultured in DMEM (Gibco) supplemented with 10% foetal bovine serum, 50 units/mL penicillin, 0.25 mg/mL streptomycin. All cells were incubated at 37°C in 5% CO_2. Cell lines were routinely tested for mycoplasma using MycoStrip Mycoplasma Detection Kit (InvivoGen, San Diego, CA). Cell line authentication was done by short tandem repeat analysis (Australian Genome Research Facility, Melbourne, Vic).

2.1.3 Drugs and Reagents

Table 2-1: Drugs and reagents used throughout thesis.

Drugs	Company	Cat#	Location	Solvent
3-Methyladenine (3-MA)	Selleck	S2767	Houston, TX	H_2O
Arachidonic acid	Sigma-Aldrich	10931	Burlington, MA	DMSO
Bafilomycin A1 (Baf-A1)	Selleck	S1413	Houston, TX	DMSO
Bortezomib	MedKoo	100100	Morrisville, NC	DMSO
Erastin	AdooQ Bioscience	A13822	Irvine, CA	DMSO
Etoposide	Selleck	S1225	Houston, TX	DMSO
Ferric Ammonium Citrate	MedKoo	592821	Morrisville, NC	H_2O
iFSP1	Selleck	S9663	Houston, TX	DMSO
Lenalidomide	AdooQ Bioscience	A10522	Irvine, CA	DMSO
Liproxstatin-1	Selleck	S7699	Houston, TX	DMSO
Necrostatin 2 racemate (Nec-1s)	Selleck	S8641	Houston, TX	DMSO
OB 24 Hydrochloride	Tocris Bioscience	RD611910	Bristol, UK	DMSO
PR-171/Carfilzomib	AdooQ Bioscience	A11278	Irvine, CA	DMSO
Rapamycin (AY-22989)	Selleck	S1039	Houston, TX	DMSO
Recombinant Human TNF-alpha Protein	R&D Systems	210-TA	Victoria, AU	PBS + 0.1% bovine serum albumin
RSL3	Selleck	S8155	Houston, TX	DMSO
SM-164	New England BioLabs	56003S	Ipswich, MA	DMSO
Vincristine sulphate	Selleck	S1241	Houston, TX	DMSO
Zinc(II) Protoporphyrin IX	Enzo Life Sciences	ALX-430-049	Farmingdale, NY	DMSO
Z-VAD-FMK	Selleck	S7023	Houston, TX	DMSO
Cell culture				
(+)-Sodium L-ascorbate	Sigma-Aldrich	A4034	Burlington, MA	
DMEM, powder, low glucose, pyruvate	Gibco	31600034	Waltham, MA	
FBS QUALIFIED, USA ORIGIN 500ML	Gibco	26140079	Waltham, MA	
Heparin sodium salt from porcine intestinal mucosa	Sigma-Aldrich	H3149	Burlington, MA	
HEPES	Gibco	15630080	Waltham, MA	
L-glutamine	Gibco	25030081	Waltham, MA	
Minimum Essential Medium Eagle, alpha modification	Sigma-Aldrich	M4526	Burlington, MA	
MycoStrip™ - Mycoplasma Detection Kit	InvivoGen	rep-mysnc-50	San Diego, CA	
Penicillin/streptomycin	Gibco	15070063	Waltham, MA	

RPMI 1640 Medium, powder	Gibco	31800022	Waltham, MA
Sodium bicarbonate	Sigma-Aldrich	S5761	Burlington, MA
Sodium pyruvate	Sigma-Aldrich	P5280	Burlington, MA
Trypan blue	Gibco	15250061	Waltham, MA
Tryple Express	Gibco	12604021	Waltham, MA
Western blotting			
Kaleidoscope Prestained Protein Standards	Bio-Rad	1610375	Hercules, CA
4–20% Mini-PROTEAN® TGX Stain-Free™ Protein Gels	Bio-Rad	various sizes	Hercules, CA
Clarity Western ECL Substrate	Bio-Rad	1705061	Hercules, CA
cOmplete EDTA-free Protease Inhibitor Cocktail	Roche	11873580001	Basel, CH
Nitrocellulose Transfer Kit	Bio-Rad	1704270	Hercules, CA
Pierce™ BCA Protein Assay Kit	ThermoFisher	23225	Waltham, MA
Molecular Biology			
1 kb Plus DNA Ladder	New England BioLabs	N3200S	Ipswich, MA
Ampicillin sodium salt	Sigma-Aldrich	A8351	Burlington, MA
Doxorubicin (Adriamycin) HCl 10 mg	Selleck	S1208	Houston, TX
GPX4 (Human) - 3 unique 27mer siRNA duplexes	OriGene	SR320383	Rockville, MD
lentiCRISPR v2-sgFSP1	AddGene	186026	Watertown, MA
lentiCRISPRv2 puro	AddGene	98290	Watertown, MA
Lipofectamine™ 2000 Transfection Reagent	Invitrogen	11668019	Waltham, MA
Lipofectamine™ RNAiMAX Transfection Reagent	Invitrogen	13778150	Waltham, MA
Monarch® Plasmid Miniprep Kit	New England BioLabs	T1010L	Ipswich, MA
Opti-MEM™ Reduced Serum Medium, GlutaMAX™ Supplement	Gibco	51985034	Waltham, MA
Polybrene Transfection Reagent	Sigma-Aldrich	TR-1003	Burlington, MA
Puromycin dihydrochloride from *Streptomyces alboniger*	Sigma-Aldrich	P8833	Burlington, MA
Patient samples			
SepMate™-50	StemCell Technologies	85450	Vancouver, CA
500mL Lymphoprep	StemCell Technologies	7851	Vancouver, CA
Vacutainer Lithium Heparin	BD	367526	Franklin Lakes, NJ
Other			
Cell Proliferation Kit I (MTT)	Roche	11465007001	Basel, CH
RNeasy Mini Kit	Qiagen	74106	Hilden, DE

2.1.4 Antibodies and dyes

Table 2-2: Flow cytometry and Western blotting antibodies and dyes used throughout thesis.

Flow Cytometry

Antibody	Company	Cat#	Final concentration/ Dilution	Location
Alexa Fluor™ 647 Annexin V	BD Biosciences	567356	1:100	San Jose, CA
APC Annexin V	BD Biosciences	550474	1:100	San Jose, CA
APC Mouse Anti-Human CD138	BD Biosciences	347193	3:100	San Jose, CA
BODIPY™ 581/591 C11 (Lipid Peroxidation Sensor)	Invitrogen	D3861	400 nM	Waltham, MA
FITC Annexin V	BD Biosciences	556419	1:100	San Jose, CA
FITC Rabbit Anti- Active Caspase-3	BD Biosciences	559341	1:20	San Jose, CA
Propidium iodide	Sigma-Aldrich	P4170	20 µg/mL	Burlington, MA
V450 Annexin V	BD Biosciences	560506	1:100	San Jose, CA
V450 Mouse Anti-Human CD38	BD Biosciences	646851	3:100	San Jose, CA
Annexin V Binding Buffer, 10X concentrate	BD Biosciences	556454		San Jose, CA
Cytofix/Cytoperm™ Fixation/Permeabilization Kit	BD Biosciences	554714		San Jose, CA

Western blotting

Antibody	Company	Cat#	Dilution	Location
ACSL4 Antibody (A-5) Mouse mAb	Santa Cruz Biotechnology	sc-271800	1:1000	Dallas, TX
AMID/AIFM2/FSP1 Antibody (B-6) Mouse mAb	Santa Cruz Biotechnology	sc-377120	1:1000	Dallas, TX
Anti-Actin Antibody, clone C4	Sigma-Aldrich	MAB1501	1:5000	Burlington, MA
Anti-alpha Tubulin antibody [DM1A] Mouse mAb	Abcam	ab7291	1:5000	Cambridge, United Kingdom
CD71 (D7S5Z) Rabbit mAb	Cell Signaling	13208S	1:1000	Danvers, MA
Ferroportin-1 Antibody (B-4) Mouse mAb	Santa Cruz Biotechnology	sc-518125	1:1000	Dallas, TX
FTH1 (D1D4) Rabbit mAb	Cell Signaling	4393S	1:1000	Danvers, MA
Goat anti-Mouse IgG (H+L) Secondary Antibody, HRP	Invitrogen	31430	1:10000	Waltham, MA
Goat anti-Rabbit IgG (H+L) Secondary Antibody, HRP	Invitrogen	31460	1:10000	Waltham, MA
GPX4 Polyclonal Antibody	Invitrogen	PA5-79321	1:1000	Waltham, MA
GPX4 Rabbit pAb	Cell Signaling	52455S	1:1000	Danvers, MA

HO-1 (E3F4S) Rabbit mAb	Cell Signaling	43966S	1:1000	Danvers, MA
LC3B Rabbit pAb	Cell Signaling	2775S	1:500	Danvers, MA
MLKL (D2I6N) Rabbit mAb	Cell Signaling	14993S	1:1000	Danvers, MA
Pan-Actin (C4) Mouse mAb	Cell Signaling	41185S	1:5000	Danvers, MA
Phospho-MLKL (Ser358) (E7G7P) Rabbit mAb	Cell Signaling	18640S	1:1000	Danvers, MA
RIP3 (E1Z1D) Rabbit mAb	Cell Signaling	13526S	1:1000	Danvers, MA
xCT/SLC7A11 (D2M7A) Rabbit mAb	Cell Signaling	12691S	1:1000	Danvers, MA

2.2 Cell Biology

2.2.1 Cell counts

Trypan blue was mixed 1:1 with cell suspension and 10 µL was pipetted onto a haemocytometer slide. Cells within the four corner 4 x 4 grids were counted and averaged; blue cells were considered dead and unstained cells considered viable. The concentration of cells was determined by the following equation: *n* x *d* x 10,000 = cells/mL where *n* is the number of cells counted and *d* is the dilution factor (i.e. 2).

2.2.2 Measurement of cellular proliferation

Cell Proliferation Kit 1 (MTT) (Roche, Basel, Switzerland) was used to determine cell proliferation as per kit instructions. Approximately 10,000 – 50,000 cells were cultured with or without drugs of interest in a 96-well plate at a final volume of 100 µL per well. Four hours before the final time point, MTT (5 mg/mL stock) was added to each well at a final concentration of 0.5 mg/mL and the plate was returned to a humidified atmosphere (37°C, 5% CO_2). After this 4-hour incubation period, 100 µL of solubilisation buffer (10% sodium dodecyl sulphate in 0.01 M hydrochloric acid (HCl)), was added to each well. The plate was then incubated overnight to allow complete solubilisation of formazan crystals and absorbance was read at 570 nm on the Packard Bioscience Fusion Microplate Reader (PerkinElmer) or CLARIOstar Plus Microplate Reader (BMG Labtech, Ortenberg, Germany). Media-only wells were used to control for background absorbance.

2.3 Molecular Biology

2.3.1 RNA extraction

RNA extraction was undertaken using the RNeasy Mini Kit (QIAGEN, Hilden, Germany). Approximately 1 million cells (>80% viable) were treated under the desired conditions before RNA was extracted following the manufacturer's instructions. For patient samples, cells were sorted into Buffer RLT (QIAGEN) and stored at -80°C before RNA was extracted using the RNeasy Micro Kit (QIAGEN).

2.3.2 RNA sequencing

Diluted RNA was provided to South Australian Genomics Centre (SAGC) who performed all library preparation and RNA sequencing steps. Briefly, stranded polyA libraries from three biological replicates per condition or per cell line (or one replicate per patient) were prepared according to the Nugen Universal Plus mRNA-seq kit protocol M01442 v2. Cell line sequencing was performed on the DNBSEQ-6400 (MGI, Shenzhen, China) and patient sequencing was performed on the NovaSeq X (Illumina, San Diego, CA). Reads were mapped against the human reference genome (hg38) using STAR spliced alignment algorithm (Dobin et al., 2013).

Differential gene expression analysis was performed by SAGC using the DESeq2 program (Love et al., 2014) in R statistical program (v.4.2; https://www.R-project.org/). Briefly, the Wald test p-values from the genes that passed independent filtering were adjusted for multiple testing using the Benjamini-Hochberg test. An adjusted p-value of < 0.05 was considered statistically significant. DESeq2 reports a log2FoldChange for the differential expression of each gene and the associated Standard Error for the log2FoldChange estimate (lfcSE). We acknowledge our use of the gene set enrichment analysis (GSEA) software, and Molecular Signature Database (MSigDB) (Subramanian et al., 2005) (http://www.broad.mit.edu/gsea/).

2.3.3 Expanding bacterial colonies for plasmid extraction

LentiCRISPRv2 puro was a gift from Brett Stringer (Addgene plasmid # 98290; http://n2t.net/addgene:98290; RRID:Addgene_98290) (Stringer et al., 2019). LentiCRISPR v2-sgFSP1 was a gift from Boyi Gan (Addgene plasmid # 186026 ; http://n2t.net/addgene:186026 ; RRID:Addgene_186026) (Mao et al., 2021). Bacterial stabs (NEB stable competent *E. coli*) were streaked onto agar plates with 100 µg/mL ampicillin. Single colonies were grown up in lysogeny broth (LB) with 100 µg/mL ampicillin to a density of no higher than 15 in terms of optical density (OD). Plasmid DNA was extracted using the Monarch Plasmid Miniprep Kit (New England Biolabs) as per manufacturer's instructions. Restriction enzyme NdeI was used to confirm identity of plasmids. A Nanodrop 8000 Spectrophotometer (Thermo Scientific, Waltham, MA) was used to determine plasmid concentration and purity.

2.3.5 Plasmid cloning

Primers 5'-TAGAATTCTCGACTTCTTAACCCAACAGAAGGCTCGAGAAGGTATATTGCTGTTGACAG TGAGCG-3' and 5'-TCTCGAATTCTAGCCCCTTGAAGTCCGAGGCAGTAGGC-3' and the below 97-mer oligonucleotide templates were used to PCR amplify the mir30/shRNA target sequences (Fellmann et al., 2013) (Table 2-3).

Table 2-3: shRNA sequences

shRNA name	97-mer oligonucleotide (5'-3')
Ren713	TGCTGTTGACAGTGAGCGCAGGAATTATAATGCTTATCTATAGTGAAGCCACAGATGTATAGATA AGCATTATAATTCCTATGCCTACTGCCTCGGA
GPX4(1)	TGCTGTTGACAGTGAGCGATGGGAATAAACAGACAAATTATAGTGAAGCCACAGATGTATAATTT GTCTGTTTATTCCCACTGCCTACTGCCTCGGA
GPX4(2)	TGCTGTTGACAGTGAGCGCGTGGATGAAGATCCAACCCAATAGTGAAGCCACAGATGTATTGGGT TGGATCTTCATCCACTTGCCTACTGCCTCGGA
FSP1(1)	TGCTGTTGACAGTGAGCGACACCGACTATGTTACAGTGTATAGTGAAGCCACAGATGTATACACTGTAACAT AGTCGGTGGTGCCTACTGCCTCGGA
FSP1(2)	TGCTGTTGACAGTGAGCGAACCGACTATGTTACAGTGTATTAGTGAAGCCACAGATGTAATACAC TGTAACATAGTCGGTGTGCCTACTGCCTCGGA
HMOX1(1)	TGCTGTTGACAGTGAGCGACACCAAGTTCAAGCAGCTCTATAGTGAAGCCACAGATGTATAGAGC TGCTTGAACTTGGTGGTGCCTACTGCCTCGGA
HMOX1(2)	TGCTGTTGACAGTGAGCGCTGGTCTAACTTTTGTGTGAAATAGTGAAGCCACAGATGTATTTCACA CAAAAGTTAGACCAATGCCTACTGCCTCGGA

PCR products were digested with EcoRI and cloned into pTRIPZ(PL) to produce shRNA constructs (Powell et al., 2017). Sequencing was used to verify integrity and orientation of the respective shRNA vectors.

2.4 Gene editing

2.4.1 Small interfering RNA transfection

Small interfering RNA (siRNA) targeting the gene of interest, as well as a scramble siRNA control were purchased from Origene. Transfection was performed on cells (1 million cells/mL) plated in poly-l-ornithine-coated 6- or 12-well plates. siRNA-lipid complexes were formed by combining 7 µL Lipofectamine RNAiMAX (Invitrogen), 50 µL of each 606 nM siRNA (three siRNA against gene of interest) or 50 µL 606 nM scramble siRNA, and Opti-MEM reduced serum medium (Gibco) to reach a final volume of 507 µL. The siRNA-lipid complex solution was incubated at room temperature for 20 minutes. 2.5 mL of cells in culture media without penicillin/streptomycin were combined with 500 µL of siRNA-lipid complex so that the final concentration of each siRNA was 10 nM. After 24 and 48 hours, cells in suspension were collected and combined with trypsinised cells from the surface of the well. Approximately 400,000 cells were used to perform viability and oxidised lipids analyses by flow cytometry as described in Section 2.6. The remaining cells were lysed, and protein expression analysed by Western blot as described above.

2.4.2 Lentiviral transduction

Plasmid DNA, pVSVG (lentiviral envelope plasmid) and psPAX2 (lentiviral packaging plasmid) (lentiviral plasmids kindly provided by Professor Stuart Pitson) were added in a 1:1:1 molar ratio to OptiMEM media and mixed well. An equal volume of 4% Lipofectamine 2000 in OptiMEM media was added to the diluted DNA for a final volume of 1.5 mL with 30 µg total DNA for a T75 flask, or 0.5 mL with 10 µg total DNA for a T25 flask. The DNA-lipid complex was gently pipetted up and down to mix and incubated at room temperature, in the dark for 20 minutes. The DNA-lipid complex mix was then added dropwise to Hek293T cells at 80% confluency in 10 mL fresh DMEM with 10% FBS (no antibiotics). Cells were cultured at 37°C, 5% CO_2 for 5-16 hours, at which point the media was removed and replaced with RPMI 1640 (plus additives as per MM cell line culture conditions). After a total of 48-hours, lentivirus was harvested from the media of transfected Hek293T cells and centrifuged at 500 x g for 5 minutes. The viral supernatant was filtered through a 0.45 µm membrane and used to resuspend cell pellets to reach a cell density of 200,000 cells/mL. OPM2 and KMS-11 MM cell lines were cultured in viral supernatant containing polybrene (10 µg/mL for OPM2, 4 µg/mL for KMS-11) for 16 hours before removing polybrene. After three complete media changes, cells were cultured in 1 µg/mL puromycin for resistance selection. For doxycycline-inducible systems, cells were treated with 0.5 µg/mL doxycycline and RFP-positive cells were isolated by fluorescence-activated cell sorting (FACS) using the FACSAria Flow Cytometer (Becton Dickinson). For CRISPR KOs without a fluorescent tag, cells were

identified based on their FSC/SSC characteristics, and a single cell was sorted into each well of a 96-well plate. Transduced clones were selected for using 1 µg/mL puromycin and knockout confirmed by Western blot.

2.5 Western blotting

Approximately 3 to 5 million cells were cultured with drugs of interest for the times and at the doses indicated in the relevant figures, washed twice in cold PBS and then pellets resuspended in lysis buffer (10 mM Tris/HCl (pH 7.4), 137 mM NaCl containing 10% glycerol, 1% NP40 with the following reagents added fresh: 10 mM β-glycerophosphate, 2 mM sodium fluoride and cOmplete EDTA-free protease inhibitor cocktail). Cells were lysed in this buffer for 10 minutes on ice before centrifugation at 14,000 x g to clarify the lysate. Pierce BCA Protein Assay Kit (Thermo Scientific) was used as per the manufacturer's protocol to measure protein concentration. Samples were diluted in running buffer (50 mM Tris/HCl (pH 8.0), 5 mM EDTA, 100 mM DTT), 5% SDS, 50% glycerol and 0.1% bromophenol blue) and boiled at 100°C for 5 minutes before equal amounts of protein were loaded onto a Mini-PROTEAN TGX Precast Gel (Bio-Rad). The Trans-Blot Turbo Transfer System was used to transfer protein onto a nitrocellulose membrane (Bio-Rad). Total protein was imaged on a ChemiDoc MP system (Bio-Rad) using a Stain Free Blot protocol. Membranes were then blocked in 5% non-fat dairy milk powder in tris-buffered saline with Tween-20 (TBS-T) buffer (50 mM Tris (pH 7.4), 154 mM NaCl and 1% Tween20) at room temperature for a minimum of two hours or overnight at 4°C. Total protein or β-actin were primarily used as loading controls for densitometric analyses. To avoid unnecessary stripping of blots which may cause a reduction in signal, α-tubulin was used if there was an overlap in molecular weight between the protein of interest and actin (i.e. FSP1). Primary and secondary antibodies were diluted in 5% milk in TBS-T as per dilutions in Table 2-2. Membranes were imaged on the ChemiDoc MP after incubation in Clarity Western ECL Substrate (Bio-Rad). Image Lab Software (Bio-Rad) was used for densitometric analysis of Western blot images.

2.6 Flow cytometry

2.6.1 Cell viability

Approximately 300,000 cells/mL were cultured with or without drugs of interest for up to 72 hours. Cell suspensions were washed in 1X phosphate buffered saline (PBS) and cell pellets stained with 1 µL FITC Annexin-V, 2 µL 20 µg/mL propidium iodide (PI) in 97 µL 1X Annexin V Binding Buffer for 10 minutes in the dark at room temperature. Data was acquired from a minimum of 10,000, intact, single cells per sample on a CytoFLEX S flow cytometer (Beckman Coulter, Brea, CA). Data analysis was performed using CytExpert Software (Beckman Coulter). Dual Annexin-V FITC and PI negative cells were considered viable.

2.6.2 Analysis of oxidised lipid levels

Oxidised lipids were quantified using the BODIPY 581/591 C11 (C11-BODIPY) lipid peroxidation sensor (Invitrogen). Approximately 300,000 cells/mL were seeded in cell culture plates with or without drugs of interest for up to 72 hours. Following treatment, C11-BODIPY was added to the wells at a final concentration of 400 nM. After a 20-minute incubation at 37°C, cells were washed twice in 1X PBS. Lipid ROS generation was determined by measuring fluorescence due to oxidised C11-BODIPY, with excitation at 488nM and emission of 525nm. Data from a minimum of 10,000 intact, single cells was acquired per sample using a CytoFlex S (Beckman Coulter) flow cytometer.

2.6.3 Analysis of cleaved caspase-3 protein

Approximately 300,000 cells/mL were cultured with or without drugs of interest for up to 72 hours in cell culture plates. Cells were then harvested, washed in cold 1X PBS and resuspended in Cytofix/Cytoperm Fixation and Permeabilization Solution (Becton Dickinson) for 20 minutes at 4°C. Cells were then washed twice in Perm/Wash Buffer (Becton Dickinson) before 5 µL FITC anti-cleaved caspase-3 antibody (Table 2-2) was added. Cells were incubated at room temperature in the dark for 30 mins, followed by a final wash in Perm/Wash Buffer. The proportion of cleaved caspase-3-positive cells was determined by measuring FITC fluorescence (excitation at 488nM and emission of 525nm). Data from a minimum of 10,000 intact, single cells was acquired per sample using a CytoFlex S (Beckman Coulter) flow cytometer.

2.8 Patient samples

2.8.1 Patient recruitment and consent

Patients who were suspected of having MM and who underwent a bone marrow biopsy for diagnostic purposes at Flinders Medical Centre were provided with information concerning participation in the study. Ethical approval for the study was provided from the Southern Adelaide Local Health Network (SAHLN) human research ethics committee (approval number 2023_HRE00059). Excess bone marrow aspirate from those patients who provided informed consent was collected in lithium heparin tubes (Becton Dickinson) and processed within 24 hours of collection, according to the protocol described below. Only samples from patients with newly-diagnosed MM according to the International Myeloma Working Group criteria were used for this study. Clinical information from the patients used in this study are provided in Table 2-4.

Table 2-4: Patient clinical characteristics

Sex n (%)	
Males	5 (50)
Females	5 (50)
Age (years)	
Mean ± SD	73.0 ± 8.2
Median	75.6
Range	58-83

2.8.2 Sample collection – mononuclear cells

After collection, all patient samples were assigned a unique code, which did not contain any identifiable information. A 250μL aliquot of whole marrow aspirate was removed to establish primary stromal layers, as described below. The residual bone marrow aspirate was then diluted 1:2 with sterile PBS and layered onto 15 mL Lymphoprep (StemCell Technologies) in a 50 mL SepMate™ Isolation Tube (StemCell Technologies) and processed according to the manufacturer's protocol. The samples were centrifuged at 1,200 x g for 10 minutes. The top layer, containing Lymphoprep, mononuclear cells (MNCs) and serum, was poured off into another tube and washed in sterile PBS followed by centrifugation at 500 x g for 5 minutes. The cell pellet was then resuspended in a 50:50 solution (1:1 ratio of RPMI media and FBS). A 5 μL aliquot of cells were diluted 1:10 in PBS and viability was measured by trypan blue exclusion on a haemocytometer. Additionally, a 1:10 dilution of cells in PBS were added in a 1:1 ratio to white cell fluid (crystal violet and acetic acid) to lyse any red blood cells (RBCs) present and enable an accurate count of the mononuclear cells only. Dimethyl sulfoxide (DMSO) was then added to the MNCs in 50:50 solution, to make a final DMSO content of 10%. The cells were then pipetted into labelled cryovials and frozen to -80C in controlled rate freezing containers. After at least 18 hours, the vials were transferred to liquid nitrogen tanks for long term storage.

2.8.3 Sample collection – establishing stromal cell layers

Whole bone marrow aspirate (250 μL) was added to a T25 flask containing 5 mL of minimum essential medium eagle, alpha modification (α-MEM; Sigma-Aldrich), supplemented with 250 μM sodium ascorbate, 1 mM sodium pyruvate, 10 mM HEPES, 10% FBS, 50 units/mL penicillin, 0.25 mg/mL streptomycin, 2 mM L-glutamine and 10 μg/mL heparin. The flasks were then placed in an incubator for up to 7 days without media changes to allow for cell adhesion. Following this, the media was replaced every 3-4 days until the adherent cells reached approximately 70-80% confluence, at which point the cells were harvested using Tryple Express (Gibco) and placed into T75 flasks with 10ml of complete medium. The cells were then maintained by feeding every 3-4 days and passaging as necessary in T75 flasks until required for experiments.

2.9 Other

2.9.1 Trace metal inductively coupled plasma mass spectrometry (ICP-MS)

Inductively coupled plasma mass spectrometry (ICP-MS) was performed by our collaborators in the Biometals Facility at The Florey Institute of Neuroscience and Mental Health (Melbourne, Australia). Briefly, cell pellets ($1x10^6$ cells) were lysed, lyophilised, digested and resuspended in nitric acid as per a recently published method (Pyun et al., 2022). ICP-MS was performed on an Agilent 7700 instrument (Agilent Technologies) under routine multi-element operating conditions using a Helium Reaction Gas Cell. The final concentration of metals was normalised to total protein (measured using BCA assay) as per the following equations:

$$\mu mol/L\ element = \frac{raw\ ppb\ value\ x\ final\ sample\ volume}{molecular\ weight\ of\ the\ element}$$

Where ppb = parts per billion and the final sample volume was 0.5 mL

$$\frac{\mu mol/L\ element}{mg/mL\ protein} = \mu mol\ element\ /\ gram\ protein$$

Some elements were excluded from the analysis as per the below criteria:

- Samples with ppb readings below the empty tube reading (sample result not a true reading)
- Samples with ppb readings below the elements respective detection limit (DL) on the day of the run (below detection limit, data is extrapolated)
- Samples with ppb readings above the 500 ppb range (beyond detection limit, data is extrapolated)
- Sample results with RSD above 5% excluded (result is not reproducible)
- Elements whose calibration (5-500ppb) had a relative standard deviation (RSD) above 5% (known range is unstable)

Table 2-5: Details pertaining to reliability and stability of ICP-MS results

	Sample ppb less than empty tube (n (%))	Sample ppb below respective DL (n (%))	Sample ppb above 500 ppb DL (n (%))	Sample reading with RSD above 5%	Element calibration (5-500ppb) had RSD above 5% (n (%))
Sodium	0 (0)	0 (0)	33 (100)	0 (0)	2 (40)
Magnesium	0 (0)	0 (0)	31 (94)	0 (0)	0 (0)
Aluminium	30 (91)	0 (0)	0 (0)	22 (67)	0 (0)
Phosphorus	0 (0)	0 (0)	33 (100)	0 (0)	3 (60)
Potassium	0 (0)	0 (0)	33 (100)	0 (0)	2 (40)
Calcium	0 (0)	0 (0)	27 (82)	19 (58)	5 (100)
Chromium	0 (0)	0 (0)	0 (0)	26 (79)	0 (0)
Manganese	0 (0)	0 (0)	0 (0)	3 (9)*	0 (0)
Iron	0 (0)	0 (0)	0 (0)	0 (0)	0 (0)
Cobalt	6 (18)	0 (0)	0 (0)	31 (94)	0 (0)
Nickel	0 (0)	0 (0)	0 (0)	32 (97)	0 (0)
Copper	0 (0)	0 (0)	0 (0)	1 (3)*	0 (0)

Zinc	0 (0)	0 (0)	0 (0)	1 (3)*	0 (0)
Selenium	0 (0)	16 (48)	0 (0)	33 (100)	0 (0)
Rubidium	0 (0)	0 (0)	0 (0)	0 (0)	0 (0)

* Low percentage of samples met exclusion criteria, so this element was used for downstream analyses. ppb, parts per billion; DL, detection limit; RSD, relative standard deviation.

2.9.2 Lipid peroxidation assay (Melbourne)

The cell-free lipid peroxidation assay was performed by our collaborators at The Florey Institute of Neuroscience and Mental Health. Cell pellets ($4x10^6$ cells) were resuspended in Tris-buffered saline (TBS), sonicated and snap frozen at -80°C. Before assaying, samples were sonicated and 10 µM iron was added for 30 minutes at room temperature. Lipid peroxidation was measured using the Lipid Peroxidation Malondialdehyde (MDA) Assay Kit (Abcam) according to the manufacturer's protocol. The final concentration of MDA was normalised to total protein (measured using BCA assay).

2.9.3 Lipidomic analysis (LC-MS)

Cell suspensions were washed in PBS and stored at -80°C before processing. Sample processing and analysis by liquid chromatography/mass spectrometry (LC-MS) was performed by Ali Habib at the Lipidomics and Metabolomics core facility at the South Australian Health and Medical Research Institute (SAHMRI). Briefly, 100 µL fresh extraction buffer (acetonitrile/isopropanol/splash mix (99:99:2, v/v)) was added and samples were sonicated for 10 minutes before being incubated at –20°C for one hour. Samples were centrifuged at 16,000 x g for 15 minutes and the supernatant transferred to a glass vial. Samples were run on a XEVO G2-XS QTOF liquid chromatography/mass spectrometer (Waters Corporation, Milford, MA) according to a lipidomics assay protocol established at SAHMRI (White et al., 2022). Sample data was processed and analysed using Skyline Targeted Mass Spec Environment (Pino et al., 2020) and MetaboAnalyst (Wishart Research Group, Alberta, Canada).

2.10 Statistical Analysis

GraphPad Prism was used statistical analyses; comparisons between two groups were performed using t-tests, and comparisons between three or more groups were performed using two-way analysis of variance (ANOVA). Following ANOVA, multiple comparisons tests were performed; Tukey test was used when correction for multiple comparisons was necessary, and Fisher's least significant test was used when multiple comparisons did not need to be corrected for. Synergistic effects of drug combinations were determined using the fractional product method (Webb, 1963) with a value of < -0.1 indicating synergy and > 0.1 indicating an antagonist effect.

CHAPTER 3. INVESTIGATING FERROPTOSIS IN MULTIPLE MYELOMA (MM) CELLS

3.1 Introduction

The overall aims of this project were formed based on the findings of Yang *et al.* who previously showed that MM cells are more resistant to ferroptosis compared to another B-cell malignancy, diffuse large B-cell lymphoma (DLBCL) (Yang et al., 2014). Specifically, the xCT inhibitor, erastin, was shown to have significantly greater inhibitory effects on the growth of DLBCL cells compared to MM cells (Yang et al., 2014). Class 1 ferroptosis inducers, such as erastin, sulfasalazine and buthionine sulfoximine (BSO), directly inhibit xCT, reducing cellular GSH levels, thus reducing the activity of the selenoprotein GPX4 (Yu et al., 2017). Erastin was first described to selectively kill oncogenic RAS cells, resulting in a nonapoptotic form of cell death (Dolma et al., 2003). Later studies suggested the mechanism of action of erastin involved mitochondrial voltage-dependent anion channels (VDACs) as well xCT (Yagoda et al., 2007, Dixon et al., 2012). After only 2 hours of xCT inhibition by erastin, NRAS-mutant HT-1080 fibrosarcoma cells displayed an increase in total and lipid reactive oxygen species (ROS) before cell death was observed after 6 hours of treatment (Dixon et al., 2012). Exogenous iron amplified this cell death while the iron chelator deferoxamine (DFO) prevented it, supporting the important role iron plays in ferroptosis (Dixon et al., 2012). A number of agents commonly used to inhibit apoptosis, necrosis or autophagy-mediated cell death do not consistently prevent the cell death induced by erastin and other compounds that deplete GSH, further supporting the idea that ferroptosis represents a distinctive mode of cell death (Dixon et al., 2012, Beatty et al., 2021, Yang and Stockwell, 2008).

Erastin treatment was shown to be the most effective means of inhibiting xCT in mouse embryonic fibroblast (MEF) cells that overexpressed the protein (Sato et al., 2018). However, erastin does not represent a viable means of inducing ferroptosis *in vivo* due to its pharmacokinetic profile and poor solubility (Zhang et al., 2019). Despite this, xCT inhibition by other means, including by drugs such as sorafenib (Feng and Stockwell, 2018), may have potential as pro-ferroptotic agents in cancer and should be investigated further for *in vivo* use.

Yang *et al.* found that in seven DLBCL cell lines (DoHH-2, LY-19, WSY DLCL-2, LY-3, SU-DHL-7, SU-DHL-8 and SU-DHL-9), erastin had half-maximal inhibitory effects on growth (EC_{50}) at concentrations less than 1 μM, whereas in the five MM cell lines tested (EJM, KMS-11, LP-1, RPMI-8226 and SKM1) the EC_{50} values were greater than 10 μM (Yang et al., 2014). In some cell types, erastin has also been shown to have little to no effect, while direct inhibition of GPX4 by RSL3 can induce ferroptosis in these cells (Dixon et al., 2012). This is because not all cells express xCT and increases in the intracellular pool of cysteine can be due to mechanisms other than system Xc^-. It is thought that the sensitivity of DLBCL cells to xCT inhibition is due to their inability to use the transsulfuration pathway to generate cysteine from methionine (Zhang et al., 2019).

They are therefore reliant on xCT to import cystine, which is subsequently reduced to cysteine to fuel GSH production. In an xCT-inhibited state, DLBCL cells that cannot use the transsulfuration pathway would not be able to produce *de novo* GSH. As GSH is a crucial GPX4 co-factor, this would presumably result in reduced activity of this important ferroptosis-related protein. For MM cells which can produce cysteine from methionine, the transsulfuration pathway would be able to compensate for decreased levels of GSH when xCT is inhibited. This is consistent with a study that showed that MM cell sensitivity to erastin-induced ferroptosis correlates with the expression of xCT (Zhang et al., 2024b). It was found that erastin reduced the proliferation of MM cells that had significantly higher levels of xCT at both the gene and protein level (U266 and IM-9) compared to MM cells with lower expression of xCT (MM.1S and LP-1); in the latter cell lines erastin was ineffective at any dose tested for up to 72 hours (Zhang et al., 2024b). Furthermore, in a MM xenograft model, overexpression of xCT enhanced the effects of erastin on tumour volume. The ferroptosis-related effects of targeting xCT in MM cell lines that expressed relatively high levels of the protein were confirmed by siRNA mediated knockdown of xCT, which led to malondialdehyde (MDA) and ROS accumulation, that was preventable with FDO and Fer-1. Additionally, the study showed that neither apoptosis nor cell cycle arrest were triggered by xCT knockdown (Zhang et al., 2024b).

A more direct approach of inducing ferroptosis is by targeting GPX4 directly using small molecule inhibitors such as RSL3 (Yang et al., 2014). RSL3 was first described as a ferroptosis inducer in 2008 that caused a similar phenotype to erastin but was not VDAC- or GSH-dependent (Yang and Stockwell, 2008). RSL3 and another compound called ML162, are examples of class 2 ferroptosis inducers, which are defined as compounds that directly inhibit GPX4 (Feng and Stockwell, 2018, Yu et al., 2017). Both RSL3 and ML162 covalently bind and inhibit the GPX4 protein (Moosmayer et al., 2021). At high concentrations (in a micromolar range) the effects of RSL3 cannot be reversed by ferrostatin-1, suggestive of non-ferroptosis mediated off-target effects (Eaton et al., 2020). These off-target effects likely involve ER stress, as several proteins associated with ER stress (phospho-PERK, ATF4 and SESN2) were upregulated in head and neck cancer cells following RSL3 exposure (Shin et al., 2018). The effects of RSL3 have also been shown to be independent of changes in GSH levels, but instead lead to a depletion of GPX4 protein (Kagan et al., 2017). Although the effects of erastin on MM and DLBCL cells have been studied, there is no data comparing the effects of direct GPX4 inhibition in these cells. Therefore, the aims of this chapter were to investigate the sensitivity of MM and DLBCL lines to the GPX4 inhibitor, RSL3.

In an effort to investigate mechanisms that may be associated with differences in ferroptosis sensitivity, the levels of metals and other elements, as well as the expression of ferroptosis-related proteins, were also examined in this chapter. As discussed previously, iron is a vital element involved in the oxidation of lipids

during ferroptosis. Selenium is another element of relevance to ferroptosis as GPX4 is one of the 25 selenoproteins identified in humans – the other known selenoproteins all belong to either the GPX, thioredoxin reductases or selenoprotein P families (Weaver and Skouta, 2022). A selenoprotein is defined as a protein that contains the amino acid selenocysteine (Sec), which differs from cysteine as selenium is incorporated in the place of sulphur. Selenium is an essential amino acid and has been linked to mammalian development and immune function, with selenium deficiencies resulting in a number of pathophysiological conditions in humans (Labunskyy et al., 2014). Of the eight GPX paralogues, five contain a Sec residue (GPX1-4 and GPX6) in their active site where catalytic redox reactions occur (Labunskyy et al., 2014). These five Sec-containing GPX proteins use GSH, thioredoxin or other thiol oxidoreductases to reduce soluble, small hydrogen peroxides to water (Labunskyy et al., 2014). For example, GPX1 scavenges H_2O_2 which plays a role in redox signalling (Lei et al., 2023). Because GPX4 lacks the loop structure present in the active site of other GPXs and contains positively charged residues, it has specificity for larger, complex phospholipid hydroperoxides; it is due to this specificity that GPX4 is particularly important in maintaining membrane integrity and ferroptosis (Labunskyy et al., 2014, Weaver and Skouta, 2022). GPX4 is ubiquitously expressed, and it was previously thought that its expression was not regulated by dietary selenium (Labunskyy et al., 2014). However, more recent studies have shown that exogenous selenium supplementation can influence the expression of GPX4 mRNA, protein and/or activity in a number of cell types, including primary cortical neurons, MEFs, triple negative breast cancer cells and human umbilical vein endothelial cells (Alim et al., 2019, Ingold et al., 2018, Vande Voorde et al., 2019, Sneddon et al., 2003).

3.2 Results

3.2.1 Multiple myeloma cells are generally less sensitive to cell death induced by GPX4-inhibition compared to diffuse large B-cell lymphoma cells

Initially, we demonstrated that erastin was ineffective against MM and DLBCL cell lines at concentrations up to 10 µM (Figure 3-1A). However, following treatment with 50 µM erastin, less than 50% of the Farage and HBL-1 DLBCL cells and RPMI-8226 and LP-1 MM cells were viable. Interestingly, though it has been published that 10 µM erastin resulted in a complete growth inhibition of SU-DHL-8 DLBCL cells (Yang et al., 2014), we found that 94% remained viable, compared to untreated cells (Figure 3-1A).

Next, expression of xCT was investigated by Western blotting in the MM and DLBCL cell lines (Figure 3-1B). After probing for xCT, two bands were observed: one at approximately 37 kDa, and another just above 25 kDa. When the higher molecular weight band, which is closer to the published molecular weight of 35 kDa, is considered, the DLBCL cell lines appeared to express more xCT than MM, with the exception of the Riva cell line (Figure 3-1B). Using publicly available data, levels of the xCT transcript, SLC7A11 were also found to vary between the cell lines (HBL-1 data not available) (The Human Protein Atlas, 2023j).

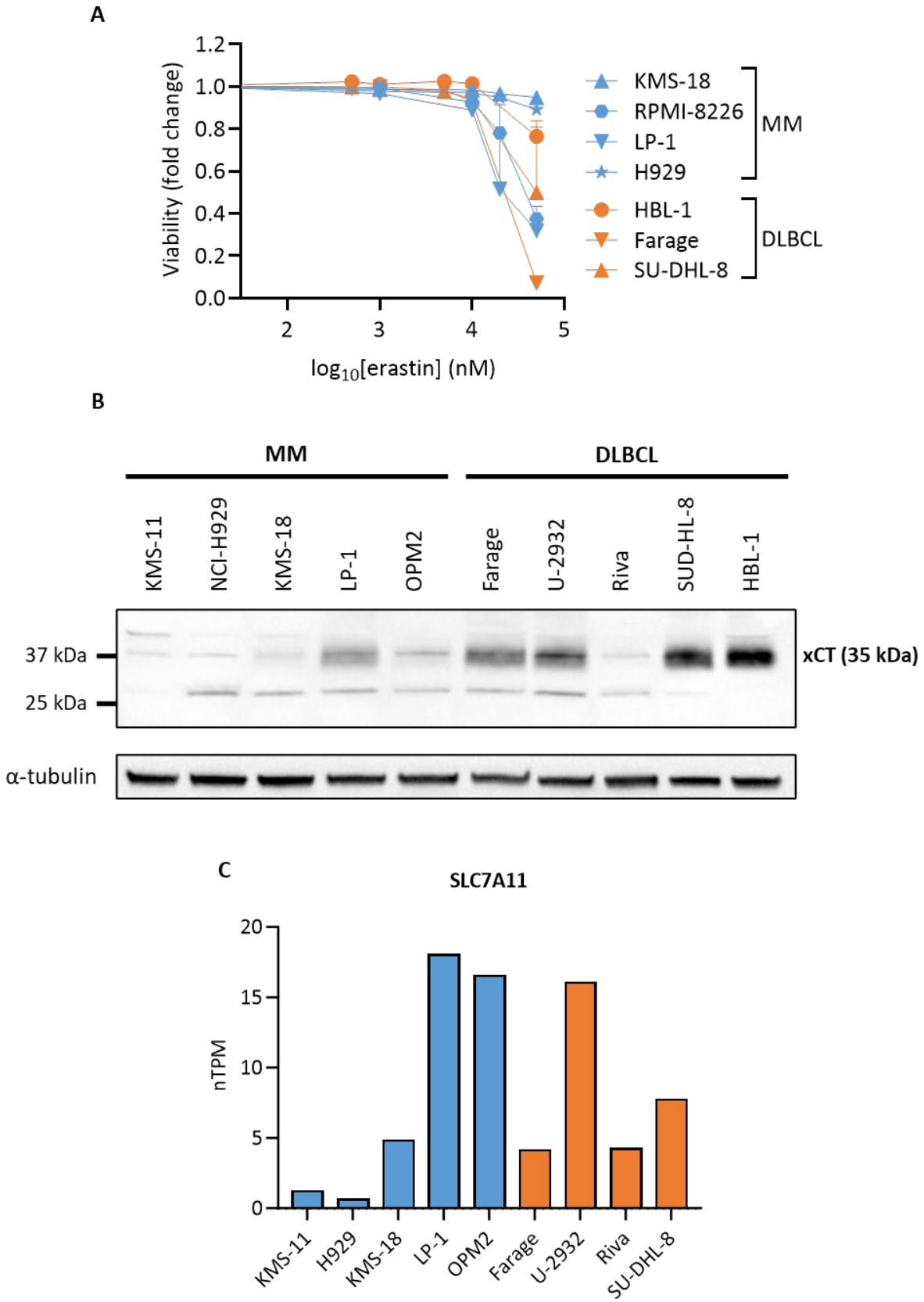

Figure 3-1: **Erastin has minimal efficacy against MM or DLBCL cell lines.**

(A) Cell lines were treated with the indicated concentrations of erastin and cell viability measured after 24 hours using Annexin V/PI and flow cytometry. Data are the mean ± standard deviation from at least two independent experiments (RPMI-8226 and H929 one independent experiment). (B) Western blot for untreated MM and DLBCL cells was probed for xCT, using α-tubulin as a loading control. (C) Normalised transcript expression (nTPM) of MM and DLBCL cell lines, taken from The Human Protein Atlas (The Human Protein Atlas, 2023j).

It was found that four out of five MM cell lines were less sensitive to RSL3-induced cell death compared to five DLBCL cell lines (Figure 3-2). The exception was the OPM2 MM cell line, which was remarkably sensitive to RSL3, with cells reaching less than 1% viable at concentrations as low as 100 nM. After 24 hours, all DLBCL cell lines had an IC_{50} for cell viability less than 560 nM RSL3, whereas most MM cell lines (excluding OPM2) had an IC_{50} well above 2.5 µM RSL3. KMS-11 MM cells were the least sensitive with an IC_{50} of 6.3 µM RSL3 (Table 3-1). Performing an ordinary one-way ANOVA with a Tukey's multiple comparisons test showed there was no statistically significant difference between the IC_{50}s of KMS-11 and H929, KMS-18 and LP-1 or any sensitive cell line (OPM2 and all DLBCL cell lines). All other comparisons had a p-value of less than 0.0001.

Table 3-1: Absolute RSL3 IC_{50} values for MM and DLBCL cell lines from Figure 3-2.

Mean IC_{50} ± standard deviation was generated by fitting a sigmoidal four parameter logistic (4PL) curve for each biological replicate from Figure 3-2 (constraints used were bottom = 0, top = 1).

	Cell line (n)	Average IC_{50} (nM)	Standard Deviation (nM)
MM	KMS-11 (7)	6251	823.1
	H929 (3)	6104	2026
	KMS-18 (5)	3845	369.8
	LP-1 (7)	2697	721.2
	OPM2 (6)	74.34	11.17
DLBCL	Farage (10)	517.9	272.9
	U-2932 (4)	557.2	202.0
	Riva (3)	259.7	67.01
	SU-DHL-8 (6)	251.7	64.10
	HBL-1 (6)	184.8	41.56

RSL3 also caused an increase in lipid oxidation, quantified using the C11-BODIPY lipid peroxidation sensor which shifts from red to green fluorescence upon oxidation (Figure 3-2B). However, despite the vast difference in RSL3 efficacy between the relatively resistant MM and sensitive DLBCL cell lines, the lipid oxidation at 24 hours was comparable in all cell lines with the exception of OPM2 MM cells. As expected, RSL3 caused the greatest increase in lipid oxidation in the low nanomolar range for the most sensitive cell line, OPM2. Lipid oxidation induced by RSL3 preceded cell death, with some lipid oxidation measured as early as 4 hours post RSL3 treatment (Supplementary Figure 3-A). It should be noted that lipid oxidation could only be measured in viable cells due to loss of fluorescence as the cells die and become permeable.

As well as an increase in lipid ROS, the mechanism of cell death of RSL3 was confirmed to involve ferroptosis with the use of the lipophilic antioxidant liproxstatin-1 (Lip-1). Lip-1 prevents the accumulation of oxidised lipids, as observed in Figure 3-2D. As expected, the ability of Lip-1 to prevent lipid oxidation resulted in reduced RSL3 toxicity. At RSL3 concentrations up to 7.5 µM, Lip-1 was able to partially prevent cell death in most of the cell lines, except KMS-11 (Figure 3-2C).

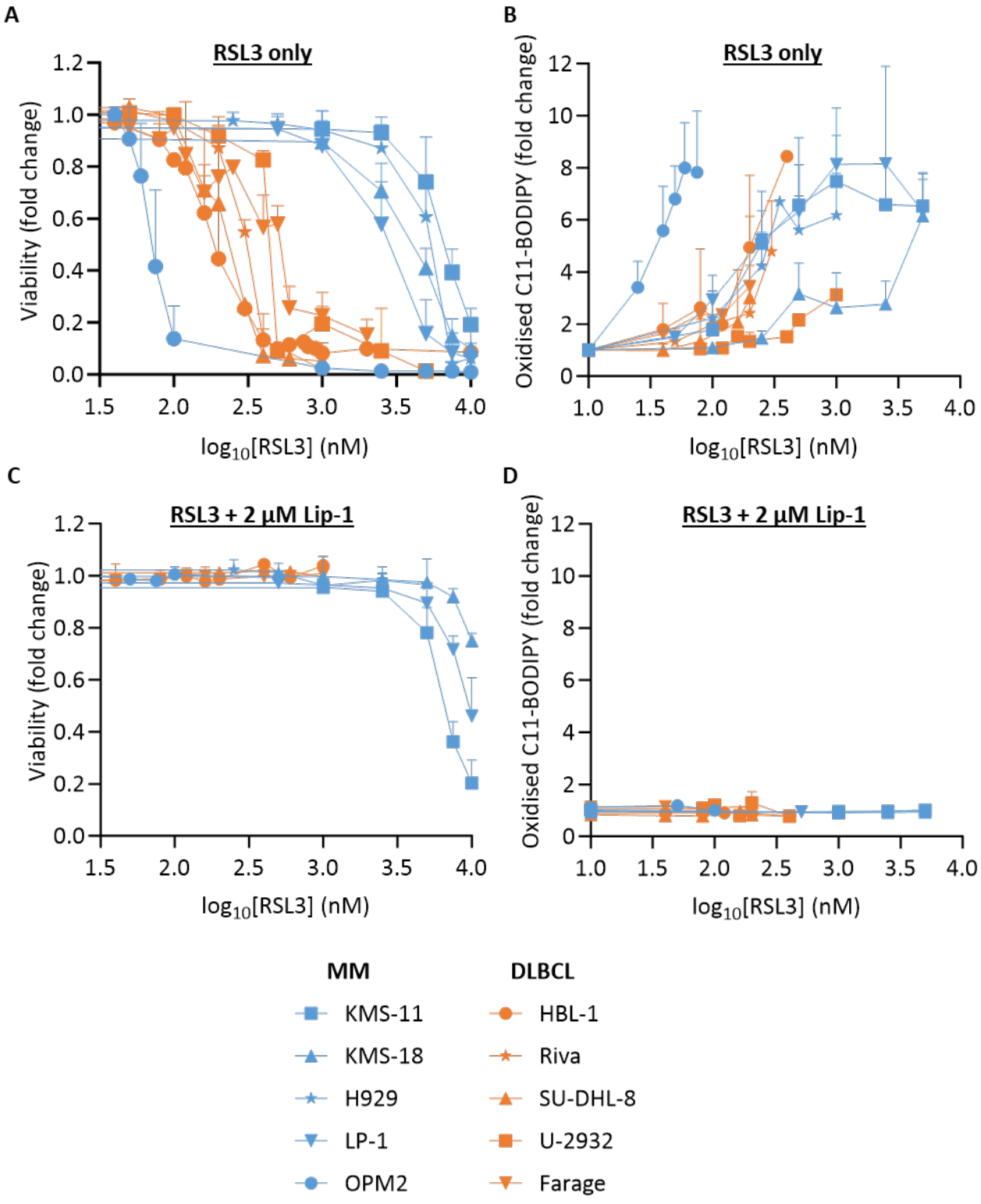

Figure 3-2: DLBCL cells are more sensitive to RSL3-induced cell death compared to most MM cells.

Cell lines were treated with the indicated concentrations of RSL3 for 24 hours and cell viability (A) and the levels of oxidised C11-BODIPY (B) were measured by flow cytometry. Cell lines were treated with the indicated concentrations of RSL3 and 2 µM liproxstatin-1 (Lip-1) for 24 hours and cell viability (C) and the levels of oxidised C11-BODIPY (D) were measured by flow cytometry. Data are the mean (fold change relative to untreated control) ± standard deviation from three or more independent experiments.

3.2.2 OPM2 MM cells are sensitive to RSL3-induced ferroptosis

OPM2 cells were highly sensitive to RSL3 with an IC_{50} of 74.3 ± 11.2 nM and less than 1% viable cells remaining after a 24-hour incubation with 100 nM (Figure 3-3A). Conversely, KMS-11 cells were consistently the least sensitive to RSL3, with an IC_{50} of 6.25 ± 0.82 µM RSL3 for over 12 accumulated biological replicates (Figure 3-3B). While KMS-11 cell death induced by RSL3 could not be prevented by Lip-1, all concentrations induced an increase in lipid ROS which was inhibited by Lip-1 (Figure 3-3D). This suggests that the cell death induced by RSL3 in KMS-11 cells results in lipid ROS but the ability of RSL3 to induce death is not dependent on this. Furthermore, the maximum 8-fold increase in lipid ROS in OPM2 cells was observed at 60 nM RSL3, whereas the maximal increase in lipid ROS in KMS-11 of 5.9-fold was induced by 2.5 µM RSL3 (Figure 3-3C,D). Moreover, MTT assays indicated that some degree of proliferation was evident in KMS-11 cells following treatment with all concentrations of RSL3 tested, as indicated by reduction of MTT to MTT formazan after 24 hours of treatment (Figure 3-3E).

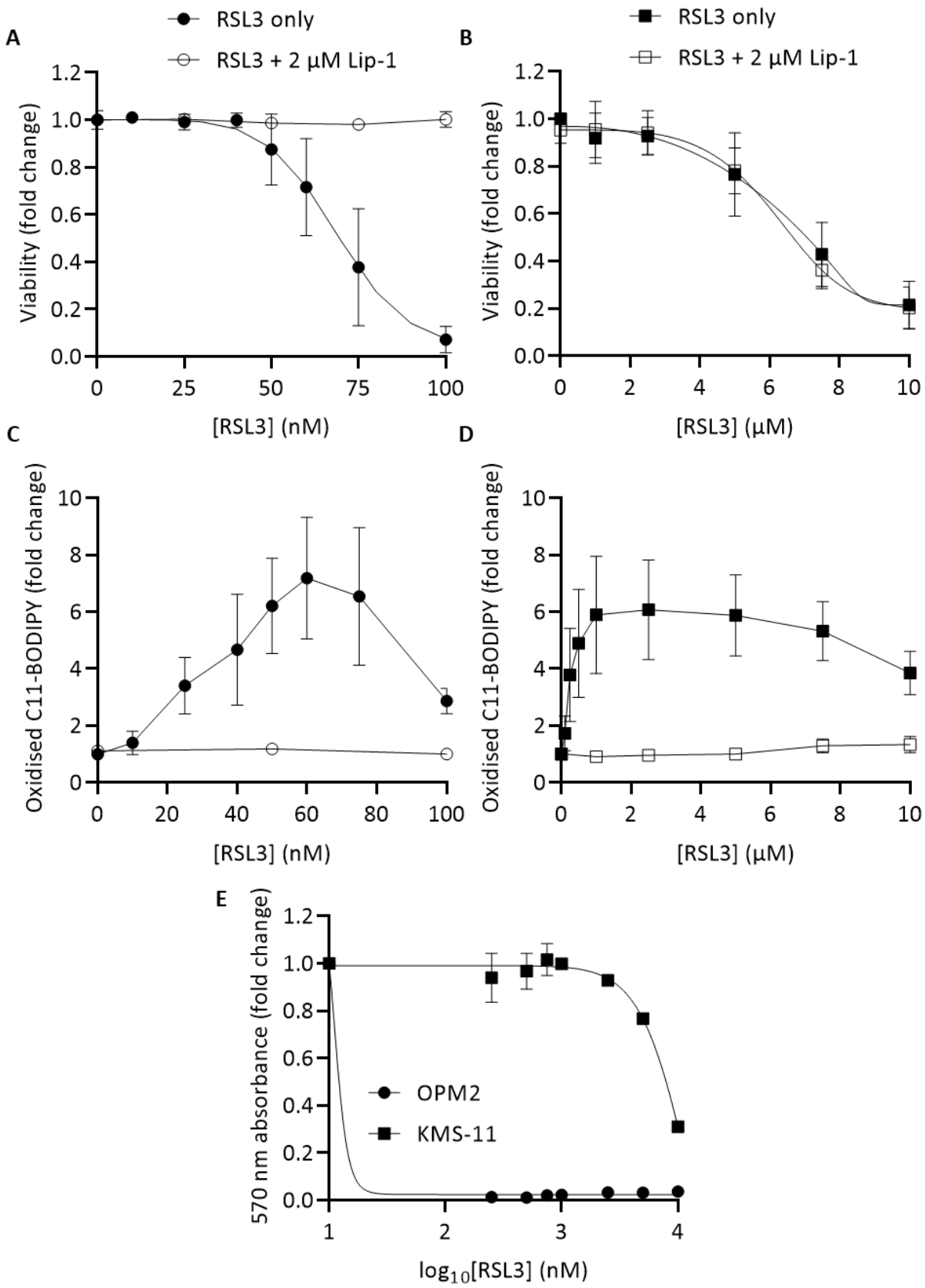

Figure 3-3: OPM2 MM cells are more sensitive to RSL3 compared to KMS-11.

OPM2 (A,C) and KMS-11 (B,D) cells were treated with the indicated concentrations of RSL3 for 24 hours and cell viability (A,B), lipid ROS (C,D) were measured by flow cytometry. Data are the mean ± standard deviation from three or more independent experiments. (E) OPM2 and KMS-11 cells were treated with the indicated concentrations of RSL3 for 24 hours and cellular proliferation was measured by MTT assay. Data are the mean ± standard deviation from two technical replicates.

3.2.3 Genetic inhibition of GPX4 does not decrease the viability of MM cells

To demonstrate that the effects of RSL3 were dependent on its target, GPX4, we aimed to knockdown GPX4 expression in MM cells. Firstly, a transient knockdown using three siRNAs against GPX4 was utilised. Previous attempts at transfecting MM cells in our lab have proven unsuccessful and unfortunately, we were again unable to transfect the MM cell lines to decrease GPX4 protein levels using siRNA. A relatively small reduction in expression was observed when the tissue culture plates were coated with poly-l-ornithine to enable adhesion of the cells, but the reduction in GPX4 protein was deemed to be insufficient for further experimentation. Furthermore, using a constitutive knockdown of GPX4 expression may unintentionally select for cells which are able to survive without GPX4. This may be particularly relevant in the RSL3 sensitive OPM2 cells, in which it is expected that full GPX4 knockout may be toxic and represents a selection pressure that enables RSL3 resistant cells to dominate. In this context, cells may need to be cultured in the presence of Lip-1 to prevent ferroptosis. In any case, GPX4 knockdown was not achieved even in the RSL3 resistant KMS-11 cells that can withstand GPX4 inhibition.

We therefore moved to a doxycycline-inducible shRNA knockdown approach. Three transduced cell lines were developed; a Renilla luciferase 713 negative control line (targets the Renilla luciferase gene that is absent in mammalian cells), and two GPX4 shRNA knockdown cells (GPX4-1 & GPX4-2) for KMS-11 and OPM2 cells. Each plasmid contained a tetracycline response element which, upon doxycycline treatment, results in expression of red fluorescence protein (RFP) and the target shRNA. Following transfection, cells were treated with doxycycline for 48 hours and the RFP-positive cells were isolated by FACS. A relatively small decrease in GPX4 expression was observed in the GPX4-1 and GPX4-2 cells after transfection, compared to the >90% reduction in expression observed for both plasmids in both cell lines after doxycycline treatment and cell sorting (Figure 3-4A).

Unfortunately, the strong fluorescent signal from RFP in the doxycycline-treated transfected cells, and spill over into the 525nm channel on the flow cytometer meant it was not possible to use the C11-BODIPY dye to measure lipid oxidation, or annexin-V FITC and propidium iodide to measure cell viability. Instead, a colorimetric MTT assay was used to determine cellular proliferation, and it was found that there was no significant difference between control cells and GPX4 knockdown cells. Interestingly, despite decreased expression of GPX4, there was no difference in the response to RSL3 in the GPX4 knockdown cells compared to control cells (Figure 3-4B). This data is from one biological replicate and should be repeated by flow cytometry to confirm, using a different viability stain that is not affected by the strong RFP signal. Our findings are consistent with a recent study showing that GPX4 knockdown had no effect on the viability of a colorectal adenocarcinoma cell line (DLD1), despite these cells being sensitive to RSL3 (DeAngelo et al., 2024). However,

DeAngelo *et al.* also showed that GPX4 knockdown using a doxycycline-inducible approach caused a 10-fold increase in the sensitivity of the cells to RSL3, which we were unable to demonstrate.

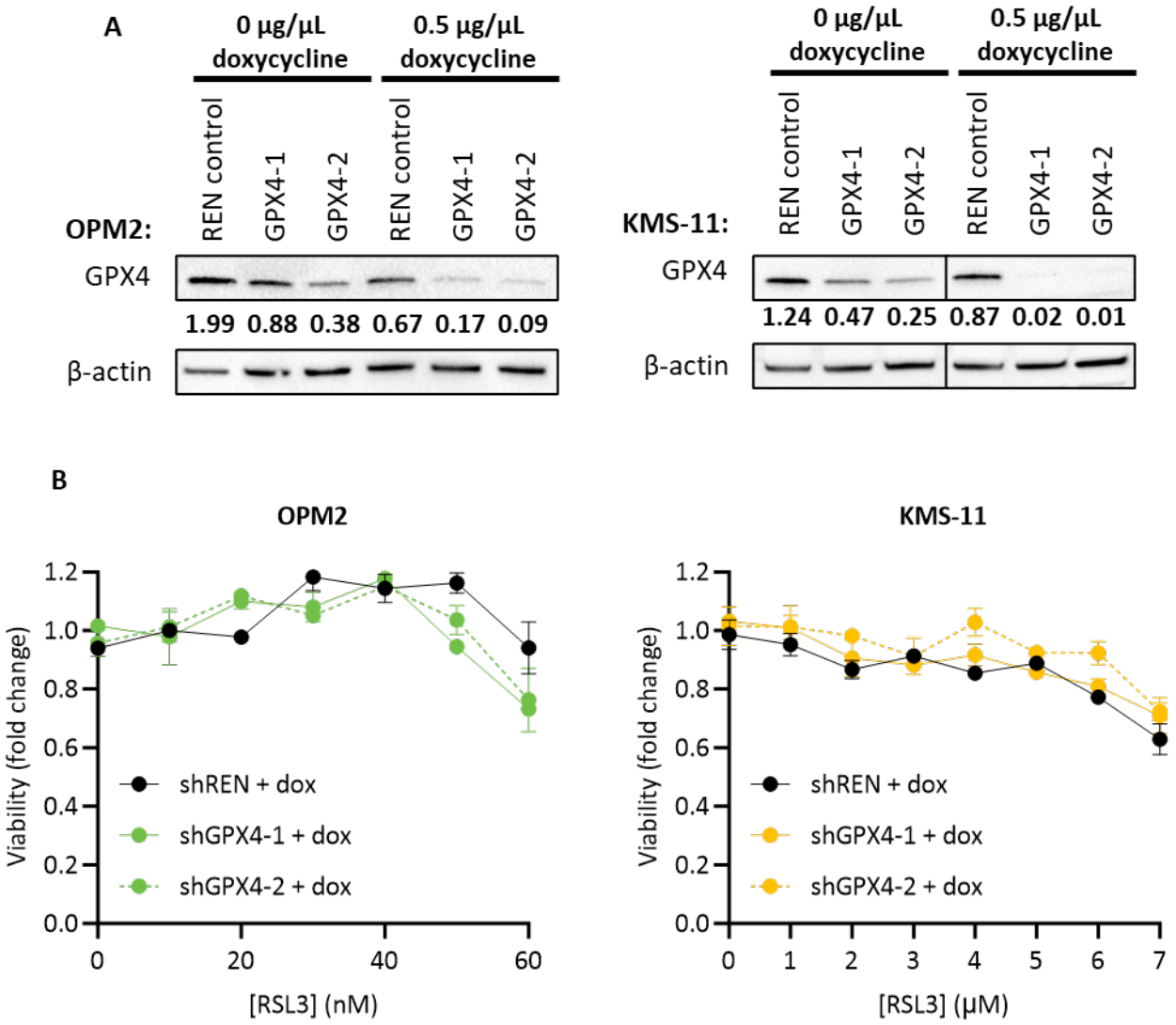

Figure 3-4: shRNA-mediated knockdown of GPX4 reduces GPX4 protein expression in KMS-11 and OPM2 cells without affecting RSL3 sensitivity.

(A) Transduced OPM2 and KMS-11 cells were treated with 0.5 µg/mL doxycycline for 48 hours and RFP-positive cells isolated by fluorescence-activated cell sorting (FACS). RFP-positive cells were cultured for at least one week before being treated again with 0.5 µg/mL doxycycline. After 48 hours, protein was extracted and GPX4 protein expression measured by Western blot. Densitometric values of GPX4 relative to β-actin are displayed under the GPX4 blots from one independent experiment. (B) Cell viability of OPM2 and KMS-11 shREN control, shGPX4-1 and shGPX4-2 cell lines were measured by flow cytometry after 48 hours of treatment with doxycycline. Data are relative to untreated controls (no RSL3 or doxycycline) of each cell line, presented as the mean ± standard deviation of two technical replicates.

3.2.4 GPX4 inhibition does not induce apoptosis in MM cells

Ferroptosis has been shown to be distinct, both biochemically and morphologically, from other forms of cell death including apoptosis, autophagy and necroptosis (Yang et al., 2014). To confirm RSL3 induces ferroptosis in MM cells, vincristine was used as an apoptosis-inducer to compare with RSL3-induced cell death. Vincristine works by inhibiting the formation of spindle fibres during mitosis, thus the cytotoxic effects of the drug require the cells to be dividing and are observed at different time points depending on the rate of cell proliferation (Kothari et al., 2016). As the doubling time varies between the different MM cell lines, different treatment times were used for the following experiments.

After trialling incubation times from 24 to 48 hours, it was found that 50 nM vincristine induced approximately 64% cell death in LP-1 cells after 38 hours, and this death could be partially prevented by the pan-caspase inhibitor, Z-VAD-FMK (Figure 3-5A). Conversely, 5 µM RSL3 caused complete cell death after 38 hours and only Lip-1, but not Z-VAD-FMK, could prevent RSL3 toxicity (Figure 3-5A).

Although vincristine was effective at killing KMS-11 and KMS-18 cells, Z-VAD-FMK was unable to completely block cell death (Supplementary Figure 3-B). This suggested that vincristine may induce caspase-independent cell death in these MM cell lines. For this reason, the proteasome inhibitor, bortezomib, which is commonly used in the clinic to treat MM patients, was used as an apoptosis-inducing agent to compare apoptosis and ferroptosis in KMS-18, KMS-11 and OPM2 cells. The viability of KMS-18 cells was decreased to 34.9% after a 28-hour incubation with 20 nM bortezomib, which could be partially prevented by pre-incubation with Z-VAD-FMK (Figure 3-5A). Bortezomib also induced caspase-dependent cell death in KMS-11 cells, whereas Lip-1 had no effect on the cytotoxicity induced by this drug (Figure 3-5A). In KMS-11, 5 µM RSL3 caused a 43% reduction in cell viability, which was reduced to a 20% drop in the presence of Lip-1, while Z-VAD-FMK had no effect. However, 10 µM RSL3 was more toxic against KMS-11 cells, and whilst Lip-1 had no effect on cell viability at this concentration of RSL3, Z-VAD-FMK could partially prevent cell death (Figure 3-5A).

Next, we examined the morphological changes observed in response to either RSL3 or bortezomib. Distinct morphological changes were observed in KMS-18 cells treated with both drugs. As early as 2 hours after RSL3 treatment was initiated, KMS-18 MM cells were morphologically different from control cells (Figure 3-5B). This difference was more evident at 24 hours with RSL3-treated cells displaying a swollen cytoplasm, consistent with the ferroptosis-associated “ballooning” morphology reported in the literature (Dodson et al., 2019). Conversely, cells treated with bortezomib became smaller, with irregular plasma membranes after 24-hours compared to control cells, which is more characteristic of apoptosis (Figure 3-5B).

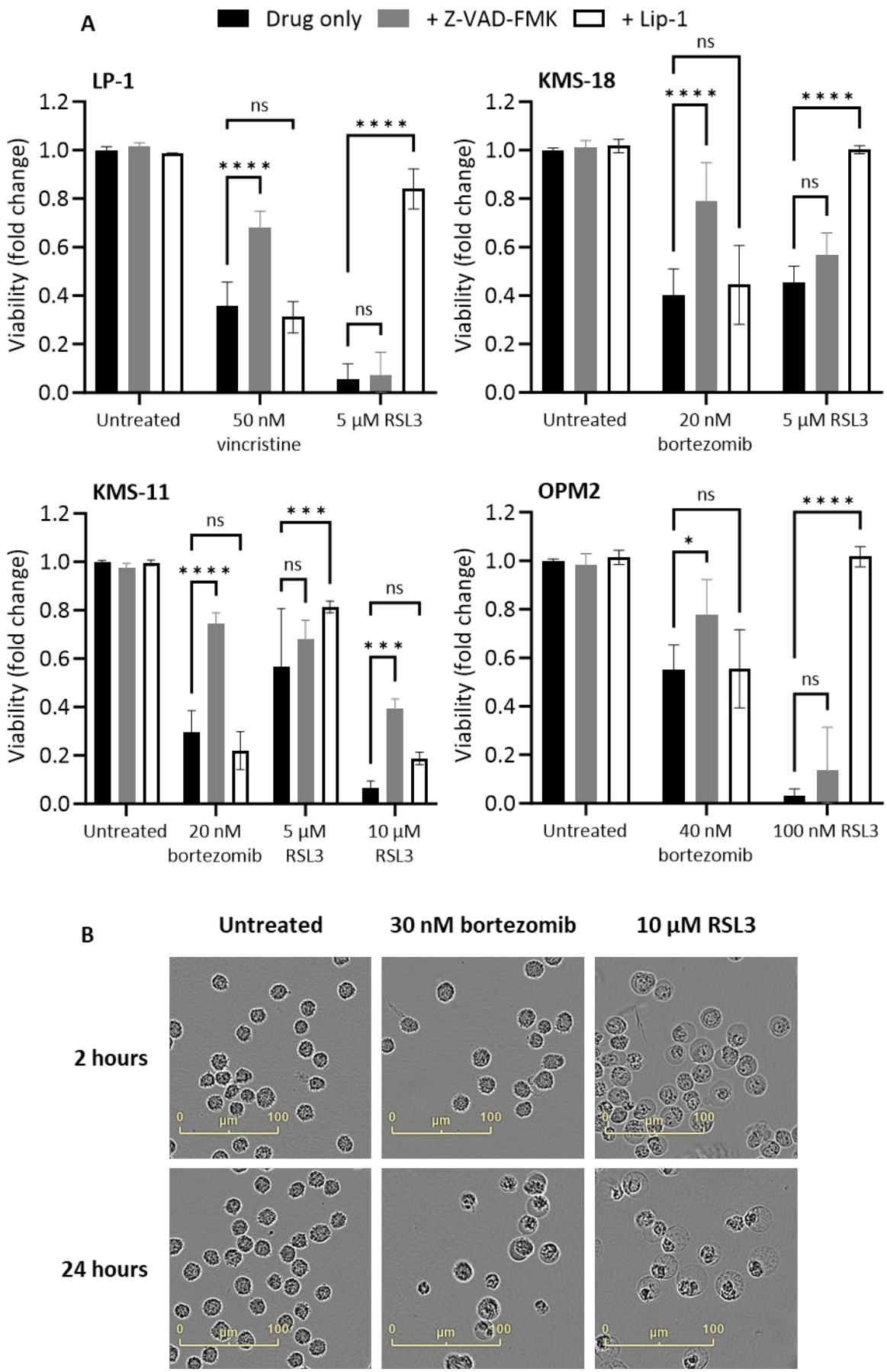

Figure 3-5: Cell death induced by RSL3 is preventable with liproxstatin-1, but not Z-VAD-FMK.

LP-1 cells were treated with the indicated concentrations of vincristine or RSL3 for 38 hours. KMS-18, KMS-11 and OPM2 cells were treated with the indicated concentrations of bortezomib or RSL3 for 28 hours. For cell death inhibition, cells were preincubated in Z-VAD-FMK for 45 minutes (LP-1: 100 µM, KMS-18, KMS-11 and OPM2: 200 µM) whereas 2 µM liproxstatin-1 (Lip-1) was added at the same time as vincristine/bortezomib/RSL3. (A) Cell viability was measured by flow cytometry. Data are the mean ± standard deviation from three independent experiments. Statistical analyses were performed by two-way ANOVA with a Tukey's multiple comparisons test; ns indicates no significant difference, * $p<0.05$, ** $p<0.01$, *** $p<0.001$, **** $p<0.0001$. (B) KMS-18 cells were treated with bortezomib or RSL3 with images acquired over 24 hours using an Incucyte Live Cell Imager.

Unlike ferroptosis, apoptosis is predominantly dependent on activation of caspases, so next we assessed the levels of cleaved caspase-3 following drug treatment. Vincristine treatment resulted in a marked increase in caspase-3 cleavage in LP-1 cells, with approximately 74% of cells positive for cleaved caspase-3, which correlated with the percentage of dead cells in this sample (Figure 3-6). As expected, given that pan-caspase inhibition prevented vincristine-induced cell death, Z-VAD-FMK effectively prevented cleavage and therefore activation of caspase-3. The proportion of KMS-18, KMS-11 and OPM2 cells that were positive for cleaved caspase-3 following bortezomib treatment correlated with the percentage of dead cells in these treatment samples (Figure 3-5A, Figure 3-6). Conversely, only 14.5% of KMS-18 cells following treatment with 5 µM RSL3 had active caspase-3, which was not significantly different from untreated. In OPM2 cells, a smaller concentration of 75 nM RSL3 was used to prevent excessive cell death (IC_{50} of RSL3 in OPM2 was 74.3 nM) and 22.7% of cells had active caspase-3 which was not significantly different from control. Conversely, in LP-1 and KMS-11 cells, 21.5% and 37.1% of cells, respectively, had active caspase-3 following treatment with 5 µM RSL3, which was significantly different from untreated controls ($p = 0.0032$ and <0.0001, respectively). Moreover, a similar proportion of active caspase-3 in KMS-11 cells was observed following treatment with either 10 µM RSL3 or 20 nM bortezomib ($p = 0.9169$) (Figure 3-6). Despite these findings that RSL3 can induce caspase-3 cleavage in some MM cells lines, Z-VAD-FMK did not prevent RSL3-induced death (at concentrations below 10 µM RSL3), indicating that the activity of RSL3 is not reliant on caspase-3 activation.

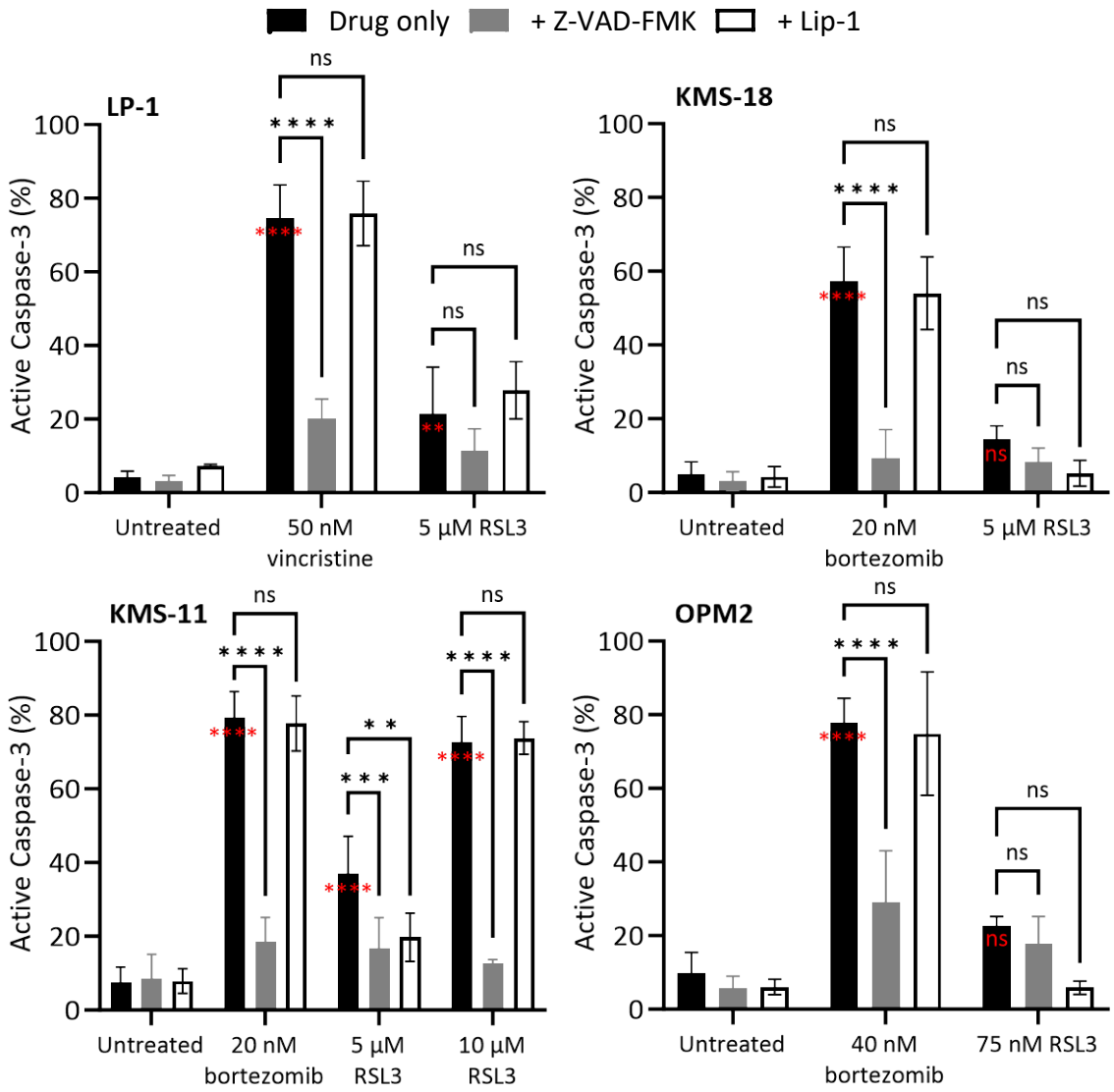

Figure 3-6: RSL3 can induce caspase-3 cleavage at high doses in MM cells, which is preventable with Z-VAD-FMK.

LP-1 cells were treated with the indicated concentrations of vincristine or RSL3 for 38 hours. KMS-18, KMS-11 and OPM2 cells were treated with the indicated concentrations of bortezomib or RSL3 for 28 hours. Cells were preincubated with Z-VAD-FMK for 45 minutes (100 µM LP-1, 200 µM KMS-18, KMS-11 and OPM2) whereas 2 µM liproxstatin-1 (Lip-1) was added at the same time as vincristine/bortezomib/RSL3. Caspase-3 cleavage was measured by flow cytometry. Data are the mean ± standard deviation from three independent experiments. Statistical analyses were performed by two-way ANOVA with a Tukey's multiple comparisons test; ns indicates no significant difference, * p<0.05, ** p<0.01, *** p<0.001, **** p<0.0001. Statistics values in red are comparisons with untreated controls.

Further support for the hypothesis that RSL3 induces ferroptosis in LP-1 cells, we observed an approximate 14-fold increase in lipid oxidation in cells treated with 1 µM RSL3, compared to a 5-fold increase following vincristine treatment (Figure 3-7). The increase in lipid oxidation levels after vincristine treatment was unexpected but is likely a consequence of cell death rather than a driver of cell death because although Lip-1 prevented lipid ROS formation, it was not able to prevent vincristine-induced death (Figure 3-5A). Bortezomib did not induce a statistically significant increase in lipid oxidation in KMS-18, KMS-11 or OPM2 cells (Figure 3-7). Conversely, RSL3 induced a marked increase in both cell death and lipid oxidation accumulation in all three cell lines which was effectively prevented by Lip-1 (Figure 3-7). In KMS-11 cells, 5 µM RSL3 caused a 5.4-fold increase in lipid oxidation, whereas 10 µM RSL3 only induced an average 3.2-fold increase; this is may be attributable to either insufficient data being acquired for 10 µM RSL3-treated cells due to a small number of viable cells available for analysis, or due to inefficient retention of the dye in dead or dying cells.

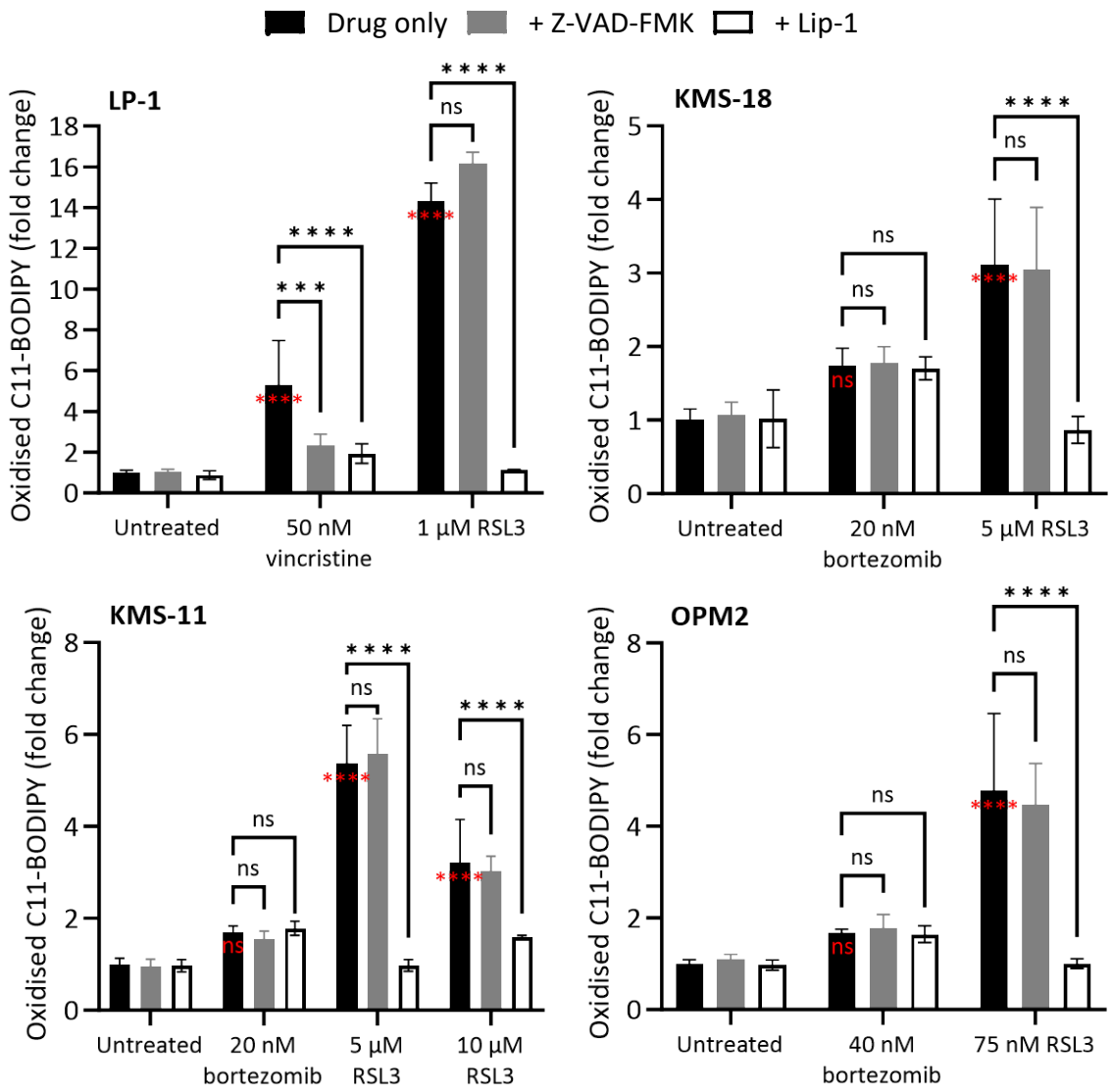

Figure 3-7: RSL3, but not bortezomib induces a marked increase in oxidised lipids in MM cells.

LP-1 cells were treated with the indicated concentrations of vincristine or RSL3 for 38 hours. KMS-18, KMS-11 and OPM2 cells were treated with the indicated concentrations of bortezomib or RSL3 for 28 hours. For cell death inhibition, cells were preincubated with Z-VAD-FMK for 45 minutes (100 µM LP-1, 200 µM KMS-18, KMS-11 and OPM2) whereas 2 µM liproxstatin-1 (Lip-1) was added at the same time as vincristine/bortezomib/RSL3. Oxidised C11-BODIPY was used to measure oxidised lipid levels by flow cytometry. Data are the mean ± standard deviation from three independent experiments. Statistical analyses were performed by two-way ANOVA with a Tukey's multiple comparisons test; ns indicates no significant difference, * p<0.05, ** p<0.01, *** p<0.001, **** p<0.0001. Statistics values in red are comparisons with untreated controls.

3.2.5 GPX4 inhibition does not induce necroptosis in MM cells

The possibility that another form of cell death, known as necroptosis, was involved in the effects of RSL3 against MM cells was investigated using the receptor-interacting serine/threonine-protein kinase 1 (RIPK1) inhibitor necrostatin-1s (Nec-1s). Nec-1s did not prevent RSL3-induced cell death or lipid oxidation (Figure 3-8). To confirm Nec-1s was functional, we attempted to induce necroptosis in MM cells using a published method combining Z-VAD-FMK, tumour necrosis factor (TNF)-α and SM-164 (Zhu et al., 2018, Akara-Amornthum et al., 2020, Ali and Mocarski, 2018). However, this approach did not cause cell death or reduce cell proliferation in OPM2 cells (Supplementary Figure 3-C). Western blotting showed that none of the MM cell lines express the target of Nec-1s, receptor-interacting serine/threonine-protein kinase 3 (RIPK3), which is a protein that is crucial for activation of necroptosis. Furthermore, even the DLBCL cell lines were found to have relatively low RIPK3 expression, indicated by the fact that a 96-hour incubation with the primary antibody was necessary to observe a signal on the Western blot. The low levels of *RIPK3*, as well as other necroptosis-related genes, *RIPK1* and mixed lineage kinase domain like pseudokinase (*MLKL*), in our panel of cell lines was confirmed by examining RNA sequencing data from The Human Protein Atlas (The Human Protein Atlas, 2023i). The fact that MM cells, including the ferroptosis-sensitive OPM2 cell line, do not express a key protein required to initiate necroptosis indicates that this type of cell death does not play a role in the toxicity of RSL3 against MM cells

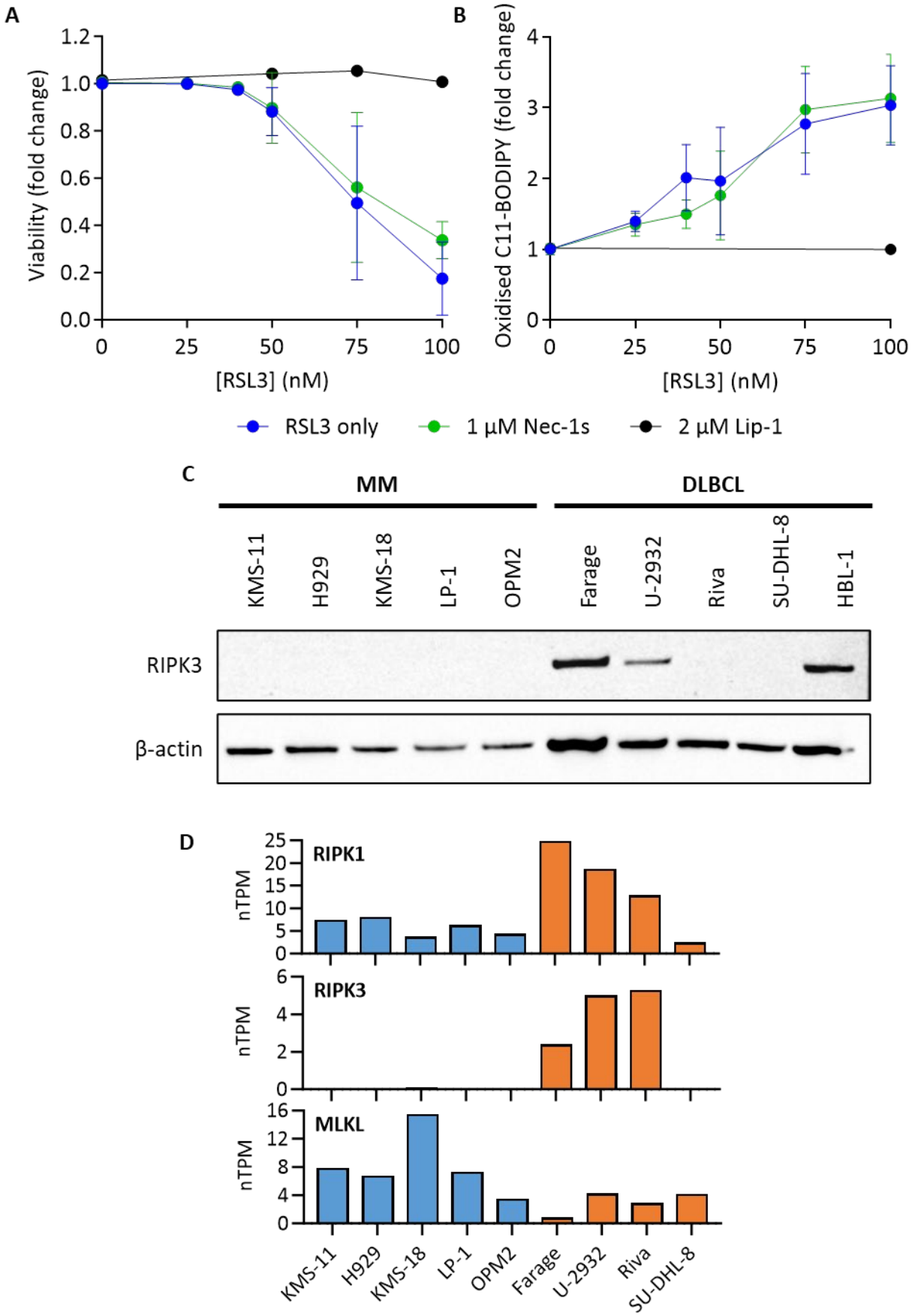

Figure 3-8: RSL3-induced death is not dependent on RIPK3 in MM cells.

OPM2 cells were treated with the indicated concentrations of RSL3 ± 2 µM Lip-1 or 1 µM Nec-1s for 24 hours. Cell viability (A) and the levels of oxidised C11-BODIPY (B) were measured by flow cytometry. Data are the

mean ± standard deviation from three independent experiments. (C) Receptor-interacting protein kinase 3 (RIPK3) protein levels were assessed in untreated MM and DLBCL cells by Western blotting, with β-actin used as a loading control. (D) Normalised transcript expression (nTPM) of *RIPK1*, *RIPK3* and mixed lineage kinase domain like pseudokinase (*MLKL*) was assessed in our panel of MM and DLBCL cell lines, taken from The Human Protein Atlas (The Human Protein Atlas, 2023i).

3.2.6 The role of autophagy in ferroptosis is cell line dependent

Autophagy was the next mechanism of cell death that was investigated to determine whether it plays a role in RSL3-induced cell death in MM cells. 3-methyladenine (3MA) is an inhibitor of the early stages of autophagy that prevents the formation of autophagosomes by inhibiting phosphatidylinositol 3-kinases (PI3K). Bafilomycin-A1 (Baf-A1) on the other hand, prevents late-stage autophagy by inhibiting V-ATPase and preventing the fusion of autophagosomes to lysosomes (Mizushima and Yoshimori, 2007).

To assess the efficacy of the two autophagy inhibitors, the conversion of LC3B-I to LC3B-II was measured by Western blotting. During autophagy, LC3B-I is converted to LC3B-II, which is expressed on the surface of autophagosomes; therefore accumulation of LC3B-II can be used as an indicator of autophagy (Mizushima and Yoshimori, 2007). However, often no LC3B-II expression is detected even in cells undergoing autophagy because autophagosomes are rapidly degraded. For this reason, it is necessary to inhibit autophagic flux to accurately determine whether autophagy is occurring (Mizushima and Yoshimori, 2007). Given that 3MA prevents the formation of autophagosomes, we did not observe an accumulation of LC3B-II in 3MA-treated OPM2, KMS-11 or LP-1 treated cells.

Consistent with previous studies, Baf-A1 caused an accumulation of LC3B-II in the MM cell lines (Moriya et al., 2013) (Figure 3-9). An accumulation of LC3B-II in cells treated with Baf-A1 alone indicated autophagic flux was occurring at baseline. In all cells, there was a modest increase in LC3B-II in cells treated with RSL3 plus Baf-A1 compared to Baf-A1 alone, but this should be confirmed through replicate experiments to enable statistical analyses of the data (Figure 3-9). Given the purpose of these blots was to confirm activity of the autophagy inhibitors, replicates were not undertaken, and we proceeded to explore the effects of the autophagy inhibitors on the efficacy of RSL3 against the MM cell lines (Figure 3-10).

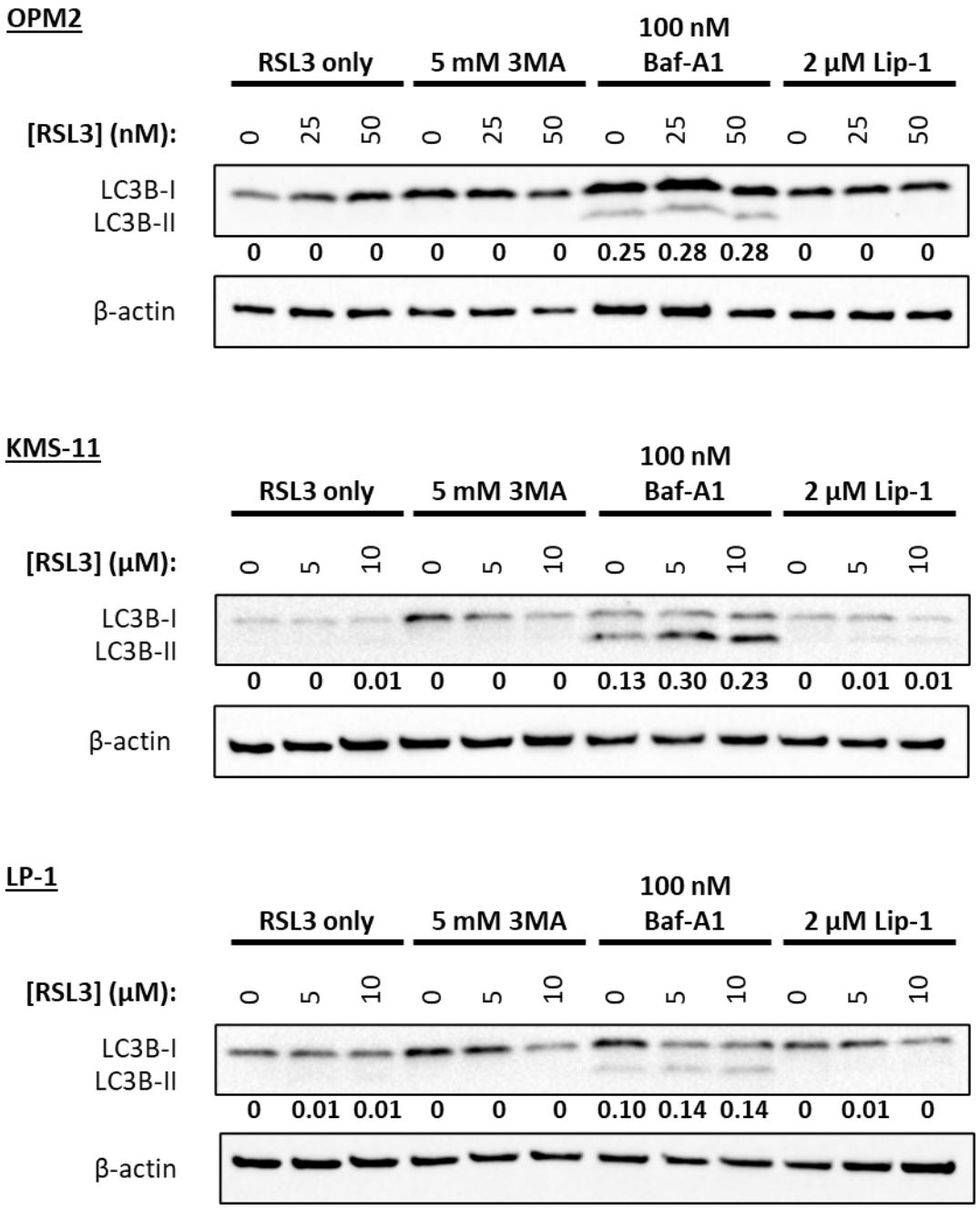

Figure 3-9: LC3B-1 to LC3B-II and autophagic flux during RSL3 treatment in MM cells.

OPM2, KMS-11 and LP-1 cells were treated with various drug and inhibitor combinations, as indicated for 6 hours and conversion of LC3B-I to LC3B-II was measured by Western blot. β-actin was used as a loading control. Densitometric values of LC3B-II relative to actin are displayed under the LC3B blots with values less than 0.005 displayed as 0.

Whether autophagy is involved in RSL3-induced cell death appeared to depend on whether the cell line uses autophagy for cell survival or cell death. OPM2 cells were not sensitive to the inhibition of autophagic flux at baseline (Figure 3-10A). In KMS-11 cells, however, and to an even greater extent in LP-1, Baf-A1 alone reduced cell viability (Figure 3-10C,E). Conversely, 3MA had no effect on any cell lines. However, it has previously been shown that MM cell lines (U266, RPMI8226 and OPM2) are sensitive to 3MA, so our results appear to contradict those from the previous study (Hoang et al., 2009). This indicates that while these cells can survive despite inhibition of autophagosome formation, the accumulation of these organelles is toxic to some degree in some MM lines.

In all three cell lines, the combination of 3MA and RSL3 did not impact the efficacy of the GPX4 inhibitor, whereas Baf-A1 had variable effects (Figure 3-10). In OPM2 cells, Baf-A1 had an antagonist effect on RSL3 efficacy where it partially prevented cell death at 75 nM ($p = 0.0500$) and 100 nM ($p < 0.0001$) RSL3 (Figure 3-10A) (Table 3-2). While this inhibition of cell death was not as effective as with the ferroptosis inhibitor Lip-1, it was statistically significant. Not only did Baf-A1 partially prevent RSL3-induced death, it also significantly reduced lipid oxidation caused by RSL3 in OPM2 cells (Figure 3-10B). In KMS-11 and LP-1 cells which were sensitive to Baf-A1 on its own, a synergistic effect was observed when combined with RSL3 (Table 3-2), suggesting the cells were more prone to cell death (Figure 3-10C,D). In KMS-11, but not LP-1 cells, Baf-A1 prevented the accumulation of lipid oxidation induced by RSL3 (Figure 3-10D,F).

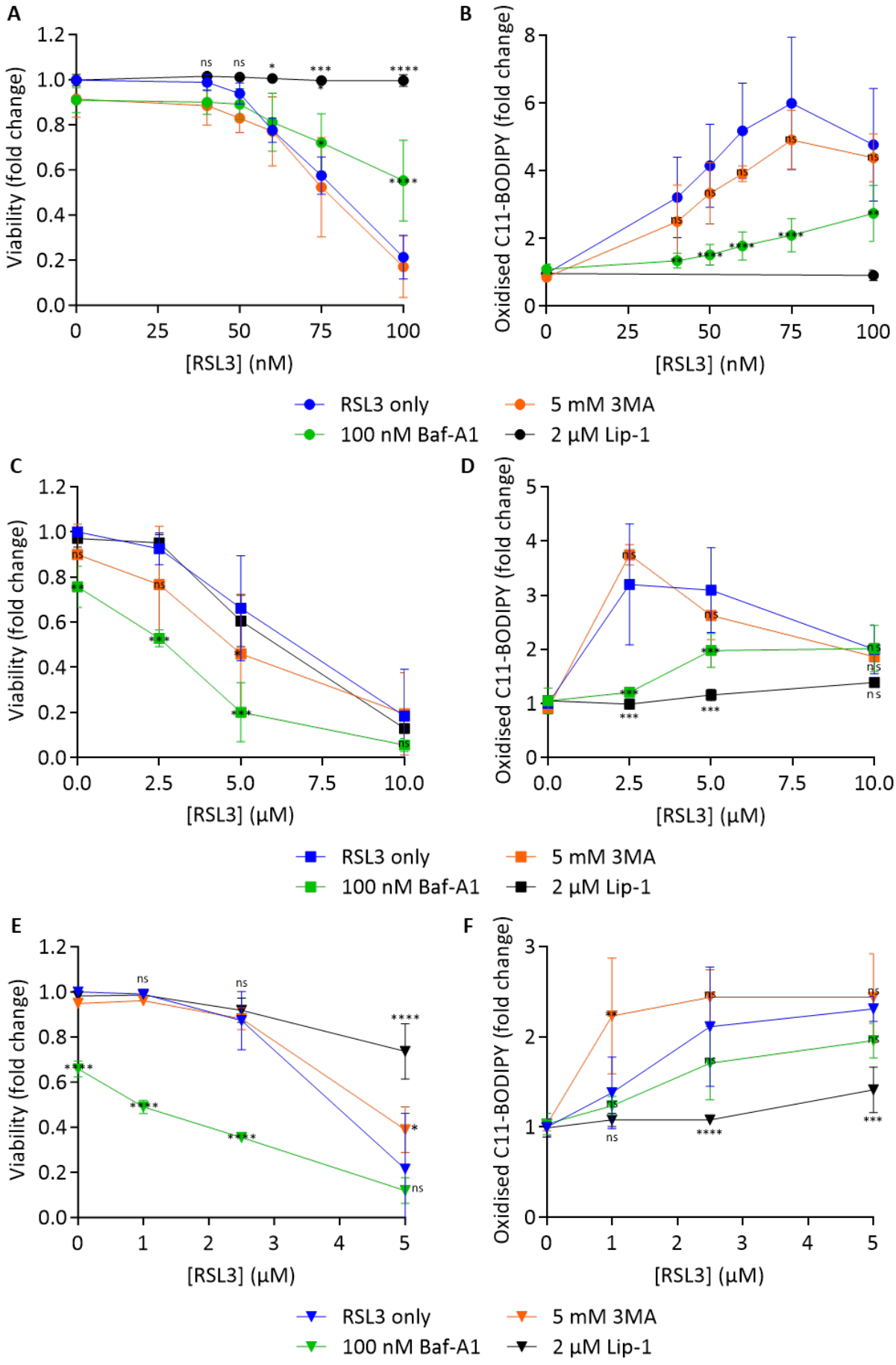

Figure 3-10: Autophagy inhibitors have varying effects on RSL3 efficacy in MM cell lines.

OPM2 (A, B), KMS-11 (C, D) and LP-1 (E, F) cells were treated with various drug and inhibitor combinations, as indicated for 24 hours. Cell viability (left) and the levels of oxidised C-11 BODIPY (right) were measured by flow cytometry. Flow cytometry data are the mean ± standard deviation from at least three independent experiments. Statistical analyses were performed by two-way ANOVA with a Tukey's multiple comparisons test; indicated statistics are relative to untreated control where ns indicates no significant difference, * p<0.05, ** p<0.01, *** p<0.001, **** p<0.0001.

Table 3-2: Synergistic effects of drug combinations.

The synergistic effect on viability of RSL3 combined with various cell death inhibitors was determined using the fractional product (FP) method (Webb, 1963). An FP less than -0.1 indicates synergism (green) whereas an FP greater than 0.1 is classified as an antagonistic effect (red).

OPM2	RSL3 (nM)			
	50	60	75	100
Baf-A1	0.04	0.11	0.20	0.36
3MA	-0.03	0.06	0.00	-0.02
Lip-1	0.07	0.23	0.42	0.78

KMS-11	RSL3 (µM)		
	2.5	5	10
Baf-A1	-0.17	-0.30	-0.08
3MA	-0.06	-0.14	0.03
Lip-1	0.05	-0.04	-0.05

LP-1	RSL3 (µM)		
	1	2.5	5
Baf-A1	-0.16	-0.22	-0.02
3MA	0.02	0.05	0.18
Lip-1	0.01	0.06	0.52

3.2.7 RSL3 causes changes in GPX4 protein expression

Next, we aimed to investigate the level of GPX4 expression in MM and DLBCL cells to determine whether differences in baseline expression could account for differences in sensitivity to its inhibitor, RSL3. Data extracted from The Human Protein Atlas indicated variable gene expression of *GPX4* across our panel of MM and DLBCL cell lines (HBL-1 data not available) (Figure 3-11A) (The Human Protein Atlas, 2023f). When grouped by malignancy, there was no statistically significant difference in *GPX4* gene expression between MM and DLBCL cells, due to the H929 outlier ($p = 0.0060$ when H929 data is excluded). Similarly, basal GPX4 protein expression varied between cell lines, with some biological variation (Figure 3-11B,C). Data from one representative Western blot is displayed in Figure 3-11B with densitometry from at least 3 biological replicates presented in Figure 3-11C. Due to the variability between biological replicates, there were few statistically significant differences in the expression of GPX4 protein between individual cell lines ($p < 0.05$ U-2932 vs. KMS-11, KMS-18, LP-1, OPM2, Farage and SU-DHL-8 only). The U-2932 DLBCL cell line had the highest expression of GPX4, which correlates with the relatively lower amount of RSL3-induced accumulation of oxidised lipids observed in this line (Figure 3-2). When grouped by malignancy, there was a slight difference in GPX4 protein expression between MM and DLBCL lines but this difference only reached statistical significance when the H929 outlier was excluded ($p = 0.0043$) (Figure 3-11C). Likewise, the IC_{50} of RSL3 did not correlate with GPX4 protein expression, with a Pearson correlation coefficient of 0.015 ($p = 0.9670$) (Figure 3-11D). These findings are consistent with data obtained from the Dependency Map (DepMap) portal where RSL3 sensitivity (Seashore-Ludlow et al., 2015, Rees et al., 2016) did not correlate with *GPX4* gene expression (DepMap, 2022, Ghandi et al., 2019) (Figure 3-11E).

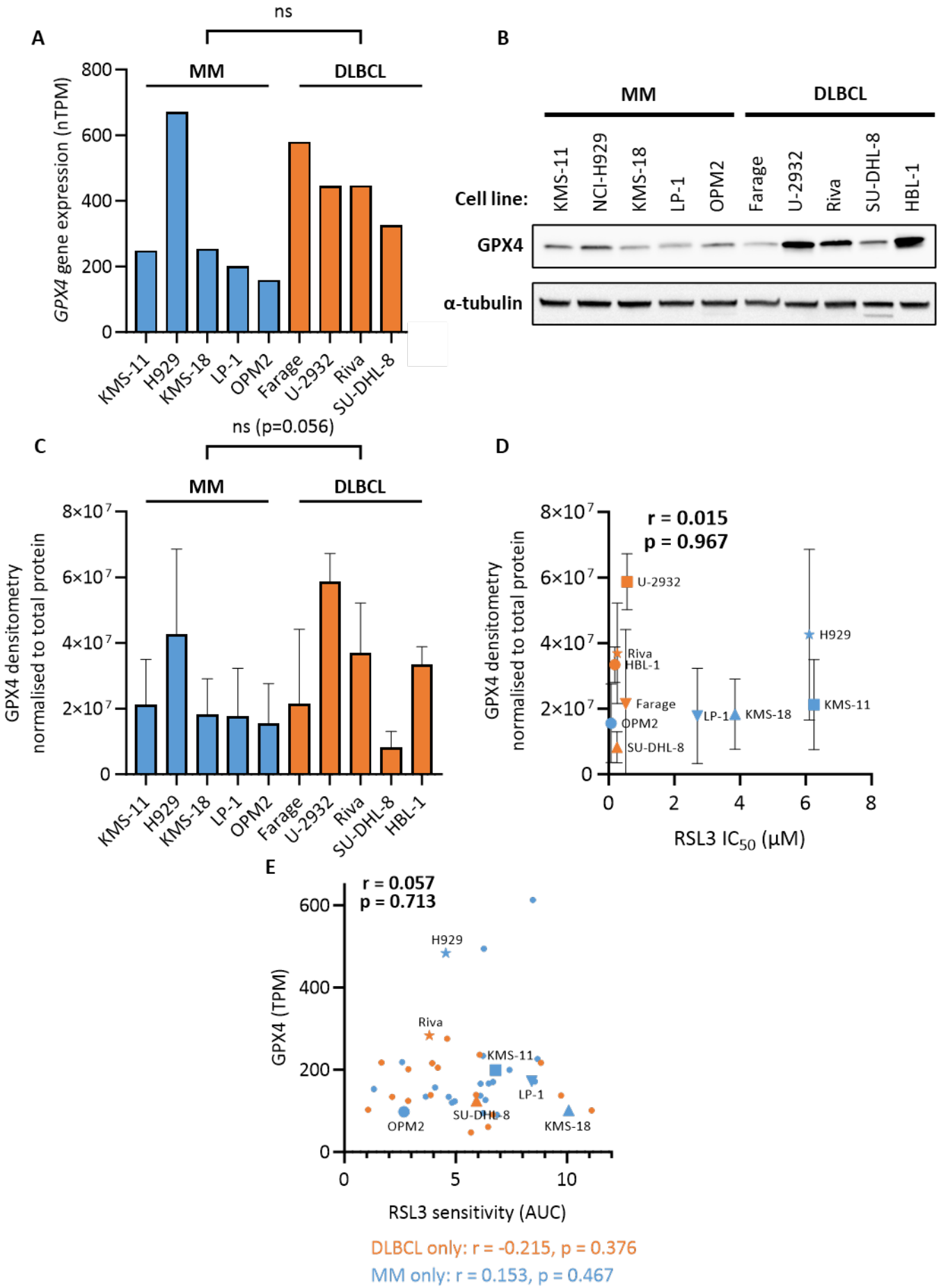
A
ns
MM
DLBCL
GPX4 gene expression (nTPM)
800
600
400
200
0
KMS-11
H929
KMS-18
LP-1
OPM2
Farage
U-2932
Riva
SU-DHL-8
ns (p=0.056)
B
MM
DLBCL
Cell line:
KMS-11
NCI-H929
KMS-18
LP-1
OPM2
Farage
U-2932
Riva
SU-DHL-8
HBL-1
GPX4
α-tubulin
C
MM
DLBCL
GPX4 densitometry normalised to total protein
8×10⁷
6×10⁷
4×10⁷
2×10⁷
0
KMS-11
H929
KMS-18
LP-1
OPM2
Farage
U-2932
Riva
SU-DHL-8
HBL-1
D
r = 0.015
p = 0.967
GPX4 densitometry normalised to total protein
U-2932
Riva
HBL-1
Farage
OPM2
SU-DHL-8
LP-1
KMS-18
H929
KMS-11
RSL3 IC50 (μM)
E
r = 0.057
p = 0.713
GPX4 (TPM)
600
400
200
0
H929
Riva
KMS-11
LP-1
SU-DHL-8
OPM2
KMS-18
RSL3 sensitivity (AUC)
DLBCL only: r = -0.215, p = 0.376
MM only: r = 0.153, p = 0.467

Figure 3-11: GPX4 protein expression in DLBCL and MM cell lines.

(A) Normalised *GPX4* transcript expression (nTPM) of MM and DLBCL cell lines, taken from The Human Protein Atlas (The Human Protein Atlas, 2023f); an unpaired t-test was used for statistical analysis of MM vs. DLBCL. (B) Representative Western blot of untreated DLBCL and MM cells, probed for GPX4 with α-tubulin as a loading control. (C) Western blot densitometry data are the mean (normalised to total protein) ± standard deviation from at least three independent experiments; an unpaired t-test was used for statistical analysis of MM vs. DLBCL. Pearson correlation was performed, and the Pearson correlation coefficient (r) and p-value (p) are displayed for GPX4 protein expression plotted vs. (D) RSL3 IC_{50} from Table 3-1, and (E) gene expression obtained from (DepMap, 2022) vs. RSL3 sensitivity (area under the curve, AUC) obtained from CTD^2 Network via DepMap portal (Seashore-Ludlow et al., 2015, Rees et al., 2016).

Next, we compared the effects of RSL3 on GPX4 protein levels in the ferroptosis-sensitive cell line, OPM2, and the resistant cell line, KMS-11 (Figure 3-12). We chose an earlier time point of 6 hours where RSL3 induces lipid oxidation, without any changes to cell viability (Supplementary Figure 3-A) to rule out the possibility of protein expression changes being linked to the presence of dead cells. Unexpectedly, in both OPM2 and KMS-11 cells, RSL3 treatment resulted in another band appearing at a slightly higher molecular weight in the Western blots probed for GPX4 (Figure 3-12A,C). In RSL3-treated OPM2 cells, two bands could be seen at approximately 20 kDa. In KMS-11 cells, only the slightly larger band could be seen in the RSL3 treated cells from 250 nM RSL3 and higher (Figure 3-12A). However, when the KMS-11 cells were treated with lower RSL3 concentrations (50-200 nM), both bands were visible (Figure 3-12C). It is worth noting that, according to the manufacturer, the antibody used in these Western blots recognises both the mitochondrial (22 kDa) and cytoplasmic (20 kDa) isoforms of GPX4. Due to the close proximity of the two bands, both were measured together as a readout of total GPX4 for densitometric analyses. In both cell lines, increasing concentrations of RSL3 caused a statistically significant increase in expression of GPX4 (Figure 3-12B). However, in KMS-11 cells, GPX4 levels began to decrease again beyond 500 nM RSL3 as the levels of GPX4 at 1 and 2.5 μM RSL3 were not significantly different from control.

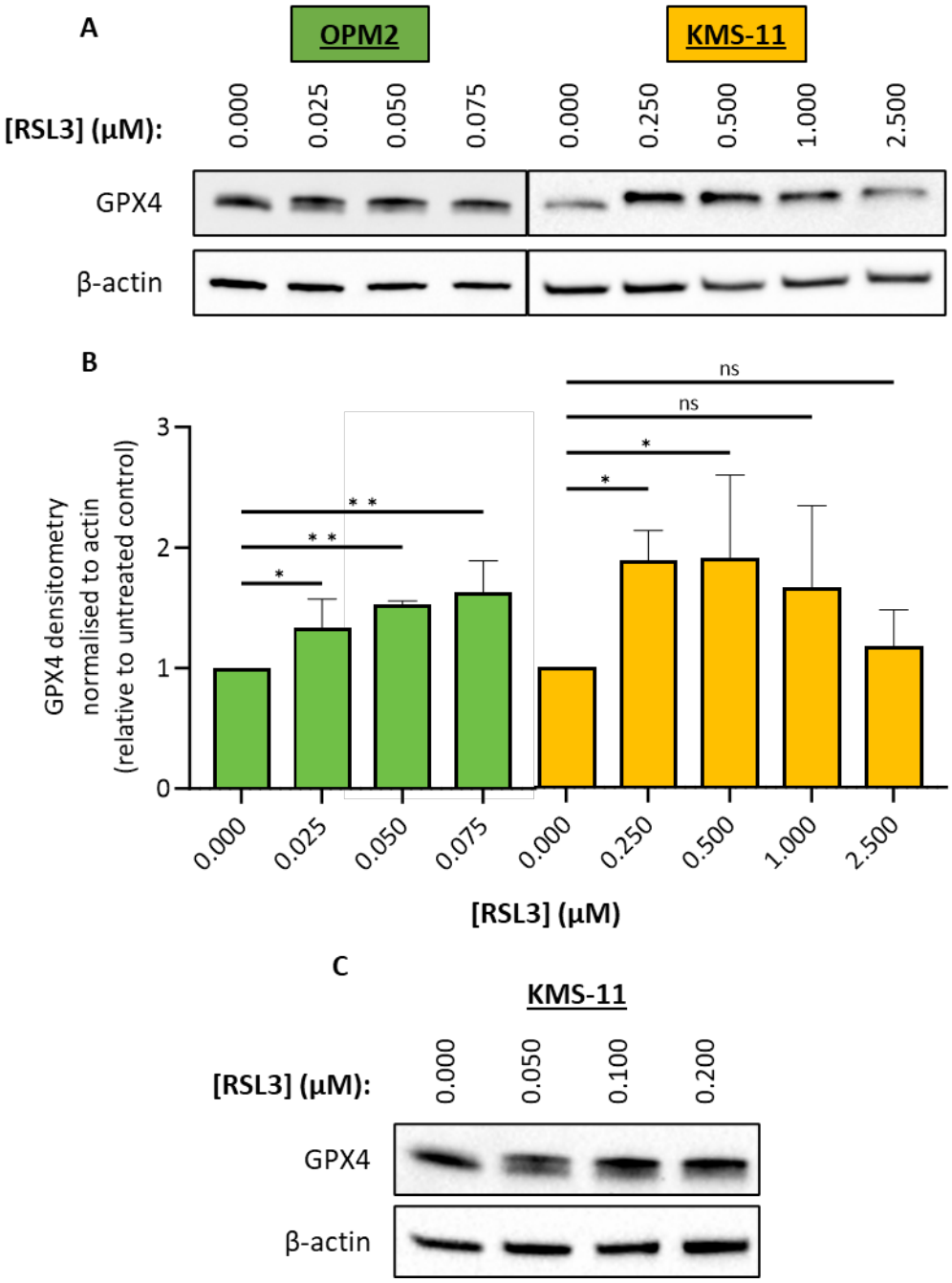

Figure 3-12: RSL3 causes changes in GPX4 protein levels in OPM2 and KMS-11 MM cells.

OPM2 and KMS-11 MM cells were treated with the indicated concentrations of RSL3 for 6 hours. (A) Representative Western blot probed for GPX4, using β-actin as a loading control. (B) Densitometry data are the mean ± standard deviation of three independent experiments. Statistical analyses were performed by one-way ANOVA with an uncorrected Fisher's least significant difference test for multiple comparisons; ns indicates no significant difference, * $p < 0.05$, ** $p < 0.01$. (C) Western blot of KMS-11 cells treated with lower doses of RSL3 for 6 hours, probed for GPX4 using β-actin as a loading control.

3.2.8 Elemental differences between MM and DLBCL cells

Given that iron and selenium play a role in ferroptosis (Ingold and Conrad, 2018), we next assessed baseline levels of these and other trace elements and metals in MM and DLBCL cells lines. This was done through inductively coupled plasma mass spectrometry (ICP-MS) performed by our collaborators at The Florey Institute of Neuroscience and Mental Health (Melbourne, VIC).Out of the fifteen elements measured, only six proceeded onto analysis as per criteria in Table 2-5. Despite the fact that the selenium results were below the detection limit, and this resulted in a high relative standard deviation, given the relevance of selenium in ferroptosis, these data were analysed further. Thus, any results concerning selenium should be interpreted with caution and should be confirmed with further analyses. Only the levels of manganese ($p = 0.0009$) and selenium ($p = 0.0006$) were statistically higher in MM cells compared to DLBCL cells (Figure 3-13A). Importantly, the levels of iron were not significantly different when the cell lines were grouped by malignancy despite differences in ferroptosis sensitivity, even when the sensitive OPM2 MM cell line was removed from the analysis (data not shown). After performing a Pearson correlation, the levels of selenium, but not manganese (Figure 3-13B), correlated with the IC_{50} of RSL3 (from Table 3-1), whereby a higher selenium content correlated with a greater IC_{50} (Figure 3-13C). Despite this correlation, selenium levels did not correlate with GPX4 protein expression (densitometry data from Figure 3-11C), indicating that higher levels of selenium are not indicative of higher levels of GPX4 protein.

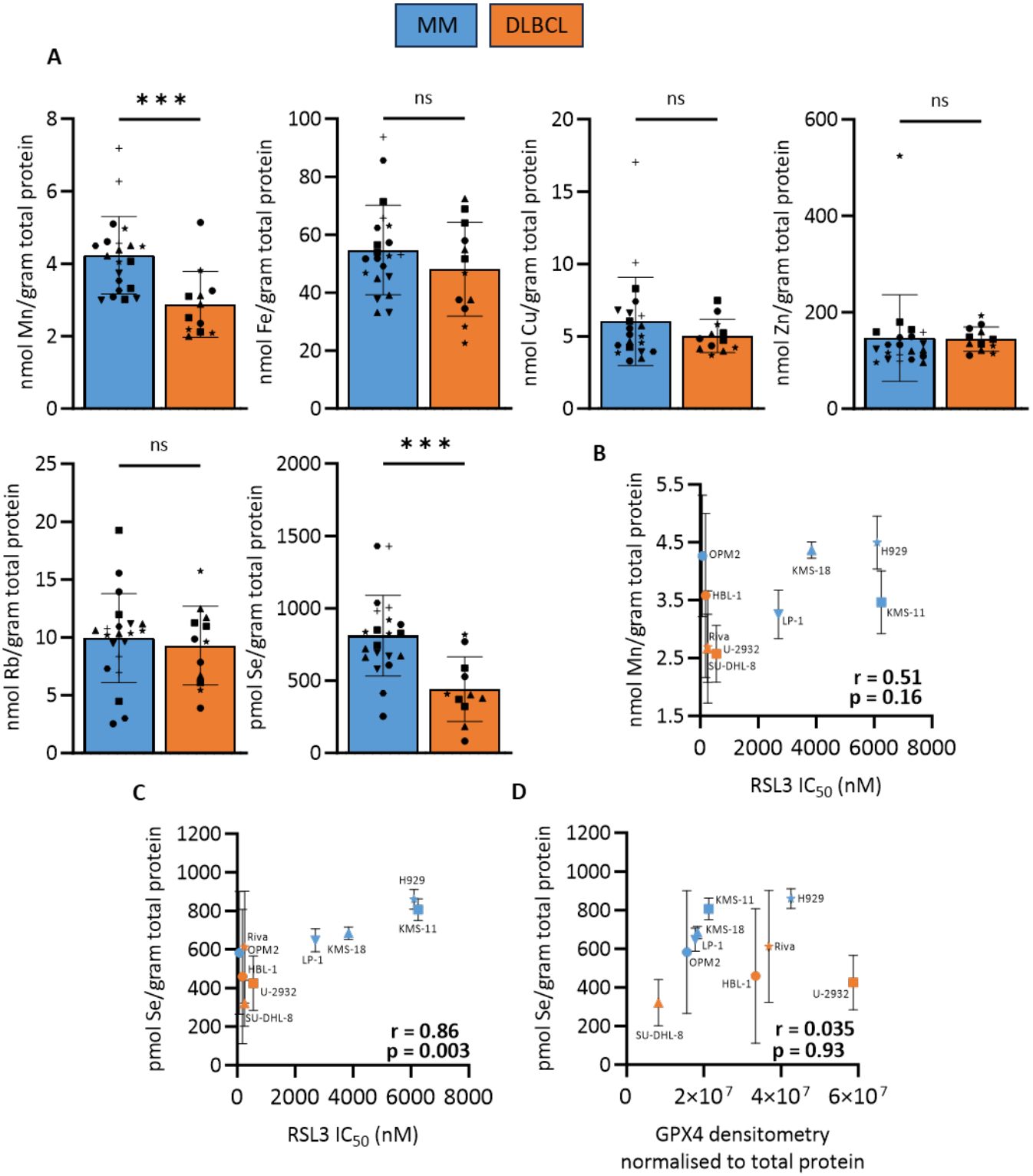

Figure 3-13: Selenium levels correlate with RSL3 sensitivity.

Inductively coupled plasma mass spectrometry (ICP-MS) was performed to assess levels of trace metals and other elements in untreated MM and DLBCL cell lines. (A) ICP-MS data were normalised to total protein and cell lines were grouped based on malignancy followed by unpaired t-tests to determine significant differences in levels of the elements between MM and DLBCL cell lines. Pearson correlation was then performed to correlate manganese (B) and selenium (C) levels with RSL3 IC_{50} values obtained from Table 3-1. (D) A Pearson correlation was also performed on selenium levels against GPX4 protein expression data from Figure 3-11C. Mn, manganese; Fe, iron; Cu, copper; Zn, zinc; Rb, rubidium; Se, selenium; ns, not significant; ***, p<0.001; r, Pearson correlation coefficient; p = p-value.

3.2.9 A higher proportion of phospholipids containing polyunsaturated fatty acids is associated with increased RSL3 sensitivity

Phospholipids are the substrates of ferroptosis and thus we were interested to compare the phospholipidomic composition of MM and DLBCL cell lines to determine whether differences in cellular phospholipid content could contribute to ferroptosis sensitivity. Despite there being significant differences in the phospholipidome of MM and DLBCL cells, there was no significant difference in the ability of the lipid content to become oxidised in the presence of iron (Figure 3-14A). While this assay was performed in a cell-free context, it does align with data from Figure 3-2where RSL3 induced a similar amount of lipid oxidation in most MM and DLBCL cell lines. It does not, however, present OPM2 as having a lipid profile more susceptible to iron-induced lipid peroxidation, despite their ferroptosis sensitivity and increased lipid oxidisation following RSL3 treatment. Lipidomic analysis of untreated MM and DLBCL cells by liquid chromatography–mass spectrometry (LC-MS) was performed to investigate the proportion of specific fatty acid groups in the phospholipidome based on saturation content. When grouped based on RSL3 sensitivity, resistant cells (MM cell lines excluding OPM2) had a higher proportion of MUFA-containing phospholipids (either 2 MUFA or 1 MUFA and 1 SFA) ($p < 0.0001$) whereas sensitive cells (OPM2 + DLBCL cell lines) had a higher proportion of PUFA (either 2 PUFA or 1 PUFA and 1 SFA) ($p = 0.0005$) or SFA-containing phospholipids ($p = 0.0044$) (Figure 3-14B). Moreover, sensitive cells had a higher proportion of phospholipids containing one or more arachidonic acid (20:4) chains ($p = 0.0015$) (Figure 3-14C). There was no statistically significant difference between RSL3 sensitive and resistant cells in the proportion of phospholipids containing both a MUFA and PUFA (Figure 3-14B). Given that the level of saturation of fatty acids has been shown to play a role in ferroptosis, we performed a Pearson correlation between the proportion of a specific fatty acid group and the RSL3 IC_{50} of MM and DLBCL cell lines (Figure 3-14D,E). Surprisingly, the proportion of phospholipids containing MUFA or PUFA, did not correlate with the IC_{50} of RSL3 (weak correlation, not statistically significant).

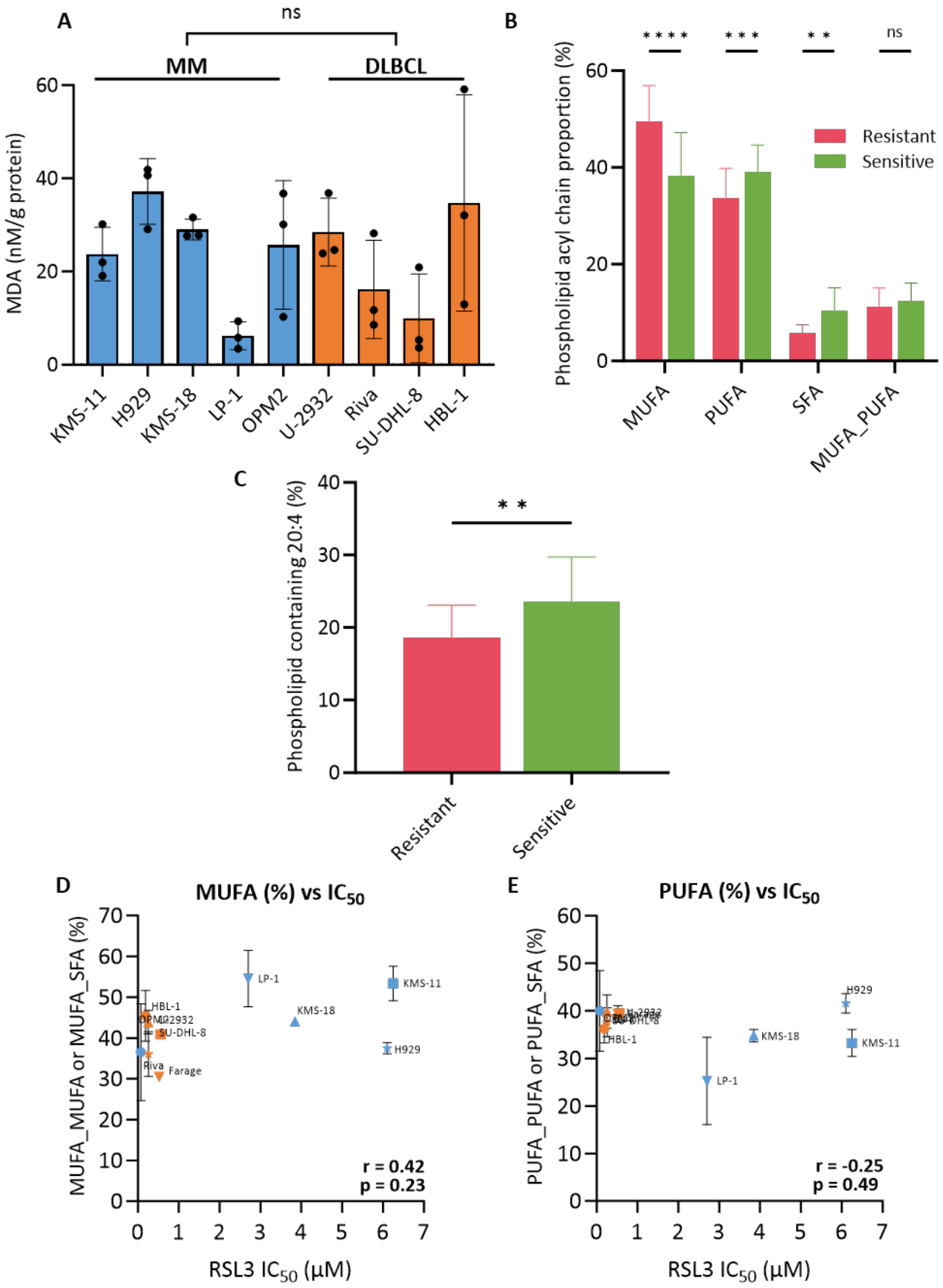

Figure 3-14: Ferroptosis-sensitive cells have a higher proportion of phospholipids containing polyunsaturated fatty acids.

(A) Generation of malondialdehyde (MDA) was measured following cell sonication and 30-minute incubation of 10 µM iron (normalised to total protein of each sample). Unpaired t-test performed; ns indicates no

significant difference. (B) Liquid chromatography–mass spectrometry (LC–MS) was performed to measure the baseline levels of phospholipids in ferroptosis-resistant (MM cell lines excluding OPM2) and -sensitive (DLBCL cell lines + OPM2 MM cells). Phospholipids were grouped and labelled according to fatty acid contents: monounsaturated fatty acid (MUFA), containing two MUFA or one MUFA and one saturated fatty acid (SFA); polyunsaturated fatty acid (PUFA), containing two PUFA or one PUFA and one SFA; MUFA_PUFA, containing one MUFA and one PUFA; or SFA, containing two SFA. Data are displayed showing the proportion of each group relative to the total number of phospholipids. Statistical analyses were performed by two-way ANOVA with an uncorrected Fisher's least significant difference test for multiple comparisons; ns indicates no significant difference, ** $p<0.01$, *** $p<0.001$, **** $p<0.0001$. (C) Proportion of phospholipids containing arachidonic acid (20:4) relative to the total number of phospholipids for ferroptosis-resistant and -sensitive cell lines. Unpaired t-test performed; ns indicates no significant difference. (D,E) Percentages from panel B were plotted against RSL3 IC_{50} values obtained from Table 3-1 to perform a Pearson correlation. r, Pearson correlation coefficient; p, p-value.

3.3 Discussion

3.3.1 Inducing ferroptosis in MM cells

While erastin did not successfully induce ferroptosis in MM cells in our study, this might be explained by the low expression of xCT in these cells (Figure 3-1B). It has been recently published that neither 10 nor 20 µM erastin causes a reduction in cell viability in a range of MM cell lines including H929, OPM2 and KMS-11 (Zhang et al., 2024a). Furthermore, another group showed that the sensitivity of MM cell lines to erastin was dependent on the level of xCT expression, with the high-expressing U266 and IM-9 MM cell lines shown to be more sensitive to the growth inhibitory effects of erastin compared to low-expressing LP-1 and MM.1s cells (Zhang et al., 2024b). However, this study suggested that in U266 cells there was no significant difference between erastin-treated and vehicle-treated cells until the 72-hour time point, and the involvement of ferroptosis was not proven through lipid oxidation or with the use of a ferroptosis inhibitor (Zhang et al., 2024b).

We also showed that DLBCL cells express relatively high levels of xCT, so it was surprising to find that concentrations in the high micromolar range were required to reduce the viability of these cells (Figure 3-1A). This inconsistency with published findings, in which DLBCL cell lines were shown to be sensitive to erastin (Yang et al., 2014) may be due to different assays being used; in the study by Yang *et al*., the effects of erastin on cellular growth, but not viability were assessed, whereas in this study, we examined cell viability in the MM and DLBCL cells. Other than Riva, the DLBCL cell lines generally had higher expression of xCT protein than the MM cells (Figure 3-1B), which is consistent with reports that DLBCL cells are reliant on xCT for generation of cysteine to fuel GSH production (Zhang et al., 2019).

Next, we examined the effects of directly inhibiting GPX4 using RSL3, which avoids the possible confounding factor of differences in GSH production pathways between MM and DLBCL cells. We found that similar to the

findings of Yang *et al.* that found DLBCL cells were more sensitive to erastin-induced ferroptosis (Yang et al., 2014), our panel of DLBCL cell lines were more sensitive to RSL3-induced death compared to 4 of the 5 MM cell lines (Figure 3-2A). Cell lines which require nanomolar concentrations of RSL3 to induce growth inhibition are generally considered to be sensitive to ferroptosis (Yang and Stockwell, 2008), which is consistent with our data suggesting that the cytotoxic effects of RSL3 exceeding 5 µM were less effectively prevented by Lip-1 (Figure 3-2B). With these factors in mind, we considered cell lines with an RSL3 IC_{50} above 2.5 µM to be resistant, and those with an IC_{50} below 2.5 µM to be sensitive. As Lip-1 was less effective at preventing cell death induced by RSL3 concentrations beyond 5 µM, and we used 2 µM Lip-1 which is much higher than what is commonly used in the literature (200 nM), this suggests off-target and/or non-ferroptotic effects occurring at these high concentrations of RSL3. It is understood that the chloroacetamide moiety of RSL3 binds to the selenocysteine residue of GPX4 which is necessary for its inhibition, so it stands to reason that RSL3 could interact with other selenoproteins, particularly at these high concentrations that exceed concentrations required to inhibit GPX4 (Mishima et al., 2023, Yang et al., 2014).

While RSL3 is a known ferroptosis inducer, we confirmed the mechanism of cell death was ferroptosis by assessing the generation of lipid ROS, which is a distinct characteristic of this form of cell death (Yang et al., 2014). This was achieved using a lipid peroxidation sensor called BODIPY™ 581/591 C11 (referred to as C11-BODIPY), which shifts from red to green fluorescence upon oxidation by nearby lipids. Increases in green fluorescence were measured and expressed relative to untreated control cells. In all 10 MM and DLBCL cell lines, a marked increase in lipid oxidation was observed following treatment with RSL3. This lipid oxidation preceded cell death in KMS-11 and OPM2 cells, as early as 4 hours, and continued to increase until the end point at 24 hours (Supplementary Figure 3-A). Furthermore, ferroptosis was confirmed as the mechanism of RSL3-induced cell death by simultaneous treatment with the lipophilic antioxidant, liproxstatin-1 (Lip-1). Lip-1 completely prevented RSL3-induced death at concentrations of RSL3 up to 2.5 µM, whereas at RSL3 concentrations above 5 µM, Lip-1 was less effective at preventing death (Figure 3-2C). Lip-1 prevents ferroptosis by reducing the levels of lipid oxidation, which was clearly evident by a lack of C11-BODIPY oxidation in cells treated with both RSL3 and Lip-1 (Figure 3-2D).

Since we found that RSL3 was more effective than erastin, we focused on the direct GPX4 inhibitor in our subsequent work. With the exception of OPM2 cells, we found that MM cell lines were less sensitive to RSL3 than DLBCL cells and were classified as resistant with IC_{50}s above 2.5 µM (Table 3-1). While the aim of this chapter was initially to determine the differences in sensitivity between MM and DLBCL and the factors that determine this variability, the outlying results from the OPM2 cell line represented an opportunity to examine differences between cell lines from the same disease. Interestingly, while OPM2 cells had the greatest

increase in oxidised lipids at lower concentrations of RSL3, the maximal levels of lipid oxidation in this line, albeit at higher concentrations of RSL3, were comparable to the other MM and DLBCL cells (Figure 3-2B). This suggests that RSL3 is effectively inhibiting GPX4 in MM cells, but they have mechanisms to withstand cytotoxicity caused by the increase in oxidised lipids.

3.3.2 Inconsistent responses to RSL3 in MM cell lines

To maintain consistency, cells were always fed the day before drug treatment and were always treated at a density of 300,000 cells/mL. Furthermore, each cell line was cultured for no longer than 3 months after being thawed from liquid nitrogen (i.e. passage <40). Despite this, inconsistencies in the RSL3 dose response were observed in KMS-18 and LP-1 cells (Supplementary Figure 3-D). 17 and 16 biological replicates were performed with KMS-18 and LP-1 cells, respectively, and from these experiments, three statistically different RSL3 dose responses were observed (Supplementary Figure 3-D A,C). After grouping replicates based on sensitivity to RSL3, the corresponding lipid oxidation data, where available, was compiled for each dose response (Supplementary Figure 3-D B,D). Interestingly, the fold change in lipid ROS between treated and untreated samples, corresponded with each dose response. For example, the most RSL3-sensitive KMS-18 biological replicates had a peak increase in lipid ROS at much lower concentrations of RSL3 compared to RSL3-resistant replicates (Supplementary Figure 3-D D). In all cases, LP-1 cells were >50% viable following treatment with 1 µM RSL3, which demonstrates that these cells are consistently less sensitive to RSL3 than all the DLBCL cell lines, which were <25% viable at this RSL3 concentration (Figure 3-2A). In 11 of 17 replicates, KMS-18 cells had an RSL3 IC_{50} for cell death greater than 3.8 µM. However, in the 6 “sensitive” replicates, KMS-18 cells were less than 20% viable after treatment with 1 µM RSL3, with an IC_{50} of only 57 nM (Supplementary Figure 3-D C). The “mid resistant” dose responses in Supplementary Figure 3-D are displayed in Figure 3-2.

The inconsistency in the data obtained for the KMS-18 and LP-1 cells in response to RSL3 alone reduces the reliability of the data obtained from these two MM cell lines, particularly for the “sensitive” KMS-18 dose responses where the data more closely resembles the response of the DLBCL lines. In any case, for all LP-1 experiments, as well as the KMS-18 “mid-resistance” and “most resistant” dose responses, it was clear that RSL3 was less effective in these cells compared to the DLBCL cells. It is, however, also clear that the cell death in the “sensitive” and “mid-resistance” cells was associated with higher levels of lipid oxidation and the opposite is true that lower levels of lipid oxidation correlated with less efficacy of RSL3. Although some variability between the biological replicates for all other cell lines was observed (evident by the large error bars), the variability was most evident in the KMS-18 and LP-1 cells. The factors that lead to this inconsistency

in lipid oxidation and consequently RSL3 sensitivity in these two cell lines, and not in the other MM or DLBCL cells, are currently unclear.

A number of factors may contribute to the data inconsistencies other than human error, given that ferroptosis is a complex process involving many cellular pathways. It has been shown in the literature that RSL3 cannot inhibit purified GPX4 unless relatively high doses are used, at which nonspecific effects may occur in intact cells (Vučković et al., 2020, Cheff et al., 2023). RSL3 has been described as a non-specific inhibitor of the selenoproteome and in fact, RSL3 has been shown to only inhibit thioredoxin reductase 1 (TXNRD1), and not GPX4 or GPX1 in a pure enzyme activity assay (DeAngelo et al., 2024, Cheff et al., 2023). Purified GPX4 can be inhibited by RSL3 in the presence of Hek293t cytosol, or in the presence of the adapter protein 14-3-3ε in a concentration dependent manner, highlighting the importance of cytosolic factors on RSL3 activity (Vučković et al., 2020). Accordingly, there may be different levels of 14-3-3ε or other cytosolic proteins or factors which vary between biological replicates, leading to the instability observed in RSL3 sensitivity. We also found that GPX4 protein levels fluctuated between biological replicates (Figure 3-11B,C), and while the average GPX4 protein we observed or publicly available gene expression data did not correlate with RSL3 sensitivity, this may have been affected by the inconsistency in protein expression (Figure 3-11D). It is not understood why there were differences in the expression of GPX4 between biological replicates given that the cell density and method of collection were consistent across replicates. This may have been due to normal biological variability, or uncontrollable changes in the environment during the process of Western blotting. It is well understood that the GPX4 dependency of drug-tolerant persister cancer cells and high-mesenchymal state cells make them markedly more sensitive to GPX4 inhibition (compared to drug-sensitive parental cells and epithelial cells, respectively) but levels of GPX4 expression have not yet been linked to dependency on this antioxidant system (Hangauer et al., 2017, Viswanathan et al., 2017). There is limited data linking GPX4 expression to RSL3 sensitivity, with one study showing non-small cell lung cancer (NSCLC) cell lines with higher expression of GPX4 are more sensitive to RSL3 (Kim et al., 2023). Future experiments should be performed in which cell lysates are prepared at the same time that RSL3 dose responses are performed to determine if there is a link between biological variations in GPX4 protein expression, or other intracellular factors, and IC_{50} values for RSL3 in MM and DLBCL cell lines. The response of KMS-11 and OPM2 MM cells to RSL3 were very consistent, which suggests that the factors that determine sensitivity to the drug are relatively stable in these cells. Due to the consistency of their response to RSL3, we decided to focus on these two cell lines for comparative work in the subsequent studies presented here.

3.3.3 Mechanisms of RSL3-induced death

It has been noted in the literature that because there is the potential for ferroptosis inducers to have different effects at different doses and in different contexts, this could result in activation of different cell death pathways (Chen et al., 2024a). Thus, it is important that we have a complete understanding of the mechanisms behind RSL3-induced death in MM cells, particularly given the high rate of drug resistance among patients with this cancer. Knowledge of the pathways involved in the cytotoxicity of RSL3 is key in order to predict potential ways in which the cancer cells might avoid death. For example, if RSL3-induced death involves caspases or proteins involved in necroptosis, the cancer cells might downregulate these proteins to avoid toxicity.

Apoptosis and caspase-dependent cell death

It is important to acknowledge that the dyes used to measure cell viability throughout this thesis are typically used to measure apoptosis. However, they are still relevant and suitable to measure the proportion of ferroptotic cells. Annexin-V binds to phosphatidylserine (PS) which is expressed on the outer leaflet of the plasma membrane during early apoptosis. Even though PS is not externalised during ferroptosis, annexin-V is able to bind PS on the inner leaflet of the plasma membrane in cells undergoing ferroptosis due to their increased permeability (Riegman et al., 2020, Pedrera et al., 2021, Seiler et al., 2008). The classic ferroptotic phenotype consisting of a swollen cytoplasm precedes cell death, and in other forms of cell death such as pyroptosis and necroptosis where swelling occurs, this is due to an influx of water and ions through pores that form in the plasma membrane (Riegman et al., 2020). In ferroptosis induced by ferric ammonium citrate (FAC), BSO, RSL3 or ML162, lactate dehydrogenase release can be prevented with the use of osmoprotectants (polyethylene glycols) to prevent osmotic cell lysis, suggesting pore formation is also occurring in ferroptosis (Riegman et al., 2020). For these reasons, cells undergoing ferroptosis are stained with both annexin-V and propidium iodide, and unlike early apoptotic cells do not go through an early ferroptotic stage in which they are stained with just annexin V (Seiler et al., 2008). To further distinguish ferroptosis from apoptosis, it is therefore necessary to employ cell death inhibitors and measure changes in cellular components associated with each individual cell death process, such as lipid oxidation and caspase-3 cleavage for ferroptosis and apoptosis, respectively.

While it is well known in the literature that RSL3 induces ferroptosis, we sought to compare RSL3-induced death to caspase-dependent death in MM cells to confirm the mechanisms behind RSL3-induced death were distinct from apoptosis. Vincristine was used in LP-1 cells as an apoptosis control for comparison with RSL3-induced death. However, the pan-caspase inhibitor, Z-VAD-FMK, did not prevent vincristine-induced death in KMS-18 and KMS-11 cells (Supplementary Figure 3-B). For this reason, the proteosome inhibitor,

bortezomib, was used in these cells instead. In bortezomib-treated, apoptosis-controls, as expected, Z-VAD-FMK partially prevented cell death, whereas Lip-1 had no effect. In contrast, only Lip-1 and not Z-VAD-FMK could prevent cell death induced by 5 μM RSL3. However, at 10 μM RSL3, a reduction in cell death was observed when KMS-11 cells were preincubated with Z-VAD-FMK (Figure 3-5). Concordant with these findings, caspase-3 cleavage was observed in KMS-11 cells treated with 10 μM RSL3, and interestingly, also at 5 μM RSL3 (Figure 3-6). This was an unexpected finding given that it has been shown that high levels of RSL3 may have non-ferroptotic effects, but historically, these effects have been independent of caspase-3 cleavage and many studies have shown that Z-VAD-FMK cannot inhibit RSL3 (Liu et al., 2022, Kim et al., 2023, Seiler et al., 2008, Hangauer et al., 2017, Dixon et al., 2012, Yang and Stockwell, 2008). However, a recent study showed that caspase-3 is cleaved in cell lines from patients with myelodysplastic syndrome following treatment with 4 or 6 μM RSL3, and that the reduced proliferation in response to 4 μM RSL3 can be inhibited by Z-VAD-FMK (Liu et al., 2024). While we observed a small but statistically significant increase in caspase-3 cleavage in LP-1 cells after treatment with 5 μM RSL3, only Lip-1 and not Z-VAD-FMK could prevent cell death in these cells (Figure 3-5, Figure 3-6). This suggests that caspase-3 cleavage occurs but is not necessary to execute RSL3-induced death in these cells.

Necroptosis and RIPK-dependent cell death

Necroptosis is a caspase-independent form of cell death that was initially found to occur when cells were treated with TNF-α and a pan-caspase inhibitor (Linkermann and Green, 2014). Necroptosis occurs when caspase-8 is inactivated, allowing RIPK3 and RIPK1 to form a necrosome complex, resulting in signalling cascade that ends in phosphorylation of MLKL (Zhang et al., 2022c). MLKL phosphorylation causes oligomerisation of the protein and necroptotic cell death by compromising the structure of the plasma membrane (Linkermann and Green, 2014, Zhang et al., 2022c). Ferroptosis has been shown to be distinct from necroptosis given that necroptosis inhibitors cannot prevent cell death induced by erastin (Dixon et al., 2012, Kim et al., 2023). A standard approach to induce necroptosis in cells is by combining TNF-α, SM-164 and a caspase-inhibitor such as Z-VAD-FMK (Zhu et al., 2018, Akara-Amornthum et al., 2020, Ali and Mocarski, 2018). However, in OPM2 cells, we did not observe a reduction in viability or proliferation using this necroptosis-inducing combination of drugs. To investigate why necroptosis could not be induced, the expression of proteins necessary for this cell death pathway were assessed by Western blotting, which revealed that the panel of MM cell lines do not express a key protein in the canonical necroptosis pathway, RIPK3 (Figure 3-8C). The Farage, U-2932 and HBL-1 DLBCL cells did express RIPK3, but this was only detected after a 96-hour incubation with an anti-RIPK3 antibody, suggesting the protein is expressed at very low levels. These findings are supported by data concerning *RIPK3* RNA expression in a range of MM and DLBCL, which is available in The Human Protein Atlas (Figure 3-8D) (The Human Protein Atlas, 2023i). A study showed that RPMI-8226, MM1.S and KMS-18 MM cells were sensitive to the combination of TNF-α, cycloheximide and Z-

VAD-FMK (Ali and Mocarski, 2018). However, when components of the necroptosis pathway were inhibited, cell death was only partially supressed in RPMI-8226 cells, and to a lesser extent in KMS-18 cells, while no effects were observed against the MM.1S cells (Ali and Mocarski, 2018). This might be explained by the fact that only the RPMI-8226 cells were shown to express RIPK3, and so KMS-18 and MM.1S cells were unlikely to be able to undergo necroptosis (Ali and Mocarski, 2018). Collectively, our data and the studies mentioned suggest that it is highly unlikely that RSL3 is inducing necroptosis in the MM cell lines given they do not express RIPK3 protein (Morgan and Kim, 2022).

Autophagic cell death and ferroptosis cross talk

Autophagy has been shown to have roles in both cell survival and cell death. Autophagy can have pro-survival effects when cells are in a nutrient-deprived or stressed environment but can also trigger cell death under certain conditions (Wallington-Beddoe et al., 2011, Gao et al., 2016). In MM cells, autophagy is required for cell survival but is tightly regulated as when it proceeds in an uncontrolled manner the cells die (Ho et al., 2019, Yun et al., 2017). Accordingly, there are various autophagy modulators being investigated in clinical trials for MM (Ho et al., 2019).

Ferroptosis was initially shown to be distinct from autophagic cell death (Dixon et al., 2012), however more recently, certain types of autophagy have been shown to play a role in ferroptosis; namely, ferritinophagy (break down of ferritin to release free iron), lipophagy (break down of lipid droplets to release free lipids), mitophagy (break down of mitochondria) and chaperone-mediated autophagy of GPX4 (Tang et al., 2021a, Chen et al., 2024a). While ferroptotic cell death is distinct from the process of autophagic cell death, the two cell death pathways have been shown to interact and enhance each other (Zhou et al., 2019). For example, the immunomodulatory drug FTY720 has been shown to induce both ferroptosis and autophagy in MM cells (Zhong et al., 2020).

Using a pooled shRNA library, the shRNAs that were enriched in ferroptosis-resistant MEF cells were identified, and included 11 autophagy-related genes (ATGs) (Gao et al., 2016). Treatment of MEFs and HT1080 cells with erastin induced conversion of LC3BI to LC3BII, which was enhanced by Baf-A1 (Gao et al., 2016). In glioma cells, both RSL3 and erastin induced an increase in LC3BII, which again was enhanced by addition of Baf-A1 (Subburayan et al., 2024, Wang et al., 2019b). In KMS-11, LP-1 and OPM2 MM cells, however, we did not observe an increase in LC3BII in cells treated with RSL3, and while Baf-A1 on its own caused accumulation of LC3BII, the addition of RSL3 had no significant effect on the expression of the protein (Figure 3-9), suggesting that RSL3 does not induce formation of autophagosomes in MM cells.

In studies where ferroptosis was associated with an upregulation of LC3BII, inhibiting autophagy through pharmacological means as well as genetic knockdown of ATGs, prevented ferroptotic cell death (Gao et al., 2016, Subburayan et al., 2024, Wang et al., 2019b). In the earlier study, however, the inhibitory effects of Baf-A1 and another autophagy inhibitor chloroquine, were most effective at preventing erastin-induced death at earlier time points and the effects decreased after 24 hours, or with higher doses of erastin (Gao et al., 2016).

Baf-A1 on its own had a cytotoxic effect against KMS-11 and LP-1 cells which was exacerbated when combined with RSL3, but not to the extent that the IC_{50} values for RSL3 were in the low nanomolar range (Figure 3-10C,E). This suggests these cells may rely, at least partially, on autophagy for survival, while the OPM2 cells do not since inhibition of autophagy in these cells had no effect on their viability (Figure 3-10A). Differences in the levels of autophagy at baseline in cell lines may have an effect on whether ferroptosis is dependent on autophagy – for example, ferroptosis-sensitive HT1080 cells have been shown to have high levels of LC3BII so may be primed for autophagic cell death (Chen et al., 2024a).

In RSL3-sensitive OPM2 cells, treatment with Baf-A1 partially prevented cell death, likely due to its ability to decrease the generation of lipid ROS (Figure 3-10A,B). In KMS-11 and LP-1 cells, in which cytotoxicity was only observed at high concentrations of RSL3, Baf-A1 did not prevent cell death (Figure 3-10C,E) despite reducing lipid ROS levels in KMS-11 cells (Figure 3-10D). The mechanisms behind how Baf-A1 reduced lipid oxidation in KMS-11 and OPM2 cells was not investigated further, however, similar to our findings, it has been shown that inhibiting autophagy can prevent both lipid and general ROS during ferroptosis (Gao et al., 2016, Subburayan et al., 2024). More specifically, this link between autophagy and ROS production during ferroptosis has been shown to involve the autophagy-dependent break-down of ferritin (ferritinophagy); when autophagy is inhibited, labile iron cannot be released from ferritin to enter the ferroptotic pathway (Gao et al., 2016, Subburayan et al., 2024). In another study, Baf-A1 could only prevent erastin- or Fin56- (class 3 ferroptosis inducer that promotes GPX4 degradation), and not RSL3-induced death in bladder cancer cells (Sun et al., 2021). Likewise, only ferroptosis induced by erastin, and not RSL3, involved ferritinophagy in HeLa cells (Gryzik et al., 2021). In NSCLC cells, chloroquine and Baf-A1 could not rescue cells from RSL3-induced death and while RSL3 was associated with an accumulation in LC3BII and autophagosome formation, there was no degradation of p62, which indicated autophagic flux was inhibited (Kim et al., 2023). Taken together, the literature suggests that autophagy does not play an important role in RSL3-induced ferroptosis, and our findings support this hypothesis in MM cells.

3.3.4 Investigating cellular characteristics that influence RSL3 susceptibility

GPX4 expression

It has been shown in Pfa1 MEF cells that GPX4 protein expression decreased with RSL3 treatment (Kagan et al., 2017). Consistent with this, we observed GPX4 degradation in HBL-1 cells treated with RSL3 for 5 hours (Supplementary Figure 3-E), which preceded cell death. A similar trend was seen in KMS-18 and LP-1 cells following treatment with RSL3, where a decrease in total GPX4 protein expression occurred as early as 6 hours after treatment initiation (Supplementary Figure 3-E), but a more prominent decrease was observed at 16 hours (Supplementary Figure 3-E). In the MM lines, this degradation was only observed at higher concentrations of RSL3, likely due to the higher IC_{50} compared to HBL-1 cells (Figure 3-2). This is consistent with a previous report that showed GPX4 expression was only reduced in RSL3-sensitive and not resistant, NSCLC cell lines (Kim et al., 2023). It is also important to point out that our data from the KMS-18, LP-1 and HBL-1 cells were obtained using an Invitrogen polyclonal antibody against GPX4 that has since been discontinued and only one biological replicate was conducted, making it hard to draw conclusions from this data until it is replicated.

Subsequently, lysates representing multiple biological replicates were prepared from KMS-11 and OPM2 cells and probed by Western blotting for GPX4 expression using a polyclonal antibody from Cell Signaling Technologies (Figure 3-12). An increase in total GPX4 protein was observed in OPM2 cells following treatment with RSL3, and while similar results were observed in KMS-11 cells, the increase in expression was only observed at much higher concentrations of RSL3, beyond which GPX4 decreased back to around baseline levels (Figure 3-12B). Interestingly, RSL3 appeared to cause expression of GPX4 at a slightly higher molecular weight in these cells, which was particularly apparent at low concentrations of RSL3 where both bands were visible, while only the higher molecular weight protein was apparent at higher RSL3 concentrations (Figure 3-12A,C). This “double banding” of GPX4 is not well reported, but has been observed in A549 and H1975 human lung cancer cells treated with class 2 ferroptosis inducers (Cheff et al., 2023). The authors observed similar, double bands at around 20 kDa in DMSO-treated cells and also found that the faster migrating, lower molecular weight band disappeared in the lysates from cells treated with RSL3, ML162 or ML210 for 6 or 24 hours. They concluded that this effect was not directly related to ferroptotic cell death as inhibition of ferroptosis with Fer-1 had no effect on the expression of the two GPX4 bands on the Western blots. In their study, Cheff *et al.*, also ran pure recombinant GPX4, which was detected at the same molecular weight as the larger, slower migrating band, leading the authors to conclude that this band represents the intact selenoprotein (Cheff et al., 2023).

There are three distinct isoforms of GPX4; mitochondrial GPX4 (~22 kDa), which contains an n-terminal, 27 amino acid mitochondrial insertion sequence that targets it to the mitochondrial matrix; cytoplasmic GPX4 (~20 kDa) has an alternate promoter, and lacks the mitochondrial insertion sequence, resulting in its enriched expression in the cytoplasm; nuclear GPX4 (~35 kDa) has an alternate exon 1, resulting in a longer, distinct n-terminus and is thought to be predominately expressed in the nuclei of spermatozoa (Tong et al., 2022, Borchert et al., 2006).

The original Invitrogen GPX4 antibody used in the current study was raised against a synthetic peptide corresponding to a sequence that is found in the n-terminus of all 3 isoforms of human GPX4. The Cell Signaling Technologies antibody is raised against a synthetic peptide corresponding to residues near the c-terminus of GPX4 and while the exact sequence has not been made available, the c-terminus is conserved across all GPX4 isoforms. With this in mind, it is reasonable to assume that both antibodies will recognise all GPX4 isoforms; this was confirmed in the data available concerning the Cell Signaling Technologies antibody, which established that their antibody would bind both mitochondrial and cytoplasmic GPX4, resulting in two bands. In the earlier blots using the Invitrogen antibody, double banding was observed in LP-1 cells, and only faintly in KMS-18 cells, suggesting that the effect of RSL3 on expression of these forms of GPX4 may differ between different cell lines (Supplementary Figure 3-E).

At baseline, MM and DLBCL cells appear to express only the smaller GPX4 band and it is not until the cells are treated with RSL3 that the larger form of GPX4 is expressed (Figure 3-11, Figure 3-12). In the literature, isoform-specific primers, or cellular fractionation are generally performed to distinguish between cytoplasmic and mitochondrial forms of GPX4 (Borchert et al., 2006, Oh et al., 2022). In our samples, it is unlikely that the larger GPX4 isoform is localised to the mitochondria given that the mitochondrial targeting sequence is cleaved once localised to this organelle (Borchert et al., 2006); therefore, cellular fractionation may not be useful. Instead, to definitively determine that the two bands observed are the different isoforms of GPX4, immunoprecipitation of the proteins from whole cell lysate could be performed using the GPX4 antibody. The precipitates could then be run on a gel and excised for sequencing. Nonetheless, the manufacturer confirmed that the antibody can produce two bands consistent with mGPX4 and cGPX4; if we assume this to be true, it appears that RSL3 causes degradation of the smaller, cytoplasmic isoform. There appears to be a RSL3 dose-dependent switch from the cGPX4 to the mGPX4 form; at low concentrations of RSL3, both isoforms can be observed before the cytoplasmic form is undetectable and only the mitochondrial form can be observed (Figure 3-12A,C). It is not well understood at this time why or under what circumstances switching between the two forms of GPX4 occurs. It is reasonable to hypothesise this could be due to either alternate transcription factor activation for different transcript variants, differential mRNA

stability, silencing of the mitochondrial start codon during translation or post-translational silencing of certain isoforms (Borchert et al., 2006). During brain development, expression of mGPX4 depends on the stage of development, whereas the cytoplasmic isoform is expressed consistently (Borchert et al., 2006). It is generally agreed that the cytosolic form of GPX4 is most relevant to ferroptosis (Mishima et al., 2023, Gan, 2021). However, there have been two studies in which mGPX4 was shown to play an important role in mitochondrial ROS-mediated ferroptosis but that this form of GPX4 cannot rescue cells from ferroptosis induced by genetic deletion of GPX4 (Mao et al., 2021, Wu et al., 2022b). A study conducted on a hepatic adenocarcinoma cell line demonstrated that transduction with either cGPX4 or mGPX4 was just as effective at preventing lipid oxidation and cell death induced by RSL3 or erastin (Oh et al., 2022). The authors suggested this could, in part, be due to the fact that mGPX4 can also be expressed in the cytoplasm. This is of particular relevance to our MM cells in which the mitochondrial insertion sequence appears to remain intact, suggesting non-mitochondrial localisation of this isoform. It might be that mGPX4 expression is upregulated to compensate for loss of cGPX4 activity when inhibited by RSL3, however, this cannot solely explain RSL3 resistance in KMS-11 cells given that RSL3 also triggers mGPX4 expression in ferroptosis-sensitive OPM2 cells.

The role of trace elements in ferroptosis

MM cell lines did contain higher levels of manganese (Mn) relative to DLBCL cells, however, the amount of this element did not correlate with RSL3 sensitivity (Figure 3-13B). Manganese plays a role in redox homeostasis and protects against cellular ROS by forming superoxide dismutase (MnSOD) and is a cofactor of other ferroptosis-relevant proteins, such as glutamine synthetase and acetyl-CoA carboxylase (Golara et al., 2023). In fact, poly(acrylic) acid-coated Mn_3O_4 nanoparticles have been used to decrease ferroptosis in a model of acute liver injury (Shan et al., 2023). Manganese has many cellular roles so further investigation would be required to understand whether the higher levels of manganese in MM cells are related to ferroptosis resistance. In other contexts, manganese may also promote ferroptosis through generation of H_2O_2 via the Fenton reaction (Cheng et al., 2021) or through inhibition of dihydroorotate dehydrogenase (DHODH), a ferroptosis suppressor (Zhang et al., 2022b). In our data, we observed a positive correlation between selenium (Se) and manganese levels, and while the reason for this is not fully understood, this could also explain why both selenium and manganese levels were elevated in MM levels, but only selenium was associated with RSL3 sensitivity.

GPX4 is classified as a selenoprotein and the importance of selenium for activity of GPX4 and its role in ferroptosis are well documented. We observed a positive correlation between selenium levels and sensitivity to RSL3, with higher levels of the trace element associated with an increase in the IC_{50} values for RSL3. However, selenium levels did not correlate with GPX4 expression and while this could be related to the wide

variability in the levels of both the element and the protein, it is not surprising given than GXP4 expression did not correlate with RSL3 IC_{50} (Figure 3-11D). Since selenium is involved in other cellular processes and there are other selenoproteins, it is not surprising that higher levels of selenium did not correlate with increased expression of GPX4. Selenium supplementation has been shown to increase the expression of selenoproteins, including GPX4 (Alim et al., 2019, Vande Voorde et al., 2019) but high doses of sodium selenite have also been shown to decrease GPX4 expression in ovarian cancer cells (Choi et al., 2023). Whether selenium supplementation would impact RSL3 sensitivity of MM cells is not yet known but it is worth noting that historically, GPX4 was considered to be a housekeeping protein that was not affected by selenium levels (Labunskyy et al., 2014). Furthermore, selenium nanoparticles have been shown to induce apoptosis in RPMI-8226 MM cells so increasing selenium levels might actually have a pro-cell death effect in MM (Li et al., 2022a). Additionally, the higher levels of selenium in MM cells could be due to higher expression of other selenoproteins which might affect RSL3 sensitivity, especially given that other selenoproteins like TXNRD1 have been implicated in ferroptosis resistance (Liu et al., 2021b).

Trace elements play a variety of roles in cells, and thus large screen analyses such as ICP-MS of total cellular content should only provide an indication of what avenues might be worth further investigation. No difference in iron levels were observed between MM and DLBCL cells when the lines were grouped by malignancy and there was no correlation with RSL3 IC_{50} (Figure 3-13A). Future analyses of the labile iron pool, rather than total iron, may provide further insight into differences in the levels of intracellular iron available for ferroptosis. The roles of exogenous iron in ferroptosis in MM cells is explored further in Chapter 4.

Cellular phospholipidome

Lipidomic analysis of the cellular phospholipidome of MM and DLBCL cells revealed that resistant cells (MM cell lines excluding OPM2) have a higher proportion of phospholipids containing MUFA, whereas sensitive cells (DLBCL cell lines and OPM2) have a higher percentage of PUFA-containing phospholipids (Figure 3-14B). Furthermore, sensitive cell lines also had a higher proportion of phospholipids containing AA, a PUFA known to enhance sensitivity to RSL3 (Yang et al., 2016, Kagan et al., 2017). Despite the lack of a strong Pearson correlation coefficient between RSL3 IC_{50} and lipidomic content, there was a clear difference between the phospholipidomic profile of RSL3-sensitive and -resistant cells. Increasing the number of cells lines with a wider range of RSL3 IC_{50}s may allow for a stronger correlation to emerge.

PUFA are known to drive ferroptosis (Yang et al., 2016, Kagan et al., 2017) so it is reasonable to assume that the high baseline level of these fatty acids essentially prime cells for ferroptosis. In this aspect of the study, the cells were not supplemented with different lipids or fatty acids and were maintained in the same media,

so that this baseline assessment could be used to determine whether there are inherent differences in the lipidome of cells from the two diseases. The difference in lipidomic content of cells that are sensitive versus resistant to RSL3 suggests that this form of analysis may represent a potential means of predicting ferroptosis sensitivity.

On the other hand, high levels of MUFA are known to prevent lipid oxidation, membrane damage and ferroptosis by displacing PUFA in membranes (Magtanong et al., 2019). Given that we observed similar levels of RSL3-induced lipid oxidation between the MM and DLBCL cells (Figure 3-2B), it appears that the RSL3-resistant cells may contain sufficient levels of PUFA to undergo ferroptosis, but the high proportion of MUFA act to protect the plasma membrane from damage and prevent ferroptosis-mediated death in these cells. These findings suggest that altering the lipid composition of ferroptosis-resistant cells may sensitise them to this form of programmed cell death.

3.3.5 Conclusions

Taken together, the data from this chapter clearly show that DLBCL cells are significantly more sensitive to RSL3-induced cell death compared to MM cells, with the exception of the OPM2 MM cell line. RSL3 clearly induces ferroptosis in MM and DLBCL cells, but at high doses, caspase-dependent cell death appears to contribute to the cytotoxicity of RSL3 in MM cells. We showed that the difference in RSL3 sensitivity between these cell lines is not due to differences in GPX4 protein expression or total cellular iron. We found that higher levels of selenium and higher proportions of phospholipids containing MUFA, rather than PUFA, appeared to be associated with resistance to RSL3-induced ferroptosis MM cells. These data highlight the importance of investigating whether modulating the levels of ferroptosis-related cellular components, such as lipid composition, may represent a means of sensitising MM cells to ferroptosis, which may lead to novel ways to treat this incurable cancer.

APPENDIX 3A. SUPPLEMENTARY FIGURES

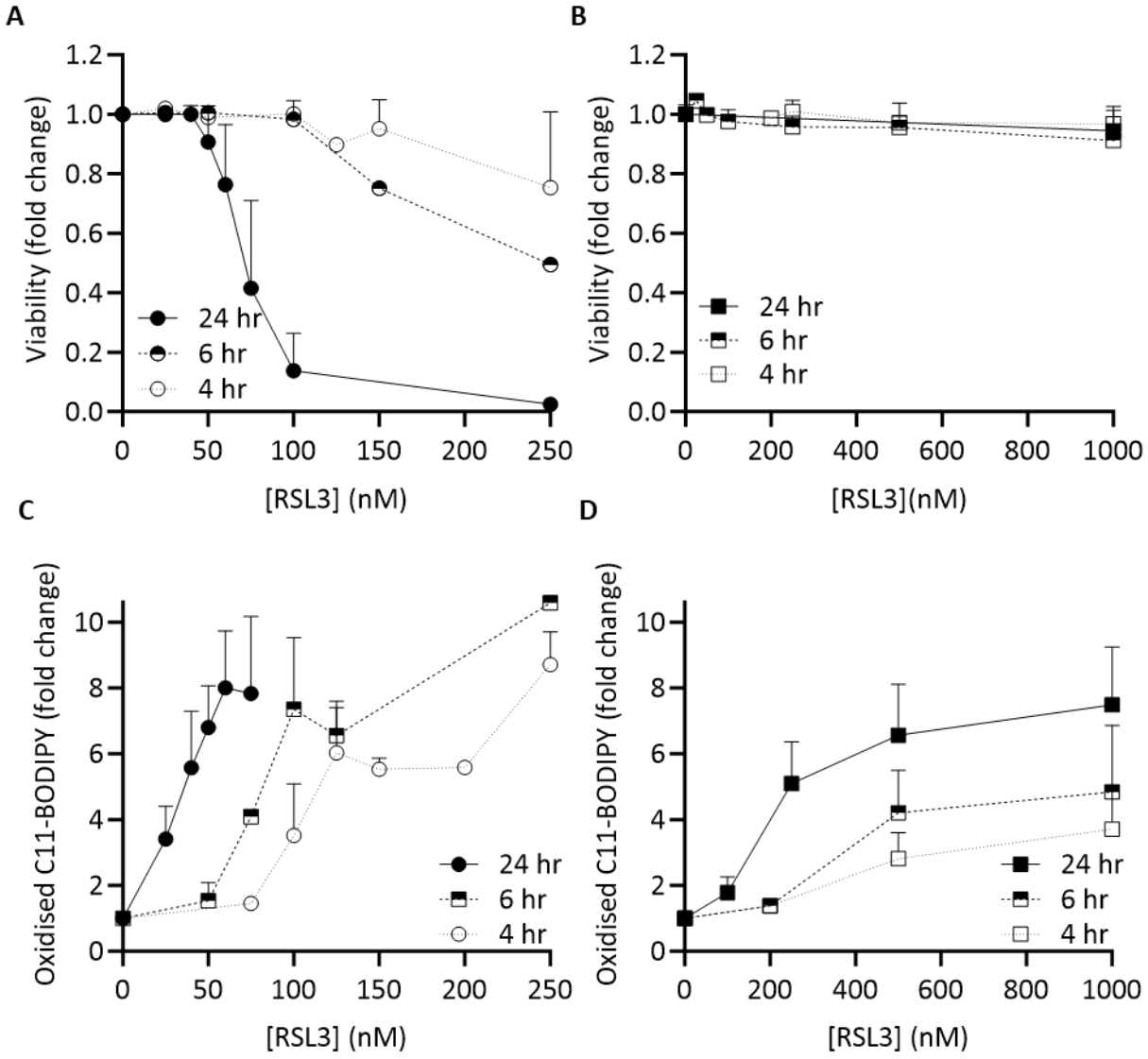

Supplementary Figure 3-A: RSL3-induced lipid peroxidation occurs as early as 4 hours post initiation of treatment.

OPM2 (A,C) and KMS-11 (B,D) cells were treated with the indicated concentrations of RSL3. After 4, 6 and 24 hours, cell viability (A,B) and lipid ROS (C,D) were measured by flow cytometry. Data are the mean ± standard deviation from at least three independent experiments.

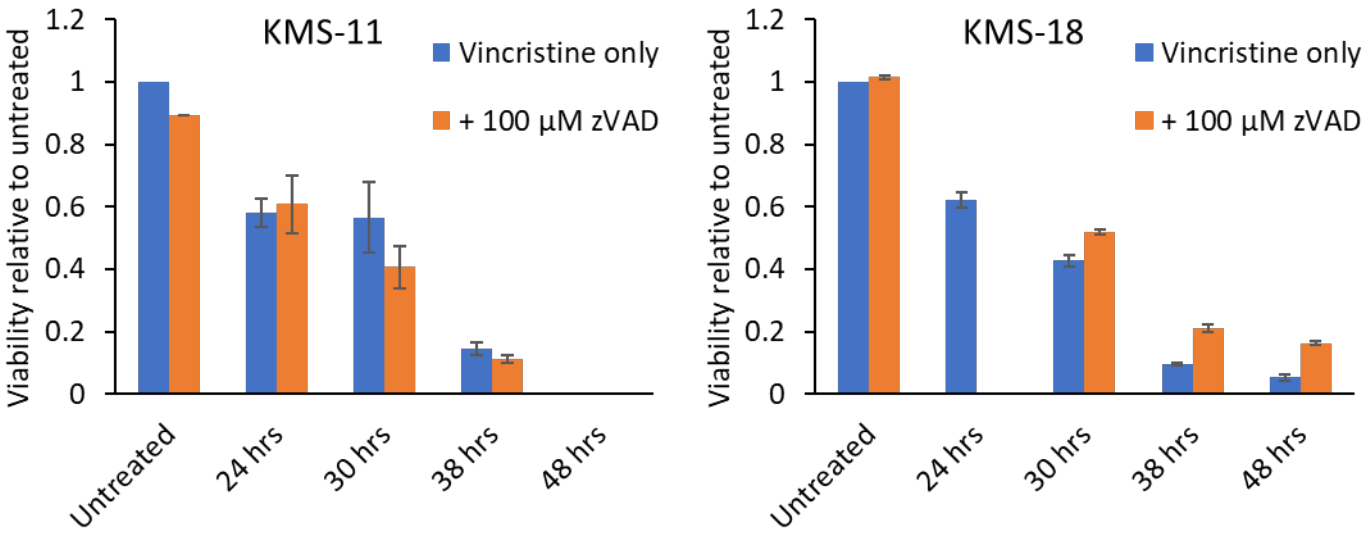

Supplementary Figure 3-B: Z-VAD-FMK does not prevent vincristine-induced cell death in KMS-11 or KMS-18 cells.

KMS-11 and KMS-18 cells were pre-treated with the pan-caspase inhibitor Z-VAD-FMK for 45 minutes, followed by treatment with 50 nM vincristine for up to 48 hours. Cell viability was assessed by flow cytometry. Data are the mean ± standard deviation from two technical replicates.

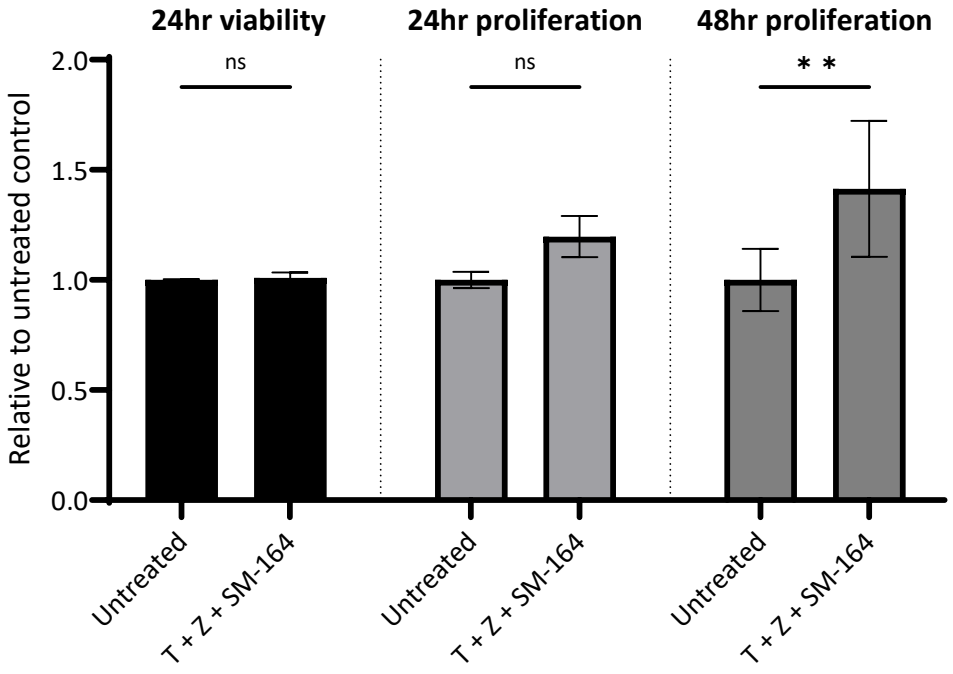

Supplementary Figure 3-C: The combination of Z-VAD-FMK, TNF-α and SM-164 does not reduce cell viability or proliferation in OPM2 MM cells.

OPM2 cells were preincubated in 200 µM Z-VAD-FMK (Z) for 45 minutes before 20 ng/mL tumour necrosis factor (TNF)-α (T) and 100 nM SM-164 was added. After 24 hours, cell viability was measured by flow cytometry. After 24 and 48 hours, cell proliferation was measured by MTT assay. Data are the mean ± standard deviation from two independent experiments. Statistical analyses were performed by two-way ANOVA with an uncorrected Fisher's least significant difference test for multiple comparisons; ns indicates no significant difference, ** $p<0.01$.

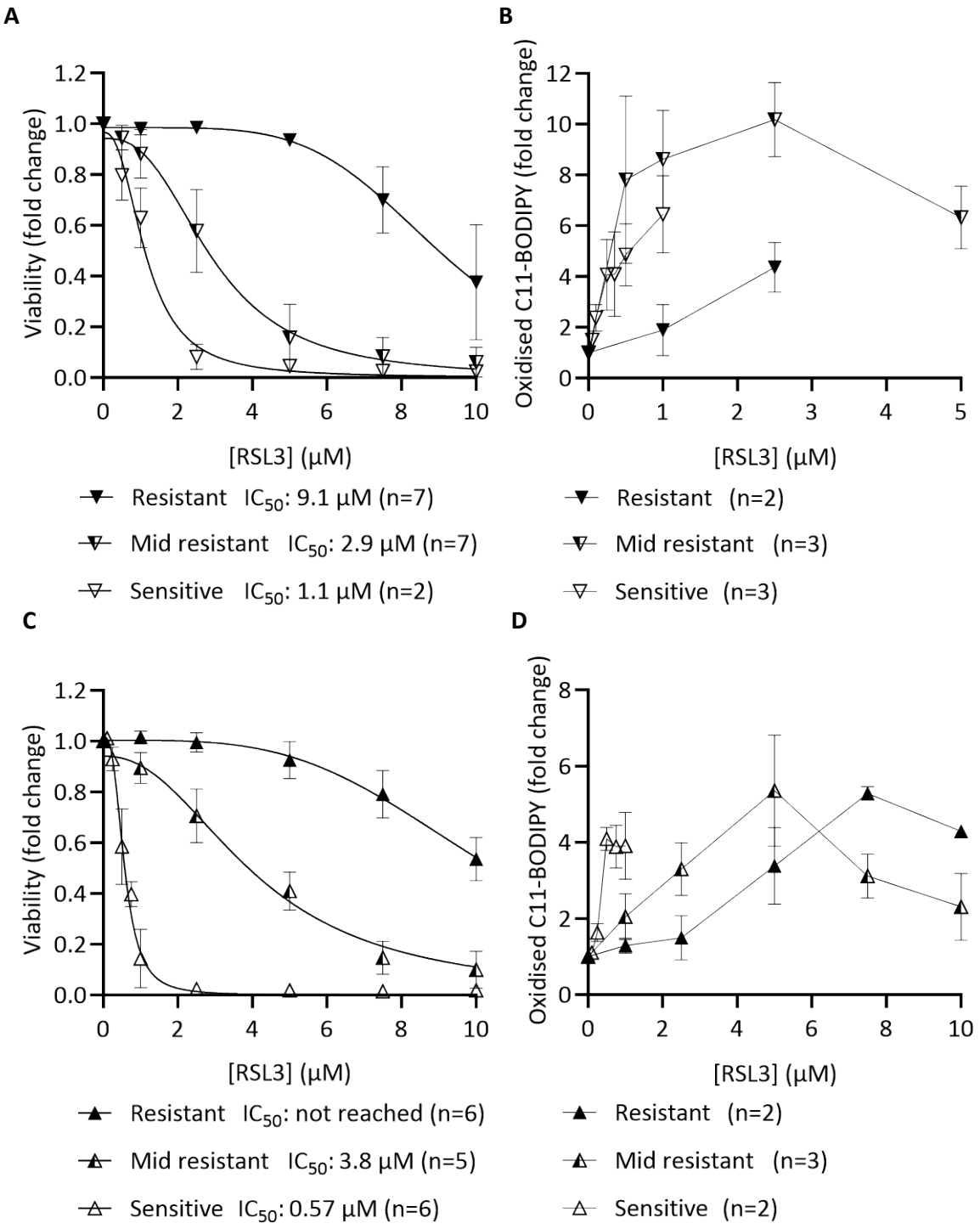

Supplementary Figure 3-D: LP-1 and KMS-18 cells have variable responses to RSL3 treatment.

LP-1 (top) and KMS-18 (bottom) cell lines were treated with the indicated concentrations of RSL3 for 24 hours and cell viability (A,B) and corresponding oxidised C11-BODIPY (C,D) were measured after 24 hours. Data are the mean ± standard deviation from the indicated number of independent experiments.

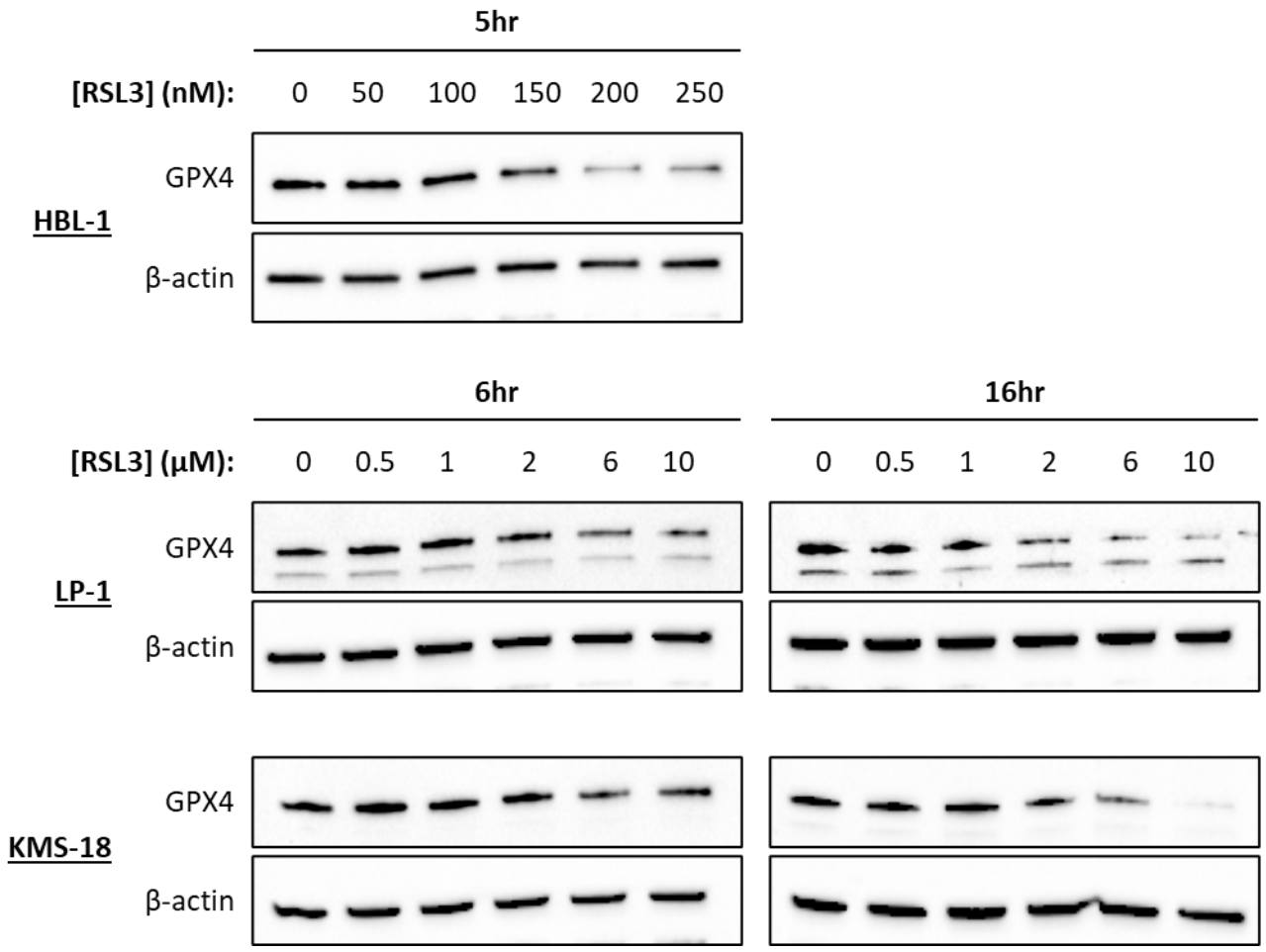

Supplementary Figure 3-E: RSL3 causes GPX4 protein degradation in LP-1, KMS-18 and HBL-1 cells.

Cells were treated with the indicated concentrations of RSL3 and protein extracted after 5, 6 or 16 hours. Western blots were probed for GPX4, with β-actin expression assessed as a loading control.

CHAPTER 4. ARACHIDONIC ACID AND IRON INCREASE THE EFFECTS OF RSL3 IN MM CELLS

4.1 Introduction

In Chapter 3, Aim 1 to "investigate the susceptibility of MM and DLBCL cells to ferroptosis" was addressed. It was established that MM cells (excluding OPM2) are more resistant to RSL3-induced ferroptosis compared to DLBCL cells. Building on this, in this chapter we aimed to investigate the susceptibility of MM and DLBCL cells to RSL3 in the presence of pro-ferroptotic substrates.

It has been reported that phospholipids containing polyunsaturated fatty acids (PUFA) are far more readily oxidised compared to those that contain monounsaturated fatty acids (MUFA) or saturated fatty acids (SFA) (Yang et al., 2016, Kagan et al., 2017). In particular, the PUFA arachidonic acid (AA), has been shown to sensitise cells from healthy human skin, human fibrosarcoma, Wilms' tumours, clear cell carcinoma and mouse embryonic fibroblasts (MEFs) to ferroptosis induced by RSL3 (Yang et al., 2016, Kagan et al., 2017, Zou et al., 2019). In intestinal-type gastric cancer cells which have reduced levels of AA, supplementation with 2.5 µM AA sensitised these ferroptosis-resistant cells to RSL3 (Lee et al., 2020). Furthermore, the omega-6 fatty acids linoleic acid and AA, and not the omega-3 fatty acid eicosapentaenoic acid, induced an increase in cell death when GPX4 expression was ablated (Seiler et al., 2008). Conversely, supplementing cells with monounsaturated fatty acids can confer resistance to ferroptosis by displacing more readily oxidised phospholipids (Magtanong et al., 2019).

In MM, high concentrations of AA as a monotherapy have been shown to induce ferroptotic and apoptotic related cell death *in vitro* and in mouse models (Panaroni et al., 2018). We showed in Chapter 3 that RSL3-sensitive DLBCL and OPM2 MM cells have a higher proportion of PUFA than MUFA, in contrast to resistant MM cells that have a higher proportion of MUFA. Moreover, RSL3-sensitive DLBCL and OPM2 MM cells had a higher proportion of phospholipids containing AA so in this chapter we sought to investigate whether exogenous AA can prime resistant MM cells to ferroptosis-mediated death in response to RSL3.

Since iron plays a major role in ferroptosis, it was also hypothesised that iron levels may, in part, play a role in the sensitivity of MM cells to this mechanism of cell death. Although we did not observe lower levels of total iron in ferroptosis resistant cells compared to sensitive cells in Chapter 3, recent reports suggest that exogenous iron increases the sensitivity of primary endometrial stroma, ovarian cancer, fibrosarcoma and prostate cancer cells to ferroptosis (Luo et al., 2024, Huan et al., 2024, Maccarinelli et al., 2023, Li et al., 2021).

Furthermore, the effects of modulating iron levels appear to vary depending on the context; for example both ferric ammonium citrate (FAC) and iron chelation induce death and cause an increase in general and lipid ROS in rhabdomyosarcoma cells (Asperti et al., 2023), whereas FAC has no effect on prostate cancer cell growth (Maccarinelli et al., 2023). In MM cells, the effects of iron supplementation appear to be cell line and/or concentration dependent. In ARP1 or OCI-My5 MM cells, up to 500 μM FAC does not affect cell proliferation (Gu et al., 2015), but another study showed that 600 μM FAC caused death of MM.1S and U266 MM cells (Bordini et al., 2020). Interestingly, reducing the labile iron pool (LIP) through iron chelation suppresses MM cell growth (Gu et al., 2015). While FAC does not affect prostate cell proliferation, it does cause a reduction in the expression of the iron import protein, transferrin receptor (TfR) and a marked increase in the expression of the iron storage protein, FTH1; despite these efforts to reduce the LIP in response to FAC, the cells became more sensitive to the cytotoxic effects of RSL3 and their migration capacity significantly decreased in a wound healing assay (Maccarinelli et al., 2023). The effects of RSL3 in combination with FAC were attributed to ferroptosis since they were inhibited by Fer-1, the treatment resulted in a significant accumulation of mitochondrial and lipid ROS, and a ferroptosis-associated gene expression profile was observed (Maccarinelli et al., 2023). These findings were also observed in a mouse xenograft model of prostate cancer, in which the combination of iron dextran and RSL3 was found to be significantly more effective at reducing tumour volume than either agent alone. There were also no measurable side effects, and similar findings were demonstrated in an immune-competent mouse model (Maccarinelli et al., 2023). Given the low toxicity of iron and its prevalent use in the clinic, these studies provide the rationale for investigating whether supplementation with iron increases the efficacy of ferroptosis-inducing agents, such as RSL3, in MM cells.

Bordini *et al.* showed that iron increased the cytotoxic effects of bortezomib in MM cells and a MM mouse model, and that ferroptosis played a role in the observed responses (Bordini et al., 2020). Recently, it was shown that increasing cellular iron levels through ferritinophagy could enhance the effects of RSL3 in MM cell lines and patient-derived cells (Zhang et al., 2024c). The authors found that relative to healthy peripheral blood mononuclear cells, MM cell lines (ARP1, OCI-My5, KMS28-PE, RPMI-8226 and MM.1S) had significantly lower levels of *SLC40A1* (encodes the iron export protein ferroportin (FPN)), while they had increased expression of *TFRC* (encodes TfR) (Zhang et al., 2024c). In correlation with this gene expression profile, MM cell lines were found to have higher levels of intracellular iron, and primary $CD138^+$ MM cells had a higher level of the iron storage protein, FTH1, relative to patient-matched $CD138^-$ cells. Knockdown of nuclear receptor coactivator 4 (NCOA4), led to an increase in FTH1 and decrease in free iron, while bortezomib effectively prevented the degradation of both NCOA4 and STEAP3, allowing for NCOA4-mediated ferritinophagy to occur. Accordingly, RSL3 and bortezomib caused a synergistic reduction in cell viability of MM cell lines and $CD138^+$ cells derived from six patients with MM. The synergy between RSL3 and bortezomib

in MM cell lines was prevented by Lip-1 and was associated with an increase in both malondialdehyde (MDA) and lipid ROS, supporting the notion that ferroptosis was involved (Zhang et al., 2024c). Collectively, these studies suggest that increasing the level of intracellular iron represents an effective means of enhancing the sensitivity of MM cells to ferroptosis.

4.2 Results

4.2.1 Expression of phospholipidome-related genes and proteins

Given the relevance of the phospholipidomic composition of MM and DLBCL cells in the context of ferroptosis sensitivity, first we investigated the basal expression of the genes and proteins introduced in Figure 1-1 that are involved in the re-modelling of phospholipids. Expression of the acyl-CoA synthetase long-chain family 4 (ACSL4) enzyme, which primes PUFA for insertion into phospholipids, varied between the MM and DLBCL cell lines, with no protein observed in SU-DHL-8 DLBCL cells (Figure 4-1A,B). However, these results are not conclusive as the gene encoding ACSL4 contain a single nucleotide variant which causes a premature stop codon in SU-DHL-8 cells, resulting in a protein that lacks the epitope to which the antibody binds. In fact, SU-DHL-8 cells do express *ACSL4* transcript, albeit at low levels relative to the other cell lines (Figure 4-1D) (The Human Protein Atlas, 2023b). ACSL4 protein expression correlated with the IC_{50} of RSL3 in MM cells, with a higher expression of the protein strongly correlating with a lower RSL3 IC_{50}. However, no correlation between ACSL4 expression and RSL3 IC_{50} was observed in the DLBCL cells alone, or when data from the MM and DLBCL lines was combined (data from SU-DHL-8 cells were excluded) (Figure 4-1C). Publicly available gene expression of lipid-related genes relevant to ferroptosis (*ACSL3*, *ACSL4*, *LPCAT3* and *ALOX15*) were assessed and the only statistically significant difference was between RSL3-sensitive (OPM2 and DLBCL lines, HBL-1 data not available) versus resistant cell lines, where sensitive cells had a higher expression of *LPCAT3* ($p = 0.0250$) (Figure 4-1D) (The Human Protein Atlas, 2023a). However, no statistically significant differences were observed between the MM and DLBCL cell lines.

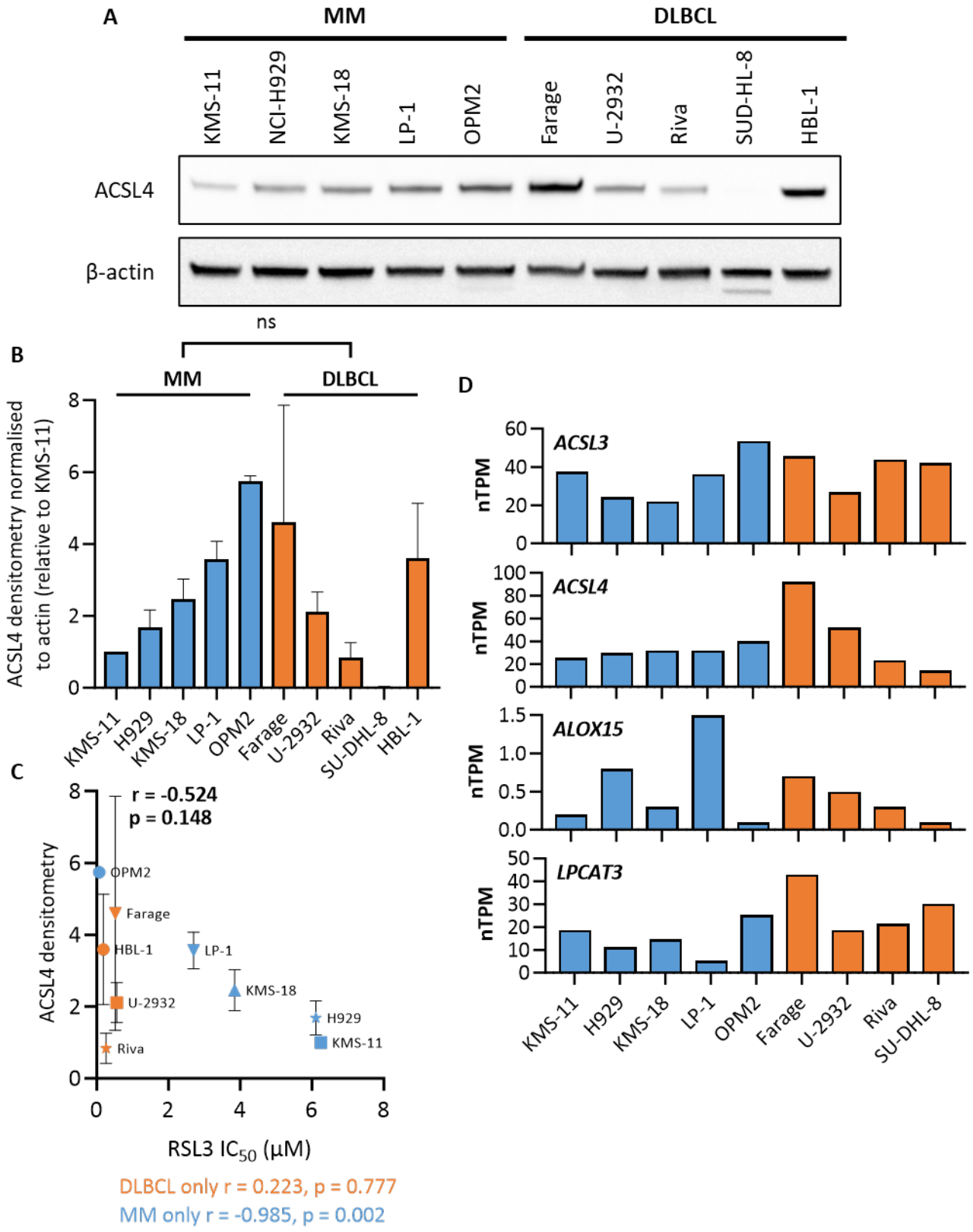

Figure 4-1: ACSL4 expression correlates with MM cell sensitivity to RSL3.

(A) Representative western blot of untreated MM and DLBCL cells, probed for ACSL4 with β-actin as a loading control. (B) Western blot densitometry data are mean (normalised to actin, relative to KMS-11) ± standard deviation from three independent experiments. An unpaired t-test was used for statistical analysis of MM vs. DLBCL. (C) A Pearson correlation was performed for ACSL4 protein expression against RSL3 IC_{50} from Table 3-1. The Pearson correlation coefficient (r) and p-value (p) are displayed. (D) Normalised gene transcript

expression (nTPM) of *ACSL3*, *ACSL4*, *LPCAT3* and *ALOX15* for MM and DLBCL cell lines. Data were derived from The Human Protein Atlas (The Human Protein Atlas, 2023a, The Human Protein Atlas, 2023b, The Human Protein Atlas, 2023c, The Human Protein Atlas, 2023g).

4.2.2 AA-induced changes in the expression of phospholipidome-related genes and proteins

Since AA has been shown to play an important role in ferroptosis, we investigated whether supplementing MM cells with AA +/- RSL3 has an effect on the expression of phospholipidome-related genes and proteins. Supplementing OPM2 cells with 60 µM AA for 6 hours did not appear to significantly affect the expression of GPX4 or ACSL4 (Figure 4-2A,B). As shown earlier (Figure 3-12), RSL3 increases the expression of GPX4 in OPM2 cells and the addition of 60 µM AA had no effect on this response (Figure 4-2B). Furthermore, AA had no effect on the expression of the two GPX4 bands induced by RSL3 (Figure 4-2A). There was a non-significant trend towards increased expression of ACSL4 in OPM2 cells following treatment with RSL3, which was inhibited by AA. However, the effect of AA on ACSL4 expression was only significant in cells treated with 50 nM RSL3 ($p = 0.0193$ for 50 nM RSL3 vs. 50 nM RSL3 + 60 µM AA) (Figure 4-2B). In KMS-11 cells, a 6-hour incubation with 60 µM AA on its own caused a small but not statistically significant decrease in GPX4 expression. However, AA prevented the RSL3-induced increase in GPX4 expression (Figure 4-2C,D). RSL3 alone had no significant effect on expression of ACSL4, but an approximate 2-fold decrease in expression was observed in cells treated with 60 µM AA, irrespective of the RSL3 concentration (Figure 4-2C,D).

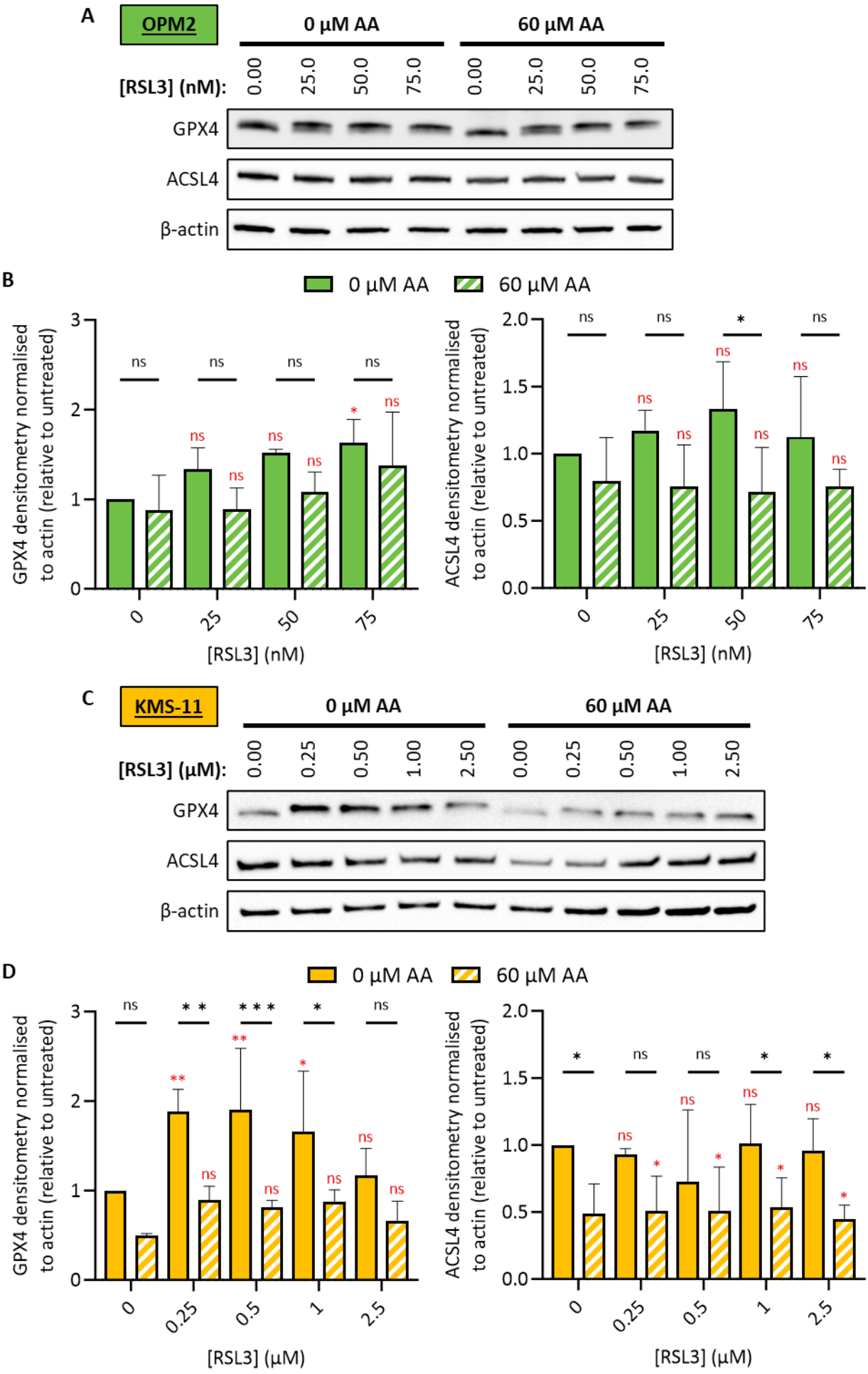
A
OPM2
0 µM AA
60 µM AA
[RSL3] (nM):
0.00
25.0
50.0
75.0
GPX4
ACSL4
β-actin
B
0 µM AA
60 µM AA
GPX4 densitometry normalised to actin (relative to untreated)
ACSL4 densitometry normalised to actin (relative to untreated)
[RSL3] (nM)
C
KMS-11
[RSL3] (µM):
0.00
0.25
0.50
1.00
2.50
D
[RSL3] (µM)

Figure 4-2: Arachidonic acid causes a decrease in GPX4 and ACSL4 protein expression in resistant KMS-11, but not sensitive OPM2 cells.

OPM2 and KMS-11 cells were treated with RSL3 ± 60 µM arachidonic acid (AA) and protein extracted after 6 hours. (A,C) Western blots were probed for GPX4 and ACSL4, with β-actin as a loading control. (B,D) Densitometry data are the mean ± standard deviation from three independent experiments, relative to untreated control (images of other Western blot replicates are included in Supplementary Figure 4-A). Statistical analyses were performed by two-way ANOVA with an uncorrected Fisher's least significant difference test for multiple comparisons; ns indicates no significant difference, * p<0.05, ** p<0.01. Statistics shown in red are relative to untreated control.

4.2.3 Arachidonic acid supplementation sensitises multiple myeloma cells to ferroptosis

Treatment of LP-1 and KMS-18 MM cells with 500 nM RSL3 and 100 µM AA individually had no significant effect on cell viability. However, in combination the agents reduced cell viability to 1.71% and 20.7%, respectively, which was preventable by Lip-1 (Supplementary Figure 4-B).

However, in OPM2 cells, 100 µM AA alone reduced cell viability by 60%, and this cell death could not be prevented with Lip-1 (Figure 4-3A). This is consistent with a previous study in which AA was shown to induce apoptosis in OPM2 cells (Abdi et al., 2014). A dose response analysis of AA was therefore performed to determine whether lower doses of AA could enhance the effects of RSL3 without causing significant cytotoxicity on its own. In OPM2 cells, 20 µM AA had no effect, but 50 and 60 µM AA significantly increased the cytotoxicity of RSL3, effectively halving its IC_{50} from 60.1 nM to 34.0 and 30.9 nM, respectively (Figure 4-3A, Table 4-1). The combined cytotoxic effect of RSL3 and AA was prevented with the addition of Lip-1, confirming ferroptosis as the mechanism of action (Figure 4-3A). Interestingly however, the addition of AA did not result in an increase in lipid oxidation, despite prevention of cell death by Lip-1 and morphological changes consistent with ferroptosis (Figure 4-3B,C).

Table 4-1: RSL3 IC_{50} values for MM cell lines treated with RSL3 + AA.

Mean RSL3 IC_{50} ± SD generated by fitting a sigmoidal 4PL curve for each biological replicate from Figure 4-3A and Figure 4-4A (constraints used were bottom = 0, top < 1).

	RSL3 IC_{50} (nM) ± SD				
Cell line	**RSL3 only**	**RSL3 + 20 µM AA**	**RSL3 + 50 µM AA**	**RSL3 + 60 µM AA**	**RSL3 + 100 µM AA**
KMS-11	6637 ± 2344	2889 ± 646 *	1735 ± 370 ***	792 ± 539 ***	554 ± 254 ***
OPM2	60.1 ± 14.3	51.1 ± 11.1 ns	34.0 ± 8.29 **	30.9 ± 10.8 ***	7.58 ± 4.48 ***

Statistical analyses performed by one-way ANOVA with a Tukey's multiple comparisons test; ns, not significant, * p<0.05, ** p<0.01, *** p<0.001 relative to RSL3 only.

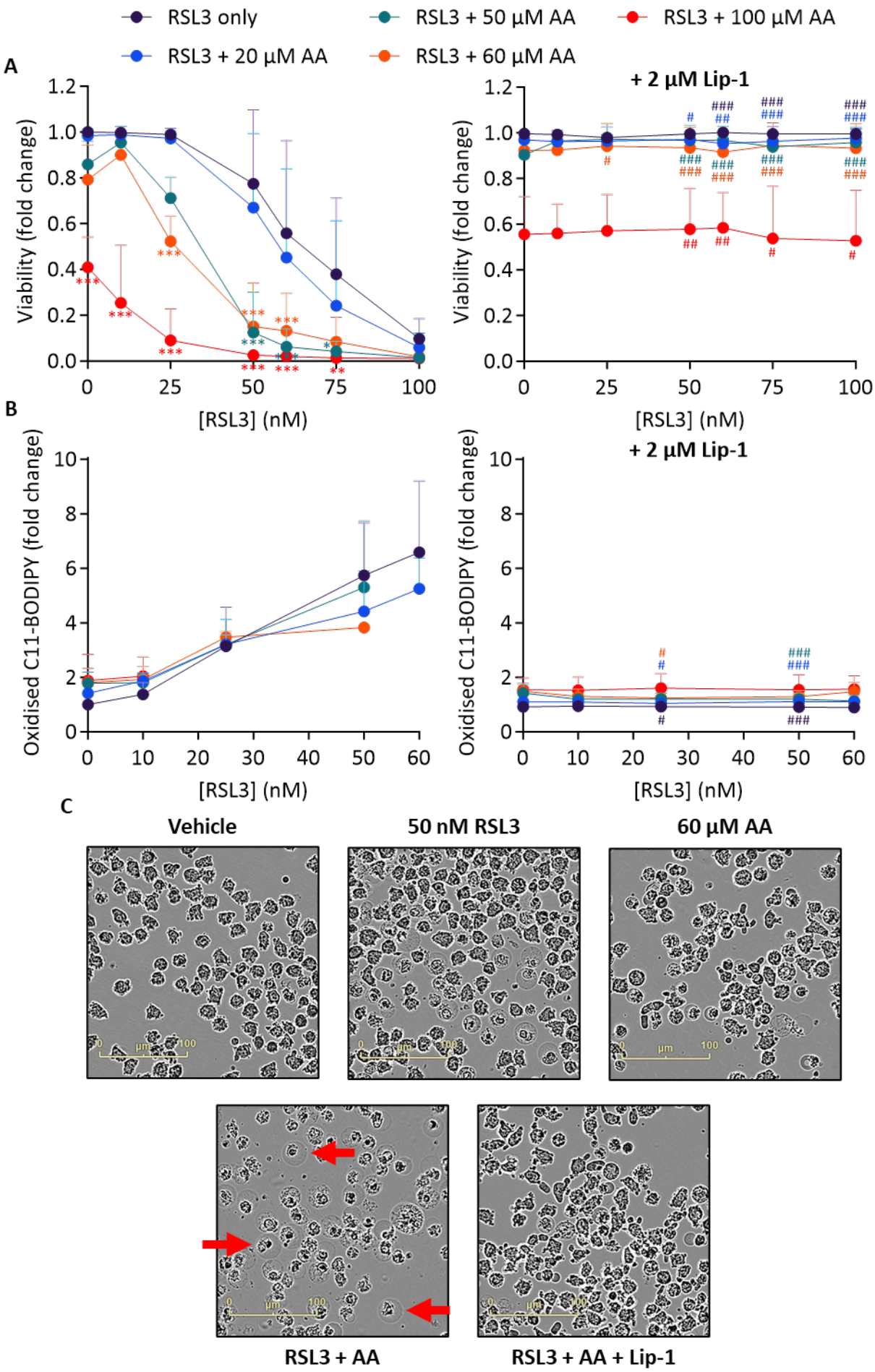
RSL3 only
RSL3 + 20 µM AA
RSL3 + 50 µM AA
RSL3 + 60 µM AA
RSL3 + 100 µM AA
A
Viability (fold change)
[RSL3] (nM)
+ 2 µM Lip-1
B
Oxidised C11-BODIPY (fold change)
C
Vehicle
50 nM RSL3
60 µM AA
RSL3 + AA
RSL3 + AA + Lip-1

Figure 4-3: AA increases the cytotoxic effects of RSL3 in OPM2 cells.

OPM2 cells were treated with combinations of RSL3, arachidonic acid (AA) and 2 μM liproxstatin-1 (Lip-1). Cell viability (A) and the levels of oxidised C11-BODIPY (B) were measured after 24 hours. Data are mean ± standard deviation from at least three independent experiments. Statistical analyses were performed by two-way ANOVA with a Tukey's multiple comparisons test; * $p<0.05$, ** $p<0.01$, *** $p<0.001$ for RSL3+AA relative to RSL3 only for each respective AA dose (as per colour); # $p<0.05$, ## $p<0.01$, ### $p<0.001$ RSL3 + AA + Lip-1 relative to RSL3 + AA for each respective AA dose (as per colour); no notation made if $p>0.05$. (C) OPM2 cells were treated with 50 nM RSL3, 60 μM AA and/or 2 μM Lip-1 with images acquired after 24 hours using an Incucyte Live Cell Imager. Red arrows indicate cells displaying the "ballooning" phenotype that is characteristic of ferroptosis.

Similar findings were observed in ferroptosis-resistant KMS-11 cells, with the exception that treatment with 100 μM AA alone resulted in only a 23% decrease in cell viability, which was not prevented by Lip-1. Unlike in OPM2, however, doses as low as 20 μM AA could effectively enhance the cytotoxic effect of RSL3 and resulted in a statistically significant reduction in the IC_{50} value for RSL3 (Figure 4-4A, Table 4-1). As with OPM2 cells, AA did not increase the levels of lipid oxidation induced by RSL3 in KMS-11 cells (Figure 4-4B). The combination of 1 μM RSL3 and 100 μM AA caused a statistically significant reduction in the levels of oxidised lipids compared to RSL3 alone ($p = 0.0014$), but this may be due to the increased permeability of dying cells, which results in less retention of the dye; this was also consistently observed in cells treated with lethal doses of RSL3. Nevertheless, Lip-1 was able to prevent cell death by reducing levels of oxidised lipids, but was less effective at preventing cell death in cells treated with >5 μM RSL3 (Figure 4-4A,B). To further confirm ferroptosis was occurring, the morphology of KMS-11 cells treated with 2.5 μM RSL3 and 60 μM AA was examined, and clearly showed a proportion of cells with morphological changes associated with ferroptosis, which was prevented by simultaneous treatment with Lip-1 (Figure 4-4C).

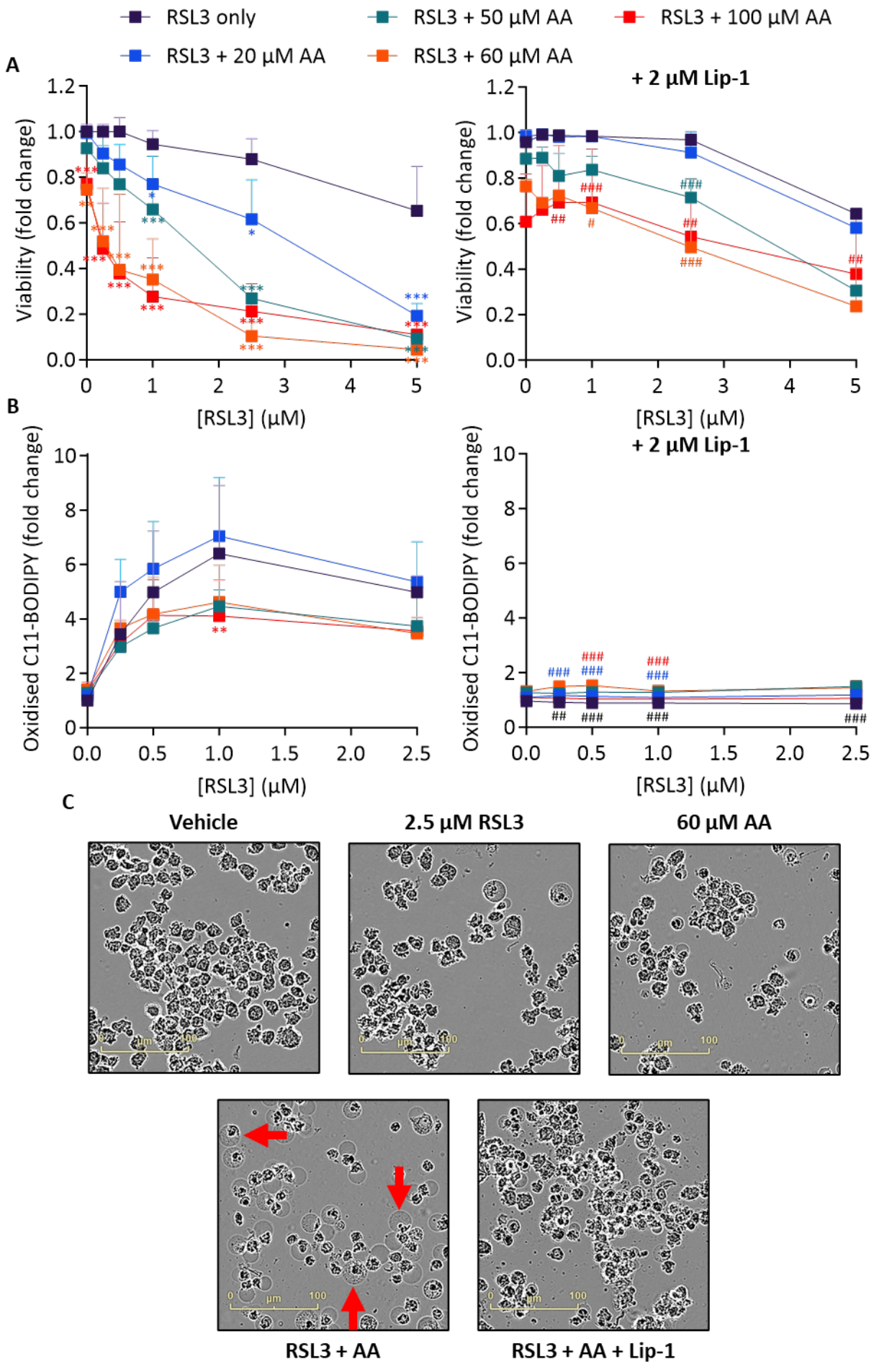
RSL3 only
RSL3 + 20 µM AA
RSL3 + 50 µM AA
RSL3 + 60 µM AA
RSL3 + 100 µM AA
A
Viability (fold change)
[RSL3] (µM)
+ 2 µM Lip-1
B
Oxidised C11-BODIPY (fold change)
[RSL3] (µM)
+ 2 µM Lip-1
C
Vehicle
2.5 µM RSL3
60 µM AA
RSL3 + AA
RSL3 + AA + Lip-1

Figure 4-4: AA increases the cytotoxic effects of RSL3 in KMS-11 cells.

KMS-11 cells were treated with combinations of RSL3, arachidonic acid (AA) and 2 µM liproxstatin-1 (Lip-1). Cell viability (A) and the levels of oxidised C11-BODIPY (B) were measured after 24 hours. Data are the mean ± standard deviation from at least three independent experiments. Statistical analyses were performed by two-way ANOVA with a Tukey's multiple comparisons test; * p<0.05, ** p<0.01, *** p<0.001 for RSL3+AA relative to RSL3 only for each respective AA dose (as per colour); # p<0.05, ## p<0.01, ### p<0.001 RSL3 + AA + Lip-1 relative to RSL3 + AA for each respective AA dose (as per colour); no notation made if p>0.05. (C) KMS-11 cells were treated with 2.5 µM RSL3, 60 µM AA and/or 2 µM Lip-1 with images acquired after 24 hours using an Incucyte Live Cell Imager. Red arrows indicate cells displaying the "ballooning" phenotype that is characteristic of ferroptosis.

Using the fractional product method (Webb, 1963) it was determined that synergy between AA and RSL3, in terms of their cytotoxic effects, was apparent in both OPM2 and KMS-11 cells (Figure 4-5). In OPM2 cells, the results appeared to suggest antagonism between 10 nM RSL3 and 50 or 60 µM AA, associated with reduced effects of the combination compared to AA alone. However, this is likely due to a high degree of variability between the replicate experiments for AA alone. Regardless, at concentrations of RSL3 of 25 nM and above, addition of 50, 60 or 100 µM AA had a synergistic effect on cell viability. Synergy was also observed between RSL3 and AA in KMS-11 cells, with the highest degree of synergy observed at the mid-range concentrations of each agent (2.5 µM RSL3 + 50 or 60 µM AA).

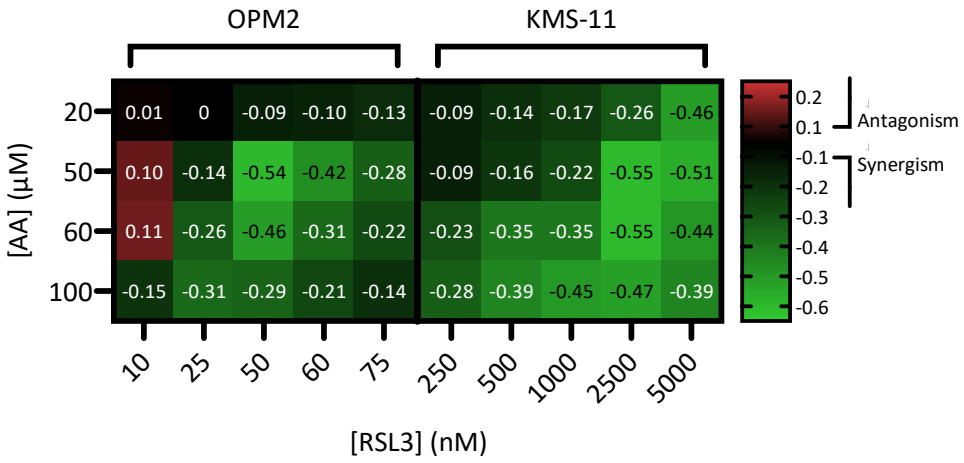

Figure 4-5: Synergistic effects of RSL3 combined with AA in OPM2 and KMS-11 MM cells.

Using the fractional product (FP) method (Webb, 1963), the combined effect of RSL3 and AA in OPM2 and KMS-11 cells was investigated using average viability data from Figure 4-3A and Figure 4-4A. An FP of less than -0.1 indicates synergy (green) whereas an FP greater than 0.1 is classified as an antagonistic effect (red).

4.2.4 Basal expression of iron-related genes and proteins

Given the importance of iron in ferroptosis, we investigated the expression of the genes and proteins displayed in Figure 1-1 that are involved in the import, storage and export of iron in MM and DLBCL cells. Expression of the iron import protein, TfR, was investigated by Western blot and while most cell lines had similar levels of expression, LP-1 MM cells had relatively high expression, whereas Riva DLBCL cells had no detectable band at the expected 90 kDa (Figure 4-6A,B). Levels of ferritin heavy chain (FTH1) were also measured by western blot. Protein bands were evident in all the cell lines, albeit at lower levels in the MM compared to the DLBCL lines. In 4/5 DLBCL and 1/5 MM lines, two bands were observed at approximately 20 kDa (Figure 4-6A). Repeats of these Western blots were not undertaken so Pearson correlations were not performed to determine whether there was a relationship between the expression of these proteins and RSL3 sensitivity.

Next, we interrogated publicly available data concerning the expression of iron-related genes that are known to play a role in ferroptosis (*FTH1*, *FTL, TFRC*, *SLC40A1* and *NCOA4*). No statistically significant differences between DLBCL (HBL-1 data not available) versus MM, or sensitive (OPM2 and DLBCL cell lines) versus resistant (MM cell lines excluding OPM2) were observed (Figure 4-6D) (The Human Protein Atlas, 2023d, The Human Protein Atlas, 2023k, The Human Protein Atlas, 2023h, The Human Protein Atlas, 2023e, The Human Protein Atlas, 2023l).

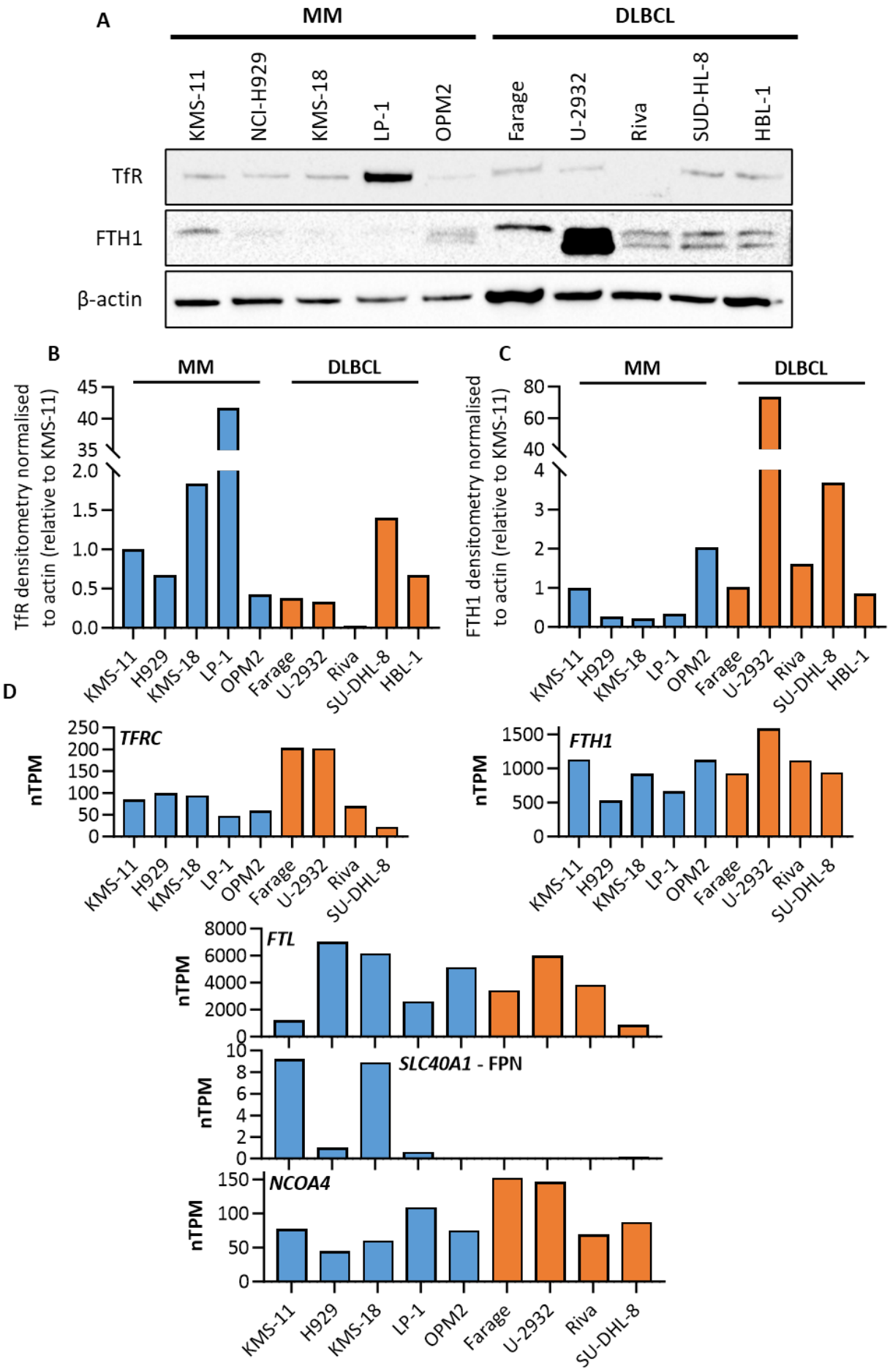

Figure 4-6: Basal expression of iron-related proteins in MM and DLBCL cells.

(A) Western blot of untreated MM and DLBCL cells, probed for transferrin receptor (TfR) and ferritin heavy chain (FTH1) with β-actin as a loading control. (B,C) Western blot densitometry data from one independent experiment, normalised to β-actin, relative to KMS-11. (D) Normalised gene transcript expression (nTPM) of *FTL*, *FTH1*, *TFRC*, *SLC40A1* and *NCOA4* for MM and DLBCL cell lines (data from HBL-1 cells was unavailable), taken from The Human Protein Atlas (The Human Protein Atlas, 2023d, The Human Protein Atlas, 2023k, The Human Protein Atlas, 2023h, The Human Protein Atlas, 2023e, The Human Protein Atlas, 2023l).

4.2.5 FAC-induced changes in the expression of iron-related genes and proteins

Next, the expression of these iron-related genes was investigated following supplementation with FAC +/- RSL3 to elucidate how OPM2 and KMS-11 cells respond to exogenous iron during ferroptosis. In OPM2 cells, the addition of FAC resulted in a reduction in expression of TfR in individual biological replicates (Figure 4-7A). However, due to biological variability, no significant changes in expression were observed when the densitometry data from three biological replicates were combined (Figure 4-7B). Similarly, treatment of OPM2 cells with FAC increased expression of FTH1, but variability in the baseline expression of FTH1 resulted in large error bars, which again impacted the statistical significance of the densitometric data (Figure 4-7B). In KMS-11 cells, FAC caused a small, but not significant reduction in TfR ($p = 0.0770$) and a significant increase in FTH1 expression ($p = 0.0080$) (Figure 4-7D). RSL3 on its own had no effect on the expression of TfR or FTH1 in either OPM2 or KMS-11 cells.

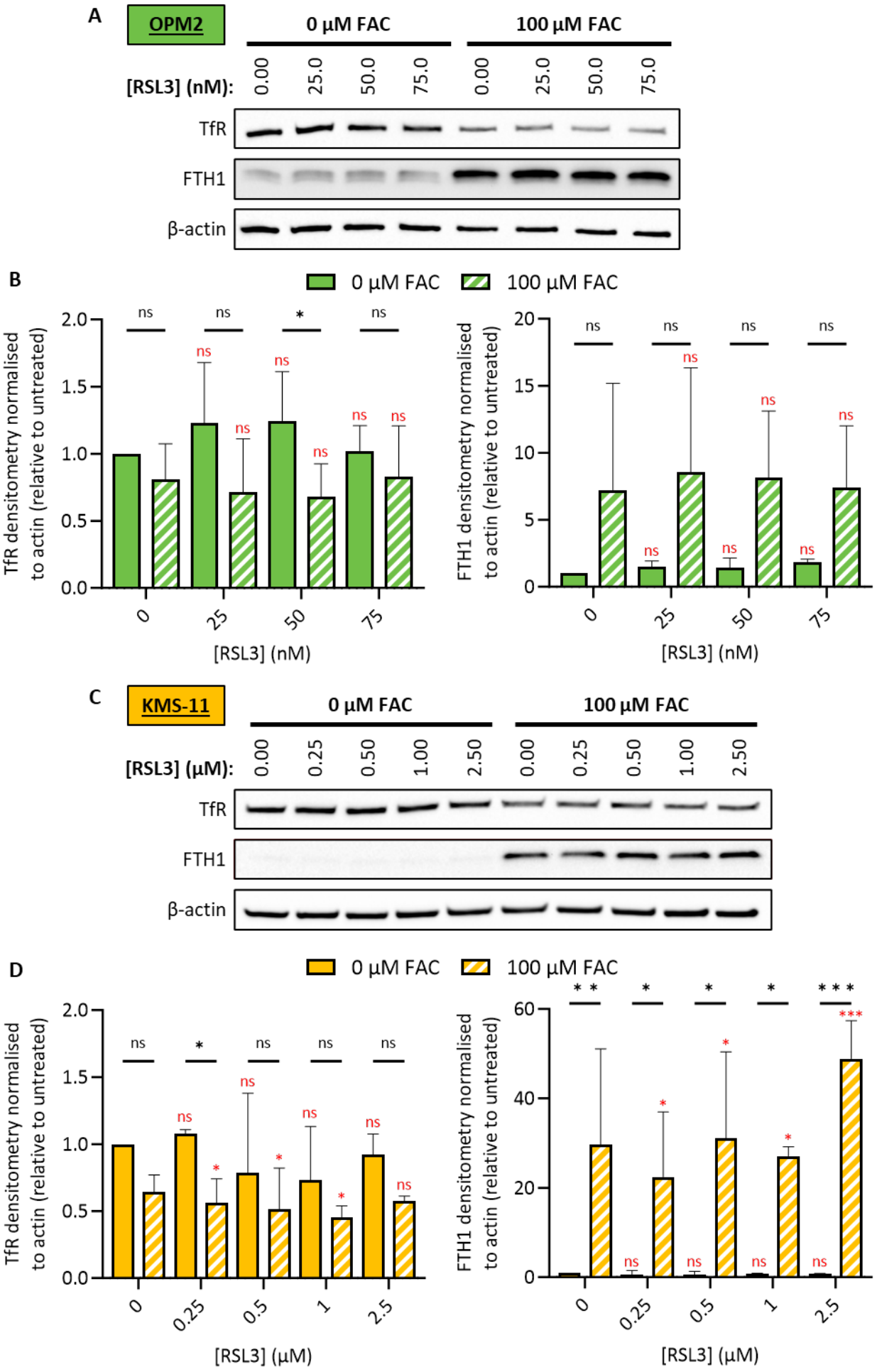
A
OPM2
0 µM FAC
100 µM FAC
[RSL3] (nM):
0.00
25.0
50.0
75.0
TfR
FTH1
β-actin
B
0 µM FAC
100 µM FAC
TfR densitometry normalised to actin (relative to untreated)
FTH1 densitometry normalised to actin (relative to untreated)
[RSL3] (nM)
C
KMS-11
[RSL3] (µM):
0.00
0.25
0.50
1.00
2.50
D
[RSL3] (µM)

Figure 4-7: Exogenous iron modulates the expression of iron-related proteins in MM cells.

OPM2 and KMS-11 cells were treated with RSL3 ± 100 μM ferric ammonium citrate (FAC) for 6 hours before harvesting for protein extraction. (A,C) Western blot probed for transferrin receptor (TfR) and ferritin heavy chain (FTH1), using β-actin as a loading control. (B,D) Densitometry data are the mean ± standard deviation from three independent experiments (images of replicate Western blot data can be found in Supplementary Figure 4-C). Statistical analyses were performed by two-way ANOVA with an uncorrected Fisher's least significant difference test for multiple comparisons; ns indicates no significant difference, * $p<0.05$, ** $p<0.01$, *** $p<0.001$, **** $p<0.0001$. Statistics in red are relative to untreated control.

4.2.6 Iron supplementation sensitises multiple myeloma cells to ferroptosis

MM cell lines (KMS-11, KMS-18, LP-1 and OPM2) were treated with FAC in combination with RSL3 for 24 hours. As a single agent, 100 μM FAC had no effect on cell viability. However, in combination with RSL3, we observed a significant reduction in cell viability (Figure 4-8). FAC reduced the IC_{50} of RSL3 by 67, 88, 67 and 31% in KMS-11, KMS-18, LP-1 and OPM2 cells, respectively (Table 4-2).

Table 4-2: RSL3 IC_{50} values for MM cell lines treated with RSL3 + FAC.

Mean RSL3 IC_{50} ± standard deviation generated by fitting a sigmoidal 4PL curve for each biological replicate from Figure 4-8 (constraints used were bottom = 0, top < 1).

	RSL3 IC_{50} (nM) ± SD	
Cell line	**RSL3 only**	**RSL3 + 100 μM FAC**
KMS-11	5242 ± 310	1731 ± 2093 *
KMS-18	5948 ± 3110	739 ± 368 *
LP-1	2894 ± 877	953 ± 633 *
OPM2	68.6 ± 8.97	47.4 ± 11.1 *

Statistical analyses were performed using an unpaired t-test; ns, not significant, * $p<0.05$ relative to RSL3 only.

Synergy between RSL3 and FAC was examined using the fractional product method. Consistent with the increased sensitivity to RSL3, fractional product values of < -0.1 for all the combinations are indicative of a high degree of synergy between the two compounds (except for 5 μM RSL3 + FAC in LP-1 cells) (Figure 4-8E).

While 100 μM FAC on its own did not cause a statistically significant increase in lipid oxidation, it enhanced the lipid oxidation induced by RSL3, an effect which was prevented with Lip-1 (Figure 4-9). Therefore, the synergy between FAC and RSL3 appeared to be due to increased levels of lipid oxidisation. These data, and evidence that the cell death induced by the combination of RSL3 and FAC was prevented with Lip-1, suggests cell death was mediated by ferroptosis.

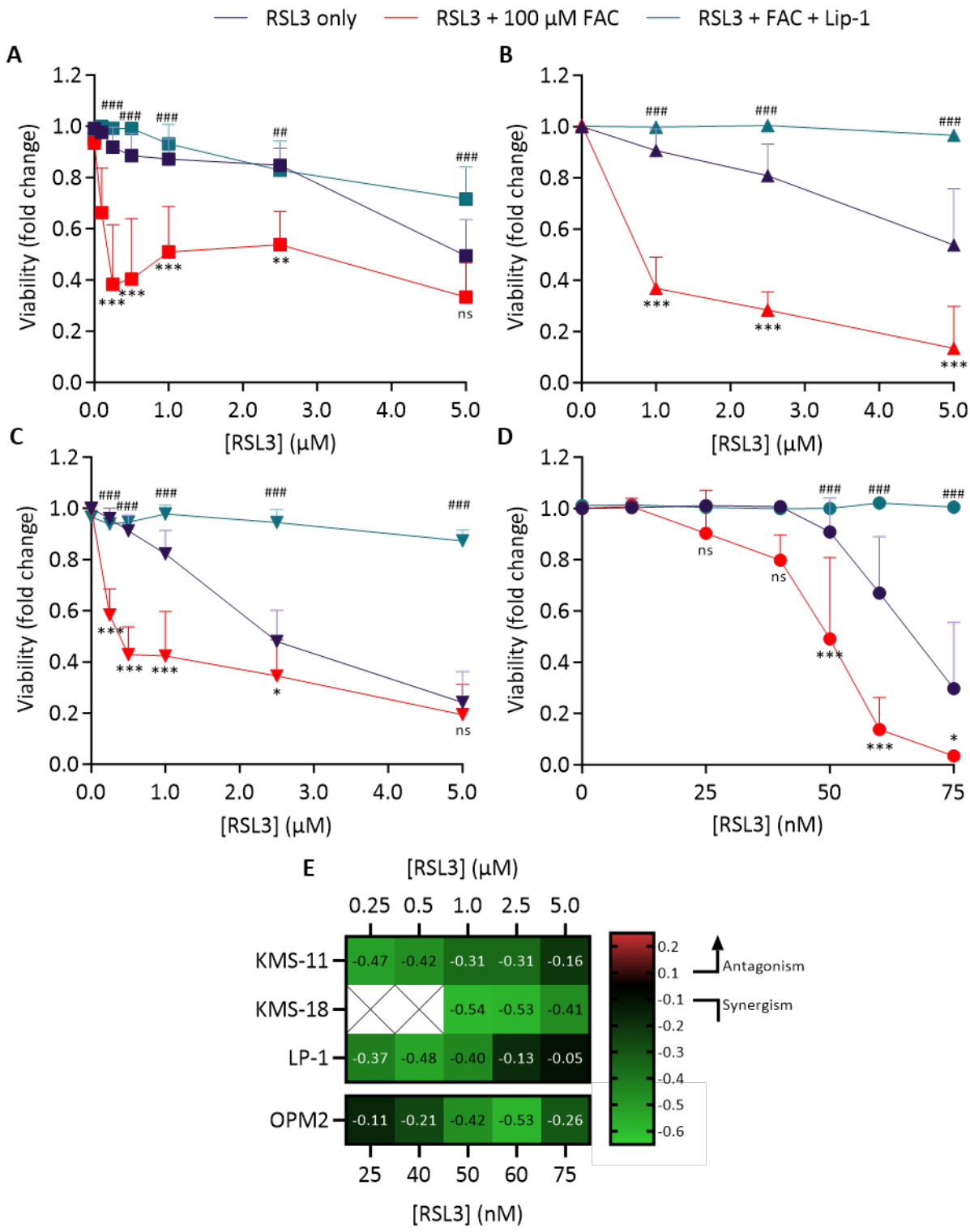

Figure 4-8: RSL3 and FAC cause a synergistic reduction in the cell viability of MM cells.

KMS-11 (A), KMS-18 (B), LP-1 (C) and OPM2 (D) cells were treated with the concentrations of RSL3 indicated and/or 100 µM ferric ammonium citrate (FAC) and/or 2 µM liproxstatin-1 (Lip-1) for 24 hours. Cell viability was measured by flow cytometry. Data are the mean ± standard deviation from at least three independent experiments. Statistical analyses were performed by two-way ANOVA with a Tukey's multiple comparisons test; ns indicates no significant difference, * $p<0.05$, ** $p<0.01$, *** $p<0.001$ RSL3 + FAC vs. RSL3 only; # $p<0.05$, ## $p<0.01$, ### $p<0.001$ RSL3 + FAC vs. RSL3 + FAC + Lip-1. (E) Potential synergy between RSL3 and FAC was examined in MM cells using the average viability data from panels A-D and the fractional product (FP) method (Webb, 1963). An FP value less than -0.1 indicates synergy (green) whereas an FP greater than 0.1 is classified as an antagonistic effect (red).

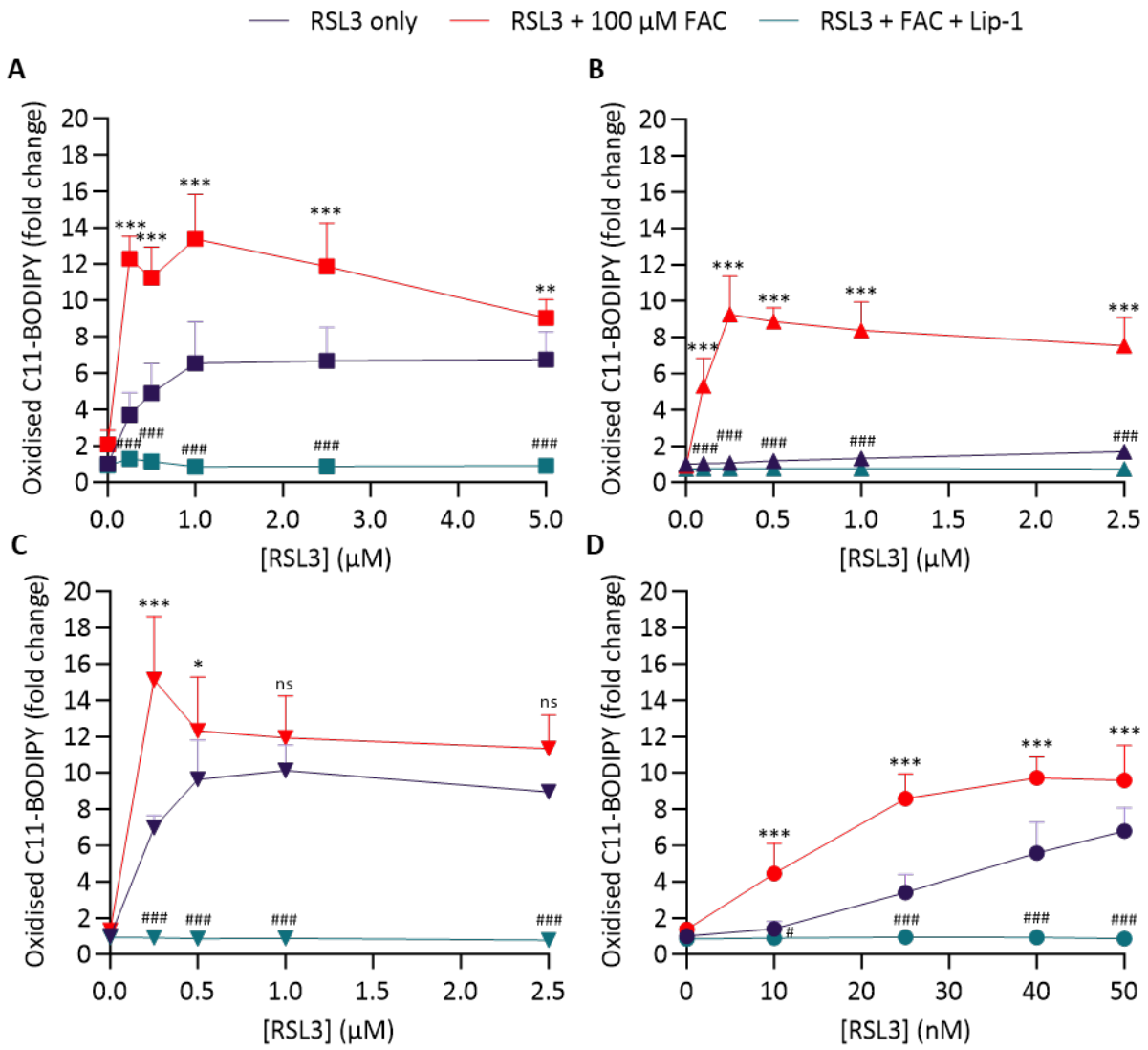

Figure 4-9: FAC increases lipid oxidation induced by RSL3 in MM cells.

KMS-11 (A), KMS-18 (B), LP-1 (C) and OPM2 (D) cells were treated with the concentrations of RSL3 indicated and/or 100 µM ferric ammonium citrate (FAC) and/or 2 µM liproxstatin-1 (Lip-1) for 24 hours. Levels of lipid oxidation were measured by flow cytometry. Data are the mean ± standard deviation from at least three independent experiments. Statistical analyses were performed by two-way ANOVA with a Tukey's multiple comparisons test; ns indicates no significant difference, * p<0.05, ** p<0.01, *** p<0.001 RSL3 + FAC vs. RSL3 only; # p<0.05, ## p<0.01, ### p<0.001 RSL3 + FAC vs. RSL3 + FAC + Lip-1

4.3 Discussion

4.3.1 Exogenous AA enhances RSL3-induced ferroptosis in MM cells

ACSL enzymes are responsible for priming free fatty acids for insertion into phospholipids by converting them to fatty acyl-CoAs. ACSL4 expression is indispensable for the execution of ferroptosis induced by inhibition of GPX4 through its activity towards long chain PUFA, with a proclivity for AA (Dixon et al., 2015, Magtanong et al., 2022). This is demonstrated by a study which showed that ACSL4 knockout in Pfa1 cells resulted in resistance to RSL3-induced death (Doll et al., 2017). Interestingly, despite ASCL4 knockout reducing RSL3 sensitivity by preventing incorporation of PUFA into phospholipid membranes, RSL3 was still able to induce oxidation of free PUFA in these cells, and moreover, exogenous AA enhanced RSL3 efficacy in ACSL4-knockout cells (Kagan et al., 2017).

We showed that in MM cells, high expression of ACSL4 correlates with a lower IC_{50} value for RSL3 (Figure 4-1B,C). This is consistent with the hypothesis that increased ACSL4 activity would increase incorporation of AA into phospholipids in the plasma membrane and might explain why OPM2 cells, which have the highest levels of ACSL4 of the MM lines (Figure 4-1), also have a higher proportion of PUFA compared to the other MM cells (Figure 3-14). These findings are consistent with another study that showed erastin-resistant LNCaP (prostate cancer) and K562 (chronic myeloid leukaemia) cells had little to no ACSL4 expression at the genetic or protein level, compared to erastin-sensitive HepG2 (liver cancer) and HL60 (acute myeloid leukaemia) cells (Yuan et al., 2016). Furthermore, ACSL4 overexpression sensitised both LNCaP and K562 cells to erastin, highlighting the important role of this protein in the execution of ferroptosis (Yuan et al., 2016). A recent study also identified a strong correlation between ASCL4 protein expression and the IC_{50} of RSL3 in a panel of MM cell lines (RPMI-8226, U-266, H929, OPM2, MM.1R, MM.1S, ARH-77 and JJN-3) (Zhang et al., 2023b). The only discrepancy between these findings and our data is that the previous study suggested that MM cells were sensitive to RSL3. This is likely due to differences in the range of MM cell lines studied, with the only overlap in lines being the H929 and OPM2 cells; in the study by Zhang *et al*., the IC_{50} values for RSL3 were determined to be 580 nM and 230 nM, in the H929 and OPM2 cells, respectively, while we calculated IC_{50} values of 6104 and 74 nM. It is difficult to understand why these differences in the IC_{50} of RSL3 were observed, although one explanation may be differences in the cell culture conditions used. In the study by Zhang *et al*., it was not apparent whether they added L-glutamine, HEPES and/or penicillin/streptomycin to their media, the cell density used was not stated nor was the method for assessment of cell viability. Nevertheless, the authors did note that ACSL4 knockdown significantly reduced the cytotoxic effects of RSL3 and reduced lipid ROS generation (Zhang et al., 2023b). Our data showed that ACSL4 expression did not correlate with RSL3 sensitivity in the four DLBCL cell lines assessed, which may suggest that mechanisms other than the level of ACSL4 expression confer ferroptosis sensitivity in these cells. However, inhibition of ACSL4 would be needed to definitively answer whether this protein plays a role in ferroptosis sensitivity in DLBCL cells. While a

pharmacological inhibitor of ACSL4 is not yet available, the published findings of Zhang *et al.* (2023b), along with our data suggest ACSL4 may be useful as a biomarker to predict ferroptosis sensitivity of MM cells.

In KMS-11, but not OPM2 cells, addition of exogenous AA reduced ACSL4 expression, suggesting a negative feedback loop, in which increased availability of AA reduces expression of the enzyme responsible for its incorporation into phospholipids (Figure 4-2C). Though only a mild reduction in ACSL4 was observed, this could, in theory, reduce the effectiveness of AA in enhancing ferroptosis given that only oxidation of fatty acids in phospholipids, and not free fatty acids, causes ferroptotic cell death (Kagan et al., 2017). Importantly, ferroptosis resistant MM cells do express ACSL4, suggesting that they have the ability to ligate PUFA to CoA, ready for insertion into phospholipids by LPCAT3, another protein essential for ferroptosis (Dixon et al., 2015, Doll et al., 2017, Kagan et al., 2017). Using publicly available data, we found that *LPCAT3* is expressed in all lines in our panel, but was expressed at significantly higher levels in ferroptosis sensitive cells (OPM2 and DLBCL cell lines) compared to resistant MM lines ($p = 0.0250$) (The Human Protein Atlas, 2023g).

ACSL3 on the other hand, has a high specificity for MUFA, so it is reasonable to hypothesise that cells with a higher proportion of MUFA in their phospholipidome would express higher levels of ACSL3. However, this is not the case as we found no difference in *ACSL3* expression between RSL3-sensitive and -resistant cells (Figure 4-1D)(The Human Protein Atlas, 2023a). Levels of ACSL3 protein or its activity could differ between the cell lines, however, unlike ACSL4, there is no evidence suggesting that levels of ACSL3 correlate with sensitivity to ferroptosis (Yuan et al., 2016). Furthermore, the literature concerning a possible role of ACSL3 in ferroptosis resistance is generally in the context of exogenous MUFA. ACSL3 expression is required to activate exogenous MUFA for insertion into phospholipids (Magtanong et al., 2019), but as we have shown in Chapter 3, the ferroptosis resistant cells studied contain higher levels of endogenous MUFA-containing phospholipids. The role of ACSL3 could be further investigated by genetic manipulation to determine whether it plays a role in shaping the phospholipidomic profile of MM and DLBCL cells. Given that resistant cell lines have a higher proportion of MUFA-containing phospholipids (Figure 3-14B), modulation of ACSL3 expression has the potential to impact ferroptosis sensitivity.

Once PUFA are inserted into membrane phospholipids, they are oxidised by lipoxygenases, which triggers ferroptosis when activity of GPX4 is unable to prevent the accumulation of lipid hydroperoxides (Seiler et al., 2008, Kagan et al., 2017). In particular, 12/15-lipoxygenase (12/15-Lox, encoded by the *ALOX15* gene) has been shown to be indispensable for ferroptosis as inhibition of this, but not other lipoxygenases, can protect GPX4 knockout cells (Seiler et al., 2008). Accordingly, 12/15-Lox knockout cells are resistant to ferroptosis induced by GSH-depletion or GPX4 inhibition (Seiler et al., 2008). Interestingly, in our study the most sensitive

MM cell line, OPM2, had the lowest expression of *ALOX15* (Figure 4-1D). However, gene expression may not directly correlate with enzymatic activity of the protein, or even low levels of activity of the protein may be sufficient to induce lipid oxidation and subsequent ferroptosis in these cells (Figure 4-1D) (The Human Protein Atlas, 2023c).

Although we did not observe a reduction in GPX4 expression in OPM2 cells following treatment with AA, we only investigated proteomic changes after 6 hours of drug treatment (Figure 4-2B). Another study showed that AA does reduce GPX4 expression and cell proliferation in U266, MM.1S and H929 MM cells after 72 hours and that these effects can be prevented by Fer-1 (Panaroni et al., 2022). In our study, AA prevented the increase in GPX4 expression observed in KMS-11 cells following RSL3 treatment (Figure 4-2D), which may increase the sensitivity of these cells to the GPX4 inhibitor and may explain the synergy between the two compounds (Figure 4-5).

The addition of AA significantly reduced the IC_{50} of not only ferroptosis-sensitive OPM2 cells, but also resistant KMS-11, LP-1 and KMS-18 cells (Figure 4-3, Figure 4-4, Supplementary Figure 4-B). This suggests that even in cells, such as OPM2, that contain a higher proportion of PUFA-containing phospholipids, the sensitivity to RSL3 can be further enhanced. These findings are similar to those observed in gastric cancer cell lines, which demonstrated that AA supplementation can increase sensitivity to RSL3 in both ferroptosis sensitive and resistant cells (Lee et al., 2020). However, the effects of AA may be dose-dependent; in a mouse MM cell line (5TGM1), low doses of AA (0.125 – 2 µM) increased cell proliferation and viability, while these were reduced by doses above 25 µM, suggesting optimising the dose of AA is important (Panaroni et al., 2022). With the exception of 10 nM RSL3 + 50/60 µM AA in OPM2 cells, we identified synergy between RSL3 and AA, associated with a reduction in the RSL3 concentrations required to induce ferroptosis (Figure 4-5). In KMS-11 cells, a synergistic reduction in cell viability was observed when RSL3 was combined with doses of AA as low as 20 µM, whereas no significant change in the IC_{50} of RSL3 was observed in OPM2 cells treated with RSL3 in combination with 20 µM AA compared to RSL3 alone (Table 4-1). This is perhaps unsurprising given that OPM2 cells have a higher proportion of PUFA-containing phospholipids at baseline (Figure 3-14), and therefore may have a reduced capacity for incorporation of AA into PUFA containing phospholipids or require higher AA concentrations than the ferroptosis-resistant cells to alter the phospholipidome.

Despite the increase in RSL3 cytotoxicity induced by AA, via a mechanism that we assume to be ferroptosis based on the morphological changes and effects of Lip-1, no increase in lipid ROS levels were observed when AA was added, compared to cells treated with RSL3 alone (Figure 4-3, Figure 4-4). These data were unexpected but could be due to several factors. Although increased lipid ROS levels were detectable as early

as 4 hours post-treatment, we assessed lipid ROS after 24 hours to align with the cell viability data. While we have shown that lipid ROS levels continue to increase beyond 6 hours (Supplementary Figure 3-A), it is possible that increase in lipid ROS induced by AA may occur prior to the 24-hour end point. For example, in one study, cells were pretreated with AA for 16 hours, followed by a 1 hour treatment with RSL3, before lipid ROS levels were assessed (Lee et al., 2020). It is well understood that the dye we used to measure lipid ROS (C11-BODIPY) localises to cellular membranes (Drummen et al., 2002), but it is plausible that AA also induces ROS accumulation in other cellular compartments. Measuring total cellular ROS or ROS in other compartments such as the cytosol or mitochondria using stains such as H_2DCFDA or MitoSox (ThermoFisher) or measurement of a byproduct of lipid peroxidation, such as MDA, may provide further insight into the role of ROS in AA and RSL3-induced ferroptosis. However, it has been shown that ROS generated by the oxidation of free PUFA does not lead to ferroptosis, indicating that the cellular location of the oxidised lipids is an important factor in the execution of ferroptosis (Kagan et al., 2017). Nevertheless, the results presented demonstrate that RSL3 and AA in combination is an effective way at causing a synergistic reduction in cell viability.

4.3.2 Exogenous iron enhances RSL3-induced ferroptosis in MM cells

The purpose of the experiments in Figure 4-6 was to confirm MM and DLBCL cells have the machinery to import, store and release iron from ferritin. We found that other than Riva cells, all the cell lines express the iron import protein TfR, and that LP-1 cells expressed the highest amount of the protein, despite levels of the corresponding *TFRC* transcript being highest in Farage and U-2932 cells (Figure 4-6A,D) (The Human Protein Atlas, 2023l). Using publicly available data, we found that the *NCOA4* transcript is expressed in all the MM and DLBCL cells studied (The Human Protein Atlas, 2023h), however, we were unable to detect NCOA4 protein by Western blot. This protein is known to be involved in ferritinophagy (Gryzik et al., 2021), but it is unclear why it was undetectable in our cell lines. Likewise, the *SLC40A1* transcript, that encodes the iron export protein, ferroportin (FPN), has been shown to be more highly expressed in KMS-11 and KMS-18 MM cells compared to the other cell lines in our panel (Figure 4-6D) (The Human Protein Atlas, 2023k). Unfortunately, the anti-FPN Western blot antibody used was unable to detect FPN in any MM or DLBCL cell lines. Without a positive control to confirm the antibody was functional, we cannot comment on the expression of this protein in MM cell lines, but future research could investigate this protein further to determine whether it plays an important role in iron export in the context of ferroptosis resistance in MM cells.

FTH1, the heavy chain of ferritin, was expressed in all the cell lines, however, no statistically significant difference in expression at either the genetic or protein level was observed between ferroptosis-sensitive

and -resistant cells, or between MM and DLBCL cell lines (Figure 4-6C,D). Likewise, no significant difference in *FTH1* transcript levels was observed between these groups. However, with the exception of Farage DLBCL cells a double band of FTH1 protein was observed in the ferroptosis sensitive OPM2 and DLBCL cells (Figure 4-6A). While the antibody used is raised against the 21 kDa heavy chain of ferritin (FTH1), the antigenic sequence has high homology with the 19 kDa light chain (FTL). Assuming the lower band observed is FTL, it appears that sensitive OPM2 and the majority of the DLBCL cells express both ferritin subunits at baseline. FTH1 is responsible for the enzymatic activity of ferritin, which oxidises ferrous iron (Fe^{2+}) to ferric iron (Fe^{3+}) for insertion into the ferritin core (Alkhateeb and Connor, 2013, Chen et al., 2020). FTL assists in iron nucleation and while both subunits are required to form the 24-subunit ferritin nanocage, even as a monomer the enzymatic activity of FTH1 can prevent oxidative damage (Alkhateeb and Connor, 2013, Asperti et al., 2023). Expression of both the heavy and light chain suggests the presence of assembled ferritin.

Consistent with findings reported in prostate cancer and rhabdomyosarcoma cells, we observed that addition of FAC to KMS-11 and OPM2 MM cell lines led to a reduction in TfR and an increase in FTH1 expression, although statistically significant changes were only observed in KMS-11 cells (Figure 4-7) (Maccarinelli et al., 2023, Asperti et al., 2023). It is possible that exogenous iron results in an increase in FPN levels and a subsequent increase in iron export, which reduces the amount of labile iron available for ferroptosis. Regardless, it was apparent that all 4 MM cell lines were sensitive to RSL3 in combination with FAC, and that the cytotoxicity of these compounds was associated with a marked increase in lipid oxidation and could be prevented by Lip-1 (Figure 4-8, Figure 4-9). Measuring the levels of labile iron in these cells, at baseline and during ferroptosis, may provide further insight into whether endogenous labile iron effects ferroptosis sensitivity. However, even RSL3-sensitive OPM2 MM cells were further sensitised to the GPX4 inhibitor by addition of FAC, suggesting that intracellular iron levels in these cells may still be a rate limiting factor.

4.3.3 Conclusions

As demonstrated in Chapter 3, ferroptosis resistant MM cells contain a lower proportion of PUFA-containing phospholipids compared to sensitive OPM2 and DLBCL cells. Accordingly, we were able to significantly increase the sensitivity of the resistant cells by supplementation with AA, a PUFA known to be readily oxidised and involved in ferroptosis. Furthermore, supplementing the cells with iron, which is another key ferroptosis substrate, was also shown to enhance the ferroptosis-mediated effects of RSL3 in MM cells. These findings highlight that MM cells may be deficient in important substrates that are necessary for execution of ferroptosis. In the subsequent work presented in Chapter 6 of this thesis, these findings were investigated in patient-derived MM cells.

APPENDIX 4A. SUPPLEMENTARY FIGURES

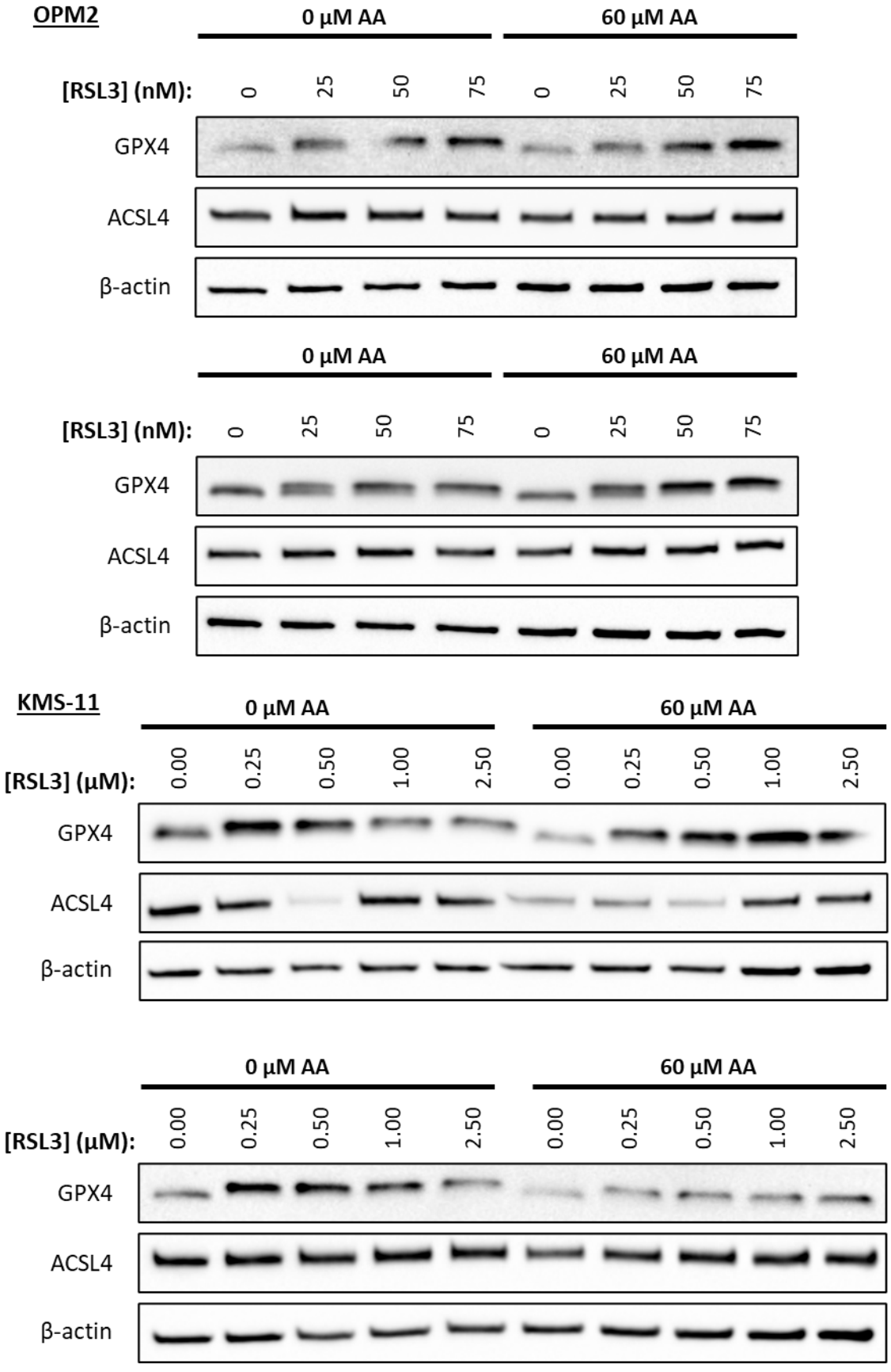

Supplementary Figure 4-A: Western blot biological replicates used to generate densitometry data in Figure 4-2B,D.

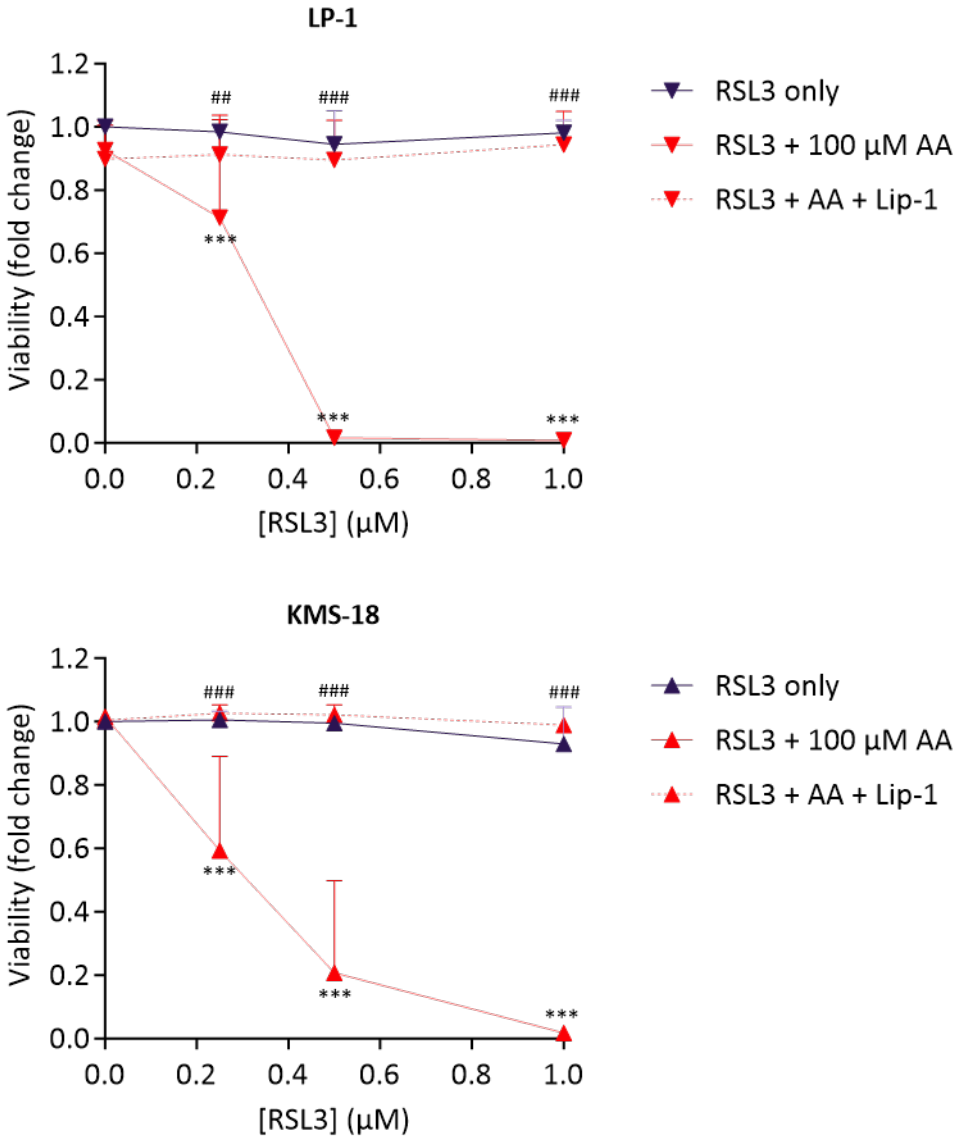

Supplementary Figure 4-B: AA increases the cytotoxic effects of RSL3 in LP-1 and KMS-18 MM cells.

LP-1 (top) and KMS-18 (bottom) cells were treated with the concentrations of RSL3 indicated, 100 µM arachidonic acid (AA) and/or 2 µM liproxstatin-1 (Lip-1) for 24 hours. Cell viability was measured by flow cytometry. Data are the mean ± standard deviation from at least three independent experiments. Statistical analyses were performed by two-way ANOVA with a Tukey's multiple comparisons test; *** $p<0.001$ RSL3 + AA vs. RSL3 only; ### $p<0.001$ RSL3 + AA vs. RSL3 + AA + Lip-1.

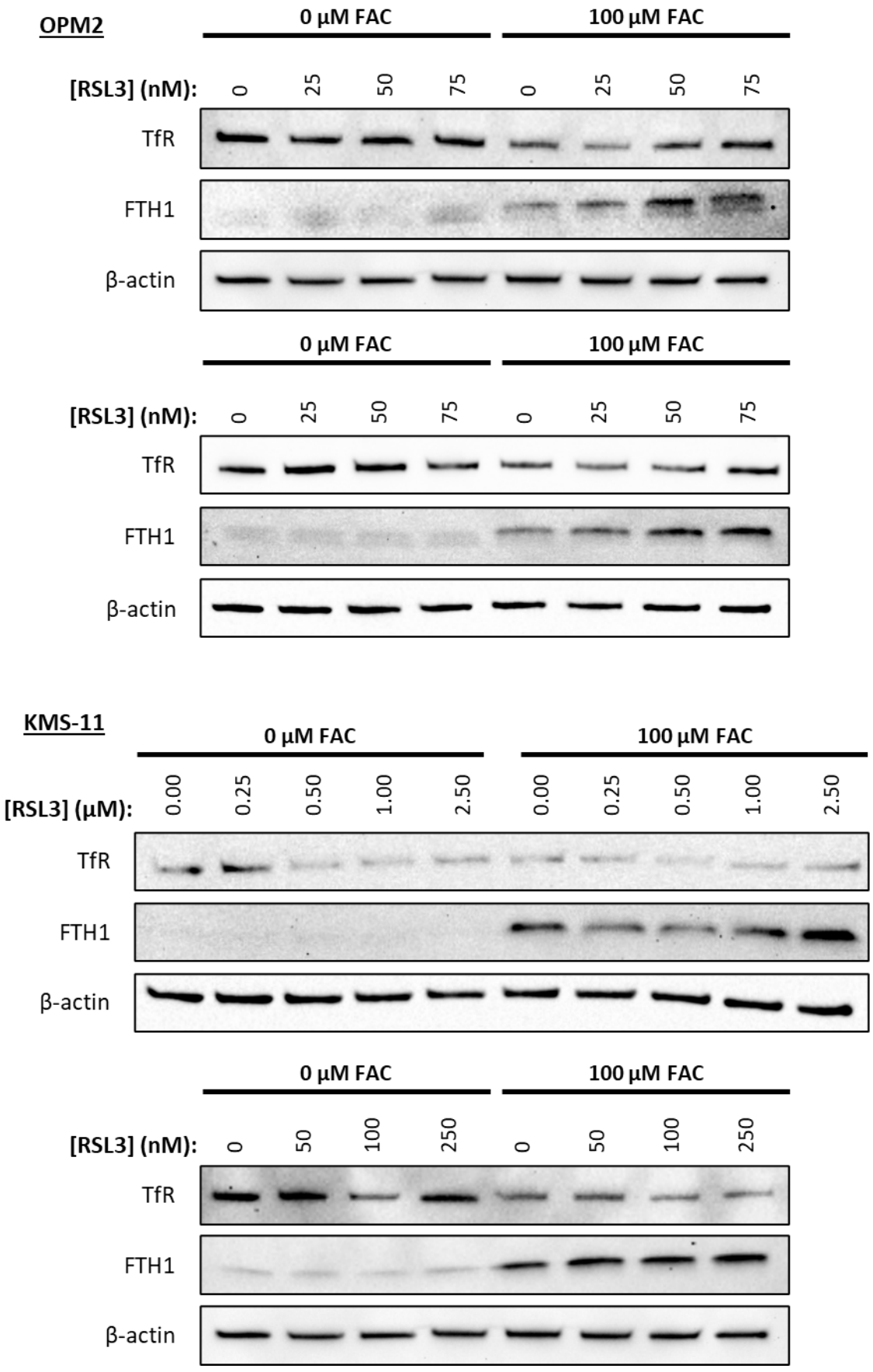

Supplementary Figure 4-C: Western blot biological replicates used to generate densitometry data in Figure 4-7B,D.

CHAPTER 5. FERROPTOSIS-RELATED GENOMIC DIFFERENCES IN MM CELLS

5.1 Introduction

Ferroptosis involves a series of complex cellular pathways and various genes, proteins and metabolites (Figure 5-1). According to the online ferroptosis database, FerrDb, there have been 565 genes identified as drivers, suppressors and/or markers of ferroptosis to date (Zhou et al., 2023). In the preceding chapters, we have introduced the important roles that GPX4, phospholipid composition and iron storage, import and export have on ferroptosis. Other important pathways involved in ferroptosis include glutathione (GSH) synthesis, phospholipid remodelling and iron metabolism (Figure 5-1). Furthermore, briefly introduced in Chapter 1, the mevalonate pathway leads to the production of not only isopentenyl pyrophosphate (IPP), which is required for selenocysteine synthesis, but also farnesyl pyrophosphate (FPP), which feeds into coenzyme Q_{10} (CoQ_{10}, ubiquinone) biosynthesis (Warner et al., 2000, Yang and Stockwell, 2016, Turunen et al., 2004) (Figure 5-1).

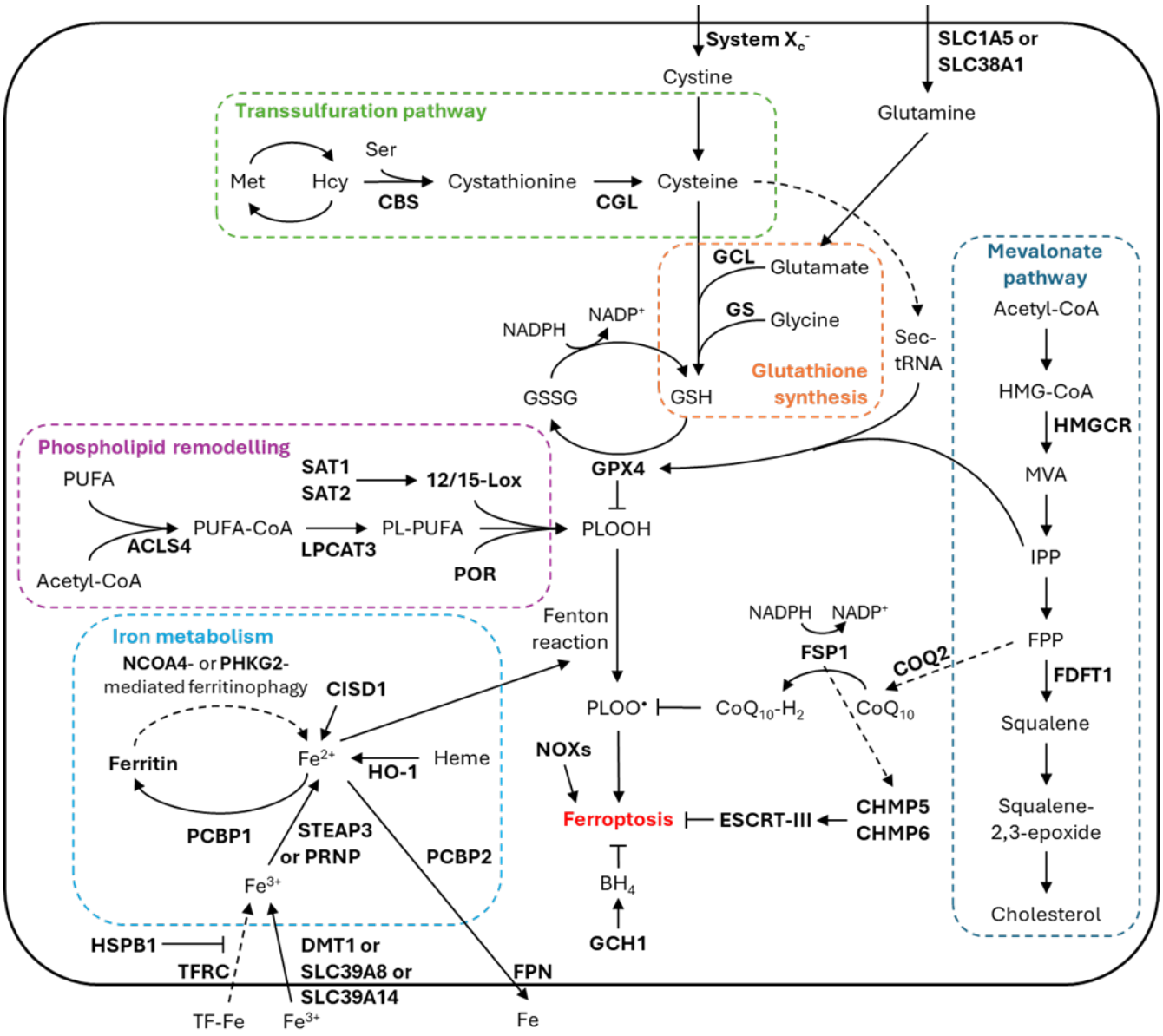

Figure 5-1: Key proteins involved in the ferroptosis pathway.

Dotted arrows represent multiple steps within a pathway. Adapted from (Tang et al., 2021a, Kuang et al., 2020, Chen et al., 2020). ACSL4, acyl-CoA synthetase long chain family member 4; BH_4, tetrahydrobiopterin; CBS, cystathionine beta-synthase; CGL, cystathionine gamma-lyase; CHMP5/6, charged multivesicular body protein 5/6; CISD1, CDGSH iron sulphur domain 1; CoA, coenzyme A; CoQ_{10}, coenzyme Q_{10}, ubiquinone; $CoQ_{10}H_2$, ubiquinol; DMT1, divalent metal transporter 1; ESCRT-III, endosomal sorting complexes required for transport III; FDFT1, farnesyl-diphosphate farnesyltransferase 1 (aka squalene synthase); $Fe2^+$, ferrous iron; $Fe3^+$, ferric iron; FPN, ferroportin; FPP, farnesyl pyrophosphate; FSP1, ferroptosis suppressor protein 1; GCH1, guanosine-5'-triphosphatecyclohydrolase-1; GCL, glutamate-cysteine ligase; GPX4, glutathione peroxidase 4; GS, glutamine synthetase; GSH, glutathione; GSSG, glutathione disulfide; Hcy, homocysteine ; HMG-CoA, 3-hydroxy-3-methylglutaryl coenzyme A; HMGCR, 3-hydroxy-3-methyl-glutaryl-coenzyme A reductase; HO-1, heme oxygenase; HSPB1, heat shock protein beta-1; IPP, isopentenyl pyrophosphate; 12/15-Lox, 12/15-lipoxygenase; LPCAT3, lysophosphatidylcholine acyltransferase 3; Met, methionine ; MVA, mevalonic acid; NADP, nicotinamide adenine dinucleotide phosphate; NCOA4, nuclear receptor coactivator 4; NOX, NADPH oxidase; PCBP1/2, poly(RC) binding protein 1/2; PL, phospholipid; PLOO, phospholipid hydrogen peroxide radical; PLOOH, phospholipid hydroperoxides; POR, cytochrome P450 reductase; PHKG2, Phosphorylase kinase catalytic subunit gamma 2; PRNP, prion protein; PUFA, polyunsaturated fatty acid; SAT1/2, spermidine/spermine N1-acetyltransferase 1/2; Sec-tRNA, selenocysteine tRNA; SLC1A5, solute carrier (SLC) family 1 member 5; SLC38A1, SLC family 38 member 5; SLC39A14, SLC family 39 member 14; SLC39A8, SLC family 39 member 8; STEAP3, six-transmembrane epithelial antigen of prostate 3 metalloreductase; TF, transferrin; TFRC, transferrin receptor.

5.1.1 Regulation of ferroptosis-related genes

Nuclear factor erythroid 2-related factor 2 (Nrf2) is a transcription factor of interest in the context of ferroptosis due to its involvement in regulating a number of genes involved in oxidative stress. Basal levels of Nrf2 are generally low due to constant ubiquitination and degradation regulated by Kelch-like ECH-associated protein 1 (KEAP1) which is bound to Nrf2 (Dodson et al., 2019, Tonelli et al., 2017). Under oxidative stress, KEAP1 is inactivated, permitting Nrf2 to translocate to the nucleus where it binds to small musculoaponeurotic fibrosarcoma (sMaf) proteins, which enables binding of Nrf2 to promoter regions of target genes, specifically antioxidant response elements (ARE) (Tonelli et al., 2017, Li et al., 2023a). Of interest in ferroptosis, these genes include *xCT*, *GPX4*, genes involved in GSH synthesis and metabolism, and iron-related genes such as *FTH1* and *HMOX1* (Barrera et al., 2012, Dodson et al., 2019).

Another important protein in the regulation of ferroptosis-related genes is iron-responsive element binding protein 2 (IREB2). When iron levels are low, IREB2 expression is stable, and it acts to regulate expression of genes containing iron responsive elements (IRE); however, when iron levels are high, IREB2 is degraded (Chen et al., 2020). IREB2 decreases the translation of genes involved in depleting intracellular, iron such as *SLC40A1* (encodes iron exporter, ferroportin; FPN)*, FTH1* and *FTL* (subunits of the iron storage protein ferritin), and upregulates genes involved with iron import, including transferrin receptor (*TFRC*) and *SLC11A2* (encodes divalent metal transport 1; DMT1) (Chen et al., 2020).

BTB domain and CNC homolog 1 (BACH1) is a transcription factor that has been shown to promote ferroptosis (Nishizawa et al., 2020, Wang et al., 2024). Like Nrf2, BACH1 regulates ferroptosis-related gene expression, but unlike Nrf2 which upregulates anti-ferroptotic genes, BACH1 promotes ferroptosis by suppressing the expression of genes, including heme oxygenase 1 (*HMOX1*), *FTH1, FTL* and those involved in GSH biosynthesis (Nishizawa et al., 2020, Wang et al., 2024). BACH1-null mouse embryonic fibroblasts (MEFs) were shown to be more resistant to erastin compared to wild type cells and had significantly higher levels of GSH; furthermore, HO-1 knockdown enhanced ferroptotic cell death in MEFs, in a BACH1-dependent manner (Nishizawa et al., 2020).

5.1.2 GPX4-independent anti-ferroptotic pathways

While ferroptosis was previously thought to be controlled primarily by the xCT/GPX4 axis, other intracellular antioxidant systems, that are independent of GPX4 have also been implicated in ferroptosis. Doll *et al*. investigated genes that compensate for knockout of GPX4 in ferroptosis-resistant MCF7 breast cancer cells (Doll et al., 2019). They found that apoptosis-inducing factor mitochondrial 2 (AIFM2), now known as ferroptosis suppressor protein 1 (FSP1), was expressed in GPX4 knockout cells and overexpression of this

protein in ferroptosis-sensitive HT1080 cells could protect the cells from various ferroptosis inducers (Doll et al., 2019). The authors also showed that FSP1 is only protective against ferroptosis-inducing agents and not apoptosis-inducing compounds/conditions. Importantly, FSP1 overexpression in HT1080 cells was only effective at suppressing ferroptosis in cells that express coenzyme Q2 (*COQ2*), an enzyme involved in ubiquinone biosynthesis (Doll et al., 2019) (Figure 5-1). This is because unlike GPX4, which alone is able to reduce lipid peroxides, FSP1 prevents lipid oxidation by reducing ubiquinone to ubiquinol, which traps lipid peroxyl radicals (Doll et al., 2019, Bersuker et al., 2019) (Figure 5-1).

Using a whole-genome activation screening approach, Kraft *et al*. found that GTP cyclohydrolase-1 (*Gch1*) was overexpressed in mouse fibroblast cells resistant to ferroptosis induced by either RSL3, IKE or *Gpx4* knockout (Kraft et al., 2020). Overexpression of *Gch1* reduced ferroptosis-induced lipid oxidation and protected against cell death via ferroptosis but not apoptosis induced by doxorubicin. Overexpression of *GCH1* and supplementation with its metabolic derivative, tetrahydrobiopterin (BH_4), also prevented ferroptosis in human HT1080 cells, independent of GSH, whereas *GCH1* knockdown increased sensitivity to ferroptosis (Kraft et al., 2020). Other ferroptosis suppressors implicated in ferroptosis resistance include thioredoxin reductase 1 (TXNRD1) (Liu et al., 2021b, Hsieh et al., 2024) and endosomal sorting complexes required for transport III (ESCRT-III) and its subunits, charged multivesicular body protein 5 (CHMP5) and CHMP6 (Dai et al., 2020).

Heme oxygenase 1 (HO-1, encoded by *HMOX1*) cleaves heme into biliverdin, carbon monoxide and ferrous iron (Alaoui-Jamali et al., 2009). HO-1 has been described as an antioxidant system in some contexts, in part due to its generation of biliverdin, which is reduced to the ROS-scavenging antioxidant, bilirubin (Chiang et al., 2018). Conversely, the release of iron during heme degradation may also contribute to the labile iron pool (LIP) and therefore enhance ferroptosis. However, to mediate this increase in labile iron, ferritin can be upregulated and/or iron efflux can be promoted through an increase in the expression of FPN, providing protection from oxidative stress (Alaoui-Jamali et al., 2009). As such, HO-1 has been described to be the "double-edged sword" of ferroptosis and its role appears to be context dependent and dependent on how increases in intracellular iron are managed (Nishizawa et al., 2020). Accordingly, HO-1 has been shown to both drive (Hassannia et al., 2018, Chang et al., 2018, Kwon et al., 2015, Tang et al., 2021b, Meng et al., 2021, Guo et al., 2024) or prevent ferroptosis (Adedoyin et al., 2018, Sun et al., 2016, Nishizawa et al., 2020, Luo et al., 2022).

In Chapter 5, we use RNA sequencing to identify key genes that are differentially expressed in ferroptosis-sensitive and -resistant MM cells. Through pharmacologic and genetic inhibition of the proteins encoded by

these differentially expressed genes, we aimed to investigate the specific role they play in ferroptosis sensitivity of MM cells.

5.2 Results

5.2.1 Comparing the genetic profile of a ferroptosis-sensitive and a ferroptosis-resistant MM cell line

RNA sequencing was performed to investigate the differential expression of genes between a ferroptosis-sensitive MM cell line, OPM2, and a ferroptosis-resistant cell line, KMS-11. Both cell lines harbour the t(4;14) translocation (Table 5-1).

Table 5-1: Cell line characteristics.

Cell line	Sex	Age	Race	Ab	Genetics
OPM2	Female	56	Japanese	IgG lambda	t(4;14)
KMS-11	Female	67	Japanese	IgG kappa	t(4;14)

Normalised gene counts were converted to a row z-score to allow for the expression of genes to be visualised on the same scale (Figure 5-2A). A differential gene expression analysis between each cell line was performed using the DESeq2 program (Love et al., 2014) in R (v.4.2; https://www.R-project.org/). Differentially expressed genes (DEG) were defined by a $\log_2$ fold change of >1 or <-1 with an adjusted p-value of < 0.05 considered statistically significant. There were 4375 DEG that fit these criteria (33% of the total 13,071 genes analysed), 130 of which overlapped with the 565 ferroptosis-related genes extracted from FerrDb (Zhou et al., 2023) (Figure 5-2B). Of these 130 DEG that are ferroptosis-related, 76 were upregulated in KMS-11 and 54 were upregulated in OPM2. Of the 76 FerrDb genes upregulated in KMS-11, 29 genes (38%) were known ferroptosis drivers, 30 (39%) were suppressors, 16 (21%) were unclassified and 1% have been demonstrated to be either drivers or suppressors of ferroptosis in different contexts (Figure 5-2C). In OPM2, 17 genes (31%) were drivers, 26 (48%) were suppressors, 7 (13%) were unclassified and 4 (7%) were classed as both drivers and suppressors (Figure 5-2C).

Gene set enrichment analysis (GSEA) was performed on all genes, regardless of their fold change or p-value, to determine gene pathways enriched in KMS-11 versus OPM2 cells. This analysis allowed for investigation of genes that are co-regulated, including specific genes that might have a small or insignificant individual fold change. Using the C2 collection of curated gene sets (Subramanian et al., 2005), it was found that 690 gene sets were significantly enriched in KMS-11 cells and 40 gene sets were enriched in OPM2 cells (nominal p-value < 0.05). Of interest to ferroptosis, the Reactome Selenoamino Acid Metabolism pathway (Williams,

2015) was enriched in OPM2 compared to KMS-11 cells (nominal p-value < 0.001) (Figure 5-2D). Genes from this pathway include those involved in synthesis of selenocysteine, which is necessary for GPX4 translation.

Conversely, the Wikipathways Ferroptosis gene set (Hanspers et al., 2024) was not enriched in one cell line compared to the other (nominal p-value = 0.527). Rather, a marked difference in the expression of ferroptosis-related genes was observed between KMS-11 and OPM2 cells (Table 5-2, Figure 5-2D, Figure 5-3A). Of the 22 ferroptosis-related genes that were significantly upregulated in KMS-11 cells, 10 (45.45%) were categorised as ferroptosis-suppressors and 5 (22.72%) were drivers, according FerrDb (Zhou et al., 2023). Of the 20 genes upregulated in OPM2 cells, 3 (15%) were suppressors and 7 (35%) were ferroptosis-driver genes in FerrDb. In particular, the *AIFM2* transcript, which encodes FSP1 was significantly upregulated in KMS-11 compared to OPM2 cells ($p < 0.0001$) (Figure 5-3B).

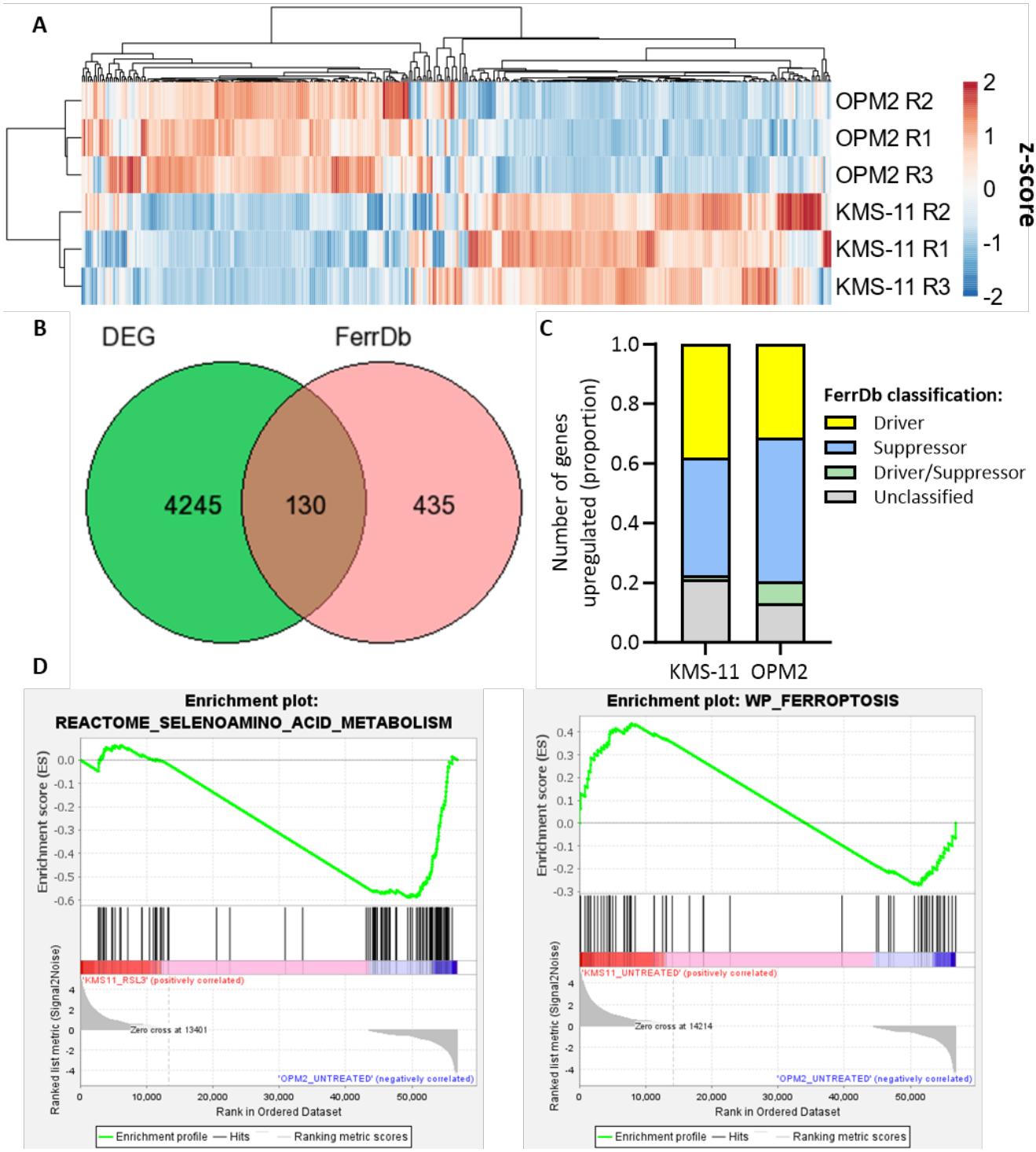

Figure 5-2: Both ferroptosis-sensitive OPM2 and ferroptosis-resistant KMS-11 MM cells express ferroptosis-related genes.

RNA sequencing was performed on untreated OPM2 and KMS-11 cells, in triplicate. (A) Heat map generated using ClustVis (Metsalu and Vilo, 2015) of normalised gene count (ferroptosis related genes from FerrDb) converted to row z-score; both rows and columns are clustered using correlation distance and average linkage. (B) Venn diagram showing overlap between differentially expressed genes (DEG) (using DESeq2, $\log_2$ fold change >1 or <-1, p<0.05 cut off) and ferroptosis-related genes from FerrDb (Zhou et al., 2023). (C) 130 genes in both DEG and FerrDb were assigned as either "driver", "suppressor", "driver/suppressor" or "unclassified" as per classification in FerrDb. The proportion of genes from each group upregulated in either cell line is displayed as a bar graph. (D) Gene set enrichment analysis (Subramanian et al., 2005) was performed on the normalised gene count of untreated OPM2 and KMS-11 cells.

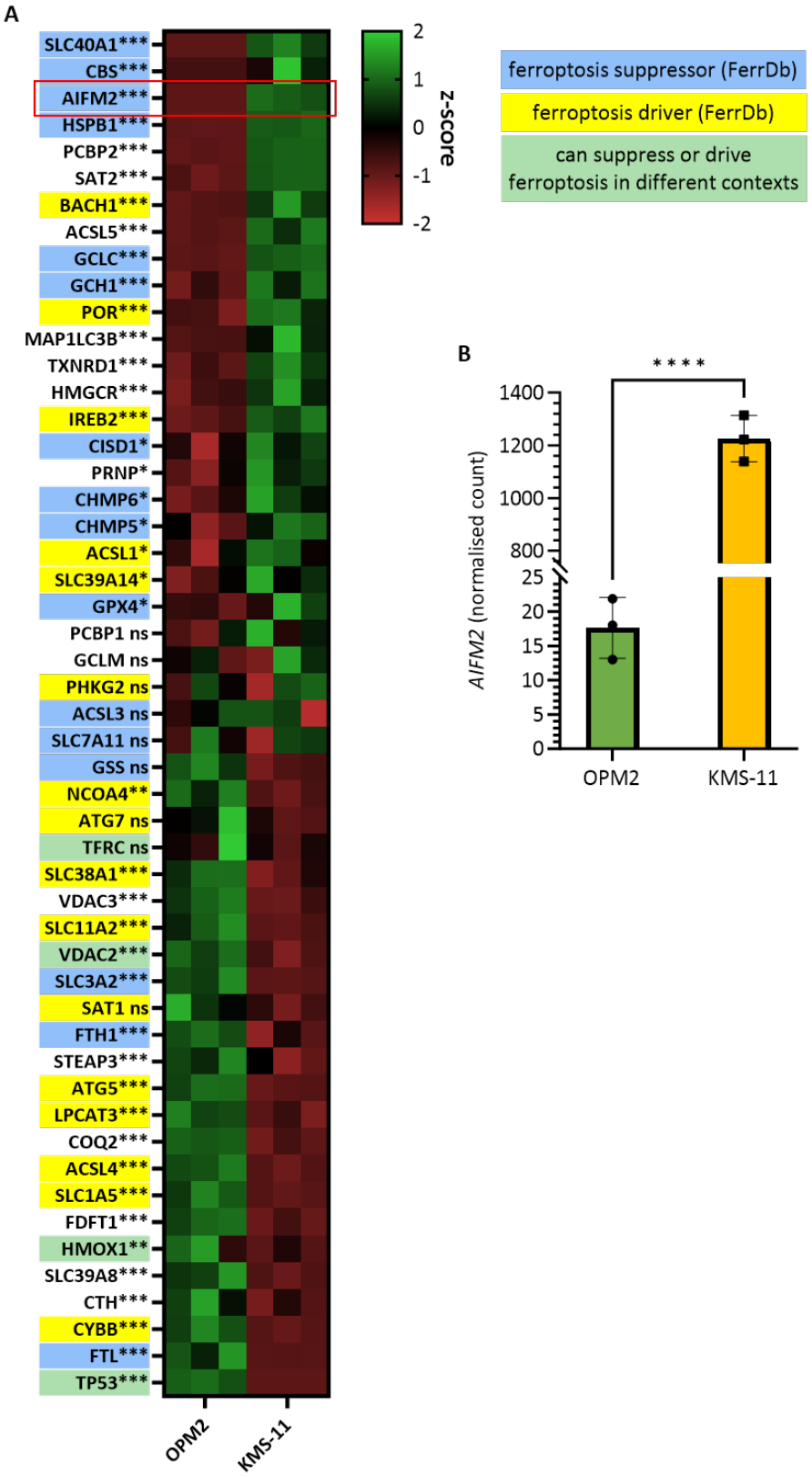

Figure 5-3: Ferroptosis-sensitive OPM2 and ferroptosis-resistant KMS-11 MM cells display a distinct signature of ferroptosis-related genes.

RNA sequencing was performed on untreated OPM2 and KMS-11 cells, in triplicate. (A) Heat map of normalised gene count converted to row z-score, for WP_Ferroptosis gene set (Hanspers et al., 2024); rows are sorted by fold change. (B) Normalised gene count of *AIFM2* transcript from RNA sequencing data. Statistical testing was performed during DESeq2; p-values were obtained by the Wald test and then corrected for multiple testing using the Benjamini-Hochberg test, ns indicates no significant difference, * $p<0.05$, ** $p<0.01$, *** $p<0.001$, **** $p<0.0001$.

Table 5-2: Genes from WP_Ferroptosis in Figure 5-3.

RNA sequencing was performed on untreated OPM2 and KMS-11 cells, in triplicate. Genes in the WP_Ferroptosis gene set (Hanspers et al., 2024) are listed. Differential gene expression analysis was performed using DESeq2 and statistical testing performed using the Wald test and then corrected for multiple testing using the Benjamini-Hochberg test.

Gene code	Full gene name (protein name if different)	log_2 fold change KMS-11 vs. OPM2	p-value	Involvement in ferroptosis (coloured as per pathways in Figure 5-1 where relevant)	Ref. in text or figure
ACSL1	Acyl-CoA synthetase long chain family member 1	-0.287	0.033	Phospholipid remodelling	Chapter 5
ACSL3	Acyl-CoA synthetase long chain family member 3	0.015	0.874	Phospholipid remodelling	Chapter 4
ACSL4	Acyl-CoA synthetase long chain family member 4	0.842	<0.0001	Phospholipid remodelling	Chapter 1 and Chapter 4, Figure 5-1
ACSL5	Acyl-CoA synthetase long chain family member 5	-1.606	<0.0001	Phospholipid remodelling	Chapter 5
AIFM2	AIF family member 2 (ferroptosis suppressor 1, FSP1)	-6.128	<0.0001	CoQ oxidoreductase	Chapter 5
ATG5	Autophagy related 5	0.684	<0.0001	Autophagy	Chapter 3
ATG7	Autophagy related 7	0.311	0.117	Autophagy	Chapter 3
BACH1	BTB domain and CNC homolog 1	-1.633	<0.0001	Transcription factor	Chapter 5
CBS	Cystathionine beta-synthase	-9.523	<0.0001	Transsulfuration pathway	Figure 5-1
CHMP5	Charged multivesicular body protein 5	-0.337	0.018	Membrane repair – subunits of endosomal sorting complexes required for transport (ESCRT)-III	Figure 5-1
CHMP6	Charged multivesicular body protein 6	-0.340	0.024		
CISD1	CDGSH iron sulphur domain 1	-0.356	0.011	Regulates mitochondrial iron and ROS metabolism	Figure 5-1
COQ2	Coenzyme Q_2	0.833	<0.0001	Ubiquinone biosynthesis	Chapter 5, Figure 5-1
CTH	Cystathionine gamma-lyase (GCL)	1.546	<0.0001	Transsulfuration pathway	Figure 5-1
CYBB	Cytochrome B-245 beta chain (NADPH oxidase 2, NOX2)	2.349	<0.0001	Contribute to ROS production	Figure 5-1
FDFT1	Farnesyl-diphosphate farnesyltransferase 1 (squalene synthase)	0.962	<0.0001	Mevalonate Pathway	Figure 5-1
FTH1	Ferritin heavy chain 1	0.638	<0.0001	Iron storage	Chapter 4
FTL	Ferritin light chain	3.019	<0.0001	Iron storage	Chapter 4
GCH1	GTP cyclohydrolase 1	-0.793	<0.0001	BH_4 synthesis	Figure 5-1
GCLC	Glutamate-cysteine ligase catalytic subunit	-0.956	<0.0001	Glutathione synthesis	Figure 5-1

GCLM	Glutamate-cysteine ligase modifier subunit	-0.114	0.452	Glutathione synthesis	Figure 5-1
GPX4	Glutathione peroxidase 4	-0.240	0.025	Reduces lipid hydroperoxides	Throughout thesis, Figure 5-1
GSS	Glutathione synthetase (GS)	0.185	0.092	Glutathione synthesis	Figure 5-1
HMGCR	3-hydroxy-3-methylglutaryl-CoA reductase	-0.562	<0.0001	Mevalonate Pathway	Figure 5-1
HMOX1	Heme oxygenase 1 (HO-1)	1.053	0.009	Iron metabolism	Chapter 5, Figure 5-1
HSPB1	Heat shock protein family B (small) member 1	-2.277	<0.0001	Inhibits TfR recycling to prevent iron uptake	Figure 5-1
IREB2	Iron responsive element binding protein 2	-0.446	<0.0001	Regulates expression of iron-related proteins	Chapter 5
LPCAT3	Lysophosphatidylcholine acyltransferase 3	0.701	0.001	Phospholipid remodelling	Chapter 1 and Chapter 4, Figure 5-1
MAP1LC3B	Microtubule associated protein 1 light chain 3 beta	-0.564	<0.0001	Autophagy	Chapter 3
NCOA4	Nuclear receptor coactivator 4	0.280	0.002	Ferritinophagy	Chapter 4, Figure 5-1
PCBP1	Poly(RC) binding protein 1	-0.116	0.224	Iron storage	Figure 5-1
PCBP2	Poly(RC) binding protein 2	-1.785	<0.0001	Iron export	Figure 5-1
PHKG2	Phosphorylase kinase catalytic subunit gamma 2	-0.007	0.965	Ferritinophagy	Figure 5-1
POR	Cytochrome P450 oxidoreductase	-0.717	<0.0001	Phospholipid remodelling	Figure 5-1
PRNP	Prion protein	-0.341	0.020	Ferrireductase	Figure 5-1
SAT1	Spermidine/spermine N1-acetyltransferase 1	0.594	0.051	Mediates expression of ALOX15	Chapter 4, Figure 5-1
SAT2	Spermidine/spermine N1-acetyltransferase 2	-1.714	<0.0001	Mediates expression of ALOX15	Chapter 4, Figure 5-1
SLC11A2	Solute carrier (SLC) family 11 member 2 (divalent metal transporter 1, DMT1)	0.555	<0.0001	Iron import	Figure 5-1
SLC1A5	SLC family 1 member 5 (alanine/serine/cysteine transporter 2, ASCT2)	0.915	<0.0001	Glutamine import	Figure 5-1
SLC38A1	SLC family 38 member 1 (sodium-coupled neutral amino acid symporter 1, SNAT1)	0.447	<0.0001	Glutamine import	Figure 5-1
SLC39A14	SLC family 39 member 14 (ZRT/IRT-like protein 14, ZIP14)	-0.247	0.020	Iron import	Figure 5-1
SLC39A8	SLC family 39 member 8 (ZRT/IRT-like protein 8, ZIP8)	1.329	<0.0001	Iron import	Figure 5-1
SLC3A2	SLC family 3 Member 2	0.593	<0.0001	System Xc^-	Chapter 1 and Chapter 3, Figure 5-1

SLC40A1	SLC family 40 member 1 (ferroportin, FPN)	-10.966	<0.0001	Iron export	Chapter 4, Figure 5-1
SLC7A11	SLC family 7 member 11 (xCT)	0.123	0.827	System Xc^-	Chapter 1 and Chapter 3, Figure 5-1
STEAP3	STEAP3 metalloreductase (ferrireductase)	0.682	<0.0001	Ferrireductase	Chapter 4
TFRC	Transferrin receptor	0.367	0.223	Iron import	Chapter 4
TP53	Tumour protein p53	13.284	<0.0001	Transcription factor	Chapter 5
TXNRD1	Thioredoxin Reductase 1	-0.564	<0.0001	Antioxidant and redox regulator	Chapter 1 and Chapter 3
VDAC2	Voltage dependent anion channel 2	0.557	<0.0001	Erastin mechanism of action	Chapter 3
VDAC3	Voltage dependent anion channel 3	0.554	<0.0001	Erastin mechanism of action	Chapter 3

5.2.2 Investigating the role of FSP1 in MM ferroptosis sensitivity

Since FSP1 can mediate resistance to ferroptosis, expression of this protein was investigated in a wider range of MM and DLBCL cell lines to determine whether expression of this protein could account for resistance to RSL3 in MM cells. KMS-11 cells showed markedly higher expression of FSP1 compared to all other MM cell lines (Figure 5-4A,B). However, there was no correlation observed when FSP1 densitometry was plotted against the IC_{50} of RSL3, even when MM and DLBCL cells were assessed individually (Figure 5-4C).

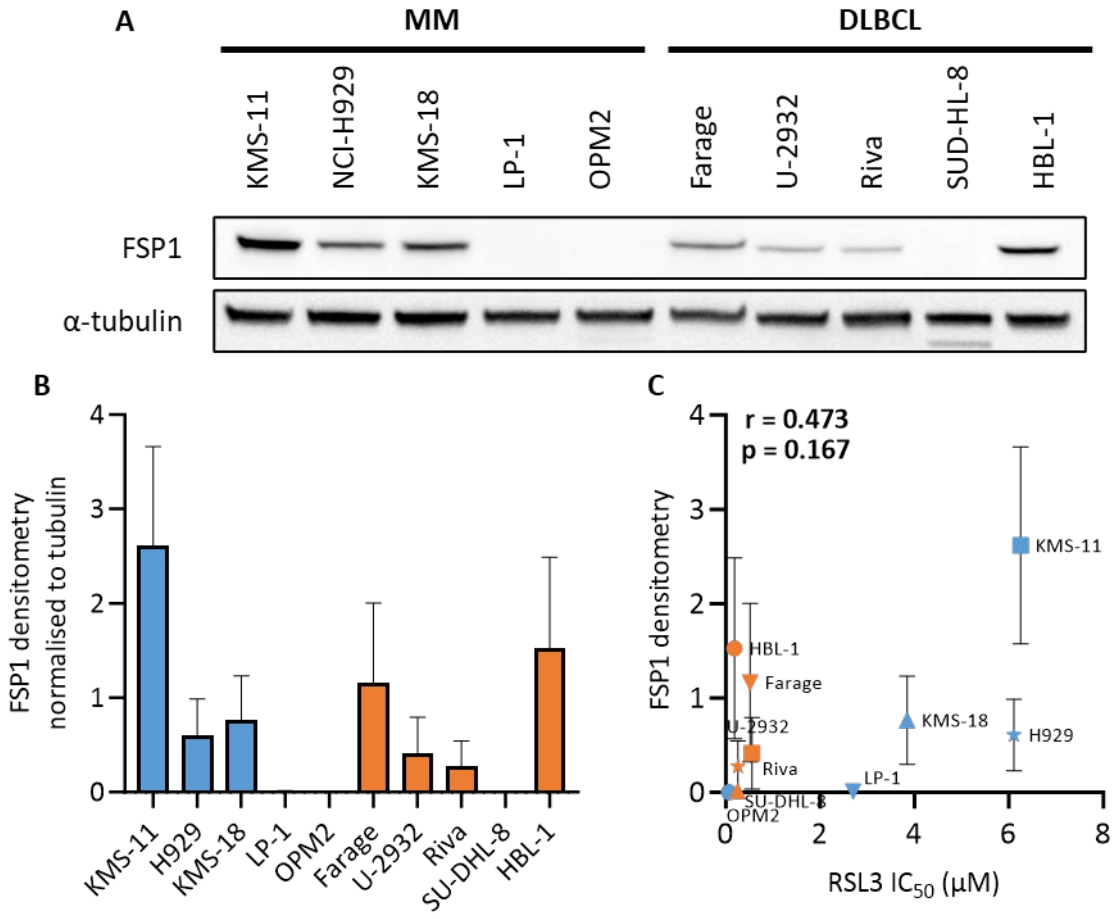

Figure 5-4: FSP1 protein expression is observed in KMS-11 but not OPM2 MM cells.
(A) Representative Western blot of untreated MM and DLBCL cells, probed for FSP1 with α-tubulin as a loading control. (B) Western blot densitometry data are the mean (normalised to tubulin) ± standard deviation from three independent experiments. (C) Pearson correlation was performed, and the Pearson correlation coefficient (r) and p-value (p) are displayed for FSP1 protein expression plotted against RSL3 IC_{50} from Table 3-1.

The FSP1 inhibitor, iFSP1, was combined with RSL3 and there was no significant difference between RSL3 alone and RSL3 plus iFSP1 in terms of cytotoxicity or lipid oxidation in OPM2 cells (Figure 5-5A,B). Conversely, in KMS-11 cells, which had higher FSP1 expression, 1 μM iFSP1 on its own had no effect, but induced a synergistic reduction in cell viability when combined with RSL3 (Figure 5-5C, Table 5-3). The ability of iFSP1 to enhance the effects of RSL3 was also observed in terms of lipid oxidation, whereby at any given concentration of RSL3, the addition of iFSP1 caused an increase in lipid oxidation, despite there being no increase in lipid oxidation induced by the FSP1 inhibitor alone (Figure 5-5D). Lip-1 was effective at preventing both cell death and lipid oxidation, consistent with ferroptosis, which was further supported by ferroptotic morphological changes in KMS-11 cells treated with the combination of RSL3 and iFSP1 (Figure 5-5E). Taken together, these findings suggest FSP1 contributes to ferroptosis resistance in KMS-11 cells which strongly express this protein.

Table 5-3: FSP1 inhibition synergises with GPX4 inhibition in KMS-11 MM cells.

Using the fractional product (FP) method (Webb, 1963), the combined effect of RSL3 and iFSP1 was investigated using average viability data from panel A. An FP value of less than -0.1 indicates synergy.

	[RSL3] (μM)					
	0.10	**0.25**	**0.50**	**0.75**	**1.00**	**2.50**
+ 1 μM FSP1	-0.09	-0.23	-0.40	-0.49	-0.65	-0.62

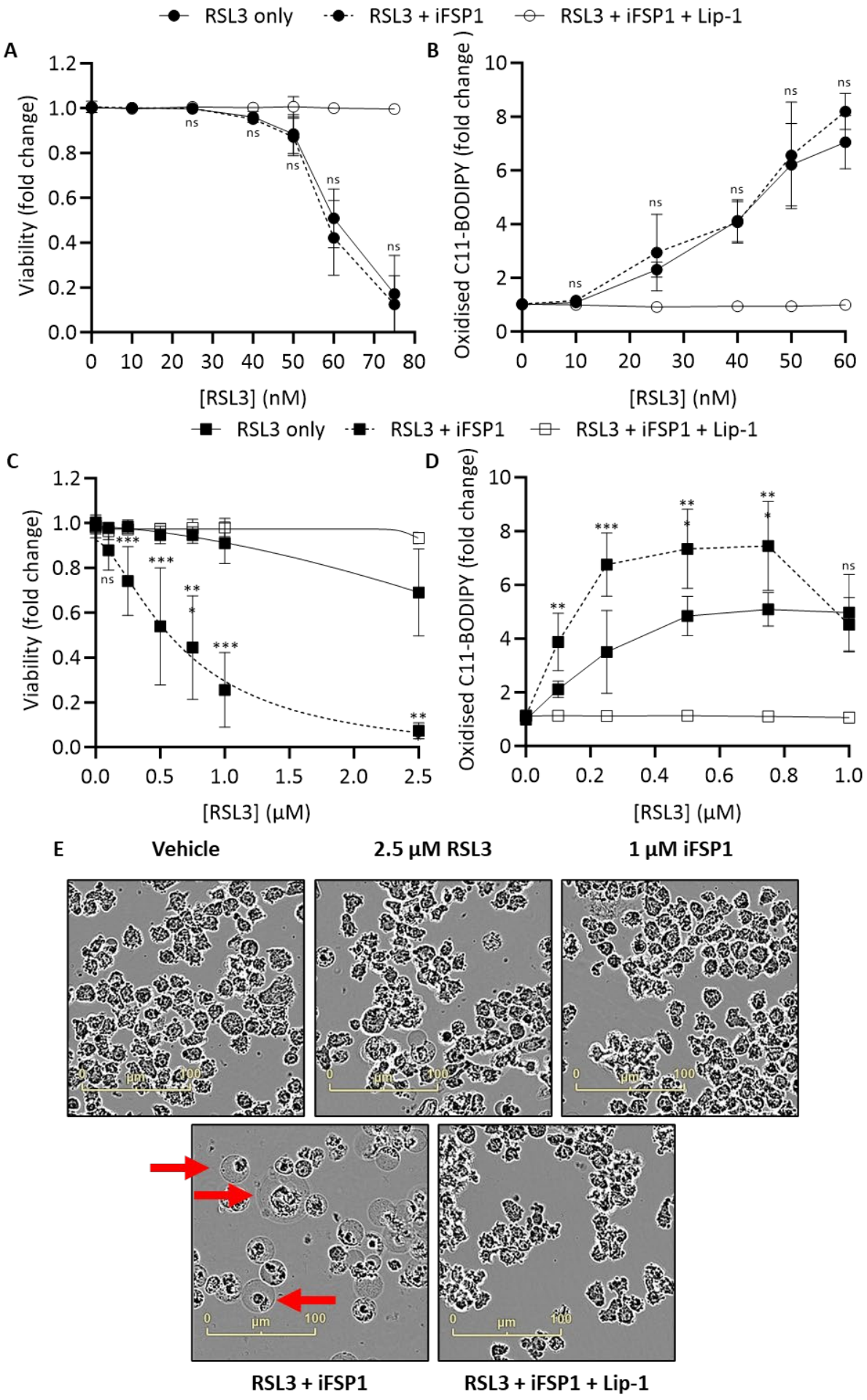
RSL3 only
RSL3 + iFSP1
RSL3 + iFSP1 + Lip-1
A
Viability (fold change)
[RSL3] (nM)
B
Oxidised C11-BODIPY (fold change)
[RSL3] (nM)
C
Viability (fold change)
[RSL3] (µM)
D
Oxidised C11-BODIPY (fold change)
[RSL3] (µM)
E
Vehicle
2.5 µM RSL3
1 µM iFSP1
RSL3 + iFSP1
RSL3 + iFSP1 + Lip-1

Figure 5-5: FSP1 inhibition enhances the effects of RSL3 in KMS-11, but not OPM2 MM cells.

OPM2 (A,B) and KMS-11 (C-E) cells were treated with the indicated concentrations of RSL3, 1 µM iFSP1 and/or 2 µM liproxstatin-1 (Lip-1) for 24 hours. Cell viability (A,C) and the levels of oxidised C11-BODIPY (B,D) were measured by flow cytometry. Data are the mean ± standard deviation from at least three independent experiments. Statistical analyses were performed by two-way ANOVA with a Tukey's multiple comparisons test; * $p<0.05$, ** $p<0.01$, *** $p<0.001$ for RSL3+iFSP1 relative to RSL3 only. (E) KMS-11 cells were treated with 2.5 µM RSL3, 1 µM iFSP1 and/or 2 µM Lip-1 with images acquired after 24 hours using an Incucyte Live Cell Imager. Red arrows indicate cells displaying the "ballooning" phenotype that is characteristic of ferroptosis.

A doxycycline-inducible shRNA-mediated knockdown of FSP1 was attempted in KMS-11 cells but proved unsuccessful (Supplementary Figure 5-A). Given that iFSP1 did not affect cell viability on its own, a CRISPR knockout was subsequently used to further investigate the role of FSP1 in the sensitivity of KMS-11 cells to RSL3 (Figure 5-6). Without a fluorescent marker in the CRISPR plasmid, puromycin selection was used to culture transformed cells, before fluorescence activated cell sorting (FACS) was performed to isolate a single-cell into each well of a 96-well plate. Given that suspension cells can be difficult to culture from single cells, cells were also sorted at 5 cells/well. Colonies were assigned a name based on the number of cells grown from (B = 1 cell/well, C = 5 cells/well) and the well number. Eight sub-clones were established: four with the empty lentiCRISPRv2 puro plasmids, and four with the lentiCRISPRv2-sgFSP1 plasmid with complete FSP1 knockout observed by Western blot (Figure 5-6). KMS-11 empty C2 (referred to as empty vector in subsequent figures), sgFSP1 C10 and sgFSP1 B8 were selected for downstream analyses.

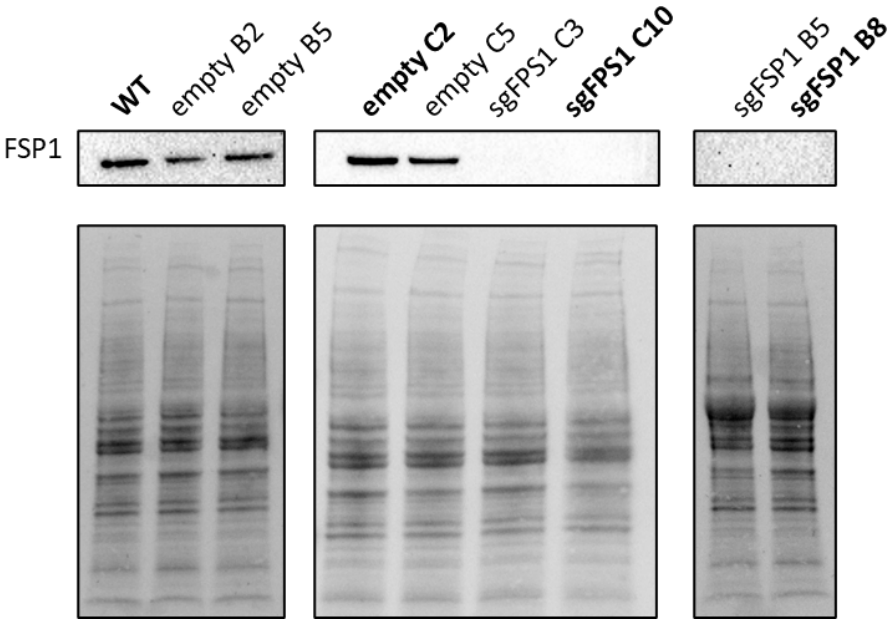

Figure 5-6: CRISPR knockout of FSP1 in KMS-11 MM cells.

KMS-11 wild-type (WT), KMS-11 CRISPR clones with empty lentiCRISPRv2 plasmid and lentiCRISPRv2-sgFSP1 plasmid were harvested for protein extraction after puromycin selection and fluorescence activated cell sorting (FACS). Western blots were probed for FSP1, with total protein in each lane assessed to control for equal loading.

Cell viability and lipid oxidation following 24 hours of RSL3 treatment was investigated in the selected CRISPR cell lines, alongside KMS-11 wild type cells (Figure 5-7). Whilst wild type and empty vector cells responded similarly to RSL3 with no cell death up to 500 nM and minimal lipid oxidation, both FSP1 KO C10 and B8 were significantly more sensitive with IC_{50}s for RSL3 of 166 ± 41.3 and 91.3 ± 14.3 nM RSL3, respectively (Figure 5-7A,B). While RSL3 had no obvious effect on the morphological features of the wild type and empty vector cells, the FSP1 KOs C10 and B8 displayed the classic swollen cytoplasm associated with ferroptosis following treatment, which was prevented by Lip-1 (Figure 5-8).

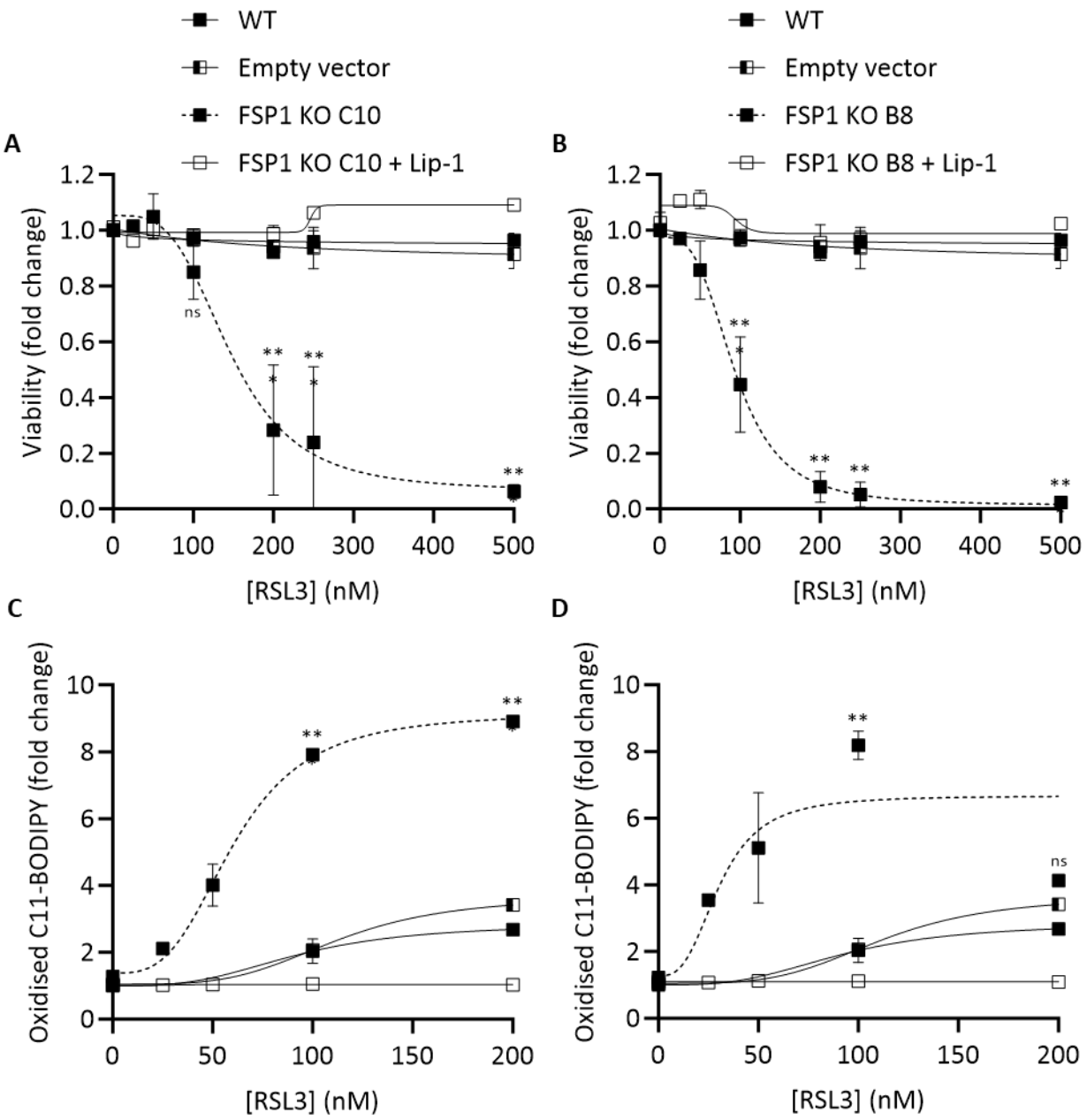

Figure 5-7: FSP1 knockout KMS-11 cells are markedly more sensitive to RSL3 compared to control cells.

KMS-11 wild type (WT), empty vector (empty C2), FSP1 KO C10 and FSP1 KO B8 cells were treated with the indicated concentrations of RSL3 and/or 2 µM liproxstatin-1 (Lip-1) for 24 hours. Cell viability (A,B) and the levels of oxidised C11-BODIPY (C,D) were measured by flow cytometry. Data are the mean ± standard deviation from at least three independent experiments. Statistical analyses were performed by two-way ANOVA with a Tukey's multiple comparisons test; ns indicates no significant difference, ** $p<0.01$, *** $p<0.001$ for FSP1 knockout relative to WT cells.

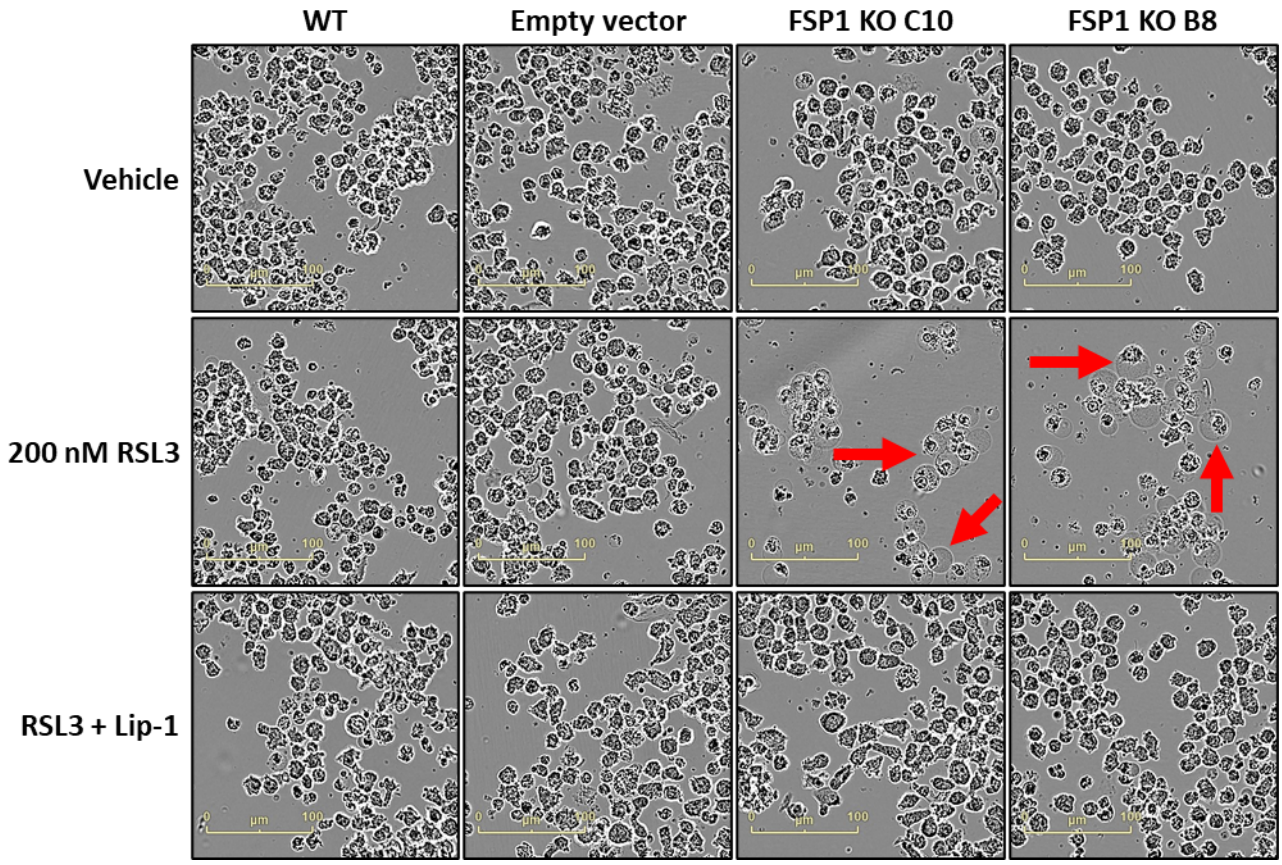

Figure 5-8: FSP1 knockout cells treated with RSL3 exhibit the characteristic ferroptosis-associated morphology.

KMS-11 wild type (WT), empty vector (empty C2), FSP1 KO C10 and FSP1 KO B8 cells were treated with 200 nM RSL3 and/or 2 µM liproxstatin-1 (Lip-1) with images acquired after 24 hours using an Incucyte Live Cell Imager. Red arrows indicate cells displaying morphological changes associated with ferroptosis.

5.2.3 Investigating the role of HO-1 in MM ferroptosis sensitivity

Heme oxygenase 1 (*HMOX1*) encodes the HO-1 protein, and given that it can act as both a suppressor or driver of ferroptosis depending on the cellular context, we aimed to investigate its role in ferroptosis sensitivity in MM cells. We observed significantly higher expression of HO-1 in OPM2 compared to KMS-11 cells ($p = 0.0090$) (Figure 5-9A). HO-1 was expressed to varying degrees across our panel of MM and DLBCL cell lines, with no apparent correlation with RSL3 sensitivity (Figure 5-9C,D). Given the variable role of HO-1 in ferroptosis sensitivity, we aimed to determine whether modulating the activity and expression of this protein effects ferroptosis sensitivity in OPM2 and/or KMS-11 MM cells.

In KMS-11 cells, the HO-1 inhibitor, zinc protoporphyrin IX (ZnPPIX), had no effect on cellular viability or lipid oxidation after 24 hours of treatment at doses ranging from 0.5 to 10 µM (Figure 5-10). At 5 µM RSL3, the mean viability of KMS-11 cells was 50.1% (relative to untreated), and the addition of 10 µM ZnPPIX caused a small, but statistically significant increase in the mean viability to 62.3% ($p = 0.0410$) (Figure 5-10A). In the absence of an easily accessible assay to measure HO-1 activity and determine the efficacy of the drug at inhibiting HO-1 activity, we decided on a genetic knockdown approach to definitively investigate the role HO-1 plays in the RSL3 sensitivity of MM cells.

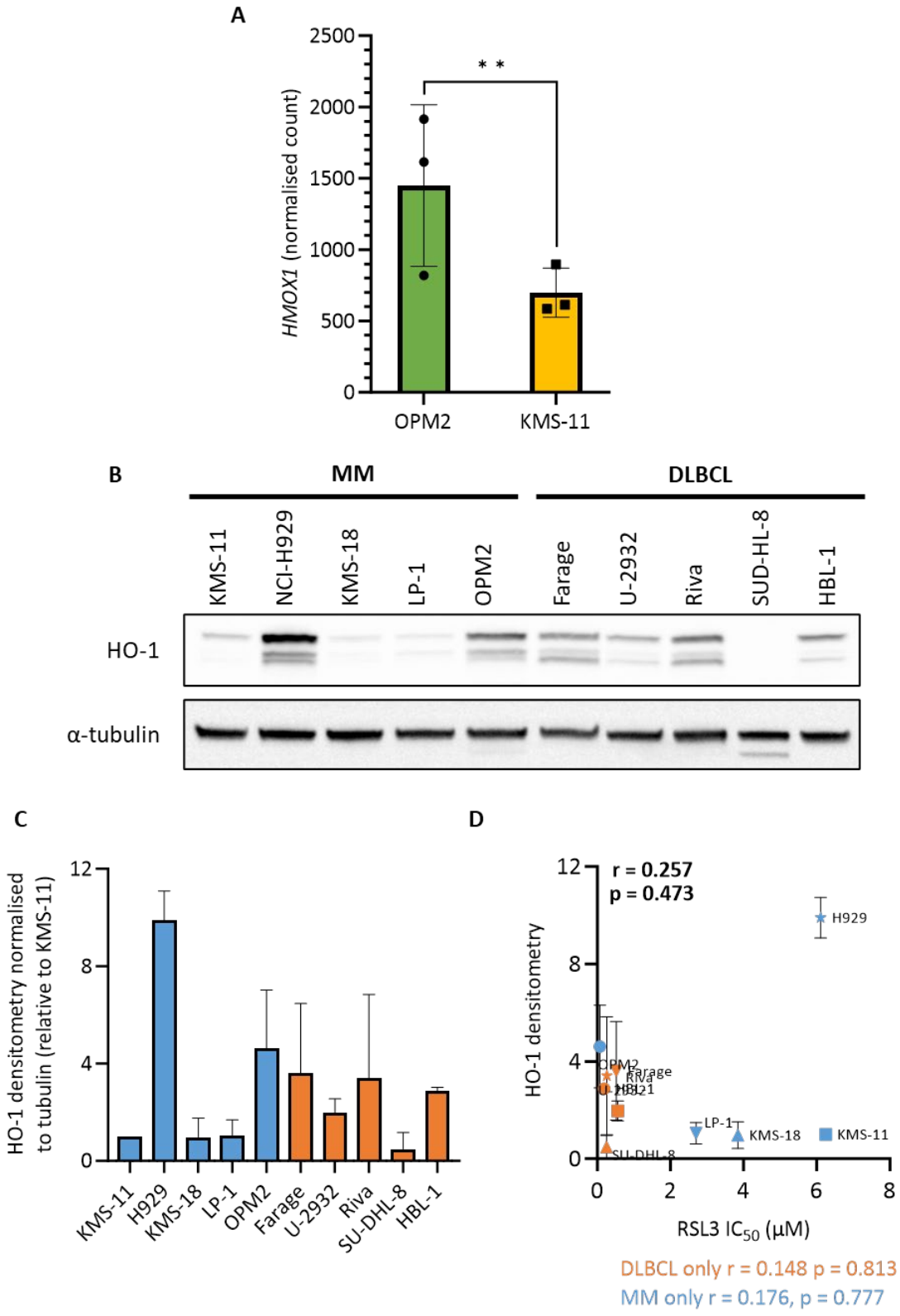

Figure 5-9: HO-1 expression is increased in OPM2 cells compared to KMS-11 cells.

(A) Normalised gene count of *HMOX1* RNA sequencing data. Statistical testing was performed during DESeq2; p-values obtained by the Wald test and then corrected for multiple testing using the Benjamini-Hochberg test, **, p<0.01. (B) Representative Western blot of untreated MM and DLBCL cells, probed for HO-1 with α-tubulin as a loading control. (C) Western blot densitometry data are the mean (normalised to tubulin, relative to KMS-11) ± standard deviation from two independent experiments. (D) Pearson correlation was performed, and the Pearson correlation coefficient (r) and p-value (p) are displayed for HO-1 protein expression plotted against RSL3 IC_{50} from Table 3-1.

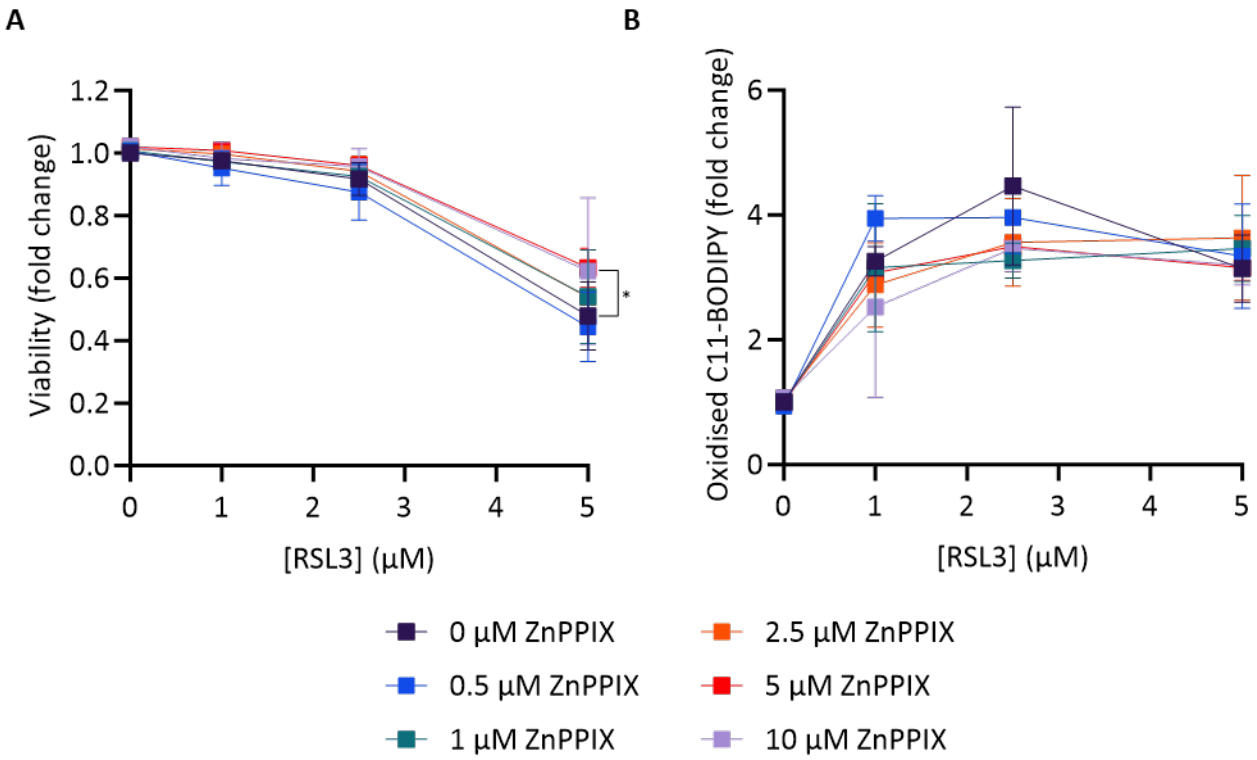

Figure 5-10: KMS-11 cells are not sensitive to the HO-1 inhibitor ZnPPIX.

KMS-11 cells were treated with the indicated concentrations of RSL3 ± ZnPPIX for 24 hours. Cell viability (A) and the levels of oxidised C11-BODIPY (B) were measured by flow cytometry. Data are the mean ± standard deviation from three independent experiments. Statistical analyses were performed by two-way ANOVA with a Tukey's multiple comparisons test; * $p<0.05$.

Using a doxycycline-inducible knockdown, HO-1 expression was successfully reduced in KMS-11 shHMOX1(1) and shHMOX1(2) cells (Figure 5-11A,B). While there was some biological variability in HO-1 expression, significantly lower levels were observed in the doxycycline-induced knockdown cells compared to KMS-11 shREN control cells (Figure 5-11B). Despite this difference in the protein expression of HO-1, no significant difference in RSL3 sensitivity was observed between the knockdown and control cells (KMS-11 shREN ± doxycycline, and shHMOX1(1) and (2) without doxycycline) (Figure 5-11C,D).

HO-1 was also successfully knocked down in OPM2 cells, which had a higher baseline level of HO-1 mRNA and protein compared to KMS-11 (Figure 5-9). In these cells, however, expression of HO-1 was lower in shHMOX1(1) and (2) even before doxycycline was added (Figure 5-12B). This resulted in no statistically significant difference in HO-1 expression in knockdown cells before and after doxycycline treatment. However, after treatment with doxycycline, there was a significant decrease in HO-1 expression in shHMOX1(1) ($p = 0.0036$) and shHMOX1(2) ($p = 0.0041$) knockdown cells compared to untreated OPM2 shREN control cells (Figure 5-12B). The addition of doxycycline produced a small and statistically insignificant decrease in the IC_{50} of RSL3; this effect was also observed in the OPM2 shREN cells which retained expression of HO-1, indicating a doxycycline-mediated effect, independent of HO-1 (Figure 5-12C,D).

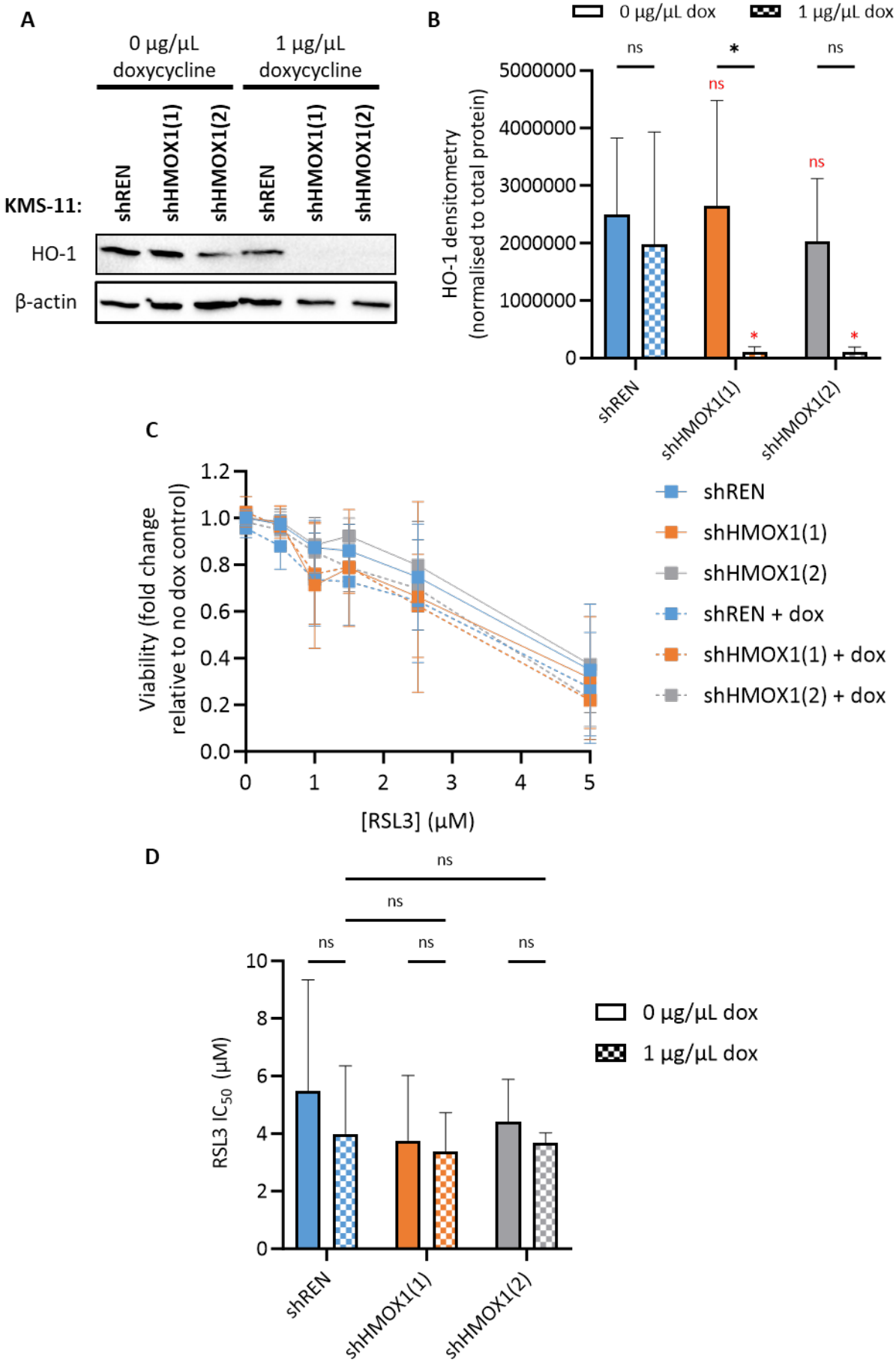
A
0 µg/µL doxycycline
1 µg/µL doxycycline
shREN
shHMOX1(1)
shHMOX1(2)
shREN
shHMOX1(1)
shHMOX1(2)
KMS-11:
HO-1
β-actin
B
0 µg/µL dox
1 µg/µL dox
HO-1 densitometry (normalised to total protein)
5000000
4000000
3000000
2000000
1000000
0
ns
*
ns
ns
ns
*
*
shREN
shHMOX1(1)
shHMOX1(2)
C
Viability (fold change relative to no dox control)
1.2
1.0
0.8
0.6
0.4
0.2
0.0
0
1
2
3
4
5
[RSL3] (µM)
shREN
shHMOX1(1)
shHMOX1(2)
shREN + dox
shHMOX1(1) + dox
shHMOX1(2) + dox
D
ns
ns
ns
ns
ns
RSL3 IC50 (µM)
10
8
6
4
2
0
shREN
shHMOX1(1)
shHMOX1(2)
0 µg/µL dox
1 µg/µL dox

Figure 5-11: Knockdown of HO-1 does not affect RSL3 sensitivity in KMS-11 MM cells.

(A) KMS-11 shREN, shHMOX1(1) and shHMOX1(2) were treated with 1 μg/μL doxycycline (dox) and the expression of HO-1 was assessed after 48 hours by Western blot, with β-actin used as a loading control. (B) Western blot densitometry data are the mean ± standard deviation from three independent experiments (normalised to total protein) (images of replicate Western blot data can be found in Supplementary Figure 5-B). Statistical analyses were performed by two-way ANOVA with an uncorrected Fisher's least significant difference test for multiple comparisons; ns indicates no significant difference, * $p<0.05$; statistics values in red are relative to shREN untreated control. (C) KMS-11 shREN, shHMOX1(1) and shHMOX1(2) were first treated with 1 μg/μL doxycycline for 48 hours, and then RSL3 was added for a further 24 hours before cell viability was measured by flow cytometry. Data are the mean ± standard deviation from three independent experiments. (D) The mean IC_{50} of RSL3 ± standard deviation was generated by fitting a sigmoidal 4PL curve for each biological replicate from panel C (constraints used were bottom = 0, top < 1). Statistical analyses were performed by two-way ANOVA with an uncorrected Fisher's least significant difference test for multiple comparisons; ns indicates no significant difference.

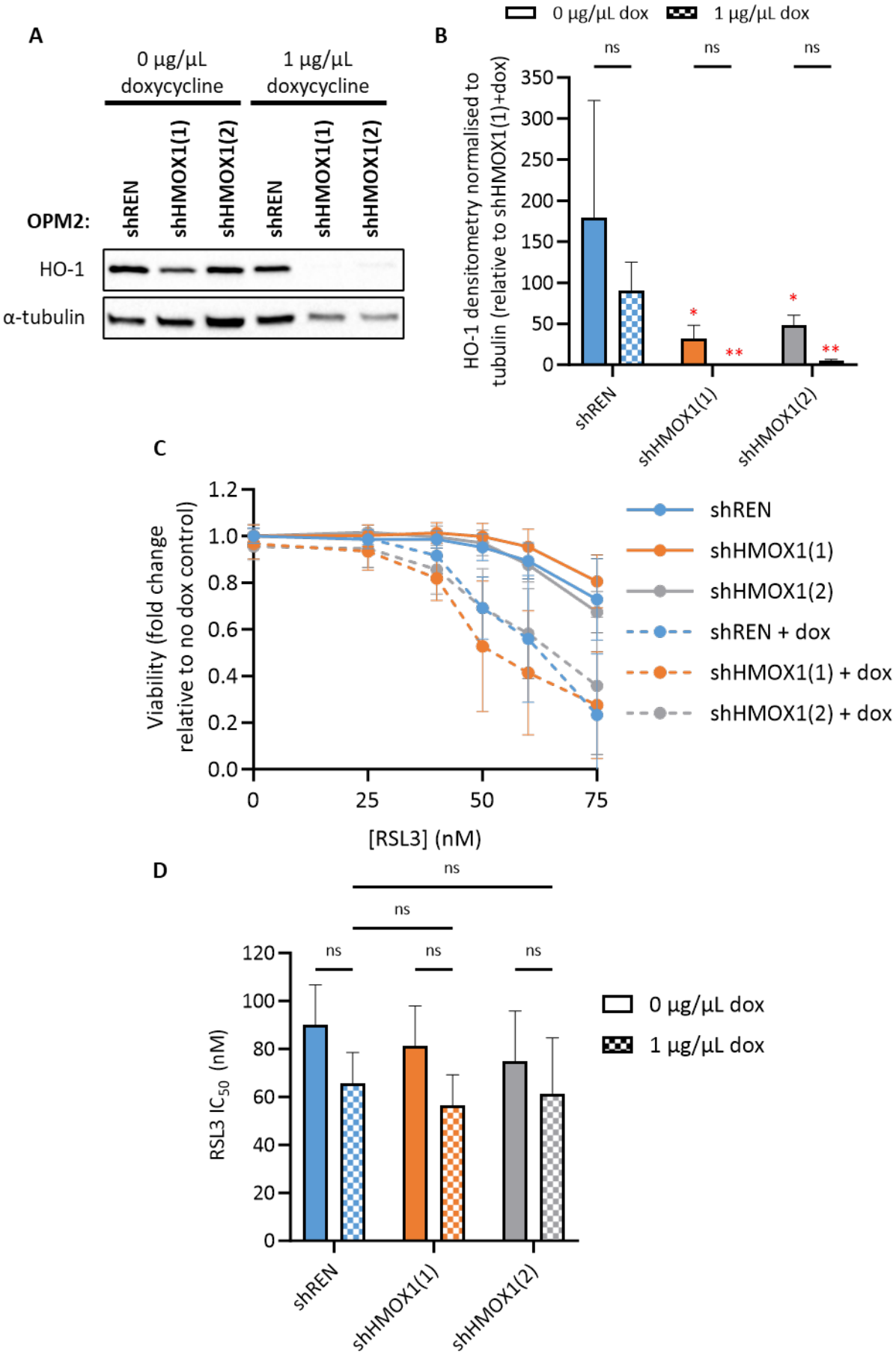
A
0 µg/µL doxycycline
1 µg/µL doxycycline
shREN
shHMOX1(1)
shHMOX1(2)
shREN
shHMOX1(1)
shHMOX1(2)
OPM2:
HO-1
α-tubulin
B
0 µg/µL dox
1 µg/µL dox
HO-1 densitometry normalised to tubulin (relative to shHMOX1(1)+dox)
ns
ns
ns
shREN
shHMOX1(1)
shHMOX1(2)
C
Viability (fold change relative to no dox control)
[RSL3] (nM)
shREN
shHMOX1(1)
shHMOX1(2)
shREN + dox
shHMOX1(1) + dox
shHMOX1(2) + dox
D
RSL3 IC50 (nM)
ns
ns
ns
ns
0 µg/µL dox
1 µg/µL dox
shREN
shHMOX1(1)
shHMOX1(2)

Figure 5-12: Knockdown of HO-1 does not affect RSL3 sensitivity in OPM2 MM cells.

(A) OPM2 shREN, shHMOX1(1) and shHMOX1(2) were treated with 1 μg/μL doxycycline (dox) and the expression of HO-1 was assessed after 48 hours by Western blot, with α-tubulin used as a loading control. (B) Western blot densitometry data are the mean ± standard deviation from three independent experiments (normalised to α-tubulin, relative to the cell line with the smallest standard deviation; OPM2 shHMOX1(1)+dox) (images of replicate Western blot data can be found in Supplementary Figure 5-C). Statistical analyses were performed by two-way ANOVA with an uncorrected Fisher's least significant difference test for multiple comparisons; ns indicates no significant difference, * $p<0.05$, ** $p<0.01$; statistics values in red are relative to shREN untreated control. (C) OPM2 shREN, shHMOX1(1) and shHMOX1(2) were first treated with 1 μg/μL doxycycline for 48 hours, and then RSL3 was added for a further 24 hours before cell viability was measured by flow cytometry. Data are the mean ± standard deviation from three independent experiments. (D) The mean IC_{50} of RSL3 ± standard deviation was generated by fitting a sigmoidal 4PL curve for each biological replicate from panel C (constraints used were bottom = 0, top < 1). Statistical analyses were performed by two-way ANOVA with an uncorrected Fisher's least significant difference test for multiple comparisons; ns indicates no significant difference.

We sought to investigate whether treating HO-1 knockdown cells with RSL3 results in re-expression of HO-1 (Figure 5-13). In OPM2 cells, no significant increase in HO-1 expression was observed following RSL3 treatment compared to their respective controls, across three biological replicates (Figure 5-13A,B). In KMS-11 cells, however, an increase in HO-1 was observed in KMS-11 shREN control, shHMOX1(1) and (2) cells after treatment with 1 μM RSL3 for 24 hours (Figure 5-13A,C). A statistical analysis of the effects of RSL3 on HO-1 expression in the KMS-11 HO-1 knockdown cells was not performed as data was only available from one biological replicate. However, the effects of RSL3 on HO-1 expression in wild type KMS-11, as well as OPM2 cells were investigated, and the data is presented in the subsequent sections.

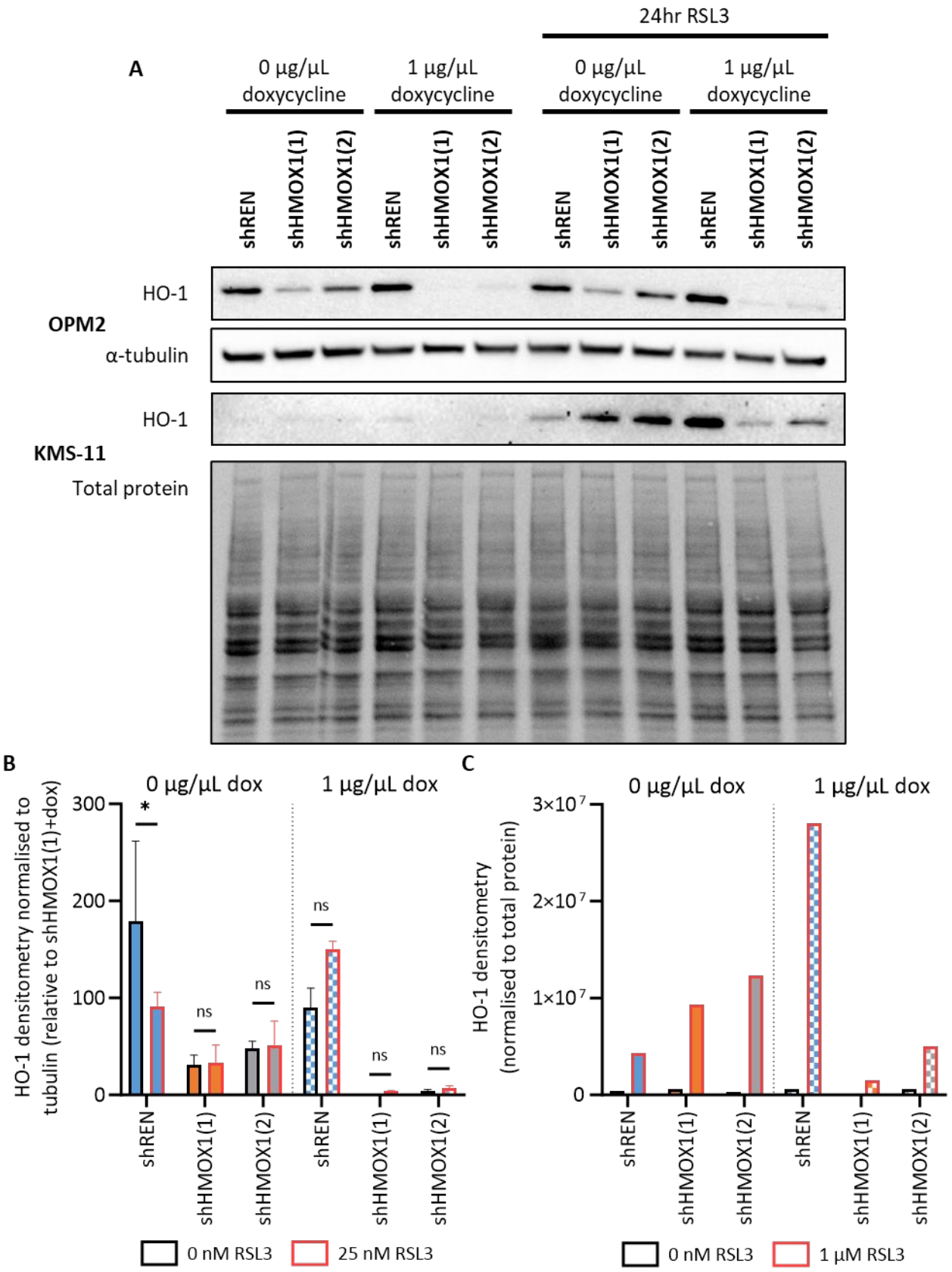

Figure 5-13: RSL3 causes re-expression of HO-1 in KMS-11 HO-1 knockdown cells.

(A) OPM2 and KMS-11 shREN, shHMOX1(1) and shHMOX1(2) were treated with 1 µg/µL doxycycline (dox) for 48 hours, and RSL3 was added for a further 24 hours (25 nM RSL3 for OPM2 and 1 µM RSL3 for KMS-11). At the final time point of 72 hours, HO-1 expression was assessed by Western blot, with α-tubulin or total

protein in each lane used as loading controls. (B) OPM2 Western blot densitometry data are the mean ± standard deviation from three independent experiments (normalised to α-tubulin, relative to cell line with the smallest standard deviation; OPM2 shHMOX1(1)+dox) (images of replicate Western blot data can be found in Supplementary Figure 5-C). Statistical analyses were performed by two-way ANOVA with an uncorrected Fisher's least significant difference test for multiple comparisons; ns indicates no significant difference, * $p<0.05$. (C) KMS-11 Western blot densitometry data are from one biological replicate (normalised to total protein).

Similar to OPM2 shREN, shHMOX1(1) and (2) cells, RSL3 had no effect on HO-1 expression in OPM2 WT cells at either the genetic or protein level (Figure 5-14A-C, Table 5-4). Although the addition of 100 µM FAC on its own did not cause a significant change in *HMOX1* transcript levels, HO-1 protein levels increased by 2.1-fold in OPM2 cells (Table 5-4). When 100 µM FAC was combined with 25, 50 or 75 nM RSL3, a significant increase in HO-1 protein, but not gene, expression was observed (Figure 5-14C, Table 5-4). Although this difference may reflect post-translational effects, samples for RNA sequencing and protein expression were prepared from cells treated for 4 and 6 hours, respectively, and so the difference may simply be due to treatment time.

Conversely, a significant increase in HO-1 expression was observed in KMS-11 WT cells treated with RSL3 only; 0.5 µM RSL3 caused a 2.1-fold increase at both the transcript and protein levels in KMS-11 cells, and a 30.5-fold increase in protein expression after a 6-hour treatment with 2.5 µM RSL3 (Figure 5-14D-F, Table 5-4). Treatment with 100 µM FAC alone caused a 2.2-fold increase in *HMOX1* transcript levels, and a 4.1-fold increase in expression of the protein. While the combination of 100 µM FAC and 0.5 µM RSL3 caused a greater fold change in *HMOX1* transcript levels compared to each compound alone, the same effect was not seen at the protein level, with no effect of 100 µM FAC observed on expression induced by RSL3 alone (Figure 5-14E,F, Table 5-4).

In contrast, AA caused a marked increase in HO-1 expression in both cell lines (Figure 5-15). AA (20 µM) caused a 6.3 and 9.6-fold increase in *HMOX1* transcript expression in OPM2 and KMS-11 cells, respectively (Figure 5-15B,E, Table 5-4). At the protein level, 60 µM AA induced a 9.2-and 247-fold increase in HO-1 expression in OPM2 and KMS-11 cells, respectively (Figure 5-15C,F, Table 5-4). RSL3 had no effect on the levels of HO-1 expression induced by AA in OPM2 cells, however, it appeared to dampen the AA-induced expression of HO-1 in KMS-11; while 20 µM AA combined with 0.5 µM RSL3 caused a greater fold change in *HMOX1* transcript levels compared to each compound alone, 60 µM AA combined with RSL3 resulted in a smaller fold change in protein levels compared to AA alone (Figure 5-15E,F, Table 5-4).

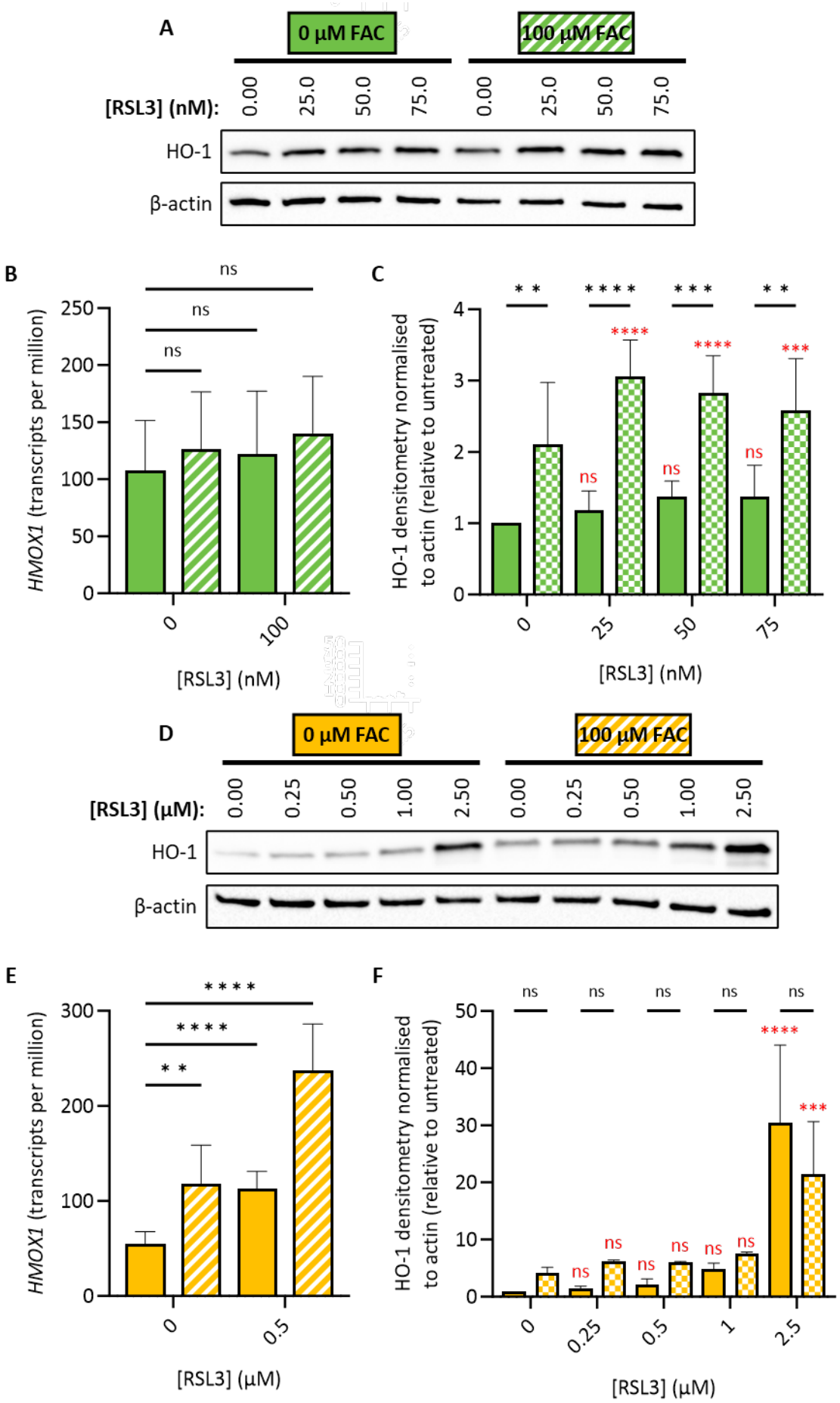
A
0 µM FAC
100 µM FAC
[RSL3] (nM):
0.00
25.0
50.0
75.0
HO-1
β-actin
B
HMOX1 (transcripts per million)
[RSL3] (nM)
C
HO-1 densitometry normalised to actin (relative to untreated)
[RSL3] (nM)
D
0 µM FAC
100 µM FAC
[RSL3] (µM):
0.00
0.25
0.50
1.00
2.50
HO-1
β-actin
E
HMOX1 (transcripts per million)
[RSL3] (µM)
F
HO-1 densitometry normalised to actin (relative to untreated)
[RSL3] (µM)

Figure 5-14: Ferroptosis induction causes changes to HO-1 expression.

(A,D) OPM2 and KMS-11 cells were treated with the indicated concentrations of RSL3 ± 100 μM ferric ammonium citrate (FAC) for 6 hours. Heme oxygenase 1 (HO-1) expression was measured by Western blot and β-actin was used as a loading control. (B,E) OPM2 and KMS-11 cells were treated with the indicated concentrations of RSL3 ± 100 μM FAC for 4 hours. Normalised *HMOX1* transcripts per million were obtained from RNA sequencing and statistical testing was performed during DESeq2; p-values obtained by the Wald test and then corrected for multiple testing using the Benjamini-Hochberg test; ns indicates no significant difference, ** $p<0.01$, **** $p<0.0001$. (C,F) Western blot densitometry data are the mean (normalised to actin) fold changes relative to untreated controls ± standard deviation from three independent experiments (images of replicate Western blot data can be found in Supplementary Figure 5-D). Statistical analyses were performed by two-way ANOVA with an uncorrected Fisher's least significant difference test for multiple comparisons; ns indicates no significant difference, ** $p<0.01$, *** $p<0.001$, **** $p<0.0001$. Statistics values in red are comparisons with untreated controls.

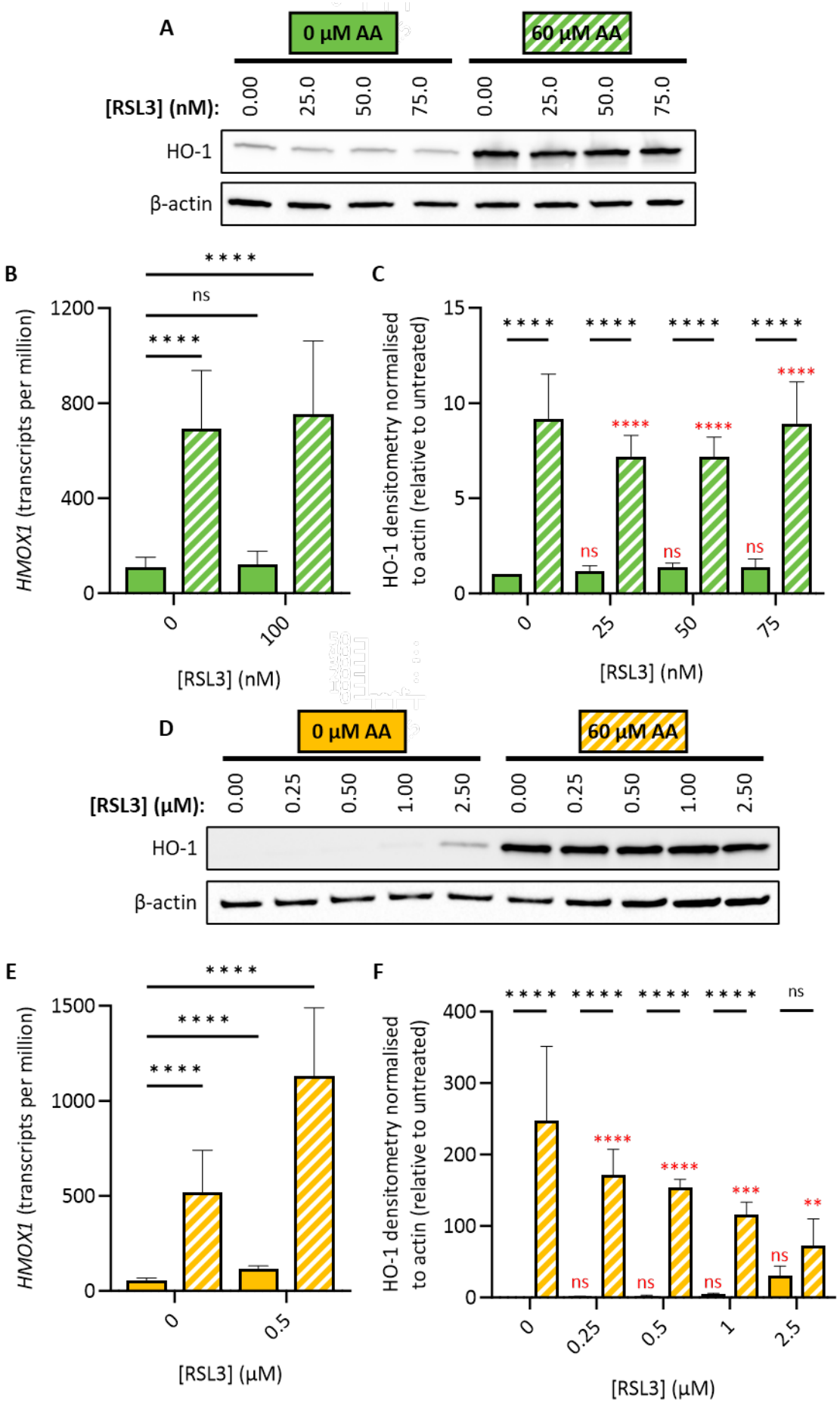
A
0 µM AA
60 µM AA
[RSL3] (nM):
0.00
25.0
50.0
75.0
HO-1
β-actin
B
HMOX1 (transcripts per million)
[RSL3] (nM)
C
HO-1 densitometry normalised to actin (relative to untreated)
[RSL3] (nM)
D
0 µM AA
60 µM AA
[RSL3] (µM):
0.00
0.25
0.50
1.00
2.50
HO-1
β-actin
E
HMOX1 (transcripts per million)
[RSL3] (µM)
F
HO-1 densitometry normalised to actin (relative to untreated)
[RSL3] (µM)

Figure 5-15: RSL3 induces HO-1 expression in KMS-11, but not OPM2 cells, whilst AA induces marked expression of the protein in both cell lines.

(A,D) OPM2 and KMS-11 cells were treated with the indicated concentrations of RSL3 ± 60 μM arachidonic acid (AA) for 6 hours. Heme oxygenase 1 (HO-1) expression was measured by Western blot with β-actin as a loading control. (B,E) OPM2 and KMS-11 cells were treated with the indicated concentrations of RSL3 ± 20 μM AA for 4 hours. Normalised *HMOX1* transcripts per million were obtained from RNA sequencing and statistical analyses were performed using DESeq2; p-values were obtained using the Wald test and then corrected for multiple testing using the Benjamini-Hochberg test; ns indicates no significant difference, ** $p<0.01$, **** $p<0.0001$. (C,F) Western blot densitometry data are the mean (normalised to actin) fold changes relative to untreated controls ± standard deviation from three independent experiments (images of replicate Western blot data can be found in Supplementary Figure 5-E). Statistical analyses were performed by two-way ANOVA with an uncorrected Fisher's least significant difference test for multiple comparisons; ns indicates no significant difference, ** $p<0.01$, *** $p<0.001$, **** $p<0.0001$. Statistics values in red are comparisons with untreated controls.

Table 5-4: Average fold change values for HO-1 transcript and protein levels following ferroptosis induction.

Average fold change relative to untreated control for RNA sequencing and protein densitometry data in Figure 5-14 and Figure 5-15 panels B, C, E, F.

		RSL3 only		100 μM FAC		20 μM AA	60 μM AA
		RNA	**Protein**	**RNA**	**Protein**	**RNA**	**Protein**
KMS-11	0 μM RSL3	1	1	2.2	4.1	9.6	247.0
	0.5 μM RSL3	2.1	2.1	4.4	6.0	20.4	154.3
	2.5 μM RSL3	NA	30.5	NA	21.4	NA	72.0
OPM2	0 nM RSL3	1	1	1.2	2.1	6.3	9.2
	75 nM RSL3	NA	1.4	NA	2.6	NA	8.9
	100 nM RSL3	1.1	NA	1.3	NA	6.9	NA

5.3 Discussion

5.3.1 Differential expression of ferroptosis-related genes in KMS-11 and OPM2

In general, KMS-11 and OPM2 cells had marked differences in baseline gene expression, with 4375 genes differentially expressed between the two cell lines (Figure 5-2A). Of these 4375 genes, 130 were ferroptosis-related according to the FerrDb ferroptosis database (Figure 5-2B) (Zhou et al., 2023). When looking at the specific role these genes play in ferroptosis, both KMS-11 and OPM2 expressed genes that drive ferroptosis as well as genes that suppress ferroptosis, despite the significant difference in their sensitivity to RSL3 (Figure 5-2C, Figure 5-3A). It is therefore likely that the interaction between the proteins encoded by these genes, their relative activity levels, and other cellular contexts might contribute to ferroptosis sensitivity. Assessing the expression of individual genes is not always a useful tool in these types of analyses given that the genes are often not regulated in isolation. Gene set enrichment analysis (GSEA) allows for the investigation of large datasets of genes, and assessment of changes in gene expression associated with specific pathways. This allows for genes with only small changes in expression to be included in the analysis, as they may modulate the activity of a broader pathway. In the current study, we used GSEA to determine whether specific gene sets were enriched in one cell line compared to the other. This analysis identified genes with known roles in the Selenoamino Acid Metabolism pathway (Williams, 2015) as being enriched in ferroptosis-sensitive OPM2 compared to KMS-11 cells (nominal p-value < 0.001) (Figure 5 2C). Conversely, we found that genes included in the Wiki Pathways Ferroptosis gene set (Hanspers et al., 2024) were not enriched in one cell line compared to the other (nominal p-value = 0.527) (Figure 5-2D). Rather, we observed a marked difference in the expression of ferroptosis-related genes between KMS-11 and OPM2 cells (Figure 5-2D, Figure 5-3A).

While KMS-11 cells expressed higher levels of *CBS*, which encodes the cystathionine beta-synthase enzyme that converts Hcy to cystathionine in the transsulfuration pathway, OPM2 cells had higher levels of other genes involved in GSH synthesis, including *SLC38A1, SLC3A2, SLC1A5* and *CTH* (Figure 5-1, Figure 5-3A, Table 5-2). The levels of GSH were not assessed to confirm whether an increase in the expression of these genes correlates with higher intracellular levels of GSH. However, since RSL3 directly inhibits GPX4, its efficacy should not be impacted by changes in GSH levels (Yang et al., 2014). The higher expression of genes involved in GSH synthesis in OPM2 cells suggests these cells are more reliant on GPX4 to regulate lipid ROS levels. This could explain the sensitivity of OPM2 cells to RSL3, compared to KMS-11 cells which might rely on other GSH-independent antioxidant pathways. Accordingly, we found that KMS-11 cells express higher levels of FSP1, an anti-ferroptotic protein whose mechanism of action does not involve intracellular GSH, GPX4 activity, ACSL4 expression or fatty acid composition (Doll et al., 2019, Bersuker et al., 2019).

Consistent with protein levels and publicly available data (Figure 4-6A,D), OPM2 cells expressed higher levels of the *FTL* transcript compared to KMS-11 cells (Figure 5-3A, Table 5-2). We also found that OPM2 cells had higher expression of *FTH1* transcript, despite publicly available data indicating similar levels to KMS-11 cells (Figure 4-6D). Although higher expression of these genes, which are involved in iron storage, might indicate ferroptosis resistance through reduction of the labile iron pool (LIP), these OPM2 cells also had higher levels of *NCOA4* compared to KMS-11, which suggests an enhanced ability to undergo ferritinophagy. Furthermore, expression of genes that encode proteins involved in iron import (*SLC11A2* and *SLC39A8*) was higher in OPM2 cells, while KMS-11 cells expressed higher levels of genes involved in iron export (*SLC40A1* and *PCBP2*) as well as *HSPB1*, which decreases iron uptake by preventing TfR recycling (Tang et al., 2021a) (Figure 5-3A, Table 5-2). Tumour protein p53 (*TP53*) transcript levels were higher in OPM2 compared to KMS-11 cells (Figure 5-3A, Table 5-2). *TP53* is often mutated in cancer and has been shown to be hypermethylated in KMS-11 cells, which prevents its transcription (Hurt et al., 2006). In contrast, OPM2 cells express the protein encoded by *TP53,* p53, due to lower levels of gene methylation (Hurt et al., 2006). p53 can play a role in ferroptosis, albeit in a context-dependent manner; while p53 can contribute to ferroptosis by decreasing *SLC7A11* and increasing *SAT1* expression, it can also enhance GSH production to prevent ferroptosis (Tang et al., 2021a). However, neither *SLC7A11* nor *SAT1* transcript levels were significantly different between KMS-11 and OPM2 (Figure 5-3A, Table 5-2). Furthermore, we extracted publicly available *TP53* gene expression data for our panel of DLBCL and MM cell lines (The Human Protein Atlas, 2023m), and found that although DLBCL cells have a higher level of *TP53* compared to MM cells ($p = 0.0300$), there was no correlation between the levels of *TP53* transcript and the IC_{50} of RSL3 (Pearson $r = -0.587$, $p = 0.0970$). This suggests that the mechanisms behind RSL3 sensitivity in MM and DLBCL cells are not *TP53*-dependent. Furthermore, whilst FSP1 was previously identified as a *TP53*-responsive gene it has since been shown to be unaffected by *TP53* mutational status (Doll et al., 2019).

Whilst acyl-CoA synthetase long-chain family (ASCL) members have different substrate preferences, they are all responsible for converting long-chain fatty acids into fatty acyl-CoA esters (Klett et al., 2017, Quan et al., 2021). It has been shown that each isoform can interact with a range of fatty acid substrates including 16:0, 18:0, 18:1 and 20:4 lipids. However, as we have previously discussed, ACSL4 has a preference for polyunsaturated fatty acids (PUFAs), including arachidonic acid (AA, 20:4). Conversely, ACSL1, -3 and -5 have a preference for saturated fatty acids such as palmitic acid (16:0) and other shorter chain fatty acids (16-18 carbons) including oleic acid (18:1) (Klett et al., 2017, Quan et al., 2021). Not only did we show that ferroptosis sensitive cells (OPM2 and DLBCL cells) have more AA-containing phospholipids than resistant MM cells (Figure 3-14), OPM2 cells specifically had 1.4-fold more AA-containing phospholipids compared to KMS-11 cells ($p < 0.0001$). It is therefore unsurprising that OPM2 cells have a higher expression level of *ACSL4*. Relative to OPM2, KMS-11 cells had a higher expression of *ACSL1* and *ACSL5* (Figure 5-3A, Table 5-2). ACSL5 is pro-

apoptotic, can act as a tumour suppressor, and is expressed in the mitochondria, but there is minimal evidence that demonstrate its involvement in ferroptosis (Zhang et al., 2023d, Zhang et al., 2023f). Zhang *et al.* showed that ACSL5 overexpression in hepatocellular carcinoma cells resulted in lipid peroxidation, whereas its inhibition reduced RSL3 efficacy (Zhang et al., 2023f). ACSL1 on the other hand, has been shown to induce ferroptosis by incorporating linoleic acids into neutral lipids (Beatty et al., 2021) but is also responsible for driving ferroptosis resistance through myristoylation of FSP1 (Zhang et al., 2023e). FSP1 myristoylation is required to prevent degradation and enables its expression in the plasma membrane, which is necessary for its anti-ferroptotic effects (Zhang et al., 2023e, Doll et al., 2019). This was demonstrated by Doll *et al*. who showed that GFP-tagged, mutant FSP1 without its predicted myristoylation site, can be seen throughout cells, while GFP-tagged wild type FSP1 is localised to the perinuclear region, endoplasmic reticulum and Golgi apparatus (Doll et al., 2019) Therefore, the higher expression of *ACSL1* in KMS-11 cells compared to OPM2 cells could be related to FSP1 expression in these cells.

It is important to consider that transcript levels do not always correlate with the level or activity of the corresponding protein when drawing conclusions from the RNA sequencing data. These data provide insight into gene expression levels and their association with ferroptosis sensitivity. From the data, two genes were chosen for further investigation, namely *FSP1* and *HMOX1*.

5.3.2 FSP1 inhibition sensitises resistant KMS-11 MM cells to RSL3-induced ferroptosis

Bersuker *et al.* extracted data concerning *FSP1* mRNA expression and sensitivity to RSL3, ML210 and ML162 on 800 cell lines from the Cancer Therapeutics Response Portal (CTRP). The authors showed that *FSP1* expression positively correlated with resistance to GPX4 inhibition, however, this analysis only included non-haematopoietic cancer cells (Bersuker et al., 2019). We extracted *FSP1* mRNA expression and RSL3 sensitivity data for 19 DLBCL cell lines and 26 MM cell lines from the CTRP and did not observe a correlation between *FSP1* mRNA expression and RSL3 sensitivity.

We found that the ferroptosis-resistant cell line, KMS-11, had very high levels of FSP1 protein and the ferroptosis-sensitive cell line, OPM2, did not express FSP1. However, we found that 3 of the 4 ferroptosis resistant MM lines expressed FSP1, with the exception being LP-1 cells, which had undetectable levels of the protein (Figure 5-4A,B). Furthermore, the expression of FSP-1 varied among the RSL3-sensitive DLBCL cell lines, ranging from similar levels to H929 and KMS-18, to undetectable levels in SU-DHL-8 DLBCL cells (Figure 5-4A,B). Accordingly, there was no correlation between FSP1 protein expression and the IC_{50} of RSL3 when all cell lines were assessed together, nor when each malignancy was assessed individually (Figure 5-4C).

Since KMS-11 cells were found to be the most RSL3-resistant among the MM lines and had markedly higher expression levels of FSP1 compared to all other cell lines, we decided to investigate whether these cells could be sensitised to RSL3 by inhibition of FSP1. Doll *et al.* showed that knockout of FSP1 increased the sensitivity of cancer cells to RSL3 and that resistance could be restored by re-expression of mouse FSP1 in MDA-MB-436 breast cancer cells (Doll et al., 2019). However, the role that FSP1 plays in ferroptosis sensitivity in MM is yet to be explored in the literature. We found that, unsurprisingly, iFSP1 did not have an effect on RSL3 cytotoxicity or lipid oxidation in FSP1-null OPM2 cells supporting that iFSP1 specifically targets to FSP1 (Figure 5-4). Conversely, KMS-11 cells were very sensitive to the combination of RSL3 and iFSP1 (Figure 5-5). While iFSP1 on its own had no effect on cell viability or lipid oxidation, it synergised with RSL3, reducing the IC_{50} from 6.251 µM (Table 3-1) to 677.5 nM (Figure 5-5). Moreover, genetic knockout of FSP1 further reduced the IC_{50} of RSL3 to 166 nM and 91.3 nM in the KMS-11 FSP1 KO C10 and FSP1 KO B8 subclones, respectively (Figure 5-7). Whether FSP1 was inhibited by pharmacological means or genetic knockdown, it not only enhanced cell death induced by RSL3, but also increased lipid oxidation levels, an effect that was prevented by Lip-1. Furthermore, cells treated with the combination of RSL3 with inhibition of FSP1 through either genetic or pharmacological means exhibited the characteristic ferroptotic morphology (Figure 5-5D, Figure 5-8). Given that the induced overexpression of FSP1 in ferroptosis-sensitive HT1080 cells protects against ferroptosis (Doll et al., 2019), future research to determine whether the same is true in ferroptosis-sensitive OPM2 and DLBCL cells is feasible. Regardless, our data indicate that FSP1 inhibition effectively enhances ferroptosis induced by RSL3 in resistant KMS-11 MM cells.

5.3.3 Induction of ferroptosis increases the expression of HO-1 in MM cells

It is generally agreed upon that although HO-1 may be cytoprotective at low levels, increased expression causes an increase in labile iron that the cell cannot manage, turning it into a cytotoxic mechanism (Chiang et al., 2018, Hassannia et al., 2019). It is important to investigate the role of HO-1 in ferroptosis in MM given the multiple opposing roles it can play in other malignancies. Andrographolide, an extract from the *Andrographis paniculata* plant was shown to induce ferroptosis in MM cells by reducing the expression of Nrf2 and HO-1 through p38 mitogen-activated protein kinase (MAPK) activation (Li et al., 2023a). Inhibition of p38 reduced the andrographolide-induced downregulation of Nrf2 and HO-1 and abrogated its ability to induce ferroptosis in MM (Li et al., 2023a). Similarly, ethanol extract of *Eclipta prostrata* and the methyltransferase inhibitor, DCG006, also induced ferroptosis in MM cells associated with a decrease in the expression of Nrf2 and its downstream target HO-1 (Li et al., 2024b, Zhang et al., 2024d). However, in all these studies, reducing the expression of Nrf2 may have a broad range of effects given the number of ferroptosis-related genes that it regulates. Therefore, it cannot be concluded if reduced HO-1 expression plays a direct role in modulating ferroptosis in these contexts, or whether it is simply a marker of Nrf2 activity.

HMOX1, the gene that encodes HO-1, was expressed at significantly higher levels in ferroptosis-sensitive OPM2 compared to KMS-11 cells ($p = 0.0092$) (Figure 5-9A). However, HO-1 protein expression varied across the panel of MM and DLBCL cells and did not correlate with RSL3 sensitivity (Figure 5-9D). The HO-1 inhibitor ZnPPIX was used to determine whether HO-1 plays a role in ferroptosis in MM, but no significant effect on RSL3-induced cell death nor lipid oxidation was observed in KMS-11 cells (Figure 5-10). In the absence of a readily available HO-1 activity assay to determine whether ZnPPIX was effectively inhibiting HO-1, we took a genetic approach to reduce the expression of the protein in ferroptosis-sensitive OPM2 cells and ferroptosis-resistant KMS-11 cells. In KMS-11 cells, the expression of HO-1 was significantly reduced, but this did not affect the IC_{50} of RSL3 (Figure 5-11). Likewise, in OPM2, doxycycline caused a small, but insignificant reduction in the IC_{50} of RSL3 in not only the HO-1 knockdown cells, but also the control shREN cells; this indicates a doxycycline-mediated effect rather than an effect due to changes in HO-1 expression (Figure 5-12). Initially, the expression of HO-1 was tested at the timepoint at which RSL3 was added to the cells, to ensure that the knockdown was successful. Given the lack of effects of HO-1 knockdown on RSL3 sensitivity, we subsequently measured the expression of HO-1 at the end point of the assay, after treatment with RSL3 (Figure 5-13). It was determined that a non-lethal dose of 25 nM RSL3 did not induce re-expression of HO-1 in OPM2 cells, however, a non-lethal dose of 1 µM RSL3 caused the expression of HO-1 to increase in KMS-11 shREN, shHMOX1(1) and shHMOX1(2) cells (Figure 5-13). Only one biological replicate of this experiment was performed as we decided further investigations would focus on wild type (WT) KMS-11 and OPM2 cells.

In OPM2 WT cells, HO-1 gene and protein levels were not affected by treatment with RSL3, FAC or the combination of both compounds, with the exception of 100 µM FAC, which caused a relatively small increase in HO-1 protein (Figure 5-14A-C). Conversely, in KMS-11 WT cells, both RSL3 and FAC caused an increase in HO-1 gene and protein expression (Figure 5-14D-F). The ability of FAC to increase HO-1 expression was surprising, particularly given that HO-1 has been shown to drive ferroptosis through increasing the LIP (Hassannia et al., 2018, Chang et al., 2018, Tang et al., 2021b, Meng et al., 2021). AA, on the other hand, had marked effects on HO-1 expression in OPM2 and KMS-11 cells at both the genetic and protein levels (Figure 5-15).

Despite upregulation of HO-1 in OPM2 cells undergoing ferroptosis, it was apparent that this was not necessary for its execution given that HO-1 knockdown and control cells were equally sensitive to RSL3 (Figure 5-12). Furthermore, although RSL3 induced some re-expression of HO-1 in KMS-11 knockdown cells, its expression was less than in the control shREN cells. Taken together, these data support the notion that HO-1 is a marker of ferroptosis in MM rather than a critical element involved in its execution. A CRISPR approach to completely knockout HO-1 expression might be a useful approach to determine whether even

small levels of expression are sufficient for its activity. Given that HO-1 expression does not correlate with RSL3 sensitivity, it's role in ferroptosis might be context dependent; since HO-1 has been shown to contribute to the LIP, the expression of other iron-related proteins, such as ferritin and iron export proteins, might determine the role of HO-1 in ferroptosis in MM cells.

However, HO-1 does represent a potential therapeutic target in MM, which has been demonstrated in bortezomib-resistant MM cell lines (Raninga et al., 2016). The study showed that MM cells upregulate *TXNRD1,* and its inhibition with auranofin induced cell death in both bortezomib sensitive and resistant MM cells. However, a discrepancy was observed between the concentration required to inhibit TXNRD1 and cytotoxic concentrations (Raninga et al., 2016). Subsequently, it was shown that auranofin induced HO-1 expression and when combined with ZnPPIX, auranofin was cytotoxic towards MM cells, but not normal peripheral blood mononuclear cells. While this cell death was shown to involve caspase-3 cleavage, it was not determined whether this was necessary for cell death. Furthermore, an increase in general ROS was observed in cells treated with the TXNRD1 inhibitor alone and was enhanced when HO-1 was also inhibited (Raninga et al., 2016). While these data were not analysed in the context of ferroptosis, the study suggests that MM cells may be able to utilise multiple antioxidant systems. Although Raninga *et al*. showed that HO-1 inhibition enhanced the effects of inhibiting TXNRD1, we did not show its inhibition had any effect on the sensitivity to RSL3. However, inhibition of HO-1 and GPX4 may not be sufficient to induce ferroptosis in KMS-11 cells due to the expression of TXNRD1, as well as other antioxidants such as GCH1, CHMP5, CHMP6 and FSP1 (Figure 5-3, Table 5-2).

5.3.4 Conclusions

Ferroptosis involves the complex interaction of a number of genetic and metabolic pathways and can be induced in various contexts. Accordingly, we showed that OPM2 and KMS-11 cells both express genes that have been shown to prevent, and drive ferroptosis. Likely due to the complexity of the interaction between various genes and proteins, we did not find a correlation between HO-1 expression and RSL3 sensitivity, despite a marked difference in the expression of both *HMOX1* transcript and HO-1 protein in ferroptosis-sensitive OPM2 and resistant KMS-11 cells. However, we did find that FSP1 appears to play an important role in RSL3-resistance in KMS-11 MM cells as genetic or pharmacological inhibition of the protein significantly increased the efficacy of RSL3. Investigating FSP1 inhibition in other FSP1-expressing MM cells should be undertaken to determine whether these effects can be observed in other MM cell lines.

APPENDIX 5A. SUPPLEMENTARY FIGURES

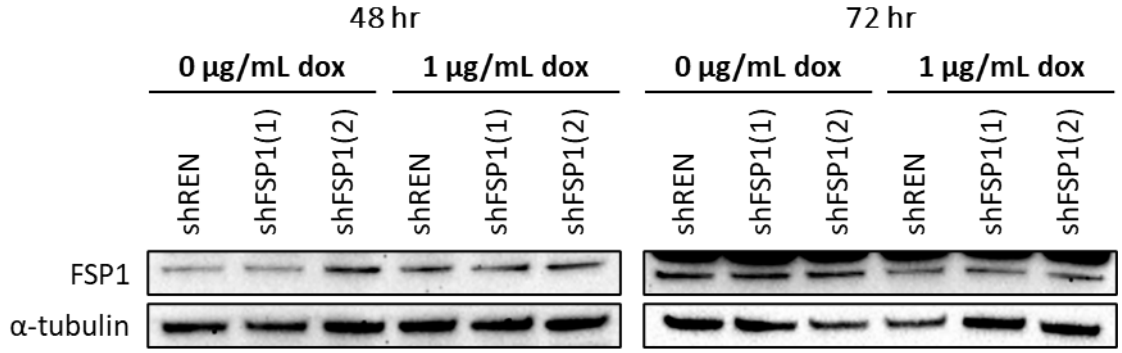

Supplementary Figure 5-A: Doxycycline-inducible knockdown of FSP1 in KMS-11 MM cells.

KMS-11 shREN, shFSP1(1) and shFSP1(2) were treated with 1 µg/mL doxycycline (dox). Cells were harvested for protein extraction after 48 and 72-hours. Western blot probed for FSP1, with α-tubulin as a loading control.

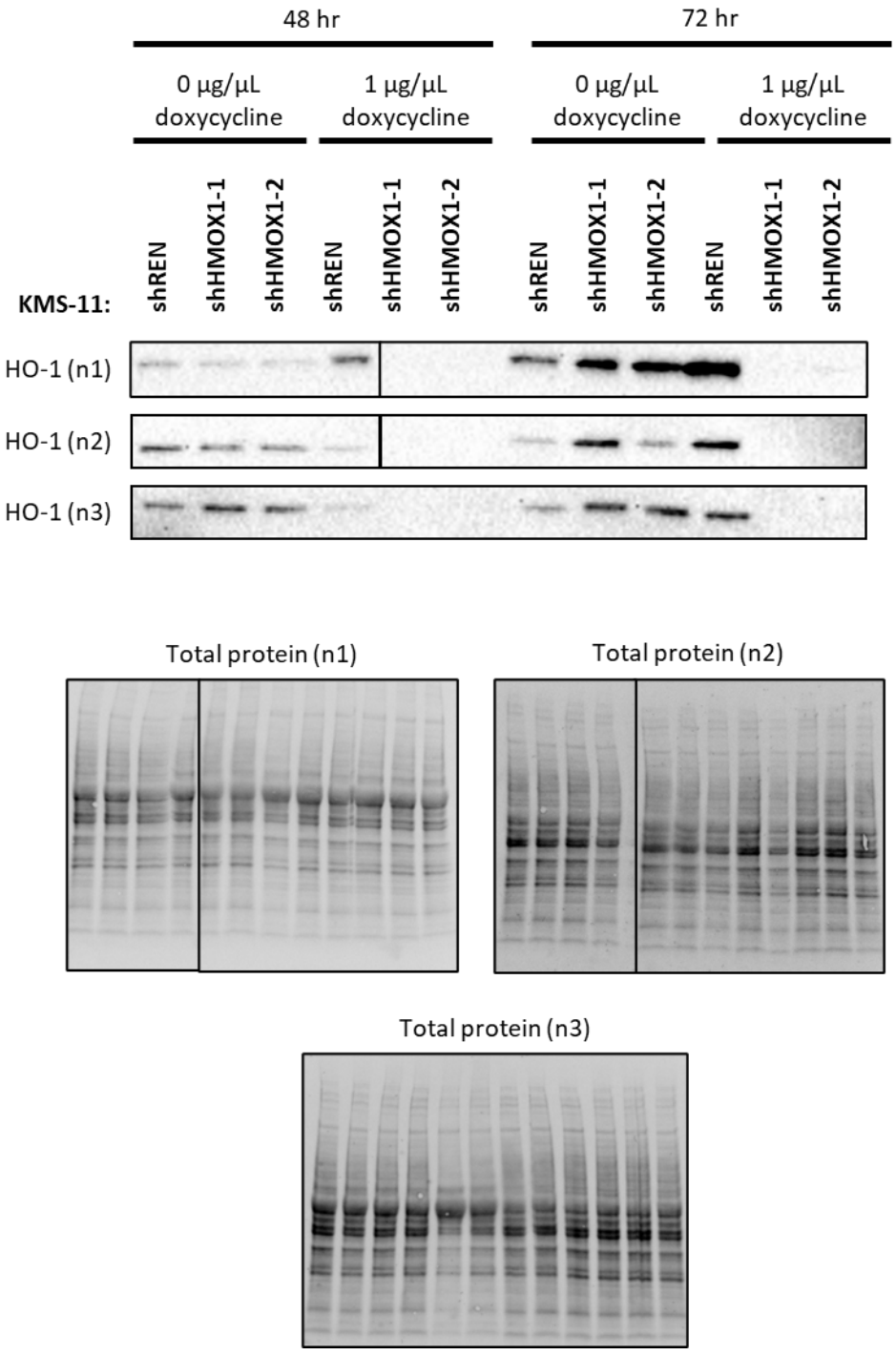

Supplementary Figure 5-B: KMS-11 HO-1 knockdown Western blot biological replicates used to generate densitometry data in Figure 5-11B.

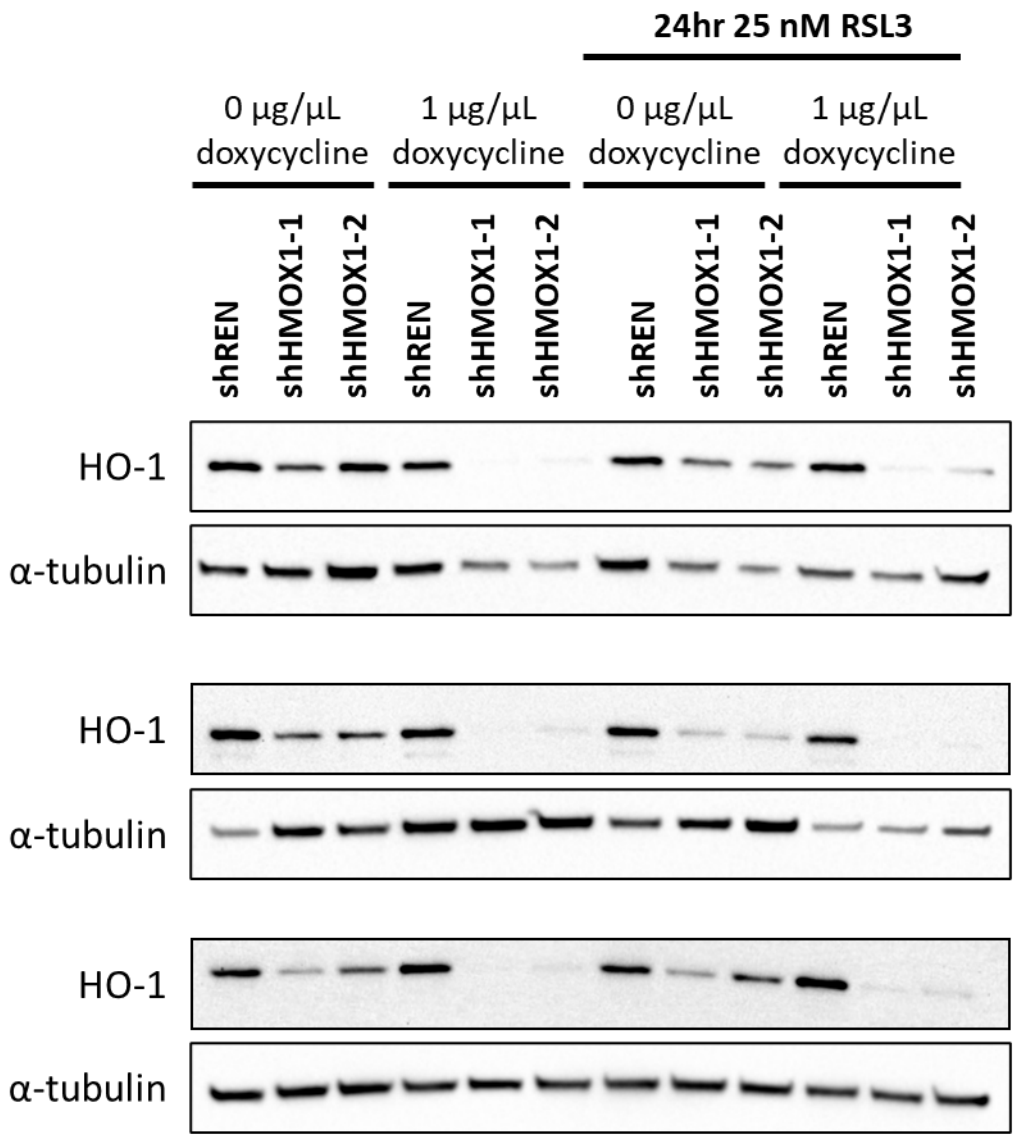

Supplementary Figure 5-C: OPM2 HO-1 knockdown Western blot biological replicates used to generate densitometry data in Figure 5-12B.

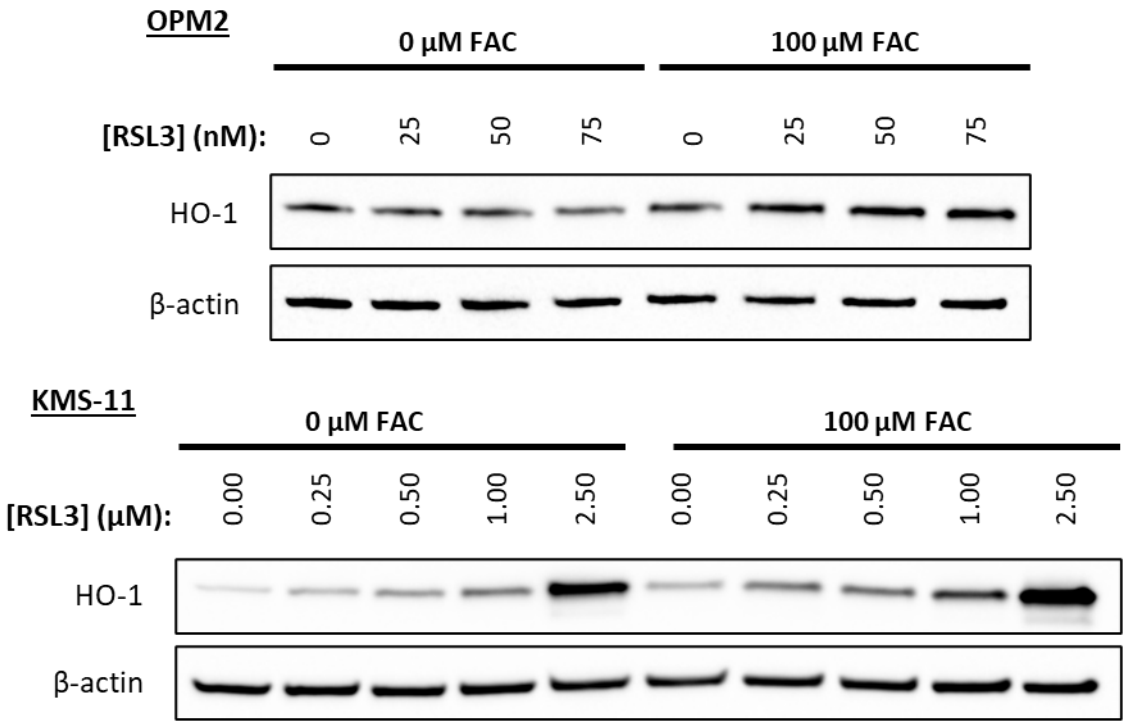

Supplementary Figure 5-D: Western blot biological replicates used to generate densitometry data in Figure 5-14C,F.

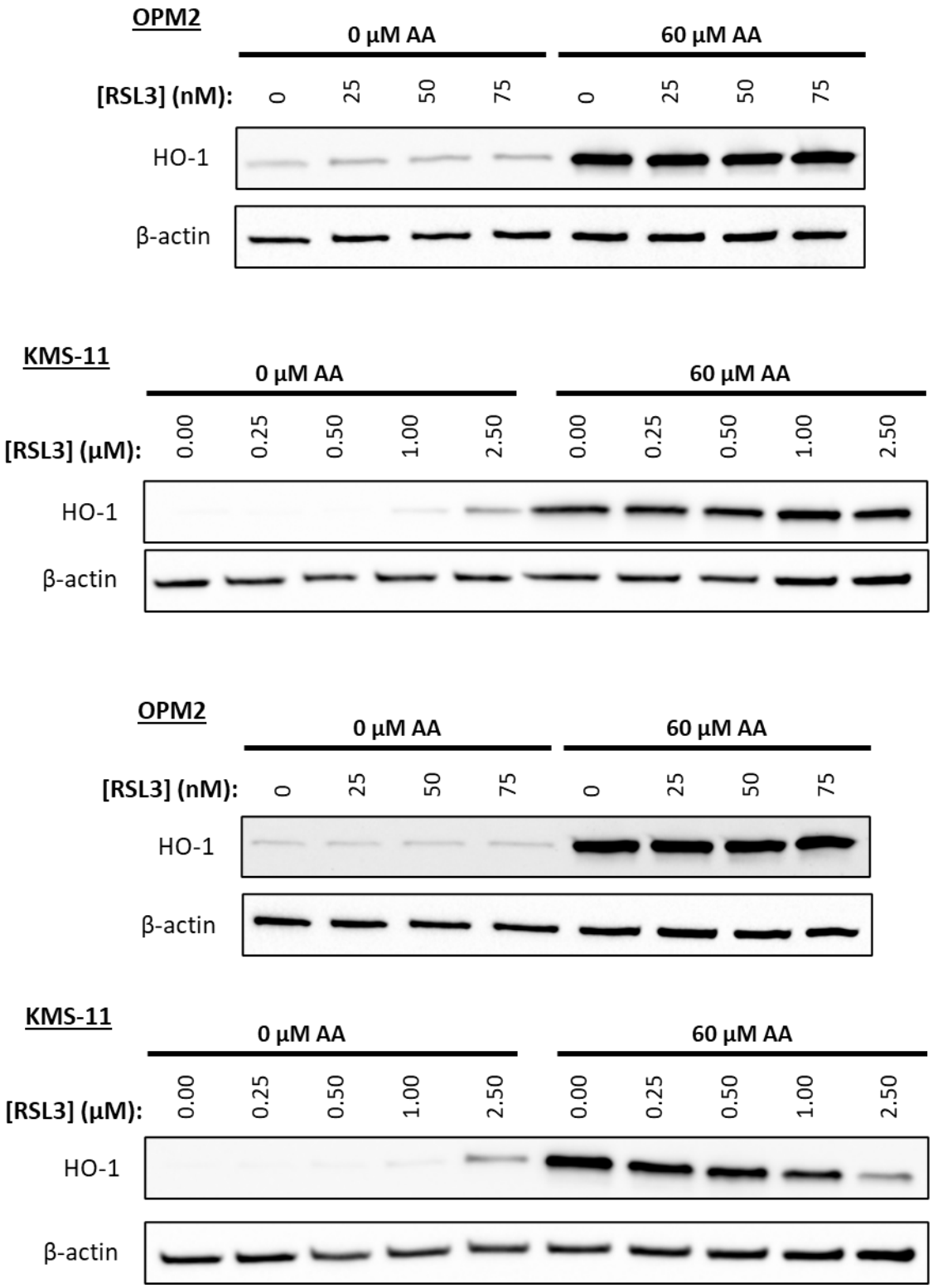

Supplementary Figure 5-E: Western blot biological replicates used to generate densitometry data in Figure 5-15C,F.

CHAPTER 6. INVESTIGATING THE SENSITIVITY OF PRIMARY PATIENT MM CELLS TO FERROPTOSIS

6.1 Introduction

Whilst *in vitro* work with cell lines is an efficient and cost-effective tool for assessing ferroptosis sensitivity in MM, it does not allow for the consideration of other factors that might influence drug sensitivity *in vivo* (Lourenço et al., 2022). This is of particular importance in the context of MM given the prominent role the bone marrow microenvironment plays in disease development. Unfortunately, RSL3 has poor pharmacokinetics and while some studies have reported its effectiveness in mouse models, it is generally not recommended to be used *in vivo*, partly due to unknown off-target or off-tumour effects (Berndt et al., 2024, Dai et al., 2024). Systemic GPX4 knockout is embryonic lethal and its inhibition not only affects cancer cells, but also healthy tissues, manifesting as acute renal failure and liver damage, amongst others (Yang et al., 2014, Friedmann Angeli et al., 2014, Diao et al., 2024). An alternative method that bridges the gap between cell line work *in vitro* and animal models is the *ex vivo* use of patient-derived cells. In this chapter, we utilised a co-culture system whereby patient-derived mononuclear cell (MNC) fractions, containing the malignant plasma cells, were co-cultured with autologous bone marrow stromal cells (BMSCs). These BMSCs and other non-cancer MNCs provide an environment that more closely resembles the tumour microenvironment compared to a monoculture of immortalised cell lines. This model enabled us to investigate not only how RSL3 affects MM cells in the presence of other cell types, but also whether the drug is toxic to healthy lymphocytes. Previous chapters have demonstrated that the phospholipidomic profile and expression of ferroptosis-related genes in MM cell lines can be linked to ferroptosis sensitivity, and thus the aim of this chapter is to determine whether the same is true for patient-derived MM cells.

6.2 Results

6.2.1 Determining differences in cell viability and lipid oxidation in patient-derived MM cells and lymphocytes in the presence or absence of patient-matched stromal cells

Patients at Flinders Medical Centre undergoing a bone marrow aspirate and trephine biopsy for known or suspected MM were recruited to this study. Additional bone marrow aspirate to what was required for clinical investigations was obtained after informed consent. At the time of the biopsy, the diagnosis may be unknown, and thus some patients may ultimately not have a diagnosis of MM. Instead, these patients may receive a diagnosis of monoclonal gammopathy of undetermined significance (MGUS), smouldering MM, or other, thereby limiting the number of bone marrow aspirate available for this study. Furthermore, as priority was given to the samples collected for diagnostic purposes, the samples we received were often the final draw of aspirate and frequently contained a lower percentage of MM cells than expected compared to the diagnostic results.

Rather than treat patient-derived MM cells in a monoculture, we wanted to better mimic the tumour microenvironment by including a range of haematopoietic cells, other than just MM cells and a supportive stromal cell layer, to assess ferroptosis of the tumour cells. To do this, we co-cultured autologous BMSCs and MNCs extracted from whole marrow using density gradient centrifugation. To identify MM cells within this co-culture, all cells were harvested after drug treatment and stained with antibodies against the plasma membrane markers CD38 and CD138, which are highly expressed on MM cells. To investigate ferroptosis in non-tumour cells, we chose to assess lymphocytes due to their abundance in each sample and due to the fact that they are readily discernible from other cell types, including plasma cells, in terms of their scatter properties using flow cytometry. We employed a gating strategy that first excluded cellular debris and cell aggregates and then captured either lymphocytes, which are distinctively smaller in size (low forward scatter) and have lower granularity (low side scatter), or CD38/CD138 dual positive MM cells (Figure 6-1). We were then able to use flow cytometry to count number of events (cells) per µL, as well as measure the levels of lipid oxidation and cell viability in these two populations after being in a co-culture for 48 hours.

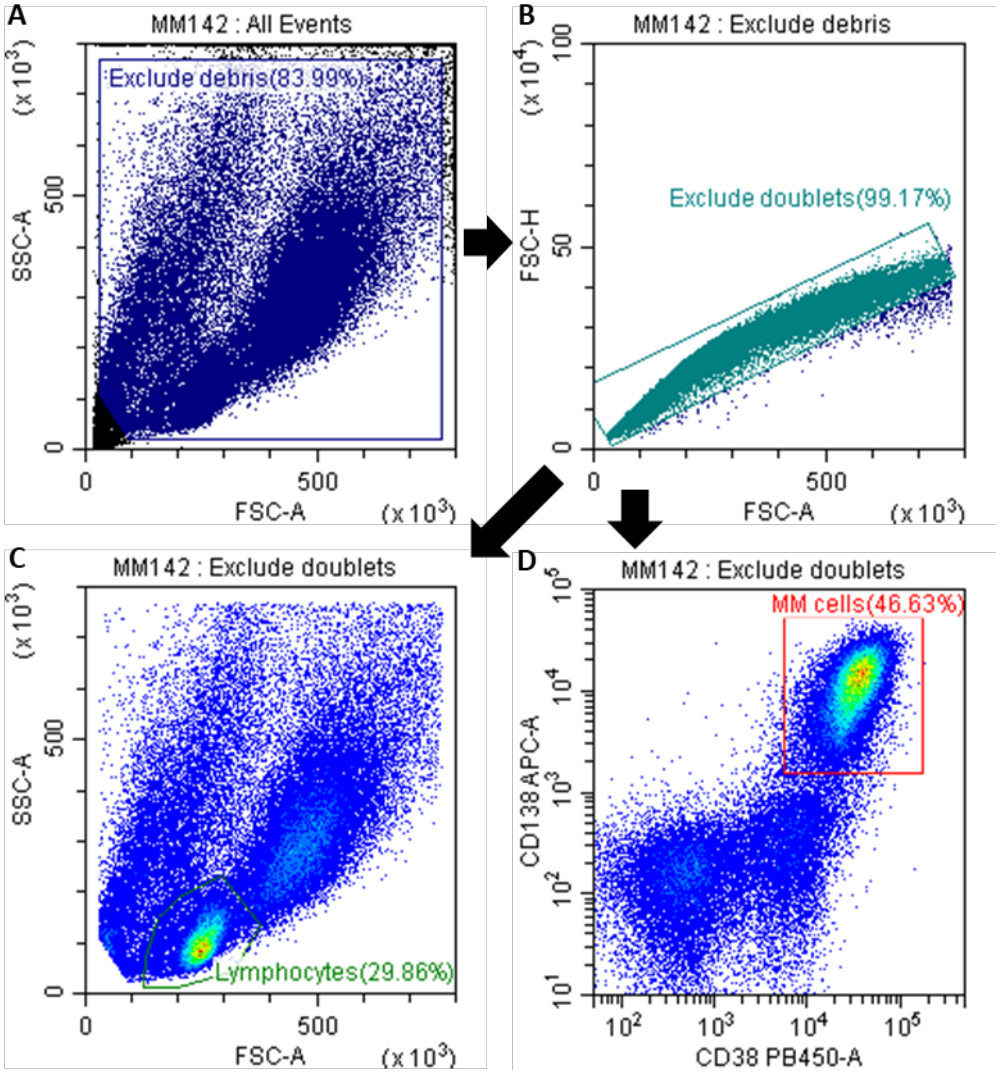

Figure 6-1: Representative gating strategy to identify lymphocytes and MM cells in the cells harvested from our co-culture model.

MM142 patient-derived MNCs were cultured with autologous BMSCs for 48 hours. (A) Forward (FSC) and side scatter (SSC) density plots were used to exclude cellular debris. (B) Next, cell aggregates were excluded using area scaling by plotting forward scatter area against forward scatter height, gating on cells in which the two parameters were proportional. (C) Lymphocytes were identified as small cells with low granularity relative to other cells on a FSC and SSC density plot. (D) MM cells were identified as those that stained positive for fluorochrome-conjugated antibodies against CD38 and CD138.

There was no significant difference in the viability, number of cells, or baseline levels of lipid oxidation in lymphocytes or MM cells cultured in the presence or absence of an autologous BMSC layer (Figure 6-2). All subsequent data presented in this chapter are from MNCs cultured on autologous BMSCs. In previous chapters, both annexin-V and PI were used to measure cellular viability but given that PI alone accurately defined the proportion of cells undergoing ferroptosis, and to avoid spillover from the fluorochromes conjugated to the other antibodies, only PI was used for the experiments on patient samples in this chapter.

When comparing lymphocytes to MM cells, the latter cell type was, on average, more viable (Figure 6-3A) with a higher baseline level of lipid oxidation (Figure 6-3C) in the co-culture system. The number of viable lymphocytes compared to viable MM cells varied between patients, with four patients having a higher number of MM cells compared to lymphocytes, and six patients having a higher number of lymphocytes (Figure 6-3B).

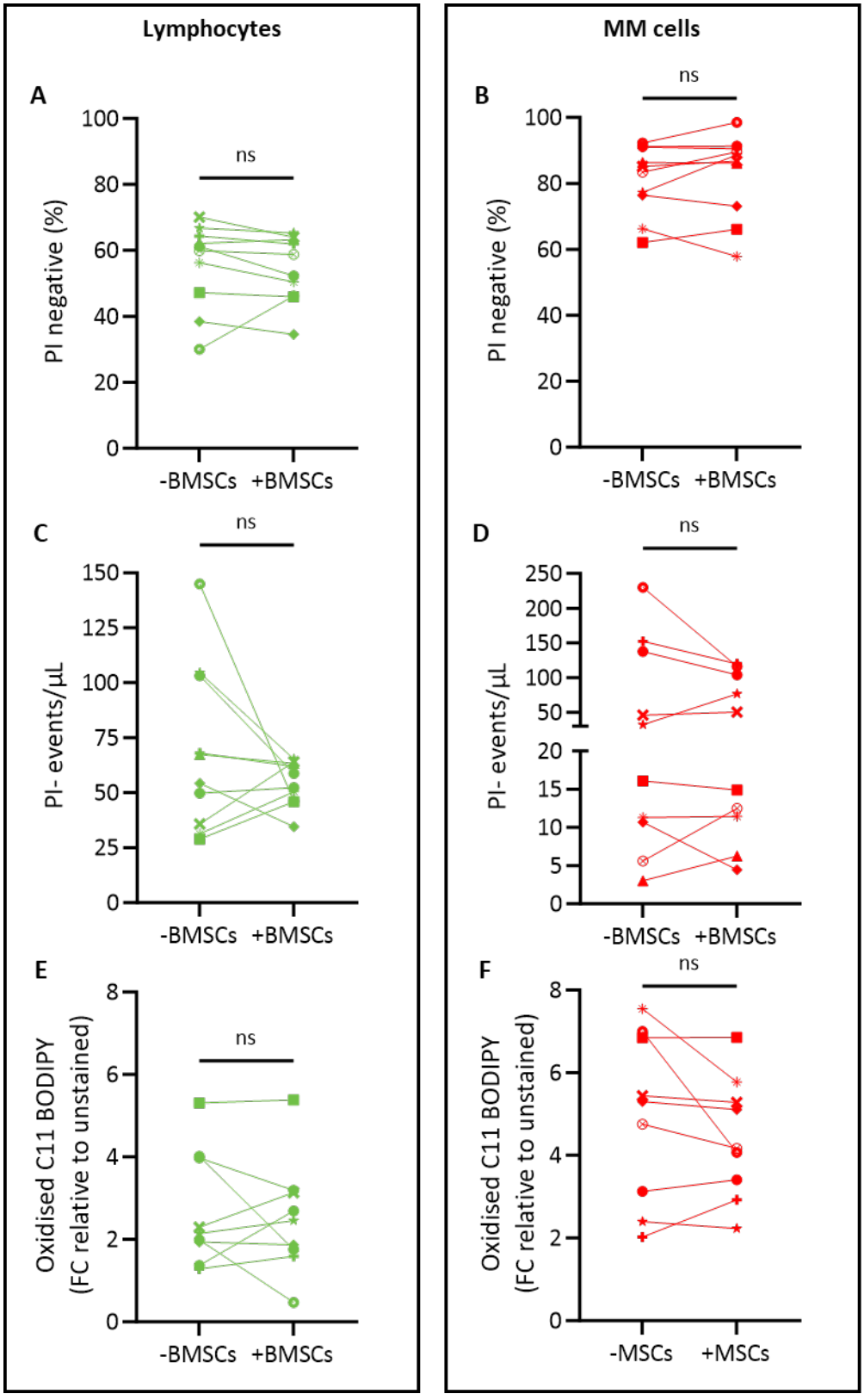

Figure 6-2: Autologous bone marrow stromal cells do not affect the viability, number of cells, or levels of lipid oxidation in patient-derived lymphocytes or MM cells.

Patient-derived MNCs were cultured with or without autologous BMSCs for 48 hours. The viability (A,B), number of viable cells (events/µL) (C,D) and levels of oxidised lipids (E,F) in lymphocytes (green) and MM cells (red) were measured by flow cytometry. Each patient sample is represented by a different shape (n=10). Statistical analyses were performed by paired t-test, ns indicates no significant difference.

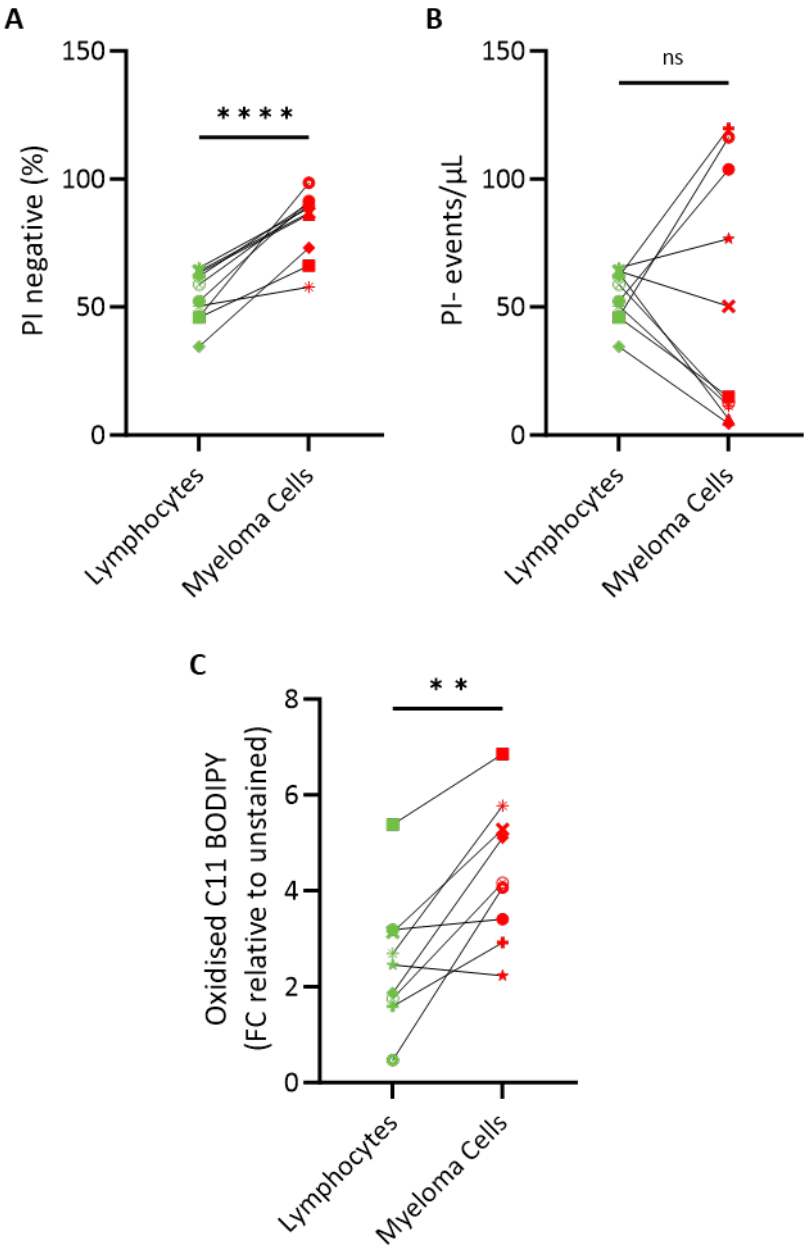

Figure 6-3: Patient-derived MM cells are more viable and have higher levels of baseline lipid oxidation than lymphocytes in the co-culture model.

Patient-derived MNCs were cultured with autologous BMSCs for 48 hours. The viability (A), number of viable cells (events/µL) (B) and levels of oxidised lipids (C) was compared between the lymphocyte (green) and MM cell (red) fractions. Each patient sample is represented by a different shape (n=10). Statistical analyses were performed by paired t-test; ns indicates no significant difference, ** p<0.01, **** p<0.0001.

6.2.2 Investigating the effects of RSL3 against patient-derived lymphocytes and MM cells

While using propidium iodide (PI) staining to measure viability was useful for the cell line work presented in previous chapters, this methodology proved challenging for patient-derived MM cells. We observed a phenomenon whereby the proportion of PI negative MM cells was unchanged after treatment with ferroptosis-inducing drugs, while the percentage of MM cells decreased (Figure 6-4). For example, in the samples from patient MM144, a reduction in the number of cells from 114.56 to 13.22 cells/µL was observed after a 24-hour incubation with 5 µM RSL3, despite a less than 1% difference in the proportion of PI negative cells (Figure 6-4C,D). This was also observed in cells treated with 5 µM RSL3 plus 60 µM AA, which were determined to be 96.56% PI negative, despite a drop in the number of MM cells from 114.56 to 1.26 cells/µL (Figure 6-4E,F). These findings led us to believe that the ferroptosis-inducing compounds were causing a rapid depletion of MM cells and the resulting dead or dying MM cells were no longer positive for CD38/CD138. We therefore decided to use changes in the number of PI negative cells per µL as a measure of drug toxicity for analysis of the subsequent data.

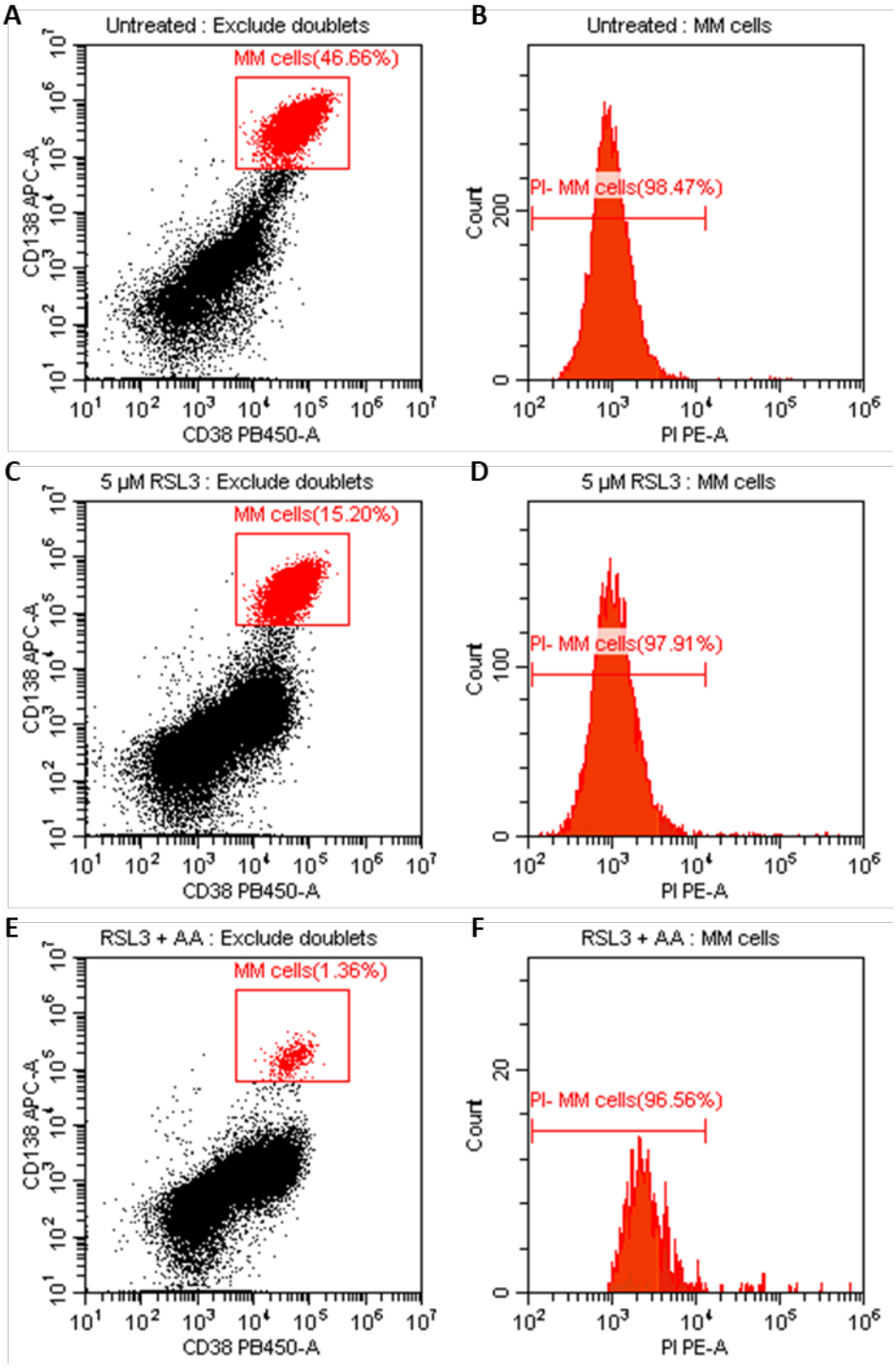

Figure 6-4: Ferroptosis results in a depletion in the number of patient MM cells.

Patient-derived MNCs were cultured with autologous BMSCs for 24 hours. 5 µM RSL3 and/or 60 µM AA were then added for a further 24 hours before flow cytometry was performed. (A,C,E) CD138 and CD38 dot plots were used to identify dual positive MM cells. (B,D,F) Histograms showing how viable cells and viable cells/µL were enumerated based on propidium iodide (PI) fluorescence.

Like MM cell lines, patient-derived MM cells had little or no response to 1 µM RSL3 (Supplementary Figure 6-A). Furthermore, in all patient samples, >50% of the lymphocytes and MM cells were viable after a 24-hour incubation with 2.5 µM RSL3 (Figure 6-5A,B). Following treatment with 5 µM RSL3, 5 of the 10 patient samples had less than 50% viable MM cells remaining compared to untreated control cultures (MM138, 140, 143, 144 and 159) (Figure 6-5D). In the lymphocyte population, however, only one patient sample was less than 50% viable relative to untreated controls at this concentration of RSL3 (MM144) (Figure 6-5C). Statistical analyses on the effects of Lip-1 in each individual patient were not performed as only one replicate per patient was analysed due to sample availability. However, data from the mean of all patient samples suggest Lip-1 had no effect on RSL3-induced death in either the MM or lymphocyte cell populations (Figure 6-5).

When comparing MM cells and lymphocytes, there was a significant difference in the average number of viable cells after treatment with 5 µM RSL3 (relative to untreated), which suggested that MM cells were more sensitive to the drug ($p = 0.0271$) (Figure 6-6B). However, there was no difference in the mean amount of lipid oxidation induced by RSL3 in lymphocytes compared to the MM cell population (Figure 6-6C,D).

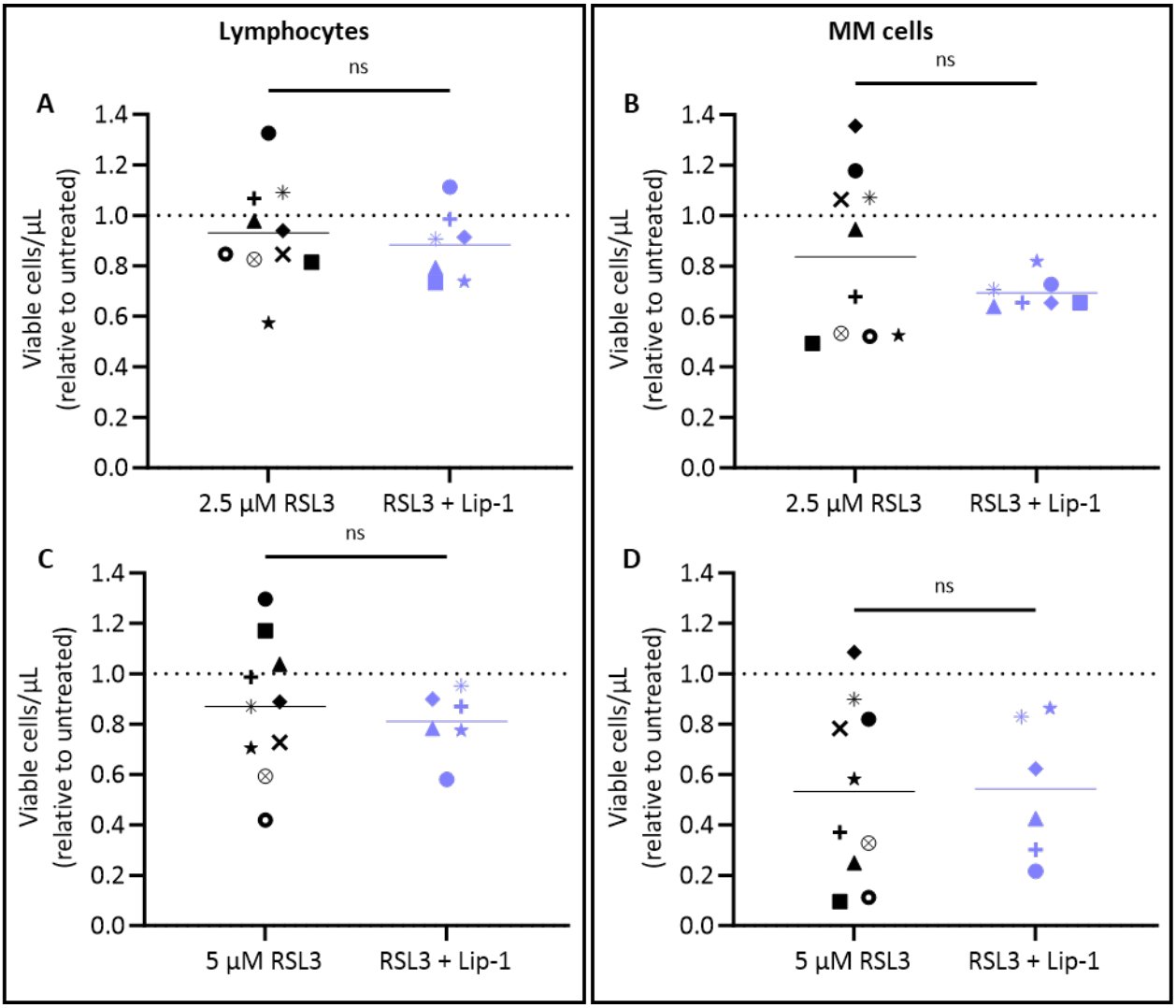

Figure 6-5: Lip-1 does not prevent RSL3-induced death in patient-derived MM cells.

Patient-derived MNCs were cultured with patient-matched BMSCs for 24 hours. 2.5 µM (A,B) or 5 µM (C,D) RSL3 with or without 2 µM Lip-1 was added for a further 24 hours and the number of viable cells was measured in the lymphocyte and MM cell populations. Propidium iodide (PI) staining and flow cytometry were performed to assess drug toxicity. PI negative cells were considered viable and the number of viable cells/µL, relative to untreated controls, were calculated. Each shape represents one patient sample, and the mean is represented by a solid line. Statistical analyses were performed by paired t-test; ns indicates no significant difference.

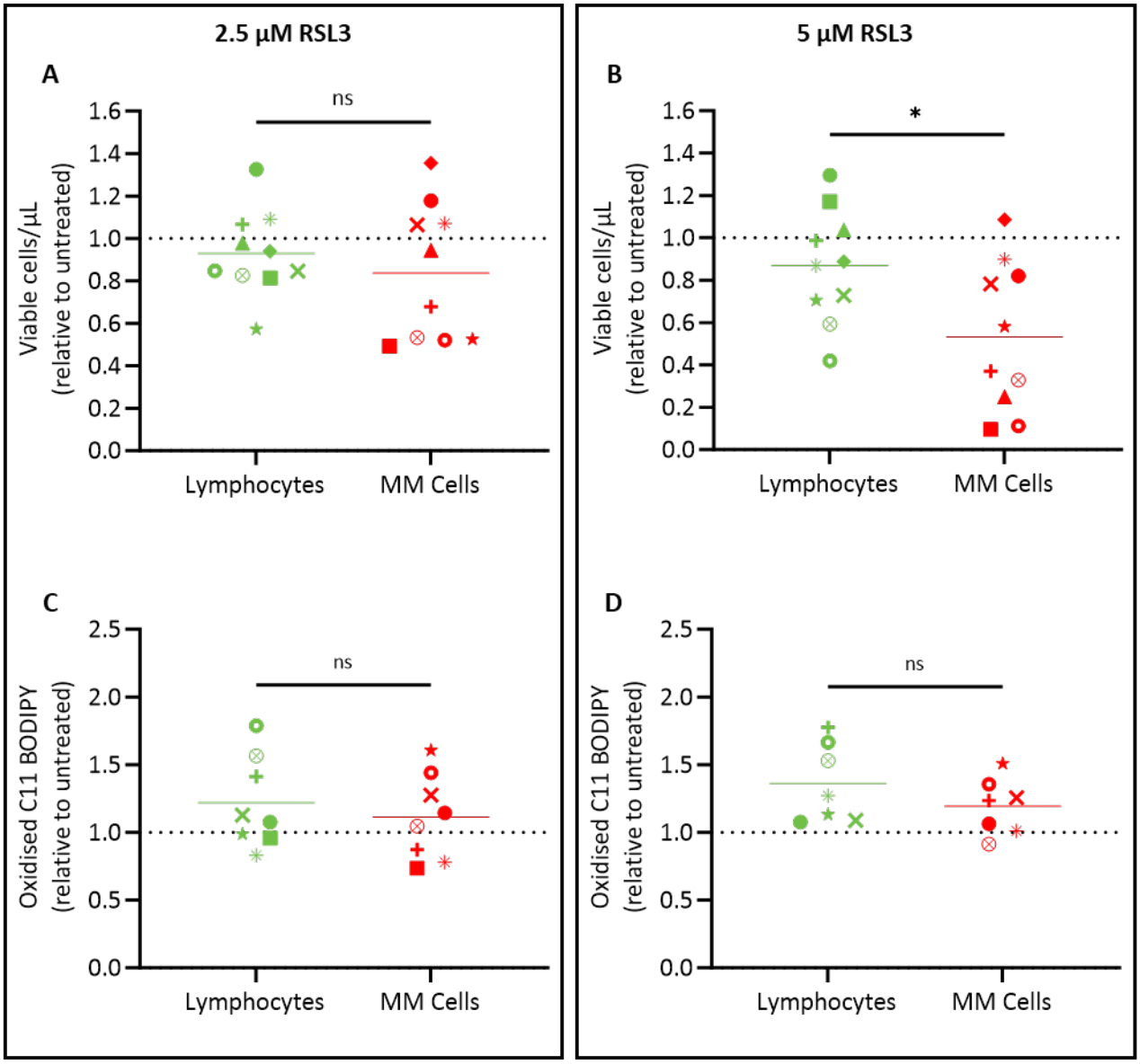

Figure 6-6: MM cells are more sensitive to high concentrations of RSL3 compared to lymphocytes.

Patient-derived MNCs were cultured with autologous BMSCs for 24 hours. 2.5 µM (A,C) or 5 µM (B,D) RSL3 was added for a further 24 hours. (A,B) Drug toxicity was measured by assessing the number of viable (PI negative) cells/µL in the lymphocyte and MM cell populations relative to untreated controls. (C,D) Levels of lipid oxidation in each cell population were measured by flow cytometry, with or without treatment with RSL3. Each shape represents one patient sample, and the mean is represented by a solid line. Statistical analyses were performed by paired t-test; ns indicates no significant difference, * $p<0.05$.

6.2.3 Using arachidonic acid to enhance the effects of RSL3 in patient-derived MM cells

Initially, it was found that patient-derived MM cells, like the OPM2 MM cell line, were sensitive to a high dose (100 µM) of AA and that Lip-1 could not prevent toxicity (Supplementary Figure 6-B). 60 µM AA was subsequently used, given that in Chapter 4 we found that in MM cell lines, this dose enhanced the effects of RSL3 with minimal toxicity as a single agent. In lymphocytes, there was no significant difference between cells treated with 2.5 µM RSL3 alone or in combination with 60 µM AA (Figure 6-7A). At the higher concentration of 5 µM RSL3, the addition of AA caused a significant reduction in the number of viable lymphocytes, with an average reduction of 36.24 ± 17.69%, relative to untreated controls ($p = 0.0013$) (Figure 6-7C). However, Lip-1 had no significant effect on death of these cells. In primary MM cells, AA enhanced the effects of both 2.5 and 5 µM RSL3, significantly reducing the number of viable cells by 55.20 ± 33.14% ($p = 0.0082$) and 85.38 ± 16.58% ($p = 0.0084$), respectively, compared to untreated controls. However, Lip-1 did not inhibit the cytotoxic effects of the combination of RSL3 and AA (Figure 6-7B,D).

No significant differences in the levels of lipid oxidation induced by the treatment with RSL3 or 60 µM AA alone was observed in either the lymphocyte or MM cell populations (Figure 6-8). However, the combination of 60 µM AA and 5 µM RSL3 significantly enhanced lipid oxidation compared to RSL3 alone in both lymphocytes ($p = 0.0010$) and MM cells ($p = 0.0440$) (Figure 6-8). Although Lip-1 had no significant effect on cell death (Figure 6-7), the antioxidant did prevent lipid oxidation induced by RSL3 in combination with AA (Figure 6-8).

When comparing the two cell types, MM cells appeared to be markedly more sensitive to the combination of RSL3 and AA compared to lymphocytes; the combination of 2.5 µM RSL3 and 60 µM AA resulted in an average 14.74 ± 28.53% decrease in the number of viable lymphocytes, which was significantly less than the 55.20 ± 33.14% reduction in the number of viable MM cells ($p = 0.0036$) (Supplementary Figure 6-C A). The higher 5 µM dose of RSL3 was more effective than 2.5 µM in both cell types, but again a significant difference in the sensitivity of the two cell populations was observed ($p < 0.0001$) (Supplementary Figure 6-C B). Despite the difference in toxicity, no significant difference was evident in the levels of lipid oxidation induced in the two cell types following treatment (Supplementary Figure 6-C C,D).

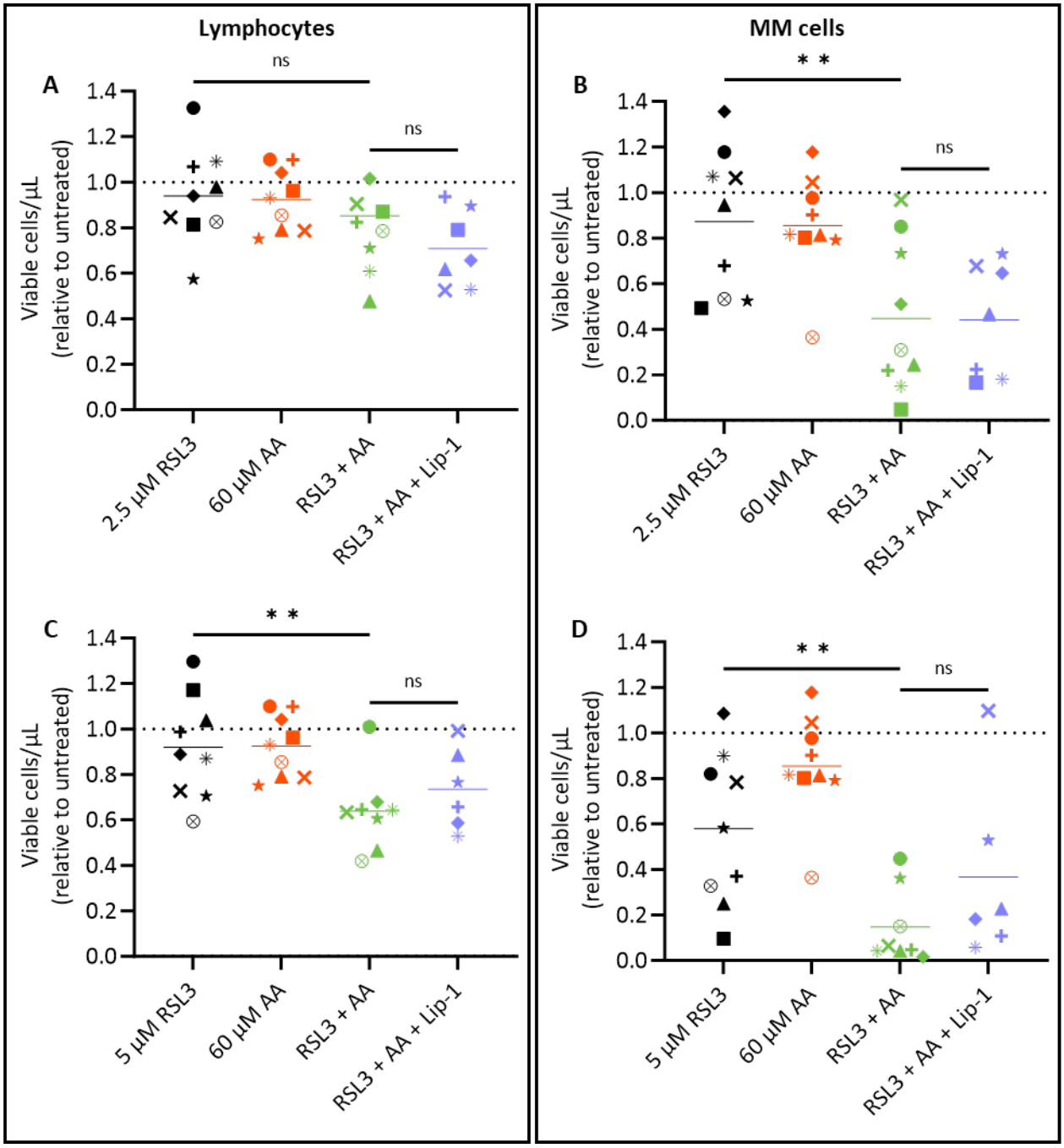

Figure 6-7: The combination of RSL3 and AA reduces the number of viable patient-derived MM cells in a co-culture model.

Patient-derived MNCs were cultured with autologous BMSCs for 24 hours. 2.5 µM (A,B) or 5 µM (C,D) RSL3 with or without 60 µM AA and 2 µM Lip-1 was added for a further 24 hours and the number of viable cells was assessed in lymphocyte and MM cell populations. Flow cytometry was performed to assess drug toxicity by calculating the number of propidium iodide (PI) negative (viable) cells/µL relative to untreated controls. Each shape represents one patient sample, and the mean is represented by a solid line. Statistical analyses were performed by uncorrected Fisher's least significant difference; ns indicates no significant difference, ** $p<0.01$.

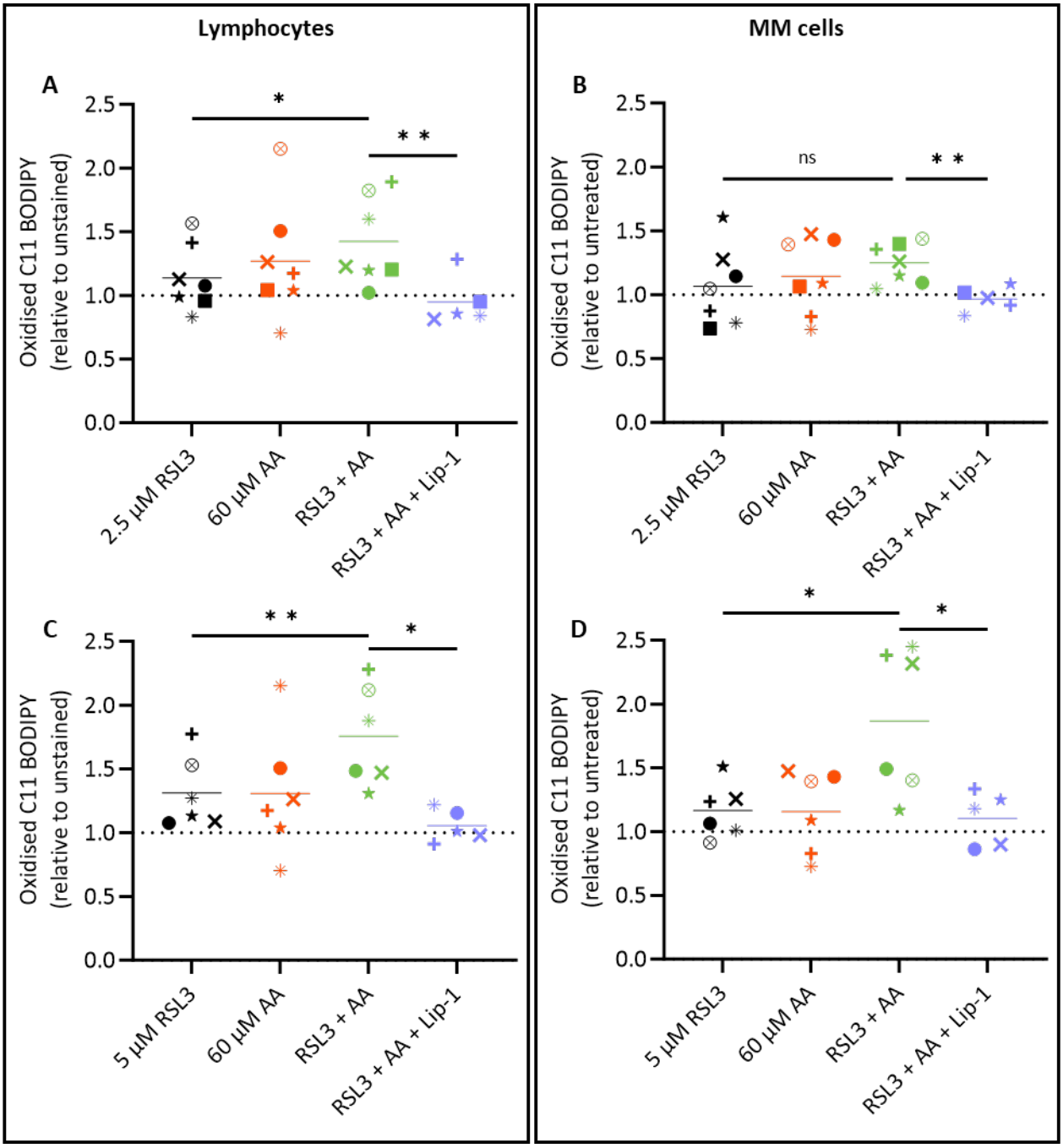

Figure 6-8: The addition of AA enhances lipid oxidation induced by high doses of RSL3 in patient-derived lymphocytes and MM cells.

Patient-derived MNCs were cultured with autologous BMSCs for 24 hours. 2.5 µM (A,B) or 5 µM (C,D) RSL3 with or without 60 µM AA and 2 µM Lip-1 was added for a further 24 hours and levels of lipid oxidation relative to untreated and unstained controls were measured in the lymphocyte and MM cell populations. Each shape represents one patient sample, and the mean is represented by a solid line. Statistical analyses were performed by uncorrected Fisher's least significant difference; ns indicates no significant difference, * $p<0.05$, ** $p<0.01$.

6.2.4 Using iron to enhance the effects of RSL3 in patient-derived MM cells

On average, addition of 100 µM ferric ammonium citrate (FAC) alone had no effect on the number of viable cells, relative to untreated controls. However, in the sample from patient MM142, we observed a 2.1-fold increase in the number of viable lymphocytes and in the samples from patients MM142 and MM139, the number of MM cells increased 1.86- and 2.03-fold, respectively (Figure 6-9).

Addition of 100 µM FAC to RSL3 caused a significant reduction in the number of viable lymphocytes, but including Lip-1 had no effect (Figure 6-9A,C). Conversely, FAC had no significant effect on the number of viable MM cells when added to either 2.5 or 5 µM RSL3 (Figure 6-9B,D). The combination of RSL3 and FAC caused the number of viable lymphocytes to decrease to a similar level to that of MM cells treated with RSL3 alone. Thus, even though the addition of FAC did not enhance the effects of RSL3 in MM cells, there was no significant difference in the viability of the lymphocyte population compared to MM cells following treatment with RSL3 and FAC (Supplementary Figure 6-D).

Accordingly, FAC had no effect on the levels of oxidised lipids induced by RSL3 in patient-derived MM cells (Figure 6-10B,D). Although FAC caused a small but significant decrease in the number of lymphocytes when combined with 2.5 µM RSL3 ($p = 0.0136$), no significant change in the levels of lipid oxidation were observed when FAC was combined with this concentration of RSL3, compared to cells treated with RSL3 alone (Figure 6-10A). However, a significant increase in the levels of lipid oxidation was observed when FAC was combined with the higher dose of 5 µM RSL3 compared to RSL3 alone in the viable lymphocyte population ($p = 0.0177$) (Figure 6-10C). Overall, the combination of RSL3 and FAC induced a greater increase in the levels of lipid oxidation in the lymphocytes, than in the MM cells (Supplementary Figure 6-D).

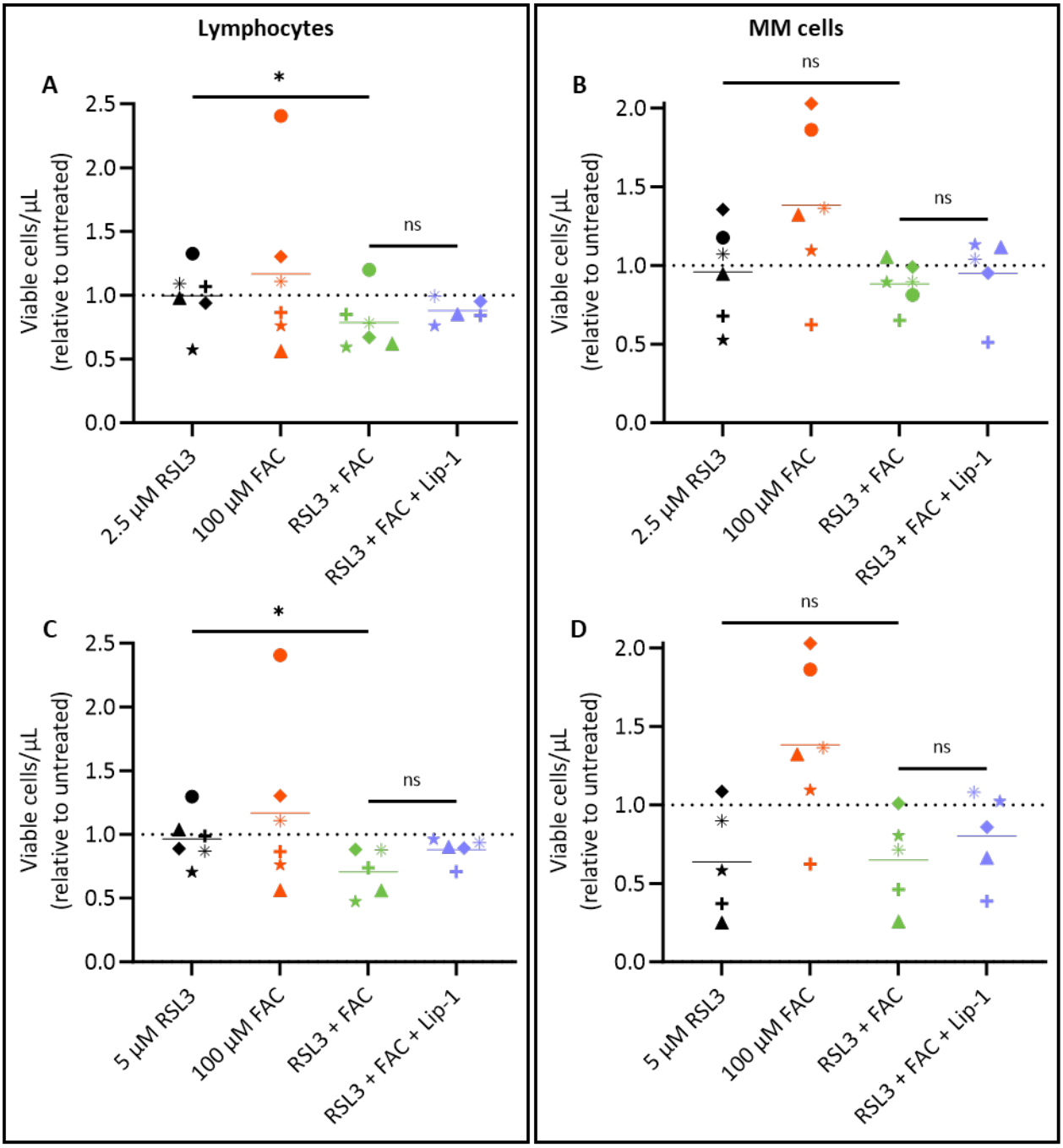

Figure 6-9: FAC does not enhance RSL3-induced death in patient-derived MM cells.

Patient-derived MNCs were cultured with autologous BMSCs for 24 hours. 2.5 µM (A,B) or 5 µM (C,D) RSL3 with or without 100 µM FAC and 2 µM Lip-1 was added for a further 24 hours and the number of viable cells was measured in the lymphocyte and MM cell populations. Flow cytometry was performed to assess drug toxicity, assessed by the number of propidium iodide (PI) negative cells/µL relative to untreated controls. Each shape represents one patient sample, and the mean is represented by a solid line. Statistical analyses were performed by uncorrected Fisher's least significant difference; ns indicates no significant difference, * $p<0.05$.

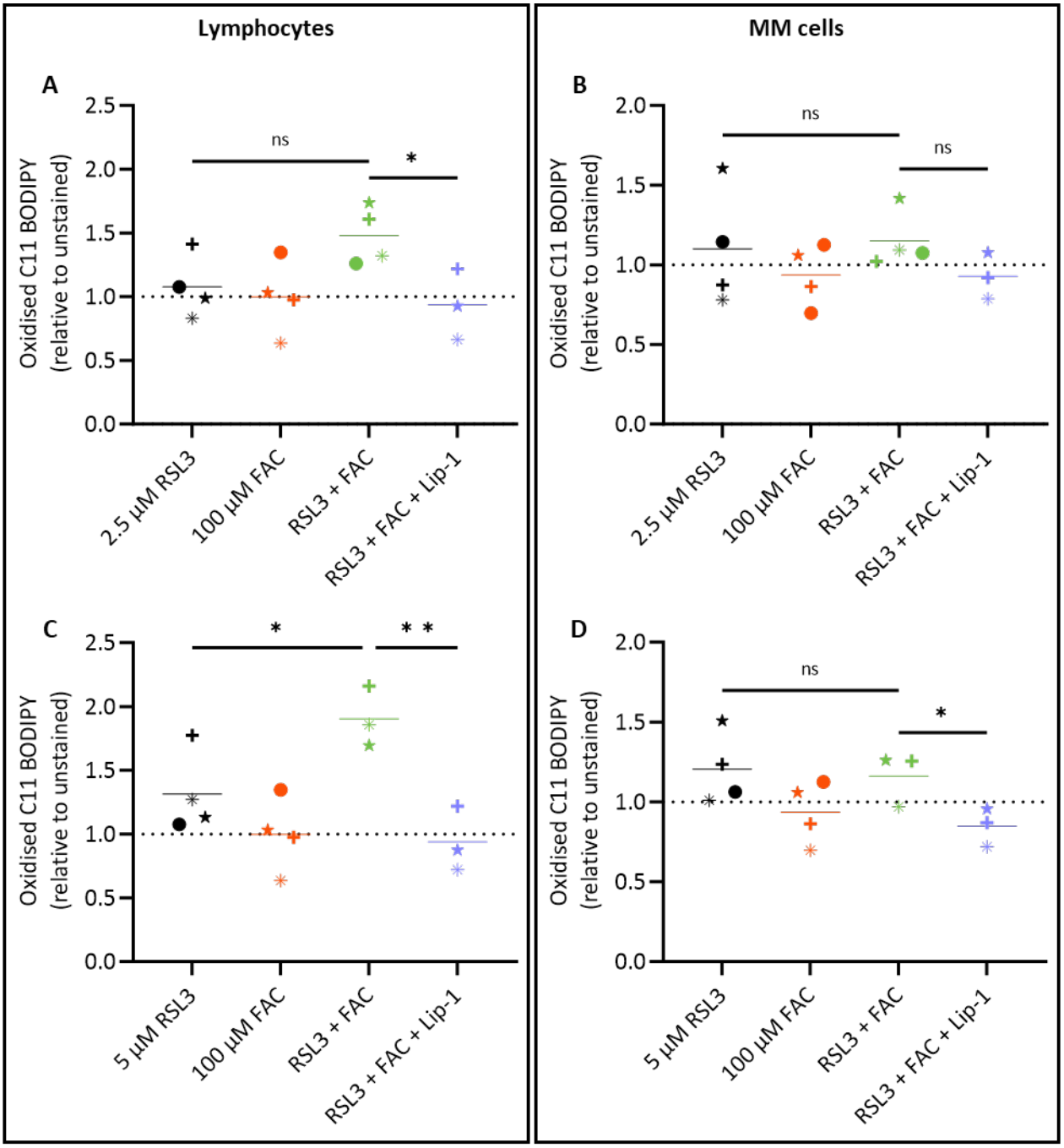

Figure 6-10: FAC enhances RSL3-induced lipid oxidation in patient-derived lymphocytes, but not MM cells.

Patient-derived MNCs were cultured with autologous BMSCs for 24 hours. 2.5 µM (A,B) or 5 µM (C,D) RSL3 with or without 100 µM FAC and 2 µM Lip-1 was added for a further 24 hours and levels of lipid oxidation relative to untreated and unstained controls were assessed in the lymphocyte and MM cell populations. Each shape represents one patient sample, and the mean is represented by a solid line. Statistical analyses were performed by uncorrected Fisher's least significant difference; ns indicates no significant difference, * $p<0.05$, ** $p<0.01$.

6.2.5 Assessing the lipidomic profile of patient-derived MM cells

The lipidomic profile of patient-derived MM cells was assessed to determine whether there was a correlation between the proportion of phospholipids containing specific fatty acids and ferroptosis sensitivity. Fresh whole marrow aspirate from patients with MM was sorted by flow cytometry to isolate CD38/CD138 dual positive MM cells for lipidomic analyses. After cryopreservation, the lipidomic profile of thirteen samples were assessed, ten of which were also included in the previous drug response experiments (Figure 6-11).

In Chapter 3, we found that ferroptosis-resistant MM cell lines tend to have a higher proportion of phospholipids containing monounsaturated fatty acid (MUFA) and less polyunsaturated (PUFA)-containing phospholipids compared to ferroptosis-sensitive OPM2 MM cells and DLBCL cell lines (Figure 3-14B). More specifically, resistant cells had an average of 1.47-fold more MUFA-containing than PUFA-containing phospholipids, whereas sensitive cells had a similar proportion of each (0.98-fold MUFA relative to PUFA) (Table 6-1). We found that patient-derived MM cells, however, had half has much MUFA-containing phospholipids compared to those containing PUFA (0.46-fold) (Figure 6-11B) (Table 6-1).

Table 6-1: Proportion of phospholipids containing specific fatty acids in patient-derived MM cells and MM cell lines.

	Proportion of phospholipids containing specific fatty acids (mean ± SD)		
	Patient-derived MM cells	**Resistant MM cell lines**	**Sensitive MM cell lines**
MUFA	0.239 ± 0.091	0.494 ± 0.076	0.383 ± 0.089
PUFA	0.519 ± 0.087	0.336 ± 0.063	0.391 ± 0.055
MUFA_PUFA	0.164 ± 0.042	0.113 ± 0.038	0.123 ± 0.038
SFA	0.078 ± 0.034	0.058 ± 0.016	0.010 ± 0.048

Phospholipids were grouped and labelled according to fatty acid contents: monounsaturated fatty acid (MUFA), containing two MUFA or one MUFA and one saturated fatty acid (SFA); polyunsaturated fatty acid (PUFA), containing two PUFA or one PUFA and one SFA; MUFA_PUFA, containing one MUFA and one PUFA; or SFA, containing two SFA. Data used were the proportion of each group relative to the total number of phospholipids.

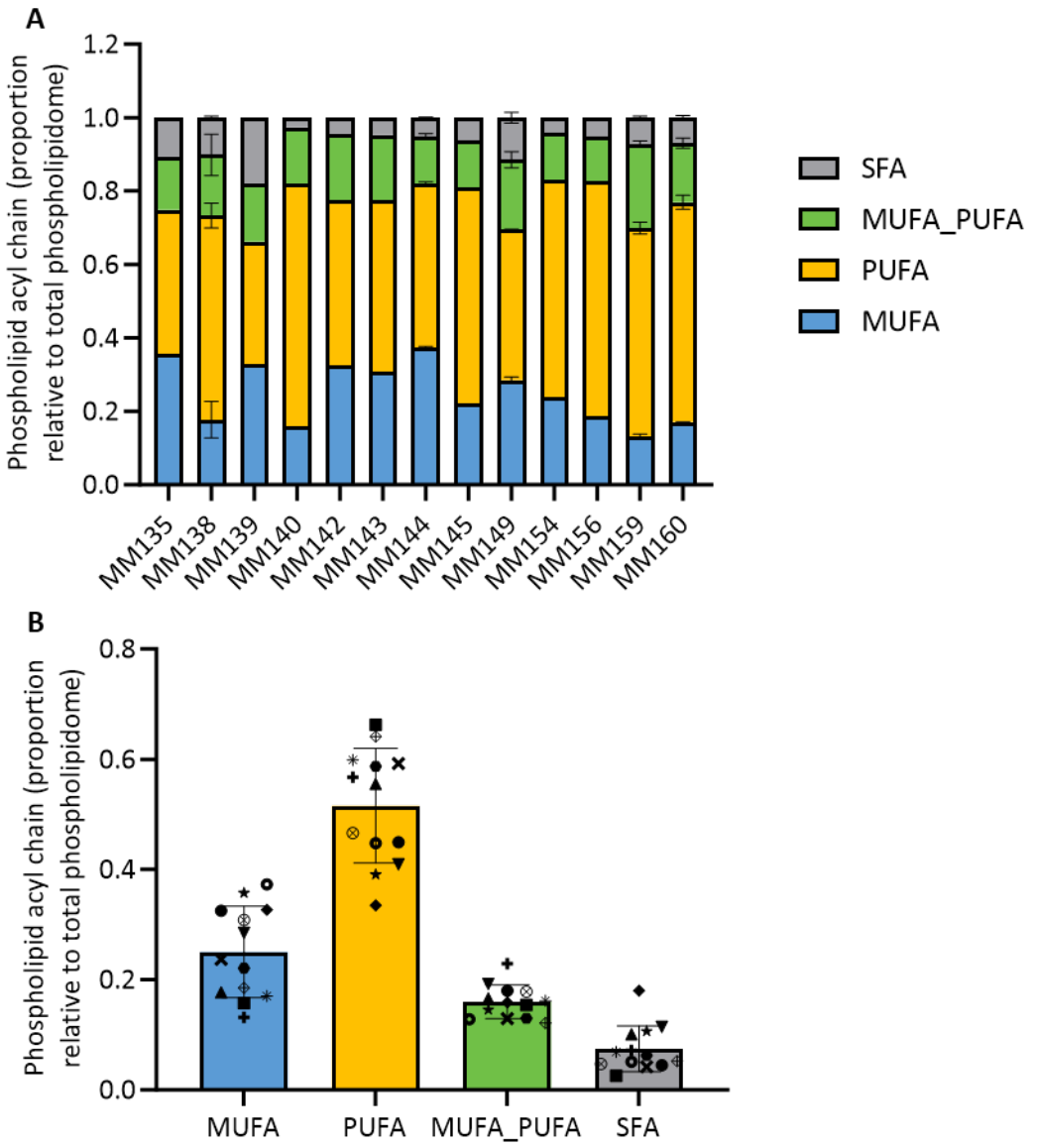

Figure 6-11: Lipidomic analyses assessing the proportion of fatty acids in patient-derived MM cells.

Liquid chromatography–mass spectrometry (LC–MS) was performed to measure the composition of phospholipids in patient-derived MM cells isolated from bone marrow aspirates by fluorescence-activated cell sorting. Phospholipids were grouped and labelled according to fatty acid contents: monounsaturated fatty acid (MUFA), containing two MUFA or one MUFA and one saturated fatty acid (SFA); polyunsaturated fatty acid (PUFA), containing two PUFA or one PUFA and one SFA; MUFA_PUFA, containing one MUFA and one PUFA; or SFA, containing two SFA. Data show the proportion of each fatty acid group relative to the total number of phospholipids. (A) The proportion of phospholipids containing specific fatty acid groups of individual patient samples. (B) The proportion of phospholipids containing specific fatty acid groups for all patient samples combined; each patient is represented by a specific shape and error bars represent the mean ± standard deviation.

To determine whether the phospholipid profile of patient-derived MM cells could be linked to sensitivity to ferroptosis-inducing agents, we separated the patient samples into "resistant" and "sensitive" groups (Figure 6-12A). Unlike MM cell lines where a line of best fit could be used to determine the IC_{50} of RSL3, due to the limited number of primary MM cells available, dose response analyses for RSL3 could not be conducted. Instead, we separated patient samples based on the number of viable cells remaining after each treatment. For example, five patient samples had a percentage of viable cells remaining that was above the mean of 53.24% after incubation with 5 µM RSL3, which were classified as resistant. Conversely, the five patient samples with less than 53.24% viable cells were deemed sensitive (Figure 6-12A). When using this stratification, there was no difference in the proportion of phospholipids containing specific acyl chains between the resistant and sensitive groups (Figure 6-12B).

When stratifying against the relative number of remaining viable cells after treatment with the combination of 5 µM RSL3 and 60 µM AA, however, differences between the two groups emerged (Figure 6-12C). In this case, patient-derived MM cells classified as resistant to the combination of RSL3 and AA had a higher proportion of MUFA-containing phospholipids, and a lower proportion of those containing PUFA, compared to patient-derived MM cells sensitive to this treatment (Figure 6-12C). Accordingly, Pearson correlation showed that there was a moderate, though not quite statistically significant, positive correlation between the proportion of MUFA-containing phospholipids and a higher number of viable cells remaining after treatment with 60 µM AA plus 2.5 µM RSL3 (Pearson r = 0.665, p = 0.051) or 5 µM RSL3 (Pearson r = 0.663, p = 0.052) (Figure 6-12D,E). Despite the observation that patient-derived MM cells classified as resistant to the combination of RSL3 and AA had a lower proportion of PUFA-containing phospholipids, no significant correlation between sensitivity and the proportion of PUFA-containing phospholipids was observed (Table 6-2). Moreover, no significant correlation between sensitivity and the proportion of phospholipids containing AA were observed (Table 6-2).

Table 6-2: Pearson correlation of sensitivity to RSL3 with or without AA and the proportion of phospholipids containing PUFA, AA or MUFA.

	PUFA		AA		MUFA	
	Pearson r	p-value	Pearson r	p-value	Pearson r	p-value
2.5 µM RSL3	-0.192	0.595	-0.025	0.945	-0.014	0.970
5 µM RSL3	-0.508	0.163	-0.339	0.373	0.460	0.213
2.5R + A	-0.454	0.220	-0.384	0.308	0.665	0.051
5R + A	-0.454	0.220	-0.410	0.273	0.663	0.052

Phospholipid proportions were plotted against the relative number of viable cells after the indicated drug treatments (data from Figure 6 7B,D) and Pearson correlation was performed. Phospholipids were grouped and labelled according to fatty acid contents: polyunsaturated fatty acid (PUFA), containing two PUFA or one PUFA and one SFA; AA, containing one or more arachidonic acid (AA); monounsaturated fatty acid (MUFA), containing two MUFA or one MUFA and one saturated fatty acid (SFA). Data used were the proportion of each group relative to the total number of phospholipids.

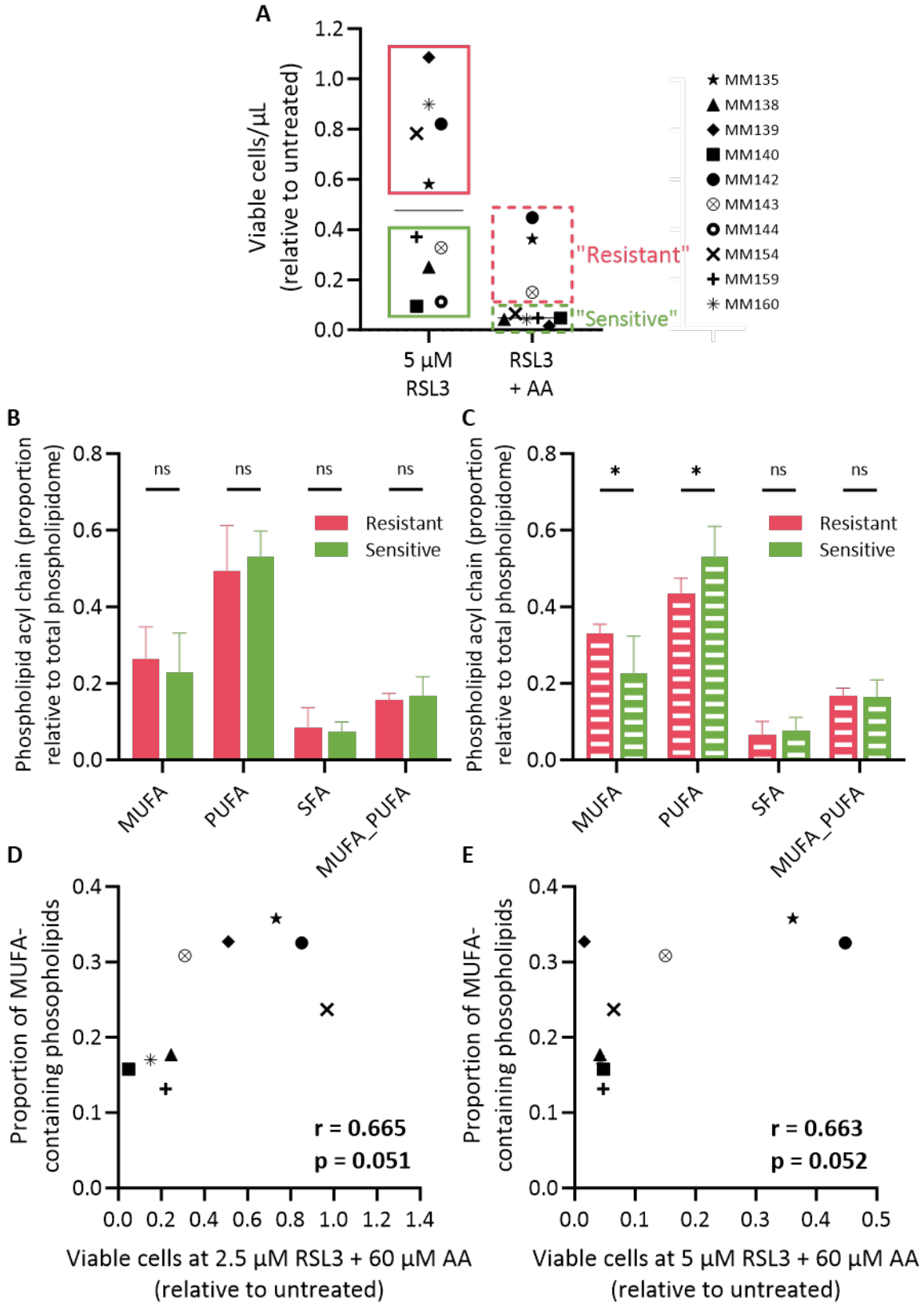

Figure 6-12: Patient-derived MM cells that are more sensitive to the combination of RSL3 and AA have a higher proportion of MUFA-containing phospholipids.

(A) Patients were stratified based on their sensitivity to RSL3 with or without AA. Liquid chromatography–mass spectrometry (LC–MS) was performed to measure the baseline levels of phospholipids in patient-

derived MM cells isolated from fresh marrow aspirate. Phospholipids were grouped and labelled according to fatty acid contents: monounsaturated fatty acid (MUFA), containing two MUFA or one MUFA and one saturated fatty acid (SFA); polyunsaturated fatty acid (PUFA), containing two PUFA or one PUFA and one SFA; MUFA_PUFA, containing one MUFA and one PUFA; or SFA, containing two SFA. Data are displayed showing the proportion of each group relative to the total number of phospholipids. (B) Based on RSL3 only sensitivity, the proportions of each fatty acid group in resistant and sensitive patient-derived MM cells were compared. (C) Based on the sensitivity to RSL3 in combination with AA, the proportions of each fatty acid group in resistant and sensitive patient-derived MM cells were compared. Statistical analyses were performed by two-way ANOVA with an uncorrected Fisher's least significant difference test for multiple comparisons; ns indicates no significant difference, * $p<0.05$. (D,E) Phospholipid proportions were plotted against the relative number of viable cells after the indicated drug treatments with analysis using Pearson correlation. r, Pearson correlation coefficient; p, p-value.

In the preceding data, whole marrow aspirate from patients was sorted by flow cytometry to isolate CD38/CD138 dual positive MM cells. These sorted cells were frozen before lipidomic analyses were performed to assess the lipidomic profile of patient-derived MM cells. In some instances where enough MM cells were present (minimum 30,000), MM cells that had been cultured in the aforementioned co-culture system in RPMI medium plus foetal bovine serum (FBS) were also sorted by flow cytometry to determine whether the lipidomic profile of these cultured cells was significantly different from patient-matched MM cells sorted from fresh whole marrow aspirates (Figure 6-13).

Of the four patient samples where lipidomic data from fresh and stroma co-cultured MM cells was available, the only significant difference in the proportion of MUFA-containing phospholipids was in sample MM160, which had a lower proportion of MUFA-containing phospholipids following co-culture ($p = 0.0291$) (Figure 6-13A). Additionally, MM160 ($p = 0.0108$) and MM159 ($p < 0.0001$), had a slightly higher proportion of PUFA-containing phospholipids after culture (Figure 6-13B). The proportion of phospholipids containing one MUFA acyl chain and one PUFA was significantly reduced after culturing in MM159 ($p < 0.0001$), but unchanged in the other 3 patient samples (Figure 6-13C). Furthermore, the proportion of phospholipids containing two SFA acyl chains was only increased in MM140 following culture ($p = 0.0026$) (Figure 6-13D). As only one biological replicate, and in some cases only one technical replicate was available due to a limited number of MM cells (MM140 fresh and cultured samples, MM154 fresh sample and MM160 cultured sample), the statistical strength of this data may be limited. Nonetheless, in all four patient samples, the proportion of AA-containing phospholipids was significantly increased following culturing (Figure 6-13E).

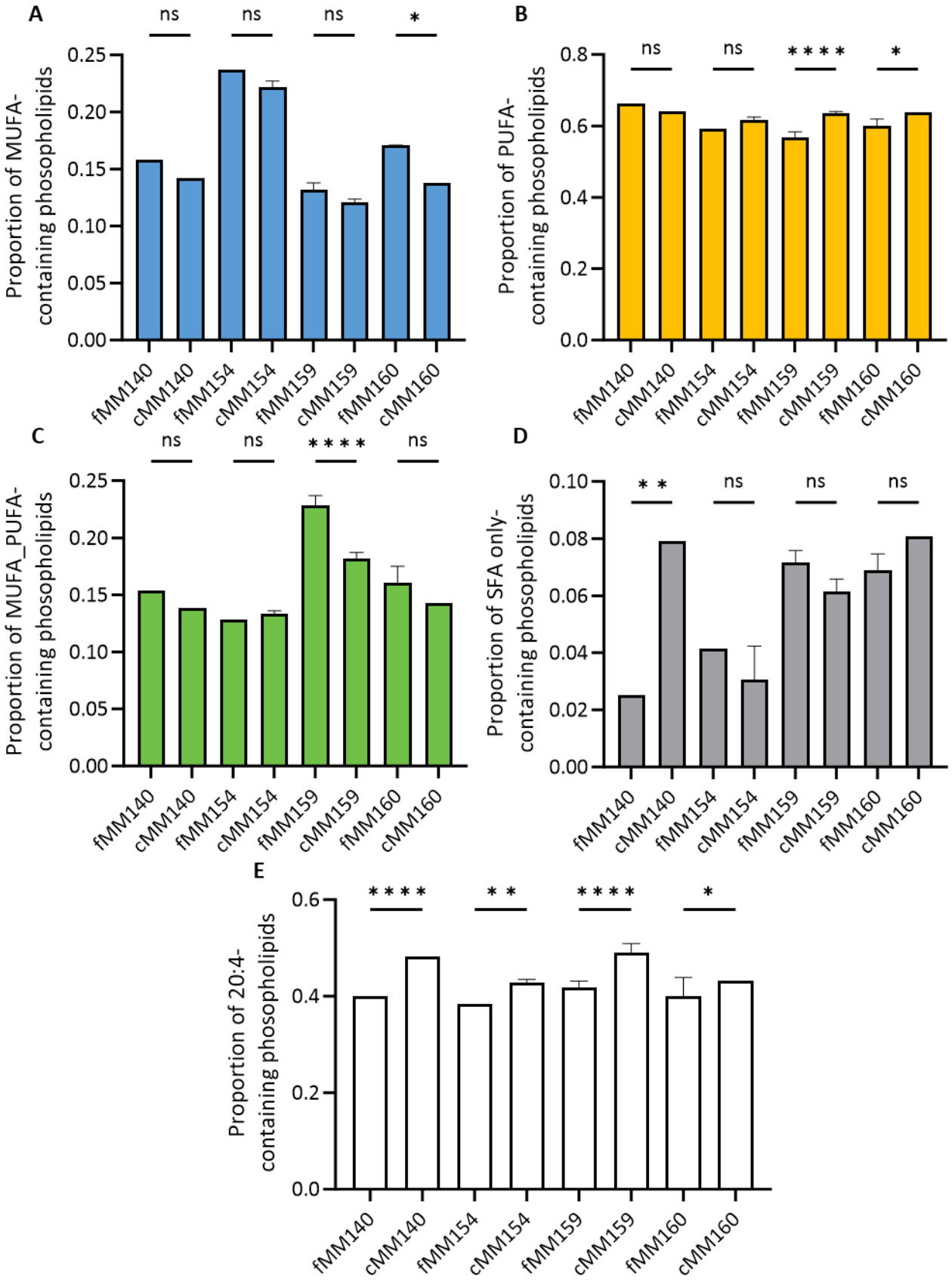

Figure 6-13: Assessing changes in the lipidomic profile of patient-derived MM cells following culturing.

Liquid chromatography–mass spectrometry (LC–MS) was performed to measure the baseline levels of phospholipids in patient-derived MM cells isolated from whole fresh marrow (fMM) and patient-derived MM cells after culturing in RPMI medium with 10% FBS in the co-culture system for 48 hours (cMM). Phospholipids were grouped and labelled according to fatty acid contents: (A) monounsaturated fatty acid (MUFA), containing two MUFA or one MUFA and one saturated fatty acid (SFA); (B) polyunsaturated fatty acid (PUFA), containing two PUFA or one PUFA and one SFA; (C) MUFA_PUFA, containing one MUFA and one PUFA; (D) SFA, containing two SFA; or (E) containing one or more 20:4 acyl chains (arachidonic acid). Statistical analyses were performed by two-way ANOVA with an uncorrected Fisher's least significant difference test for multiple comparisons; ns indicates no significant difference, * $p<0.05$, ** $p<0.01$, **** $p<0.0001$.

6.2.6 Assessing the expression of ferroptosis-related genes in patient-derived MM cells

Given that a larger number of MM cells were required for RNA sequencing (>100,000 cells compared to 30,000 cells required for lipidomic analyses), some bone marrow aspirates that were used for the drug response experiments, or lipidomic analyses did not have sufficient cells for RNA sequencing. Thus, only four patient samples with matched drug response data were assessed by RNA sequencing; MM142 and MM135 (labelled as RSL3-resistant with greater than 50% viable cells relative to untreated at 5 µM RSL3) and MM143 and MM144 (labelled as RSL3-sensitive with less than 50% viable cells relative to untreated at 5 µM RSL3) (Figure 6-12A). Normalised counts of ferroptosis-related genes from FerrDb were converted to a row z-score to allow for the expression of genes to be visualised on the same scale (Figure 6-14A). Clustering of samples using correlation distance and average linkage was performed using ClustVis (Metsalu and Vilo, 2015). No grouping of the patient samples was identified based on RSL3 sensitivity, and we found marked differences in the expression of ferroptosis-related genes between the samples (Figure 6-14A). Using the WP_Ferroptosis gene set that previously clearly distinguished RSL3-sensitive OPM2 and -resistant KMS-11 MM cell lines (Figure 5-3), distinct expression profiles were not evident between the four patient-derived MM samples, with no correlation clustering based on their sensitivity to RSL3 (Figure 6-14B). The normalised expression (transcripts per million) of ferroptosis-related genes in patient-derived MM cells, compared to resistant KMS-11 MM cells, can be found in Appendix 6B.

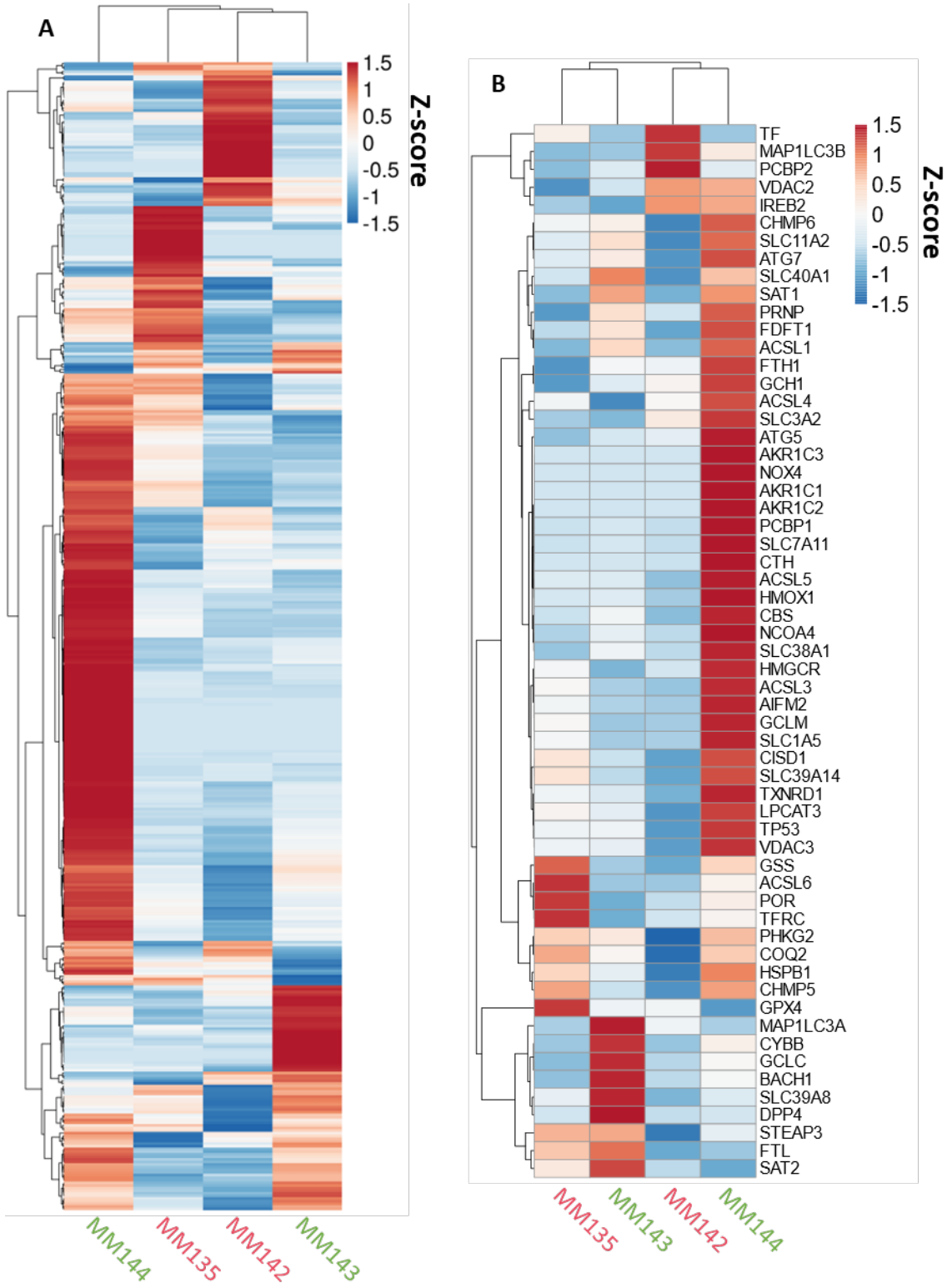

Figure 6-14: Patient-derived MM cells have different expression profiles of ferroptosis-related genes.

RNA sequencing was performed on patient-derived MM cells isolated from fresh marrow aspirate. MM135 and MM142 (pink) were categorised as resistant to 5 µM RSL3 and MM143 and MM144 (green) were classified as sensitive to 5 µM RSL3. Heat maps of normalised gene count converted to row z-score were generated using ClustVis (Metsalu and Vilo, 2015) for ferroptosis-related genes from (A) FerrDb (Zhou et al., 2023) and (B) WP_Ferroptosis gene set (Hanspers et al., 2024). Both rows and columns are clustered using correlation distance and average linkage.

In Chapter 5, we found that ferroptosis-sensitive OPM2 and -resistant KMS-11 MM cell lines differentially expressed 130 ferroptosis-related genes (Figure 5-2B). Here, we investigated the relationship between the expression of these 130 genes, and sensitivity to RSL3 in the four patient-derived MM cell samples. Pearson correlations were performed, but it should be noted that a greater number of samples is generally preferred for these types of analyses. Nevertheless, four genes were identified, which had a strong and significant correlation with the amount of cell death of patient-derived MM cells in response to 5 µM RSL3; peroxiredoxin 6 (*PRDX6*) was strongly correlated with resistance to RSL3 and microsomal glutathione S-transferase 1 (*MGST1*), solute carrier family 2 member 3 (*SLC2A3*) and toll-like receptor 4 (*TLR4*) were strongly correlated with sensitivity to RSL3 (Figure 6-15).

In Chapter 4 we found that ACSL4 protein levels strongly correlated with RSL3 sensitivity in MM cell lines, but no correlation between *ACSL4* gene expression and RSL3 sensitivity was observed in the four patient-derived samples of MM cells (Pearson r = -0.123, p = 0.878). We also previously found that *LPCAT3* levels were elevated in ferroptosis-sensitive OPM2 and DLBCL cell lines compared to resistant MM cell lines, but we did not observe a significant correlation between the expression levels of this gene and RSL3 sensitivity in our patient samples (r = -0.770, p = 0.230).

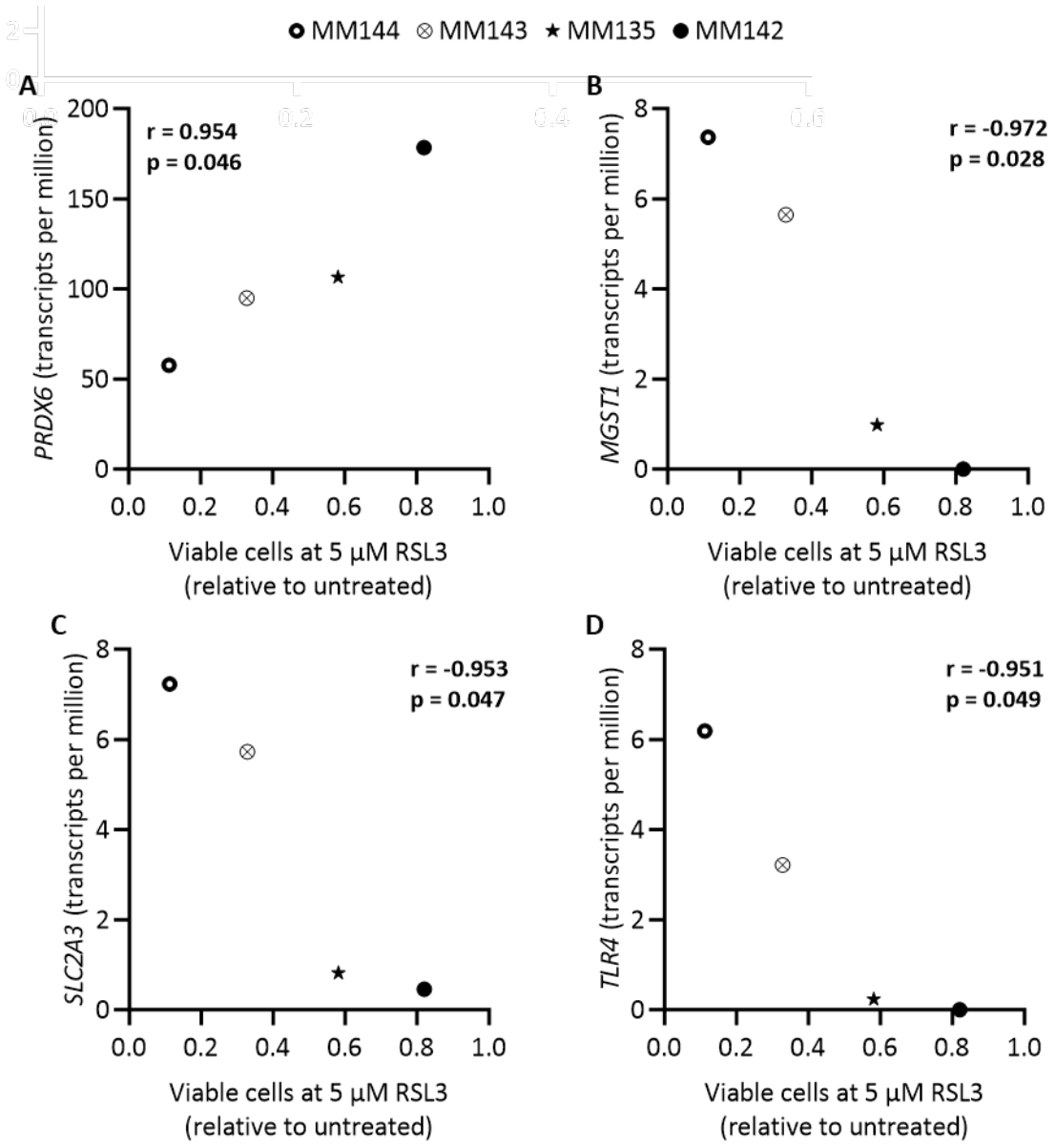

Figure 6-15: Four ferroptosis-related genes strongly correlate with RSL3 sensitivity in patient-derived MM cells.

RNA sequencing was performed on patient-derived MM cells isolated from fresh marrow aspirates of 4 MM patients. Normalised gene expression levels (transcripts per million) were plotted against the relative number of viable cells after treatment with 5 µM RSL3 (data from Figure 6-5D) and Pearson correlations were performed. Statistically significant correlations are displayed for (A) peroxiredoxin 6 (*PRDX6*), (B) microsomal glutathione S-transferase 1 (*MGST1*), (C) solute carrier family 2 member 3 (*SLC2A3*) and (D) toll-like receptor 4 (*TLR4*). r, Pearson correlation coefficient; p, p-value.

6.3 Discussion

6.3.1 AA enhances the effects of RSL3 in patient-derived MM cells, and to a lesser extent in lymphocytes

Whilst BMSCs have been shown to promote MM cell survival (Markovina et al., 2010, García-Sánchez et al., 2023), we did not observe a significant difference in viability nor in the number of viable patient-derived MM cells or lymphocytes in samples from ten patients following co-culture with primary BMSCs (Figure 6-2). Silva *et al*. used an *ex vivo* assay in combination with a mathematical model to predict clinical response of MM patients whereby bone marrow $CD138^+$ cells were cultured with allogenic human-derived BMSCs, in the presence of collagen-I and patient-matched plasma (Silva et al., 2017). An earlier study developed a similar 3D model using fibronectin as well as collagen-I and showed that plasma from patients with MM, regardless of whether it was autologous or not, was essential for MM cell growth as neither bovine nor healthy donor plasma promoted cell growth (Kirshner et al., 2008). While we did successfully maintain MM cell viability over a 48-hour period, the use of MM patient plasma and coating of cell culture plates might be important to promote survival and induce the MM cells to proliferate, which could potentially increase the number of MM cells available.

Furthermore, BMSCs have been shown to play a role in MM drug resistance through excretion of various matrix proteins and factors (Markovina et al., 2010). It was therefore important to investigate the induction of ferroptosis in MM cells in the presence of BMSCs, even if the conditions we employed may not have been optimal to promote MM cell viability or proliferation. Whilst the majority of the drug response analyses on patient samples were performed in co-culture with BMSCs (except for an MNC-only untreated control), in two patient samples there were sufficient cells to also treat with RSL3 in the absence of BMSCs. In MM142, both MM cells and lymphocytes were more sensitive to RSL3 in the absence of BMSCs, however, MM144 patient cells responded similarly with or without BMSCs (Supplementary Figure 6-E). Interestingly, it was recently reported that BMSCs actually enhance ferroptosis in MM cells through increasing intracellular iron levels in the malignant cells (Jiang et al., 2024b). The authors found that MM cell lines became more sensitive to RSL3, but not erastin, when co-cultured with BMSCs and this was enhanced by the addition of 100 µM FAC. The study found that both transferrin and transferrin receptor were upregulated in MM.1S MM cells cultured with BMSCs, which resulted in an increase in total iron. Furthermore, both exogenous iron and co-culture with BMSCs increased the production of lanosterol in MM cells, which was later found to enhance sensitivity to RSL3 (Jiang et al., 2024b). However, we found that iron had no effect on the efficacy of RSL3 in patient-derived MM cells, with a slight increase in cell death in lymphocytes (Figure 6-9). Dysregulation of iron plays a role in MM pathogenesis and drug resistance; both MM cell lines and patient samples have been shown to have low expression of the iron export protein, ferroportin (FPN), and this has been linked with poor patient outcomes (Gu et al., 2015). We showed that, on average, there was a small increase in the number of viable patient-derived MM cells following treatment with 100 µM FAC and this is in agreement

with published findings that have shown that reducing the labile iron pool (LIP) through iron chelation or increased FPN expression, suppresses MM cell growth (Gu et al., 2015).

While AA was better than FAC at enhancing the effects of RSL3 in patient-derived MM cells, high doses of RSL3 were still required, and Lip-1 was not effective at preventing the reduction in the number of viable cells (Figure 6-7). Considering the 2 µM Lip-1 used is well above the 200 nM concentration commonly used in the literature, and the fact that Lip-1 did effectively decrease lipid oxidation (Figure 6-8), the data suggest that other cell death mechanisms might be involved. In Chapter 3, we showed that high doses of RSL3, including the 5 µM used for the patient samples, induces caspase-3 cleavage in some MM cell lines. Therefore, it is plausible that the RSL3 + AA-induced death of patient-derived MM cells involves apoptosis.

Despite the combination of RSL3 and AA being more effective at reducing the number of viable MM cells compared to lymphocytes, the amount of lipid oxidation induced was not significantly different between the two cell types. These findings were similar to those in MM and DLBCL cell lines whereby other than sensitive OPM2 MM cells, the amount of lipid oxidation following treatment with RSL3 was comparable between the two malignancies, despite vast differences in their ferroptosis sensitivity (Figure 3-2). As discussed in previous chapters, differences in sensitivity to ferroptosis-inducing agents without changes to the levels of lipid oxidation, whether that be between cell lines or in the absence or presence of AA, could be due to a number of factors; differences in lipid oxidation might have occurred at an earlier time point, the C11-BODIPY dye might be saturated, differences in the intracellular location of lipid oxidation might affect sensitivity, and other antioxidant systems might be compensating for loss of GPX4 activity. If none of these factors are influencing the amount of lipid oxidation measured, this data further supports the notion that other cell death mechanisms mediate cell death of primary MM cells in response to RSL3 plus AA.

Intracellular ROS is a normal part of cellular metabolism and signalling pathways but must be tightly regulated to maintain redox homeostasis (Perillo et al., 2020). Cancer cells have long been known to exhibit increased ROS due to increased proliferation, hypoxia and genetic mutations (Perillo et al., 2020, Hayes et al., 2020). Specifically, MM cells have increased levels of baseline oxidative stress, associated with excess protein synthesis and the hypoxic environment of the bone marrow (Caillot et al., 2020). In fact, even non-malignant plasma cells are known to have relatively higher levels of ROS (Lipchick et al., 2016). This is consistent with our finding that patient-derived MM cells had a higher level of baseline lipid ROS compared to lymphocytes (Figure 6-3). Patient-derived MM cells may therefore be susceptible to additional oxidative stress and could explain why they were more sensitive to RSL3 alone and in combination with AA, compared to lymphocytes.

6.3.2 Patient-derived MM cells that are less sensitive to RSL3 and AA have a higher proportion of MUFA-containing phospholipids

We found that patient-derived MM cells had a higher proportion of PUFA-containing phospholipids compared to MM cell lines and ferroptosis-sensitive DLBCL cells; patient-derived MM cells had a lipidomic profile that was comprised of an average of 51.57% PUFA-containing phospholipids (Figure 6-11) compared to 33.56% in resistant MM cell lines and 39.07% in sensitive OPM2 MM cells and DLCBL cell lines (Figure 3-14). Vertebrate cells cannot make PUFA *de novo,* which results in cell lines generally having a lower proportion of these fatty acids (Else, 2020). It is, therefore, unsurprising that patient-derived MM cells from fresh whole marrow have a higher proportion of PUFA-containing phospholipids. This might explain their high level of basal lipid oxidation but does not explain their reduced sensitivity to RSL3 compared to the cell lines. One might expect that a higher proportion of PUFA-containing phospholipids would leave these patient-derived MM cells vulnerable to ferroptosis. However, while 5 μM RSL3 was effective in some patient samples, supplementation with exogenous AA generally increased the efficacy of the GPX4 inhibitor (Figure 6-7). Furthermore, patient-derived MM cells do harbor endogenous AA-containing phospholipids, and the proportion of this group of phospholipids increased after culture in RPMI media with 10% FBS (Figure 6-13E). Serum is the primary source of exogenous lipids in cell culture medium and there are differences in the lipid composition of bovine and human sera (Else, 2020). Given this difference, and the fact that MM patient serum has been shown to improve proliferation of patient-derived MM cells (Kirshner et al., 2008), a limitation of our study was the use of FBS. Given the small number of patient-derived MM cells available, we chose to use an already established method in our laboratory which involves culturing patient-derived cells in the same RPMI plus 10% FBS medium used for cell lines. However, it would be useful to compare the lipidomic profile of patient-derived cells in different sera, such as autologous and allogenic from healthy donors and MM-patients, to determine whether this affects ferroptosis sensitivity.

The proportion of MUFA- and PUFA-containing phospholipids was significantly different when patient-derived MM cells were stratified based on sensitivity to RSL3 plus AA, but not RSL3 alone (Figure 6-12). Like MM and DLBCL cell lines, the correlation between the proportion of MUFA-containing phospholipids and sensitivity to RSL3 alone was not significant in patient-derived MM cells (Figure 3-14D) (Table 6-2). Not all MM and DLBCL cell lines were tested with the combination of RSL3 and AA, so similar analyses could not be performed to determine whether there was a correlation between phospholipidomic composition and sensitivity to this combination treatment. In patient samples, however, there was a moderate (though not quite statistically significant) correlation between the proportion of MUFA-containing phospholipids and sensitivity to RSL3 plus AA.

Taken together, these findings suggest that the proportion of MUFA-containing phospholipids, rather than PUFA-containing phospholipids, might determine ferroptosis sensitivity in patient-derived MM cells. Given that patient-derived lymphocytes and MM cells respond differently to ferroptosis-inducing compounds, it would also be useful to investigate the lipidomic profile of patient-matched lymphocytes for comparison of MM cells to a non-malignant cell population.

6.3.3 Investigating the expression of ferroptosis-related genes in patient-derived MM cells

The high baseline level of lipid oxidation in patient-derived MM cells compared to lymphocytes suggests a robust antioxidant system is necessary in these cells to maintain homeostasis, particularly given that high doses of RSL3 are required to induce death. This has been demonstrated in the literature, in studies that found increased expression of antioxidant genes in MM cells compared to their healthy counterparts, including thioredoxin reductase 1 (*TXNRD1*), [Cu-Zn] superoxide dismutase (*SOD1*), glutaredoxin 2/3 (*GLRX2/3*), and peroxiredoxin 6 (*PRDX6*) (Raninga et al., 2015, Caillot et al., 2021, Caillot et al., 2020). Here, rather than comparing to healthy cells, we compared the expression of ferroptosis-related genes within patient-derived MM cells to determine whether differences between patient samples were associated with ferroptosis sensitivity. Specifically, we investigated the 130 ferroptosis-related genes that we identified in Chapter 5 as being differentially expressed between OPM2 and KMS-11 MM cell lines that may be involved in determining ferroptosis sensitivity (Figure 5-2).

In Chapter 5, we discovered that the high expression of FSP1 in KMS-11 MM cells likely contributed to the resistance of these cells to ferroptosis, as genetic deletion or pharmacological inhibition of the protein sensitised them to RSL3. However, compared to KMS-11, the patient samples had relatively low expression of FSP1; in fact, of the four patient samples examined, the most RSL3-sensitive patient sample, MM144, had the highest expression of FSP1 (Table 6-3).

The only gene that strongly correlated with RSL3 resistance in patient-derived MM cells was *PRDX6*, which, like GPX4, can reduce phospholipid hydroperoxides and its knockdown promotes ferroptosis (Lu et al., 2019, Chen et al., 2024b, Ito et al., 2024, Lagal et al., 2024b). Not only does PRDX6 have glutathione peroxidase activity, but it is also involved with fatty acid remodelling due to its phospholipase A2 and lysophosphatidylcholine acyltransferase (LPCAT) activity (Fujita et al., 2024, Lagal et al., 2024a). Despite these ferroptosis-relevant roles, the main mechanism by which PRDX6 is thought to contribute to ferroptosis is through its involvement in the synthesis of selenoproteins (Fujita et al., 2024, Ito et al., 2024). In MM, *PRDX6* is markedly overexpressed compared to plasma cells from healthy donors and is associated with poor prognosis (Gao et al., 2025). Knockdown of PRDX6 caused an increase in total ROS and subsequent cell death

that was associated with caspase-3 cleavage. Despite ferroptosis not being investigated in this publication, the authors showed that PRDX6 deficiency enhanced bortezomib-induced cell death of MM cells (Gao et al., 2025). *PRDX6* strongly correlated with resistance to RSL3 in our patient-derived MM cells which is unsurprising given the mounting evidence supporting its role as a ferroptosis suppressor.

Conversely, *TLR4*, *SLC2A3* and *MGST1* strongly correlated with increased RSL3 sensitivity in patient-derived MM cells (Figure 6-15). TLR4 is involved in innate immune signalling and has been shown to drive ferroptosis; its genetic knockdown reduced lipid oxidation and labile iron levels in a model of heart failure and its pharmacological inhibition reduced markers of ferroptosis such as malondialdehyde (MDA) and mitochondrial shrinkage in neuronal cells (Chen et al., 2019, Zhu et al., 2021). Encoded by the *SLC2A3* gene, glucose transporter 3 (GLUT3), is a member of the glucose transporter protein family which are typically upregulated in cancer cells due to their glucose dependence. Whilst MM cells have been shown to be reliant on various GLUT members, GLUT3 has been shown to be downregulated in MM cells compared to healthy plasma cells (McBrayer et al., 2012). GLUT3 is labelled as "unclassified" in FerrDb with minimal supporting evidence to explain its role in ferroptosis (Zhou et al., 2023). *SLC2A3* has been linked to ferroptosis as its expression was decreased following knockdown of lymphoid-specific helicase, which can inhibit erastin-induced ferroptosis (Jiang et al., 2017). More recently, knockdown of GLUT3 in a proximal tubular cell line prevented erastin-induced death through blockade of erastin-induced increases in intracellular iron and total ROS (Wei et al., 2022). These findings highlight the capacity of TLR4 and SLC2A3/GLUT3 to play roles in driving ferroptosis, which might explain why increased expression of these genes strongly correlated with ferroptosis sensitivity in our patient-derived MM cells.

Conversely, *MGST1* is a Nrf2 target gene that has been shown to prevent lipid oxidation; knockdown of *MGST1* enhanced cell death and lipid oxidation caused by a range of ferroptosis inducers in melanoma, gastric cancer and pancreatic cancer cells, whereas overexpression had the opposite effect (Zhang et al., 2023c, Kuang et al., 2021, Li et al., 2023b, Peng and Peng, 2023). In gastric cancer cells, MGST1-mediated ferroptosis resistance was shown to involve inactivation of autophagy (Peng and Peng, 2023). In pancreatic cancer cells, the ability of MGST1 to prevent ferroptosis was shown to be mediated by decreasing the activity of arachidonate 5-lipoxygenase (ALOX5), thus decreasing lipid peroxidation (Kuang et al., 2021). However, our data suggest that expression of this gene is associated with an increase in the sensitivity of primary MM cells to RSL3. This discrepancy might be due to differences in the particular ALOX protein involved in ferroptosis in the different diseases. This is particularly relevant given that none of the four patient-derived MM samples expressed *ALOX15* (Table 6-3). While *ALOX15* has previously been shown to be indispensable for ferroptosis, other lipoxygenases may compensate in its absence (Seiler et al., 2008, Friedmann Angeli et

al., 2014). Kuang *et al*. showed that during ferroptosis, there is an increase in the interaction of MGST1 with ALOX5, but not ALOX12 or ALOX15 (Kuang et al., 2021). Furthermore, the patient sample that was least sensitive to RSL3 in our study, MM142, had undetectable levels of *MGST1* (Table 6-3), indicating other ferroptosis-resistant mechanisms may be at play.

This RNA sequencing data presented here is preliminary and requires further study in a larger cohort of patient samples, either with additional RNA sequencing or analysis of specific ferroptosis-related genes using RT-qPCR. Without sufficient cells for biological replicates, nor an appropriate control (such as plasma cells from healthy donors), it was not possible to perform differential gene analyses. With further work on a wider range of patient-derived MM samples and grouping based on ferroptosis sensitivity, it may be possible to perform a more in-depth differential gene analysis between ferroptosis-sensitive and -resistant groups.

6.3.4 Conclusions

To conclude, we found that RSL3, with or without the addition of AA, but not FAC resulted in a depletion of MM cells, while healthy lymphocytes were largely spared. Whilst treatment with RSL3 and AA induced a marked increase in the levels of oxidised lipids, Lip-1 did not effectively prevent toxicity, suggesting that ferroptosis may not be the only form of cell death contributing to the depletion of MM cells. We found a correlation between the proportion of MUFA-containing phospholipids and sensitivity to RSL3 plus AA in patient-derived MM cells. Thus, assessing the lipidomic profile of patients, particularly regarding the specific fatty acids identified, may be a useful tool to predict whether patients will respond to ferroptosis-inducing drugs that rely on modulation of the lipidomic profile of the target cells. Assessing a wider range of patient samples with varying responses to RSL3 plus AA would allow for better statistical certainty to support this hypothesis. Although lymphocytes were not completely immune to the toxic effects of RSL3, with or without AA, it is promising to find that MM cells appear to be more sensitive to ferroptosis compared to lymphocytes from the same patients. It is important to note that whilst *ex vivo* cultures of patient-derived cells is a useful tool that bridges the gap between *in vitro* cell line work and animal models, it does not completely represent how a drug or cellular pathway would behave in the context of a whole organism. Data from our *ex vivo* cultures are meant to provide insight into the pathway of ferroptosis in patient-derived cells, but future work should aim to use animal models to determine the effectiveness of ferroptosis-inducers in the context of multiple body systems at play. Given that a significant challenge in the clinical translation of ferroptosis-inducing drugs is the fact that GPX4 inhibition may be detrimental to not only cancer cells but also healthy cells *in vivo*, future work should focus on targeted approaches to ensure ferroptosis-inducing agents are delivered to cancer cells and not to healthy cells or tissues.

APPENDIX 6A. SUPPLEMENTARY FIGURES

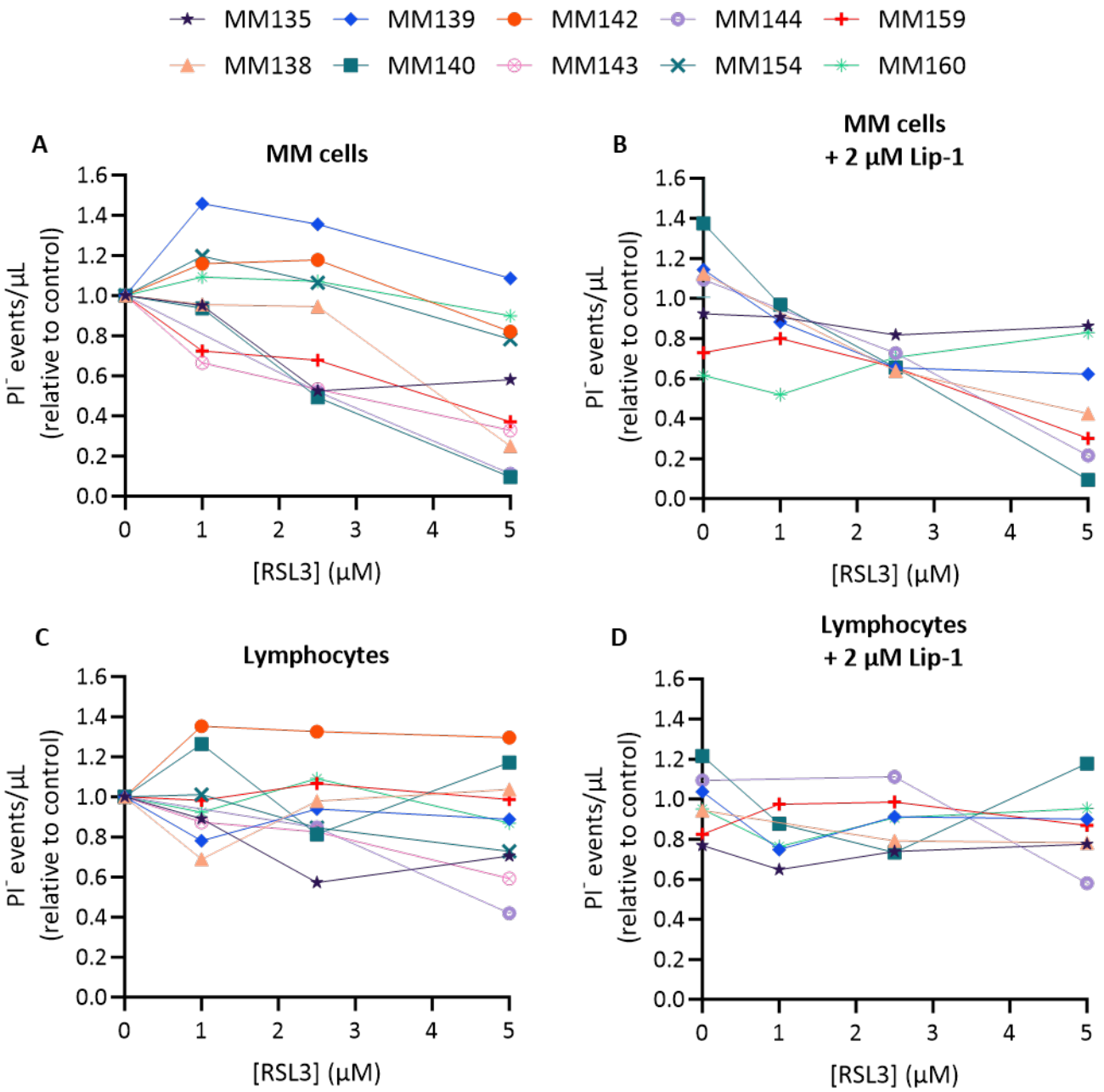

Supplementary Figure 6-A: RSL3 dose responses in 10 patient-derived samples.

Patient-derived MNCs were cultured with autologous BMSCs for 24 hours. The concentrations of RSL3 indicated, with or without 2 µM Lip-1, was added for a further 24 hours and the number of viable lymphocytes and MM cells was measured. Flow cytometry was performed to assess drug toxicity indicated by the number of propidium iodide (PI) negative cells/µL relative to untreated controls. Each shape represents one patient sample, and the mean is represented by a solid line. Statistical analyses were performed by paired t-test; ns indicates no significant difference.

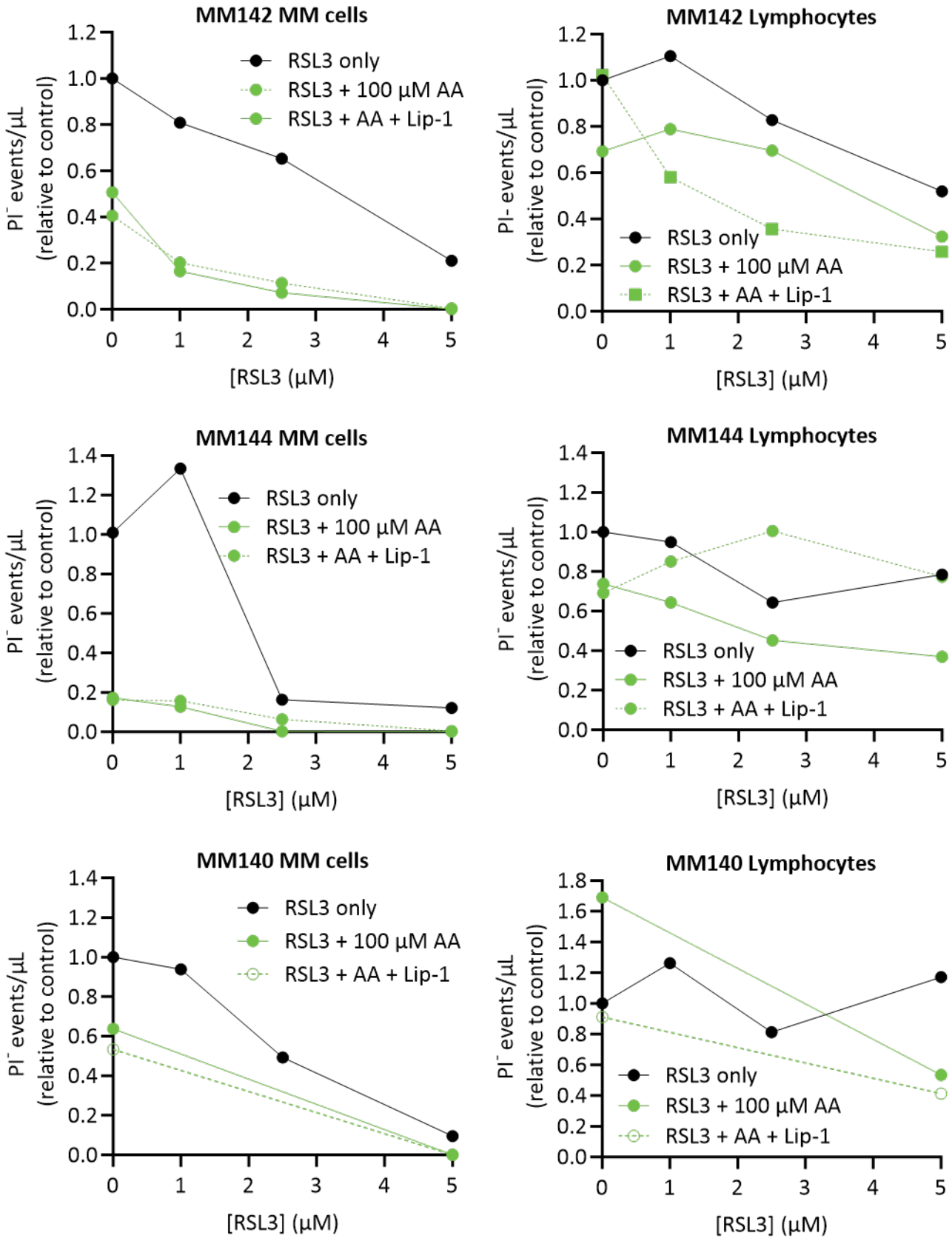

Supplementary Figure 6-B: Patient-derived MM cells are sensitive to 100 µM AA.

Patient-derived MNCs were cultured with patient-matched BMSCs for 24 hours. The concentrations of RSL3 indicated, with or without 60 µM AA and 2 µM Lip-1, was added for a further 24 hours and the number of viable lymphocytes and MM cells were measured. Flow cytometry was performed to assess drug toxicity indicated by the number of propidium iodide (PI) negative cells/µL relative to untreated controls.

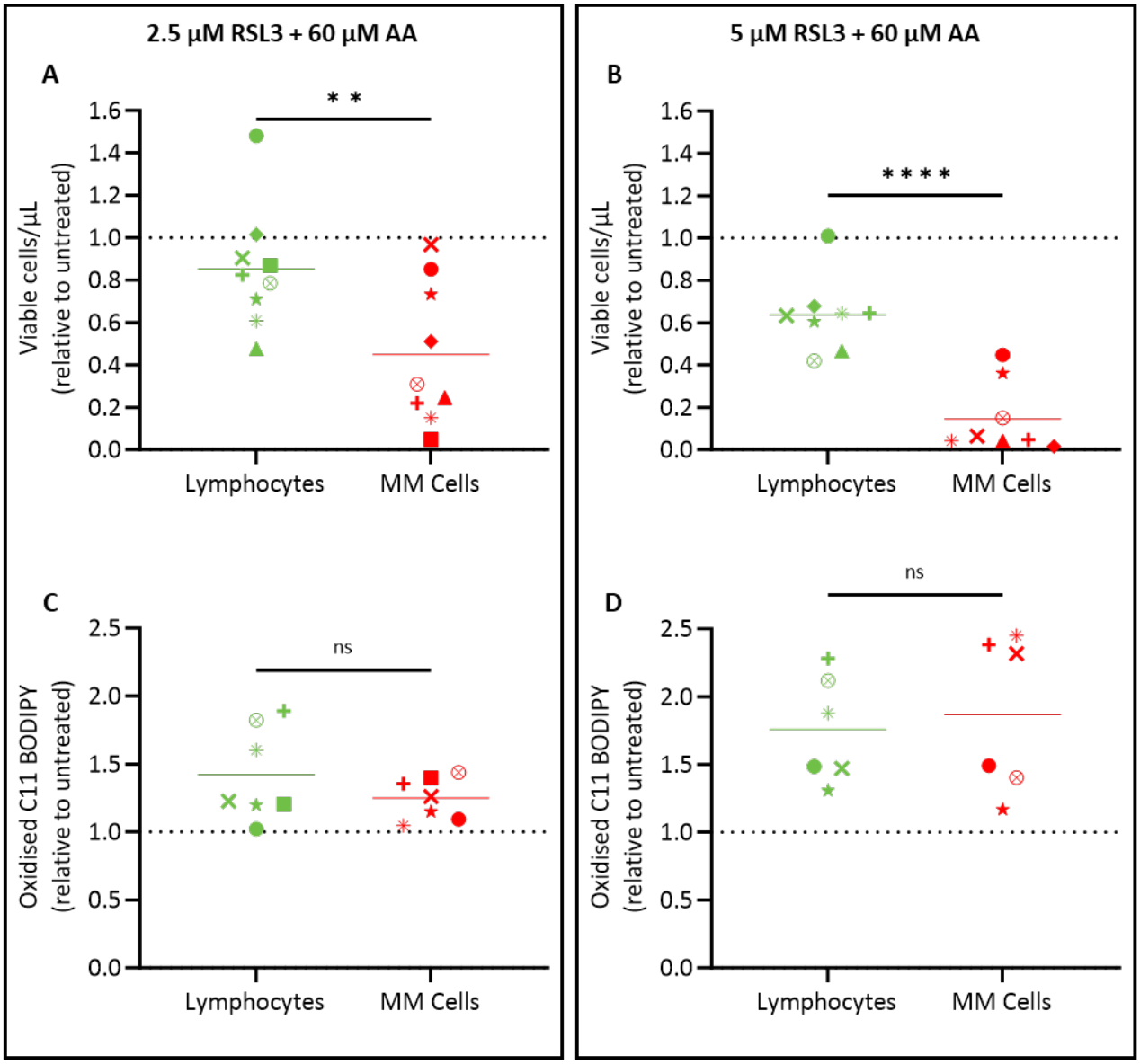

Supplementary Figure 6-C: Comparing the number of remaining viable cells and levels of lipid oxidation in patient-derived lymphocytes and MM cells after treatment with RSL3 and 60 µM AA.

Patient-derived MNCs were cultured with autologous BMSCs for 24 hours. 2.5 µM (A,C) or 5 µM (B,D) RSL3 plus 60 µM AA was added for a further 24 hours. (A,B) Drug toxicity was measured in the lymphocyte and MM cell populations as the number of propidium iodide (PI) negative cells/µL relative to untreated controls. (C,D) Levels of lipid oxidation in each cell population was measured by flow cytometry. Each shape represents one patient sample, and the mean is represented by a solid line. Statistical analyses were performed by paired t-test; ns indicates no significant difference, ** $p<0.01$, **** $p<0.0001$.

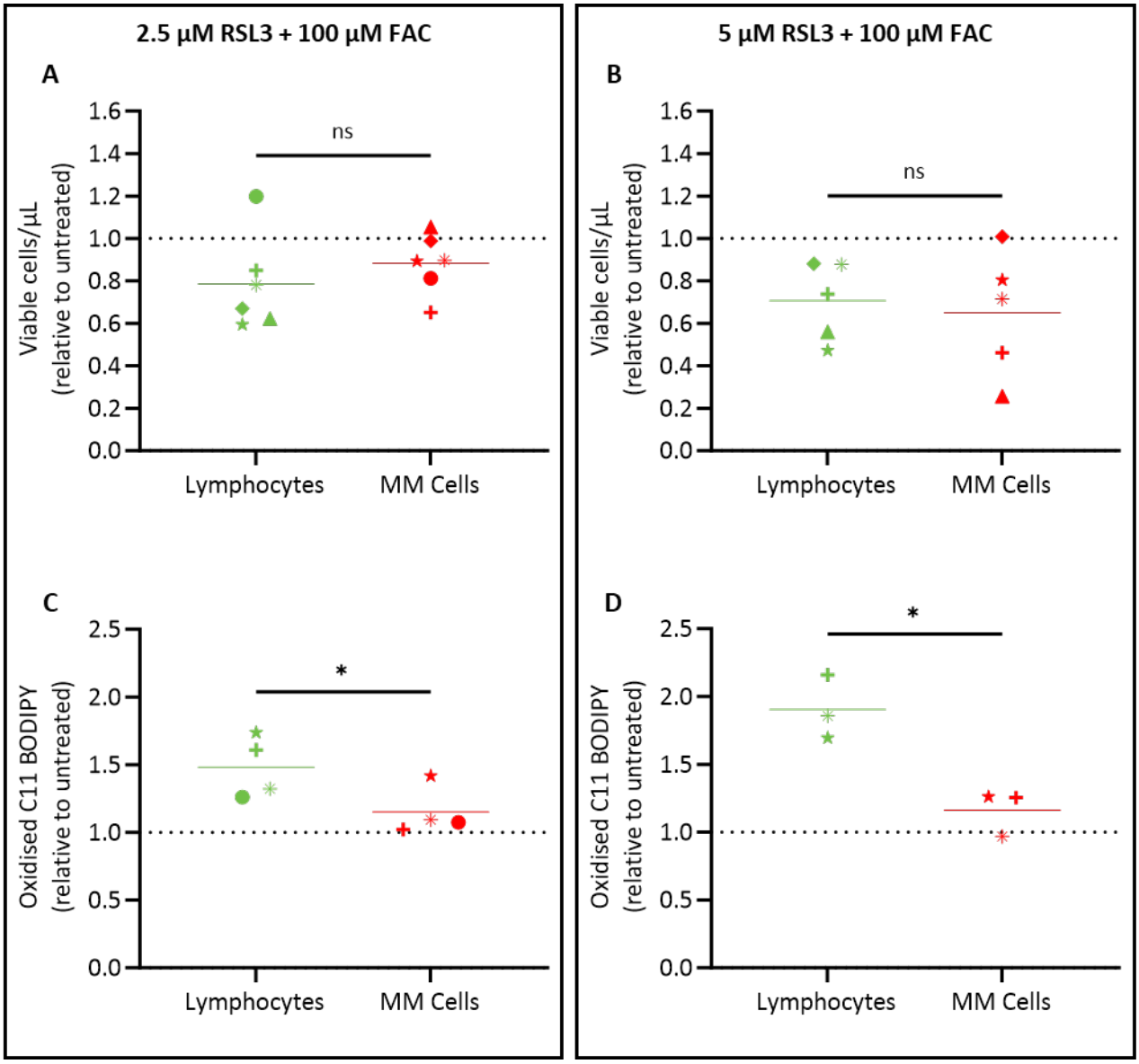

Supplementary Figure 6-D: Comparing the number of remaining viable cells and levels of lipid oxidation in patient-derived lymphocytes and MM cells after treatment with RSL3 and 100 µM FAC.

Patient-derived MNCs were cultured with autologous BMSCs for 24 hours. 2.5 µM (A,C) or 5 µM (B,D) RSL3 plus 100 µM FAC was added for a further 24 hours. (A,B) Drug toxicity was measured in the lymphocyte and MM cell populations as the number of propidium iodide (PI) negative cells/µL relative to untreated controls. (C,D) Levels of lipid oxidation in each cell population was measured by flow cytometry. Each shape represents one patient sample, and the mean is represented by a solid line. Statistical analyses were performed by paired t-test; ns indicates no significant difference, * $p<0.05$.

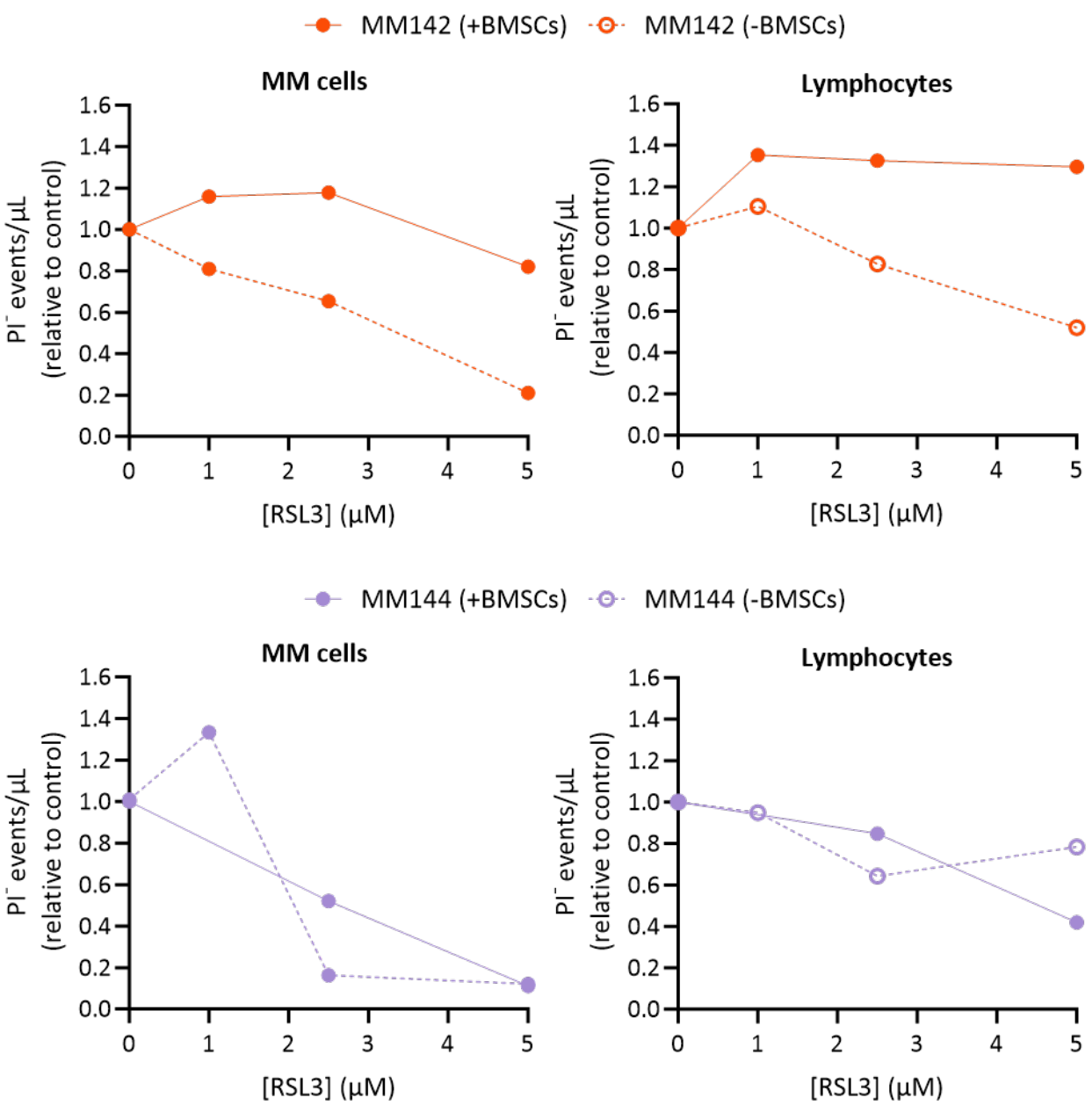

Supplementary Figure 6-E: Assessing lymphocyte and MM cell response to RSL3 in the absence or presence of BMSCs.

Patient-derived MNCs were cultured with or without autologous BMSCs for 24 hours. The concentrations of RSL3 indicated, with or without 2 µM Lip-1, was added for a further 24 hours and the number of viable lymphocytes and MM cells was measured. Flow cytometry was performed to assess drug toxicity indicated by the number of propidium iodide (PI) negative cells/µL relative to untreated controls.

APPENDIX 6B. SUPPLEMENTARY TABLES

Table 6-3: Expression of ferroptosis-related genes Figure 6-14B.

RNA sequencing was performed on untreated KMS-11 and patient-derived MM cells. Gene expression (transcripts per million) from WP_Ferroptosis gene set (Hanspers et al., 2024) are listed.

	Gene expression (transcripts per million)				
Gene	**KMS-11**	**MM135**	**MM142**	**MM143**	**MM144**
ACSL1	30.76	3.681	4.464	16.45	26.02
ACSL3	46.10	12.92	3.498	3.617	27.27
ACSL4	26.42	17.80	20.22	5.251	28.14
ACSL5	47.14	14.25	5.478	11.11	46.69
ACSL6	0.000	0.135	0.000	0.000	0.050
AIFM2	41.93	6.886	3.364	2.734	14.43
AKR1C1	0.000	0.000	0.000	0.000	25.79
AKR1C2	0.000	0.000	0.000	0.000	0.098
AKR1C3	0.549	0.000	0.000	0.000	5.320
ALOX15	0.026	0.000	0.000	0.000	0.000
ATG5	15.21	15.56	21.06	14.19	28.01
ATG7	6.160	5.243	0.897	5.552	11.17
BACH1	29.43	17.67	31.43	98.62	51.94
CBS	22.89	23.15	0.000	44.20	149.5
CHMP5	30.26	38.93	6.031	12.41	35.85
CHMP6	38.68	7.612	0.875	6.312	12.64
CISD1	51.10	11.81	1.444	4.121	17.46
COQ2	23.38	12.80	1.800	6.363	10.96
CP	0.000	0.000	0.000	0.000	0.000
CTH	1.311	3.601	0.840	6.370	165.6
CYBB	1.934	1.896	0.659	47.60	23.99
DPP4	0.020	0.076	0.000	1.553	0.093
FDFT1	87.62	27.93	25.33	31.64	48.03
FTH1	1449	885.1	1183	866.8	1266
FTL	1878	4450	3945	3606	3436
FTMT	0.000	0.000	0.000	0.000	0.000
GCH1	14.92	0.425	4.651	2.176	5.578
GCLC	51.77	4.431	6.704	17.80	10.25
GCLM	24.90	2.952	1.000	0.656	6.613
GPX4	304.5	427.5	296.9	210.3	155.1
GSS	39.34	24.71	3.124	4.486	16.69
HMGCR	45.42	10.38	9.046	4.820	16.56
HMOX1	43.88	7.044	3.285	6.771	31.51
HSPB1	1629	654.9	151.7	338.5	703.8
IREB2	42.38	8.166	22.66	4.595	18.09
LPCAT3	19.18	13.92	6.204	9.137	20.39
MAP1LC3A	0.084	0.304	1.851	4.079	0.293
MAP1LC3B	84.74	34.75	219.3	32.62	105.7
MAP1LC3C	0.000	0.000	0.000	0.000	0.000
NCOA4	100.3	27.03	32.47	35.59	101.8
NOX1	0.000	0.000	0.000	0.000	0.000
NOX4	0.000	0.000	0.000	0.000	2.589
PCBP1	635.3	201.1	213.7	166.1	405.5
PCBP2	2032	330.8	399.5	267.8	309.7
PHKG2	32.70	21.78	4.777	13.73	20.53
POR	65.18	47.46	21.30	10.83	27.79
PRNP	22.87	8.490	39.47	62.30	107.5
SAT1	5.457	52.30	50.37	110.6	133.2
SAT2	59.46	65.20	42.89	74.39	24.03
SLC11A2	8.923	7.521	3.063	9.232	14.76

SLC1A5	304.8	349.1	115.4	88.74	864.2
SLC38A1	111.8	29.00	47.58	62.82	175.1
SLC39A14	73.92	40.59	3.337	11.97	59.73
SLC39A8	62.81	39.99	18.34	82.12	32.26
SLC3A2	200.1	117.9	445.5	51.69	696.3
SLC40A1	12.81	2.365	0.000	6.379	6.066
SLC7A11	2.841	0.796	0.000	1.783	78.76
STEAP3	18.86	7.304	0.000	6.235	3.773
TF	0.000	0.158	0.415	0.000	0.000
TFRC	145.9	35.46	20.23	11.46	21.56
TP53	0.134	21.84	7.948	17.468	40.17
TXNRD1	245.2	25.71	14.38	17.593	46.44
VDAC2	186.6	94.42	140.0	90.666	124.2
VDAC3	169.5	37.31	5.377	27.734	81.35

CHAPTER 7. FINAL DISCUSSION AND FUTURE DIRECTIONS

Multiple myeloma (MM) is a still incurable disease and in 2024, it was estimated that 2,719 people were diagnosed with the disease and that it caused 1,207 deaths in Australia (Australian Institute of Health and Welfare, 2024). From 1991 to 1995, the 5-year survival rate for people with MM was 27.1% and this increased to 59.5% by 2020 (Australian Institute of Health and Welfare, 2024). Whilst the survival of MM patients has increased thanks to the development of novel therapeutic regimens being introduced in the clinic, drug resistance remains inevitable. The rate of disease-related, or drug-induced symptoms in people with MM significantly affects health-related quality of life. For example, a cross-sectional, prospective study undertaken in the United States in 2020 reported that approximately 24% of patients with MM had clinically relevant symptoms of depression, anxiety and/or post-traumatic stress disorder (O'Donnell et al., 2022).

Out of all cancers, MM incurs one of the highest costs per person to both the healthcare system and the individual. A study in Queensland, Australia determined that between 2013 and 2016, the average cost to the healthcare system per MM patient was nearly $46,000 compared to the overall average of $15,889 per person for all cancers (Merollini et al., 2022). In the 2023 State of the Nation: Blood Cancers in Australia Report, a survey of 4,600 people living with blood cancer (19% of respondents identified as having a diagnosis of MM) demonstrated that 43% of patients reported out-of-pocket costs, with more than a third of those stating costs of over $5,000 (Leukaemia Foundation, 2023).

We have described in Chapter 1 that ferroptosis is a cell death mechanism that is distinct from the types of cell death typically induced by most of the anti-cancer agents used in the clinic. Therefore, not only does ferroptosis provide a different means to try and overcome MM cell resistance to existing therapies, but it has also been shown that cancer cells are especially susceptible to this form of cell death (Lei et al., 2022). For the first time we have shown this is also true in MM whereby patient-derived MM cells are more sensitive to the combination of RSL3 and AA compared to lymphocytes within the same co-culture system. We hypothesised that MM cells can be forced to undergo ferroptosis by increasing cellular labile iron or lipid peroxidation. Throughout this thesis we have proven this hypothesis to be true by addressing the following three aims.

Aim 1: Investigate the susceptibility of MM and DLBCL cells to ferroptosis.

Aim 2: Determine mechanisms that render MM cells sensitive to ferroptosis by investigating key genes, proteins and lipids involved in ferroptosis.

Aim 3: Investigate the sensitivity of primary patient myeloma cells to ferroptosis.

7.1 Aim 1: Investigate the susceptibility of MM and DLBCL cells to ferroptosis

Throughout the production of this thesis and since the publication of our literature review describing ferroptosis studies in MM, new findings regarding ferroptosis in MM have been published. Recently, it was shown that intraperitoneal injection of 10 mg/kg RSL3 (every two days for three weeks) was well tolerated in a mouse model of MM and did not cause mortality or weight loss. In fact, RSL3 was very effective at reducing the tumour size of H929 xenograft-bearing mice and a lower dose of 5 mg/kg RSL3 caused a synergistic reduction in tumour size when combined with bortezomib (Zhang et al., 2024a).

Most publications investigating ferroptosis in MM focus on this malignancy alone and therefore fail to acknowledge that these cells are not as sensitive to inhibition of the canonical anti-ferroptosis pathway compared to solid tumours and other haematological malignancies, such as DLBCL. Yang *et al*. made this distinction in 2014 when they showed that MM cells were less sensitive to the growth inhibitory effects of the class 1 ferroptosis inducer, erastin (Yang et al., 2014). We built on this study by testing whether this was a general lack of sensitivity to ferroptosis or related to the reliance of DLBCL cells on the target of erastin, xCT, to import cystine for glutathione (GSH) production. In Chapter 3, we found that, compared to DLBCL, MM cells (except for the OPM2 cell line) are also much less sensitive to ferroptosis induced by the GPX4 inhibitor, RSL3. Whilst we did not have success in genetically knocking out GPX4 to determine whether the effects of RSL3 were related specifically to its capacity to inhibit GPX4, we found that the morphological features of MM cells treated with RSL3 were consistent with the ballooning phenotype associated with ferroptosis and showed that the activity of RSL3 was dependent on its ability to induce lipid oxidation. We found that expression of the prime target of RSL3, GPX4, did not correlate with ferroptosis sensitivity which implies this will not be a useful measure of ferroptosis sensitivity in MM patient samples. This is also an important finding as it implies that the apparent heterogenous expression of GPX4 not only between cell lines, but also within cell lines at different time points, should not affect ferroptosis induced by RSL3 in MM.

For the first time in MM, we showed that RSL3 combined with exogenous arachidonic acid (AA) or iron in the form of ferric ammonium citrate (FAC) causes a synergistic reduction in cell viability. These findings indicate that the development of GPX4-inhibiting compounds to induce ferroptosis in MM cells should also include modulation of the levels of these two important cellular components to ensure the MM cell population is completely ablated.

7.1.1 Clinical translation of iron supplementation to enhance ferroptosis

It is important to note that high iron supplementation can have detrimental effects given that healthy tissue is also susceptible to iron overload-induced ferroptosis (Table 7-1). *In vivo* studies of iron supplementation in

the context of ferroptosis often utilises iron dextran injected intraperitoneally at doses ranging from 100 mg/kg in a Vk*MYC MM mouse model (Bordini et al., 2020) to 200 mg/kg in a rhabdomyosarcoma xenograft model (Asperti et al., 2023). Bordini *et al*. injected mice with iron dextran at day 5 of every cycle of bortezomib/melphalan/prednisone and found that markers of liver function and kidney injury were not affected by the addition of iron (Bordini et al., 2020). However, various iron-overload models where C57BL/6 mice were injected with doses ranging from 100 to 500 mg/kg iron dextran, albeit at more regularly frequencies than the Bordini study, showed an association with weight loss, impaired glucose tolerance, increased intestinal permeability, damage to the structure of epithelial microvilli and osteoporosis (Table 7-1). In these studies, markers of oxidative stress and/or ferroptosis were present in various organs and cells, indicating elevated iron levels might induce ferroptosis in healthy tissue.

Table 7-1: Snapshot of recent studies involving *in vivo* use of iron

	Mouse model	Admin-istration route	Dose (mg/kg)	Frequency	Total treatment length	Adverse effects	Ref.
Iron dextran	C57BL/6	IP	100	Once per week	2 months	Ferroptosis in osteoblasts Development of osteoporosis	(Jiang et al., 2022)
	RMS NOD/SCID xenograft	IP	100	Days 5, 14, 21, 28	4 weeks	Iron deposits in spleen, liver and tumour sections (no comment on adverse effects)	(Asperti et al., 2023)
	Vk*MYC (MM)	IP	100	Once per 7 weeks	3 times	Markers of liver function and kidney injury did not deviate from reference ranges	(Bordini et al., 2020)
	C57BL/6	IP	120	Once per 2 weeks	12 weeks	Lower body weight Increased intestinal permeability Epithelial microvilli structure damage	(Zhao et al., 2024)
	RMS NOD/SCID xenograft	IP	200	Days 5, 20, 40	40 days	Iron deposits in spleen, liver and tumour sections (no comment on adverse effects)	(Asperti et al., 2023)
	C57BL/6	IP	500	Twice per week	4 weeks	Weight loss Elevated fasting blood glucose and insulin Impaired glucose tolerance Decreased insulin sensitivity	(Mo et al., 2024)
Ferric ammonium citrate	C57BL/6	IP	40	Every 3 days	8 weeks	Deterioration of trabecular bone Increased osteoclast surface Decreased osteoblast surface Decreased serum alkaline phosphatase and osteocalcin, and mineral apposition rate	(Zhang et al., 2020)
	Ovarian xenograft (BALB/c)	IP	100	Every 3 days	15 days	No change to mouse body weight (no comment on other adverse effects)	(Li et al., 2021)
	C57BL/6	Oral	333	Every day	16 weeks	Reduced mobility Impaired motor and cognitive functions	(Huang et al., 2019)
Ferrous sulphate	Kunming	IP	75	Every day	1 week	Reduced heart and liver size Reduced body weight Testis injury	(Liu et al., 2025)

IP, intraperitoneal; RMS, rhabdomyosarcoma

FAC is typically the iron source used for *in vitro* studies and lower doses from 100 to 500 µM FAC, whilst typically ineffective on their own, can synergise with ferroptosis-inducing compounds (Gu et al., 2015, Maccarinelli et al., 2023). Higher concentrations of FAC ranging from 600 µM to 1.5 mM can induce cell death, which is not limited to malignant cells (Bordini et al., 2020, Luo et al., 2024). In particular, 600 µM FAC induced ferroptotic cell death in rat cardiomyocytes, which was further exacerbated when GSH was depleted (Lyamzaev et al., 2024). *In vivo* use of 100 mg/kg FAC in an ovarian xenograft mouse model with or without GPX4 knockdown did not affect mice weight when injected intraperitoneally every three days for five cycles (Li et al., 2021). However, in a model of iron-overload, C57BL/6 mice were also injected every three days, albeit for the slightly longer period of 8 weeks, with a comparatively lower dose of 40 mg/mL FAC, and various markers of bone loss were increased compared with controls (Table 7-1) (Zhang et al., 2020).

Taken together, models of iron-overload with treatment regimens not dissimilar to those used to enhance the effects of ferroptosis-inducing agents *in vivo* may have potentially harmful systemic side effects. One way to combat this is to exploit endogenous iron to drive ferroptosis. A recent review provided an in-depth overview of enhancing ferroptosis through modulating the levels of endogenous iron by increasing uptake or releasing free iron through ferritin degradation and HO-1 activation, or decreasing iron export and utilisation (Zhu and Du, 2024). A prime example of this is the study by Zhang *et al.* introduced in Chapter 4 that showed bortezomib promotes ferritinophagy and ferric iron reduction in MM cells through prevention of NCOA4 and STEAP3 degradation, respectively (Zhang et al., 2024c). This increase in free iron, without the need for iron supplementation, allowed for the synergistic and ferroptosis-associated reduction in cell viability when bortezomib was combined with RSL3 (Zhang et al., 2024c).

7.1.2 Clinical translation of AA supplementation to enhance ferroptosis

Not only did we show that AA caused a greater reduction in the IC_{50} of RSL3 compared to FAC, but AA supplementation has already been shown to have anti-tumour effects in MM and pro-ferroptotic effects in other cancers. In MM cell lines, AA-induced death has been shown to be inhibited with ferrostatin-1 and in mice treated with 500 µg/g AA (subcutaneous injection, twice weekly for 41 days), a smaller tumour volume was observed compared to vehicle-treated mice (Panaroni et al., 2022). Intraperitoneal injection of 2 mg/kg AA, administered to immunocompetent mice every three days for 26 days, slowed melanoma, colon and Lewis lung carcinoma tumour growth (Liao et al., 2022). Furthermore, these effects were enhanced in the melanoma and colon tumour-bearing mice when co-treated with an immune checkpoint inhibitor (anti-PD-L1). Notably, tumours in immunodeficient mice were unaffected by AA and importantly, T-cells were not affected by AA *in vitro* or *in vivo* (Liao et al., 2022). Whilst the study by Panaroni *et al.* used immunodeficient mice bearing MM tumours, the findings of the latter study highlight the important role of the immune system

in AA-driven ferroptosis. In MM and other cancers, AA can play a dual role in both promoting cancer proliferation, whilst also sensitising them to ferroptosis-inducers (Panaroni et al., 2022, Zhang et al., 2025). We did not test doses below 20 μM AA to determine whether they enhance proliferation in our panel of MM cell lines, however, in two patient-derived samples the number of viable MM cells was slightly higher after treatment with 60 μM AA. Overall, we found that combining AA with RSL3 was a very effective means of inducing ferroptosis in primary MM cells without any increase in proliferation evident in the 9 patient-derived MM cell samples.

7.1.3 Repurposing drugs with other indications to induce ferroptosis in MM cells

Briefly introduced in Chapter 1, the Chinese medicinal plant extract Qinghaosu (artemisinin) and its derivatives, such as artesunate, are FDA-approved for treatment of malaria, but have also shown promise as an anti-cancer agents (Mancuso et al., 2021). Artemisinin-type compounds have been shown to have a variety of effects on cancer cells, and we discussed in Chapter 1 how its mechanism of action was found to involve ferroptosis in Burkitt's lymphoma, adult T-cell leukaemia/lymphoma and DLBCL cells (Wang et al., 2019a, Ishikawa et al., 2020, Chen et al., 2021b). Since our literature review featured in Chapter 1 was published, artesunate has been shown to induce ferroptosis in MM cells through a reduction in GPX4 expression caused by decreasing the levels of isopentenyl pyrophosphate (IPP), which is necessary in the production of Sec-tRNA (Liang et al., 2023). The bioactive components of other traditional Chinese medicinal plants, ginsenoside Rh4 and nitidine chloride (extracted from *Panax ginseng* and *Zanthoxylum nitidum*, respectively) have also recently been shown to reduce cell proliferation and induce cell death and cell cycle arrest in MM cells, through mechanisms that involve ferroptosis (Ying et al., 2023, Yin et al., 2023). Disulfiram, which is approved by the FDA to treat alcoholism, induced lipid oxidation as well as a reduction in cell viability which could be prevented with Lip-1 in MM cell lines, including against a carfilzomib-resistant cell line (Arkan and Akcora-Yildiz, 2025). Other FDA-approved drugs, sulfasalazine and sorafenib, that act as class 1 ferroptosis inducers (Feng and Stockwell, 2018, Yu et al., 2017), have also been shown to have anti-MM effects (Wang et al., 2022a, Gentile et al., 2016).

Human clinical trials with the commonly used ferroptosis-inducing agents erastin and RSL3, have not been conducted and are unlikely due to reasons discussed throughout this thesis, so it is promising that FDA-approved agents for other indications are showing promise at inducing ferroptosis in MM cells. Even if MM cells are not as sensitive to ferroptosis induced by RSL3 alone, our findings in Chapters 3 & 4, and the aforementioned studies show that MM cells do in fact have the intracellular machinery to undergo ferroptosis induced by a range of different compounds. In Aim 2, we investigated this further to determine

which intracellular factors impact or can potentially predict MM cell sensitivity to ferroptosis-inducing agents.

7.2 Aim 2: Determine mechanisms that render MM cells sensitive to ferroptosis

Ferroptosis is regulated by multiple, interconnected pathways, rather than a single linear process. Whilst research surrounding ferroptosis has grown exponentially, it is important to understand the mechanisms and cellular components that dictate sensitivity in specific contexts and cell types. For example, if a protein is found to prevent ferroptosis in prostate cancer, it may not play a similar role in MM cells, it may further sensitise MM cells, or it is also possible that the protein is not even expressed in these cells. This is especially true of proteins that have been shown to have dual, context-dependent roles in both promoting and suppressing ferroptosis such as AMP-activated protein kinase (AMPK), activating transcription factor 4 (ATF4), heme oxygenase 1 (HO-1), hypoxia-inducible factor (HIF) and tumour protein p53 (p53) (Tang et al., 2021a, Nishizawa et al., 2020, Zheng et al., 2023). Despite publications claiming certain cellular components play an indispensable role in the execution of ferroptosis, such as acyl-CoA synthetase long-chain family 4 (ACSL4) (Doll et al., 2017), new pathways independent of these "vital" proteins have been found (Chu et al., 2019, Magtanong et al., 2022, Wang et al., 2022b). Moreover, it has been shown that high expression levels of ferroptosis-driving genes, such as *ACSL4*, do not necessarily dictate ferroptosis sensitivity as other components of the pathway contribute to the overall susceptibility of cells to ferroptosis (Konstorum et al., 2020). Furthermore, MM is a highly heterogenous disease with an array of different genetic subtypes that affect how the disease develops and progresses in patients, and how the disease responds to therapy. Understanding the various cellular components that contribute to ferroptosis in MM is vital for future translational research aimed at developing ferroptosis-inducing therapeutic regimens to be used in the clinic.

To determine the mechanisms that render MM cells sensitive to ferroptosis, in this thesis we aimed to investigate key genes, proteins and lipids involved in ferroptosis in these cells. In Chapter 5, we found that a range of ferroptosis-related genes are differentially expressed between ferroptosis-sensitive OPM2 and resistant KMS-11 MM cells. In particular, KMS-11 cells appeared to have a higher expression of genes that are involved in ferroptosis suppression whereas OPM2 cells had comparatively higher levels of genes involved in driving ferroptosis. The key proteins that we have identified throughout this thesis to be differentially expressed depending on MM ferroptosis sensitivity, and the proposed way in which they relate to ferroptosis are displayed in Figure 7-1.

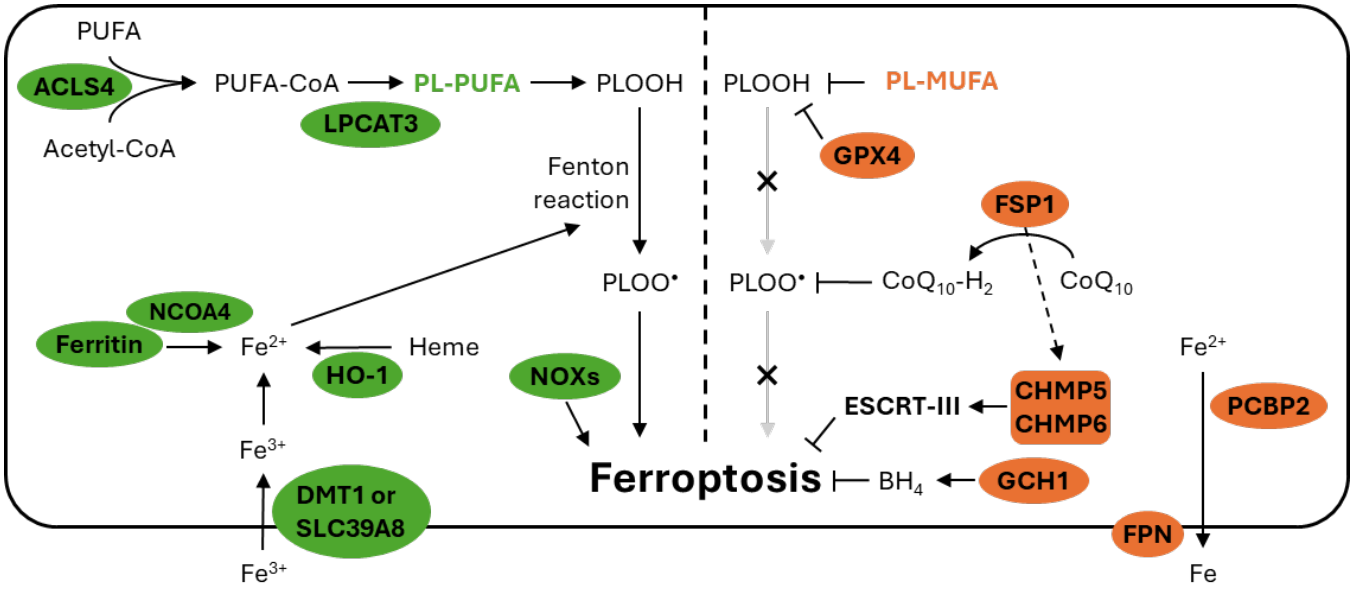

Figure 7-1: Key proteins involved in MM cell sensitivity to ferroptosis

Proteins in green were shown to be more highly expressed in ferroptosis-sensitive OPM2 MM cells compared to ferroptosis-resistant KMS-11 MM cells and are known drivers of ferroptosis. Proteins in orange were shown to be more highly expressed in KMS-11 cells and are involved in preventing ferroptosis. ACSL4, acyl-CoA synthetase long chain family member 4; BH4, tetrahydrobiopterin; CHMP5/6, charged multivesicular body protein 5/6; CoA, coenzyme A; CoQ_{10}, coenzyme Q_{10}, ubiquinone; $CoQ_{10}H_2$, ubiquinol; DMT1, divalent metal transporter 1; ESCRT-III, endosomal sorting complexes required for transport III; Fe^{2+}, ferrous iron; Fe^{3+}, ferric iron; FPN, ferroportin; FSP1, ferroptosis suppressor protein 1; GCH1, guanosine-5'-triphosphatecyclohydrolase-1; GPX4, glutathione peroxidase 4; HO-1, heme oxygenase; LPCAT3, lysophosphatidylcholine acyltransferase 3; MUFA, monounsaturated fatty acid; NCOA4, nuclear receptor coactivator 4; NOX, NADPH oxidase; PCBP2, poly(RC) binding protein 2; PL, phospholipid; PLOO, phospholipid hydrogen peroxide radical; PLOOH, phospholipid hydroperoxides; PUFA, polyunsaturated fatty acid; SLC39A8, solute carrier family 39 member 8. Dotted arrows represent multiple steps within a pathway.

7.2.1 Ferroptosis suppressor protein 1

For the first time, we identified FSP1 as an important mediator of ferroptosis resistance in MM. In Chapter 5, we found that KMS-11 MM cells were reliant on FSP1 for ferroptosis resistance given that knockout or pharmacological inhibition rendered them sensitive to RSL3. However, in Chapter 6 we found that, despite having a similar response to RSL3 as KMS-11 cells, patient-derived MM cells had a relatively lower expression of the *FSP1* gene. Whether the level of expression in these patient-derived cells is sufficient to contribute to resistance could be confirmed by using FSP1 inhibitors in the co-culture system, alongside RSL3. Given the relevance of FSP1 in KMS-11 MM cell resistance to ferroptosis, this gene initially appeared to hold potential as a marker of resistance in patient-derived MM cells. However, though not statistically significant ($p = 0.3240$), *FSP1* expression had a moderate, negative correlation with the number of viable MM cells remaining after treatment with 5 µM RSL3. This means that the patient-derived MM cells that were most sensitive to RSL3 had a higher expression of *FSP1*, suggesting it may not be useful as a marker of ferroptosis resistance in these cells. Even in the MM cell lines, expression of the FSP1 protein did not correlate with the IC_{50} of RSL3,

and in particular, even ferroptosis-resistant LP-1 MM cells did not express FSP1. The role of FSP1 in ferroptosis resistance, however, is tightly linked to the levels of coenzyme Q_{10} (CoQ_{10}, ubiquinone); in cells that do not express COQ2, the first rate-limiting enzyme in ubiquinone production, FSP1 overexpression does not contribute to ferroptosis resistance (Doll et al., 2019). Therefore, the expression of FSP1 alone may not be a good indicator of ferroptosis sensitivity in MM, but its inhibition is still a useful tool to overcome resistance in some contexts as we have shown in KMS-11 cells. In MM cell lines, Li *et al.* demonstrated COQ2 knockout caused a reduction in viability through activation of the mitogen-activated protein kinase kinase/extracellular-signal-regulated kinase (MEK/ERK) signalling pathway and this knockout enhanced RSL3-induced lipid oxidation, whereas overexpression reduced lipid oxidation (Li et al., 2024a). Combining RSL3 with the COQ2 inhibitor, 4-chlorobenzoic acid (4-CBA) was more effective at killing MM cell lines than either drug alone, and $CD138^+$ cells derived from MM patients were more sensitive to the combination of RSL3, bortezomib and 4-CBA compared to patient-matched $CD138^-$ cells (Li et al., 2024a). Furthermore, the authors showed that in a xenograft model of MM, mice treated with these three drugs had smaller tumour sizes compared to other treatment groups (control, bortezomib only and bortezomib+RSL3). Whilst this study did not comment on the expression or activity of FSP1, it suggests that reducing the levels of ubiquinone through inhibition of COQ2 might be a useful, indirect way to prevent or overcome ferroptosis resistance in MM that is mediated by FSP1.

Unlike GPX4 knockout, which is embryonic lethal, FSP1 knockout does not affect embryonic development and has no apparent phenotypic effects on mice and may therefore represent a more suitable target for ferroptosis-inducing therapies *in vivo* (Nakamura et al., 2023). Whilst the FSP1 inhibitor, iFSP1, is specific to human FSP1, it is suitable for use in mice xenografts and has been demonstrated to have anti-tumour effects as a single agent and also acts in synergy with other anti-cancer therapies in mice models of hepatocellular carcinoma, ovarian cancer and head and neck cancer (Cheu et al., 2023, Miao et al., 2024, Wu et al., 2024). In these studies, iFSP1 did not have adverse effects on mouse body weight nor did it cause significant changes in various organs.

7.2.2 Peroxiredoxin-6

The peroxiredoxin (PRDX) family of non-selenium containing peroxidases consists of PRDX1-5 which use thioredoxin, and PRDX6 which uses GSH, as cofactors for their oxidoreductase activity (Lu et al., 2019, Ito et al., 2024). Recently, PRDX6 knockout in ferroptosis-sensitive HT-1080 cells was shown to cause a reduction in the expression of selenoproteins including GPX4 at the protein, but not genetic level (Ito et al., 2024). These PRDX6-deficient cells were more sensitive to a variety of ferroptosis-inducing agents, so it is unsurprising that in Chapter 6 we found that resistance to RSL3 was strongly correlated with increased

expression of *PRDX6* in our patient-derived MM cells. Ito *et al.* also found that knockout of PRDX6 in a lung cancer xenograft mouse model resulted in a greater reduction in tumour size when combined with imidazole ketone erastin (IKE), compared to controls (Ito et al., 2024). It is important to note that whilst its knockout sensitised cells to ferroptosis, unlike overexpression of FSP1 or GTP cyclohydrolase 1 (GCH1), overexpression of PRDX6 did not protect against ferroptosis induced by deletion of GPX4 (Ito et al., 2024). Furthermore, in our MM cell lines, *PRDX6* was more highly expressed in ferroptosis-sensitive OPM2 cells compared to resistant KMS-11 cells, but assessing the expression levels in a wider range of cell lines with varying ferroptosis sensitivity may provide further insight. Since we found that *PRDX6* was more highly expressed in patient-derived MM cells that are less sensitive to RSL3, further studies investigating PRDX6 inhibition could determine whether this protein plays a role in ferroptosis resistance in MM cells, particularly given the growing evidence in the literature supporting this hypothesis.

7.2.3 Phospholipid composition

It is well known that polyunsaturated fatty acids (PUFAs) drive ferroptosis whereas monounsaturated fatty acids (MUFAs) prevent ferroptosis. In Chapter 3 we showed that while both PUFA-containing, and more specifically AA-containing phospholipids, are elevated in ferroptosis-sensitive DLBCL and OPM2 MM cells, the proportion of these phospholipids did not directly correlate with RSL3 sensitivity. The same was true of the proportion of MUFA-containing phospholipids, which were elevated in resistant MM cells. In patient-derived MM cells, however, differences in the phospholipidomic composition only became apparent when samples were stratified based on sensitivity to the combination of RSL3 and AA. These findings suggest that the phospholipidomic profile of MM cells might be a better predictor of susceptibility to ferroptosis-inducing regimens that aim to increase the levels of PUFAs, including AA, rather than agents that target GPX4 only.

Whilst phospholipids, in particular PUFA-containing phosphatidylethanolamine, have been the focus of much of the work on ferroptosis, studies have begun to associate other lipids with this form of cell death. For example, high cholesterol levels have been linked to ferroptosis resistance in breast cancer, squalene can protect against oxidative damage, and lipid droplet-lowering statins can induce ferroptosis in drug-resistant colorectal cancer cell lines (Lee and Roh, 2024, Sun et al., 2023, Jog et al., 2025). In MM, it has been shown that low-density lipoprotein, cholesterol and squalene all play a role in promoting ferroptosis resistance (Xian et al., 2024). Since cholesterol-lowering statins have been shown to reduce the risk of MM and improve survival in patients with MM (Epstein et al., 2017, Brånvall et al., 2020), investigating the levels of these lipids and how they affect ferroptosis sensitivity in MM may be a useful next step.

7.3 Aim 3: Validate the sensitivity of primary patient myeloma cells to ferroptosis

The t(4;14) status of all the patient samples used in this study was not available before the finalisation of this thesis. However, this chromosomal aberration has been shown to play a role in dictating ferroptosis sensitivity of MM cells. The t(4;14) chromosomal translocation is present in up to 15% of newly diagnosed MM and is an indicator of poor prognosis (Zhang et al., 2024a). Zhang *et al*. showed that upregulation of the oncogene MMSET, which occurs in t(4;14)(p16;q32) MM cells, is associated with sensitivity to class 2 ferroptosis inducers. They found that in patient-derived $CD138^+$ cells treated with 500 nM RSL3, t(4;14)-positive samples had an average of 30% viable cells remaining, compared to viability ranging from 60 to 90% in non-t(4;14) MM cells (Zhang et al., 2024a). However, in our study, both of the patient samples where the t(4;14) status was known (MM138 and MM140) were sensitive to RSL3, despite the fact that only patient MM138 harboured the t(4;14) lesion. Zhang *et al.* showed that because MMSET mediates ferroptosis sensitivity by upregulating ACSL4, which increases PUFA levels, PUFA supplementation can also sensitise non-t(4;14) MM cells to ferroptosis (Zhang et al., 2024a). This could explain why we observed a better response to RSL3 in patient-derived MM cells when AA was added, and suggests that PUFA supplementation may represent a means of inducing ferroptosis in MM cells regardless of their t(4;14) status.

It is important to note that Zhang *et al.* used a much lower concentration of RSL3; whilst they saw a good response in t(4;14)-positive samples with only 500 nM RSL3, none of our 10 samples responded to 1 µM RSL3. This difference may be due to normal heterogeneity in patient samples contributing to differences in drug sensitivity but might also highlight that $CD138^+$ MM cells may be more vulnerable to ferroptosis in a monoculture (the conditions in Zhang et al., 2024a), compared to our protocol which included co-culturing the cells with autologous bone marrow stromal cells (BMSCs) and other $CD138^-$ mononuclear cells (MNCs). This hypothesis was recently investigated, and it was found that BMSCs do in fact protect MM cells from ferroptosis through a signalling pathway that results in stabilisation of GPX4 (Jiang et al., 2024a). Specifically, expression of small ubiquitin-like modifier (SUMO)-specific protease 3 (SENP3) is upregulated when MM cells are co-cultured with BMCSs, and this protein removes SUMO2 from GPX4 which stabilises its expression. In two mouse models of MM, RSL3 was ineffective at reducing tumour growth. However, knock down of SENP3 combined with RSL3 was effective at decreasing tumour volume (Jiang et al., 2024a). It is interesting to note that no excess toxicity or mortality was observed in the mice after administration of RSL3 despite the general consensus that the drug is not suitable for *in vivo* use. This may be due to the drug having been delivered via an intra-tumour or intra-bone route which may overcome the poor pharmacological properties of RSL3.

Not only did we show that patient-derived MM cells can be sensitised to RSL3 through supplementation with AA, but we also discovered key intracellular components that are linked to ferroptosis sensitivity. Notably, a

higher proportion of MUFA-containing phospholipids, as well as expression of the ferroptosis suppressor gene *PRDX6* were found to correlate with ferroptosis sensitivity in patient-derived MM cells. Assessing the genetic and phospholipidomic profile of a larger cohort of patient-derived MM cells might be useful to develop predictive models of ferroptosis sensitivity. To this end, Hu *et al.* recently developed a predictive score termed "FERscore", consisting of 55 ferroptosis-related genes, that could predict sensitivity to class 2 ferroptosis-inducing agents in breast cancer (Hu et al., 2024). Furthermore, in high-grade serous ovarian cancer, a predictive model that considered expression levels of p53, transferrin receptor (TFRC), ferroportin (FPN), ACSL4 and stearoyl-CoA desaturase-1 (SCD1) was found to accurately predict whether cells would respond to RSL3 (Konstorum et al., 2020).

Personalised medicine is quickly becoming a focus in cancer therapeutics to improve clinical outcomes and avoid unnecessary adverse events. Furthermore, the development of accurate *ex vivo* systems are becoming widely recognised as a rapid means of testing a range of anti-tumour agents; Silva *et al.* developed a mathematical model that uses data from an *ex vivo* drug sensitivity assay for a range of drugs used to treat MM to predict therapeutic responses (Silva et al., 2017). Combining an *ex vivo* approach like this with predictive models described above could be a means of predicting which MM patients will respond to ferroptosis-inducing drugs based on gene expression and phospholipidomic data. Simultaneously, an array of treatment regimens could be tested in patient-derived MM cells to determine the effect on the cancer and non-malignant cells, including combining ferroptosis-inducing compounds with drugs already used in the clinic where synergy is suspected or has already been demonstrated, such as bortezomib.

7.4 The current landscape of ferroptosis-based clinical studies

Despite the exponential increase in ferroptosis research since the term was first coined in 2012, it is still a relatively new area of research and translational studies are in their infancy. To date, there are no human clinical trials focused on investigating ferroptosis as an approach to treating cancer. Several biotechnology companies are currently in the drug-discovery phase for agents that induce ferroptosis in cancer, as well as agents that prevent ferroptotic damage in neurodevelopmental disorders, macular degeneration and cardiovascular, hepatic and neurodegenerative diseases. It is therefore expected that the translational research field of ferroptosis will take off in the coming years.

A phase I clinical trial (NCT03772925) investigated the combination of the histone deacetylase (HDAC) inhibitor, belinostat, and the NEDD8 inhibitor, pevonedistat, in relapsed/refractory acute myeloid leukemia (AML) and myelodysplastic syndrome (Maher et al., 2025). Though there are limited studies drawing a link between HDAC inhibitors and ferroptosis, in some pre-clinical contexts, this class of drugs have been shown

to induce ferroptosis or enhance the efficacy of other ferroptosis-inducing agents (Jenke et al., 2024, Miyamoto et al., 2020, Zhang et al., 2021b). In the phase I trial, it was found that following treatment with belinostat and pevonedistat, the ferroptosis suppressors *SLC7A11* and *TXNRD1* were significantly increased in 5 out of 6 samples of patient-derived peripheral blood mononuclear cells (Maher et al., 2025).

Additionally, studies in AML have shown that C6-ceramide nanoliposomes enhance iron-dependent cell death induced by LCL-805, an acid ceramidase inhibitor, and enhance the efficacy of venetoclax and cytarabine in a manner independent of apoptosis and autophagy (Ung et al., 2023, Khokhlatchev et al., 2022). These studies suggest that the mechanism of action of C6-ceramide nanoliposomes might involve ferroptosis, which is particularly relevant given that ceramide accumulates during ferroptosis and can contribute to ROS production (Thayyullathil et al., 2021). A phase I trial (NCT02834611) showed that C6-ceramide nanoliposomes were well tolerated in patients with advanced/refractory solid tumours (Ciner et al., 2024). A subsequent phase I trial is planned to investigate the combination of these liposomes with other chemotherapeutic agents in AML (NCT04716452).

Additionally, carbon nanoparticles-Fe(II) complex (CNSI-Fe) has been shown to induce cell death in colon cancer cells and have anti-tumour effects in a xenograft mouse model. Accumulation of malondialdehyde (MDA) was observed both *in vitro* and *in vivo* following treatment with CNSI-Fe, suggesting ferroptosis was involved, although increased levels of caspase-3 were also observed following treatment (Gou et al., 2024, Xie et al., 2023). A phase I trial that is currently recruiting patients is being conducted to investigate the safety and efficacy of injection of CNSI-Fe in patients with advanced solid tumours (NCT06048367). Though preliminary, these studies show that the potential importance of ferroptosis in the efficacy of novel agents and drug combinations is becoming recognised and investigated in clinical trials.

7.5 Final conclusions

In this thesis we have found that MM cells, though more resistant to RSL3-induced ferroptosis, can be made more sensitive to this unique form of cell death. These results are promising, and even more so given that patient-derived MM cells were found to be sensitive to the combination of RSL3 and AA in a co-culture system. However, whilst lymphocytes were less sensitive to this drug combination, some toxicity towards this healthy population of cells was observed. Furthermore, RSL3 is widely considered unsuitable for use in clinical settings due to the likelihood of adverse effects on healthy tissues and its poor pharmacokinetics. Developing GPX4 inhibitors with better pharmacokinetic properties is one avenue to explore, however, this approach may also have issues with toxicity towards healthy tissue. As introduced in Chapter 1, another possibility is the use of nanotherapeutic delivery systems to enable targeted delivery of ferroptosis-inducing

agents to malignant cells. Specifically, liposomes are particularly promising given that we have shown a correlation between the lipidomic profile of MM and DLBCL cells and ferroptosis sensitivity, and that modulating the fatty acid content through supplementation with AA enhances the ferroptosis sensitivity of MM cells. This means that liposomes could be developed that not only encapsulate RSL3 to improve its delivery to MM cells *in vivo*, but also deliver the PUFA-containing phospholipid substrates for ferroptosis.

Whilst RSL3, which was used throughout the studies presented in this thesis, is not currently suitable for use in patients, our findings provide a strong rationale for further investigation of ferroptosis-inducing agents as potential treatments for MM. We hope that the findings of this research will provide further insight into the mechanisms of ferroptosis in MM and we are in the process of finalising manuscripts of our results for publication. Finally, the findings have already formed the basis for another project aimed at developing targeted ferroptosis-inducing liposomes for the treatment of MM.

REFERENCES

Abdi, J., Garssen, J., Faber, J. & Redegeld, F. A. 2014. Omega-3 fatty acids, EPA and DHA induce apoptosis and enhance drug sensitivity in multiple myeloma cells but not in normal peripheral mononuclear cells. *The Journal of Nutritional Biochemistry,* 25**,** 1254-1262. doi: 10.1016/j.jnutbio.2014.06.013.

Adedoyin, O., Boddu, R., Traylor, A., Lever, J. M., Bolisetty, S., George, J. F., et al. 2018. Heme oxygenase-1 mitigates ferroptosis in renal proximal tubule cells. *Am J Physiol Renal Physiol,* 314**,** F702-f714. doi: 10.1152/ajprenal.00044.2017.

Adham, A. N., Abdelfatah, S., Naqishbandi, A. M., Mahmoud, N. & Efferth, T. 2021a. Cytotoxicity of apigenin toward multiple myeloma cell lines and suppression of iNOS and COX-2 expression in STAT1-transfected HEK293 cells. *Phytomedicine,* 80**,** 153371. doi: 10.1016/j.phymed.2020.153371.

Adham, A. N., Naqishbandi, A. M. & Efferth, T. 2021b. Cytotoxicity and apoptosis induction by Fumaria officinalis extracts in leukemia and multiple myeloma cell lines. *Journal of Ethnopharmacology,* 266**,** 113458. doi: 10.1016/j.jep.2020.113458.

Akara-Amornthum, P., Lomphithak, T., Choksi, S., Tohtong, R. & Jitkaew, S. 2020. Key necroptotic proteins are required for Smac mimetic-mediated sensitization of cholangiocarcinoma cells to TNF-α and chemotherapeutic gemcitabine-induced necroptosis. *PLoS One,* 15**,** e0227454. doi: 10.1371/journal.pone.0227454.

Akiyama, H., Zhao, R., Rahhal, A., Nishida, Y., Ayoub, E., Ostermann, L. B., et al. 2021. Therapeutic Targeting of Ferroptosis Pathway in Combination with Mitochondrial Oxidative Stress Induction in Acute Myeloid Leukemia. *Blood,* 138**,** 1162-1162. doi: 10.1182/blood-2021-148248.

Alaoui-Jamali, M. A., Bismar, T. A., Gupta, A., Szarek, W. A., Su, J., Song, W., et al. 2009. A Novel Experimental Heme Oxygenase-1–Targeted Therapy for Hormone-Refractory Prostate Cancer. *Cancer Research,* 69**,** 8017. doi: 10.1158/0008-5472.CAN-09-0419.

Ali, M. & Mocarski, E. S. 2018. Proteasome inhibition blocks necroptosis by attenuating death complex aggregation. *Cell Death & Disease,* 9**,** 346. doi: 10.1038/s41419-018-0371-x.

Alim, I., Caulfield, J. T., Chen, Y., Swarup, V., Geschwind, D. H., Ivanova, E., et al. 2019. Selenium Drives a Transcriptional Adaptive Program to Block Ferroptosis and Treat Stroke. *Cell,* 177**,** 1262-1279.e25. doi: 10.1016/j.cell.2019.03.032.

Alkhateeb, A. A. & Connor, J. R. 2013. The significance of ferritin in cancer: Anti-oxidation, inflammation and tumorigenesis. *Biochimica et Biophysica Acta (BBA) - Reviews on Cancer,* 1836**,** 245-254. doi: 10.1016/j.bbcan.2013.07.002.

Arkan, C. & Akcora-Yildiz, D. 2025. FDA-approved disulfiram induces ferroptosis via alteration of redox balance and lipid peroxidation and overcomes carfilzomib resistance in multiple myeloma. *Leukemia & Lymphoma,* 66**,** 250-261. doi: 10.1080/10428194.2024.2422843.

Asperti, M., Cantamessa, L., Gryzik, M., Bugatti, M., Codenotti, S., Denardo, A., et al. 2023. The modulation of iron metabolism affects the Rhabdomyosarcoma tumor growth in vitro and in vivo. *Clinical and Experimental Medicine,* 23**,** 2487-2502. doi: 10.1007/s10238-023-01012-5.

Australian Institute of Health and Welfare. 2024. *Cancer data in Australia* [Online]. Canberra: AIHW. Available: https://www.aihw.gov.au/reports/cancer/cancer-data-in-australia/contents/summary [Accessed 5 December 2024].

Ayala, A., Munoz, M. F. & Arguelles, S. 2014. Lipid peroxidation: production, metabolism, and signaling mechanisms of malondialdehyde and 4-hydroxy-2-nonenal. *Oxid Med Cell Longev,* 2014**,** 360438. doi: 10.1155/2014/360438.

Barenholz, Y. 2012. Doxil(R)--the first FDA-approved nano-drug: lessons learned. *J Control Release,* 160**,** 117-34. doi: 10.1016/j.jconrel.2012.03.020.

Barrera, L. N., Rushworth, S. A., Bowles, K. M. & Macewan, D. J. 2012. Bortezomib induces heme oxygenase-1 expression in multiple myeloma. *Cell Cycle,* 11**,** 2248-52. doi: 10.4161/cc.20343.

Battaglia, A. M., Chirillo, R., Aversa, I., Sacco, A., Costanzo, F. & Biamonte, F. 2020. Ferroptosis and Cancer: Mitochondria Meet the "Iron Maiden" Cell Death. *Cells,* 9**,** 1505. doi: 10.3390/cells9061505.

Beatty, A., Singh, T., Tyurina, Y. Y., Tyurin, V. A., Samovich, S., Nicolas, E., et al. 2021. Ferroptotic cell death triggered by conjugated linolenic acids is mediated by ACSL1. *Nat Commun,* 12**,** 2244. doi: 10.1038/s41467-021-22471-y.

Beckmann, K., Kearney, B. A., Yeung, D., Hiwase, D., Li, M. & Roder, D. M. 2022. Changes in five-year survival for people with acute leukaemia in South Australia, 1980-2016. *Med J Aust,* 216**,** 296-302. doi: 10.5694/mja2.51423.

Berndt, C., Alborzinia, H., Amen, V. S., Ayton, S., Barayeu, U., Bartelt, A., et al. 2024. Ferroptosis in health and disease. *Redox Biology,* 75**,** 103211. doi: 10.1016/j.redox.2024.103211.

Bersuker, K., Hendricks, J. M., Li, Z., Magtanong, L., Ford, B., Tang, P. H., et al. 2019. The CoQ oxidoreductase FSP1 acts parallel to GPX4 to inhibit ferroptosis. *Nature,* 575**,** 688-692. doi: 10.1038/s41586-019-1705-2.

Birsen, R., Larrue, C., Decroocq, J., Johnson, N., Guiraud, N., Gotanegre, M., et al. 2021. APR-246 induces early cell death by ferroptosis in acute myeloid leukemia. *Haematologica,* 107**,** 403-416. doi: 10.3324/haematol.2020.259531.

Borchert, A., Wang, C. C., Ufer, C., Schiebel, H., Savaskan, N. E. & Kuhn, H. 2006. The Role of Phospholipid Hydroperoxide Glutathione Peroxidase Isoforms in Murine Embryogenesis*. *Journal of Biological Chemistry,* 281**,** 19655-19664. doi: 10.1074/jbc.M601195200.

Bordini, J., Lenzi, C., Toscani, L., Ranghetti, P., Perotta, E., Scarfò, L., et al. 2022. High dose iron impairs malignant B-cell viability in chronic lymphocytic leukemia. *HemaSphere,* 6**,** 496-497. doi: 10.1097/01.HS9.0000845276.56142.3b.

Bordini, J., Morisi, F., Cerruti, F., Cascio, P., Camaschella, C., Ghia, P., et al. 2020. Iron Causes Lipid Oxidation and Inhibits Proteasome Function in Multiple Myeloma Cells: A Proof of Concept for Novel Combination Therapies. *Cancers,* 12**,** 970. doi: 10.3390/cancers12040970.

Braham, M. V., Deshantri, A. K., Minnema, M. C., Öner, F. C., Schiffelers, R. M., Fens, M. H., et al. 2018. Liposomal drug delivery in an in vitro 3D bone marrow model for multiple myeloma. *Int J Nanomedicine,* 13**,** 8105-8118. doi: 10.2147/ijn.S184262.

Brånvall, E., Ekberg, S., Eloranta, S., Wästerlid, T., Birmann, B. M. & Smedby, K. E. 2020. Statin use is associated with improved survival in multiple myeloma: A Swedish population-based study of 4315 patients. *American Journal of Hematology,* 95**,** 652-661. doi: 10.1002/ajh.25778.

Caillot, M., Dakik, H., Mazurier, F. & Sola, B. 2021. Targeting Reactive Oxygen Species Metabolism to Induce Myeloma Cell Death. *Cancers (Basel),* 13. doi: 10.3390/cancers13102411.

Caillot, M., Zylbersztejn, F., Maitre, E., Bourgeais, J., Hérault, O. & Sola, B. 2020. ROS Overproduction Sensitises Myeloma Cells to Bortezomib-Induced Apoptosis and Alleviates Tumour Microenvironment-Mediated Cell Resistance. *Cells,* 9**,** 2357.

Cao, J. Y. & Dixon, S. J. 2016. Mechanisms of ferroptosis. *Cell Mol Life Sci,* 73**,** 2195-209. doi: 10.1007/s00018-016-2194-1.

Cao, K., Du, Y., Bao, X., Han, M., Su, R., Pang, J., et al. 2022. Glutathione-Bioimprinted Nanoparticles Targeting of N6-methyladenosine FTO Demethylase as a Strategy against Leukemic Stem Cells. *Small,* 18**,** e2106558. doi: 10.1002/smll.202106558.

Catanzaro, E., Turrini, E., Kerre, T., Sioen, S., Baeyens, A., Guerrini, A., et al. 2022. Perillaldehyde is a new ferroptosis inducer with a relevant clinical potential for acute myeloid leukemia therapy. *Biomedicine & Pharmacotherapy,* 154**,** 113662. doi: 10.1016/j.biopha.2022.113662.

Chang, L. C., Chiang, S. K., Chen, S. E., Yu, Y. L., Chou, R. H. & Chang, W. C. 2018. Heme oxygenase-1 mediates BAY 11-7085 induced ferroptosis. *Cancer Lett,* 416**,** 124-137. doi: 10.1016/j.canlet.2017.12.025.

Cheff, D. M., Huang, C., Scholzen, K. C., Gencheva, R., Ronzetti, M. H., Cheng, Q., et al. 2023. The ferroptosis inducing compounds RSL3 and ML162 are not direct inhibitors of GPX4 but of TXNRD1. *Redox Biology,* 62**,** 102703. doi: 10.1016/j.redox.2023.102703.

Chen, J., Zaal, E. A., Berkers, C. R., Ruijtenbeek, R., Garssen, J. & Redegeld, F. A. 2021a. Omega-3 Fatty Acids DHA and EPA Reduce Bortezomib Resistance in Multiple Myeloma Cells by Promoting Glutathione Degradation. *Cells,* 10**,** 2287.

Chen, X., Hu, S., Han, Y., Cai, Y., Lu, T., Hu, X., et al. 2023. Ferroptosis-related STEAP3 acts as predictor and regulator in diffuse large B cell lymphoma through immune infiltration. *Clin Exp Med*. doi: 10.1007/s10238-023-00996-4.

Chen, X., Tsvetkov, A. S., Shen, H.-M., Isidoro, C., Ktistakis, N. T., Linkermann, A., et al. 2024a. International consensus guidelines for the definition, detection, and interpretation of autophagy-dependent ferroptosis. *Autophagy,* 20**,** 1213-1246. doi: 10.1080/15548627.2024.2319901.

Chen, X., Xu, S., Zhao, C. & Liu, B. 2019. Role of TLR4/NADPH oxidase 4 pathway in promoting cell death through autophagy and ferroptosis during heart failure. *Biochem Biophys Res Commun,* 516**,** 37-43. doi: 10.1016/j.bbrc.2019.06.015.

Chen, X., Yu, C., Kang, R. & Tang, D. 2020. Iron Metabolism in Ferroptosis. *Frontiers in Cell and Developmental Biology,* 8. doi: 10.3389/fcell.2020.590226.

Chen, Y., Wang, F., Wu, P., Gong, S., Gao, J., Tao, H., et al. 2021b. Artesunate induces apoptosis, autophagy and ferroptosis in diffuse large B cell lymphoma cells by impairing STAT3 signaling. *Cellular Signalling,* 88**,** 110167. doi: 10.1016/j.cellsig.2021.110167.

Chen, Z., Inague, A., Kaushal, K., Fazeli, G., Schilling, D., Xavier Da Silva, T. N., et al. 2024b. PRDX6 contributes to selenocysteine metabolism and ferroptosis resistance. *Mol Cell,* 84**,** 4645-4659.e9. doi: 10.1016/j.molcel.2024.10.027.

Cheng, J., Zhu, Y., Xing, X., Xiao, J., Chen, H., Zhang, H., et al. 2021. Manganese-deposited iron oxide promotes tumor-responsive ferroptosis that synergizes the apoptosis of cisplatin. *Theranostics,* 11**,** 5418-5429. doi: 10.7150/thno.53346.

Chennamadhavuni, A., Lyengar, V. & Shimanovsky, A. 2022. Leukemia. *StatPearls.* Treasure Island (FL).

Cheu, J. W.-S., Lee, D., Li, Q., Goh, C. C., Bao, M. H.-R., Yuen, V. W.-H., et al. 2023. Ferroptosis Suppressor Protein 1 Inhibition Promotes Tumor Ferroptosis and Anti-tumor Immune Responses in Liver Cancer. *Cellular and Molecular Gastroenterology and Hepatology,* 16**,** 133-159. doi: 10.1016/j.jcmgh.2023.03.001.

Chiang, S.-K., Chen, S.-E. & Chang, L.-C. 2018. A Dual Role of Heme Oxygenase-1 in Cancer Cells. *International journal of molecular sciences,* 20**,** 39. doi: 10.3390/ijms20010039.

Choi, J. A., Lee, E. H., Cho, H. & Kim, J. H. 2023. High-Dose Selenium Induces Ferroptotic Cell Death in Ovarian Cancer. *Int J Mol Sci,* 24. doi: 10.3390/ijms24031918.

Chu, B., Kon, N., Chen, D., Li, T., Liu, T., Jiang, L., et al. 2019. ALOX12 is required for p53-mediated tumour suppression through a distinct ferroptosis pathway. *Nature Cell Biology,* 21**,** 579-591. doi: 10.1038/s41556-019-0305-6.

Ciner, A., Gourdin, T., Davidson, J., Parette, M., Walker, S. J., Fox, T. E., et al. 2024. A phase I study of the ceramide nanoliposome in patients with advanced solid tumors. *Cancer Chemother Pharmacol,* 93**,** 23-29. doi: 10.1007/s00280-023-04588-7.

Cluzeau, T., Sebert, M., Rahmé, R., Cuzzubbo, S., Lehmann-Che, J., Madelaine, I., et al. 2021. Eprenetapopt Plus Azacitidine in TP53-Mutated Myelodysplastic Syndromes and Acute Myeloid Leukemia: A Phase II Study by the Groupe Francophone des Myélodysplasies (GFM). *J Clin Oncol,* 39**,** 1575-1583. doi: 10.1200/jco.20.02342.

Conrad, M., Kagan, V. E., Bayir, H., Pagnussat, G. C., Head, B., Traber, M. G., et al. 2018. Regulation of lipid peroxidation and ferroptosis in diverse species. *Genes Dev,* 32**,** 602-619. doi: 10.1101/gad.314674.118.

Dächert, J., Schoeneberger, H., Rohde, K. & Fulda, S. 2016. RSL3 and Erastin differentially regulate redox signaling to promote Smac mimetic-induced cell death. *Oncotarget,* 7.

Dai, E., Chen, X., Linkermann, A., Jiang, X., Kang, R., Kagan, V. E., et al. 2024. A guideline on the molecular ecosystem regulating ferroptosis. *Nature Cell Biology,* 26**,** 1447-1457. doi: 10.1038/s41556-024-01360-8.

Dai, E., Meng, L., Kang, R., Wang, X. & Tang, D. 2020. ESCRT-III–dependent membrane repair blocks ferroptosis. *Biochemical and Biophysical Research Communications,* 522**,** 415-421. doi: 10.1016/j.bbrc.2019.11.110.

Deangelo, S. L., Dziechciarz, S., Solanki, S., Shin, M., Zhao, L., Balia, A., et al. 2024. Recharacterization of RSL3 reveals that the selenoproteome is a druggable target in colorectal cancer. *bioRxiv*. doi: 10.1101/2024.03.29.587381.

Depmap, B. 2022. DepMap 22Q4 Public. figshare.

Deshantri, A. K., Fens, M. H. a. M., Ruiter, R. W. J., Metselaar, J. M., Storm, G., Mandhane, S. N., et al. 2020. Complete Tumor Regression by Liposomal Bortezomib in a Humanized Mouse Model of Multiple Myeloma. *HemaSphere,* 4.

Desplat, V., Dulery, C., Praloran, V. & Denizot, Y. 1999. Incorporation and Effect of Arachidonic Acid on the Growth of Human Myeloma Cell Lines. *Mediators of Inflammation,* 8**,** 968415. doi: 10.1080/09629359990612.

Dev, S. & Babitt, J. L. 2017. Overview of iron metabolism in health and disease. *Hemodial Int,* 21 Suppl 1**,** S6-S20. doi: 10.1111/hdi.12542.

Devin, J., Caneque, T., Lin, Y. L., Mondoulet, L., Veyrune, J. L., Abouladze, M., et al. 2022. Targeting Cellular Iron Homeostasis with Ironomycin in Diffuse Large B-cell Lymphoma. *Cancer Res,* 82**,** 998-1012. doi: 10.1158/0008-5472.CAN-21-0218.

Diao, J., Jia, Y., Dai, E., Liu, J., Kang, R., Tang, D., et al. 2024. Ferroptotic therapy in cancer: benefits, side effects, and risks. *Molecular Cancer,* 23**,** 89. doi: 10.1186/s12943-024-01999-9.

Dixon, S. J., Lemberg, K. M., Lamprecht, M. R., Skouta, R., Zaitsev, E. M., Gleason, C. E., et al. 2012. Ferroptosis: an iron-dependent form of nonapoptotic cell death. *Cell,* 149**,** 1060-72. doi: 10.1016/j.cell.2012.03.042.

Dixon, S. J., Winter, G. E., Musavi, L. S., Lee, E. D., Snijder, B., Rebsamen, M., et al. 2015. Human Haploid Cell Genetics Reveals Roles for Lipid Metabolism Genes in Nonapoptotic Cell Death. *ACS chemical biology,* 10**,** 1604-1609. doi: 10.1021/acschembio.5b00245.

Dobin, A., Davis, C. A., Schlesinger, F., Drenkow, J., Zaleski, C., Jha, S., et al. 2013. STAR: ultrafast universal RNA-seq aligner. *Bioinformatics,* 29**,** 15-21. doi: 10.1093/bioinformatics/bts635.

Dodson, M., Castro-Portuguez, R. & Zhang, D. D. 2019. NRF2 plays a critical role in mitigating lipid peroxidation and ferroptosis. *Redox Biology,* 23**,** 101107. doi: 10.1016/j.redox.2019.101107.

Doll, S., Freitas, F. P., Shah, R., Aldrovandi, M., Da Silva, M. C., Ingold, I., et al. 2019. FSP1 is a glutathione-independent ferroptosis suppressor. *Nature,* 575**,** 693-698. doi: 10.1038/s41586-019-1707-0.

Doll, S., Proneth, B., Tyurina, Y. Y., Panzilius, E., Kobayashi, S., Ingold, I., et al. 2017. ACSL4 dictates ferroptosis sensitivity by shaping cellular lipid composition. *Nat Chem Biol,* 13**,** 91-98. doi: 10.1038/nchembio.2239.

Dolma, S., Lessnick, S. L., Hahn, W. C. & Stockwell, B. R. 2003. Identification of genotype-selective antitumor agents using synthetic lethal chemical screening in engineered human tumor cells. *Cancer Cell,* 3**,** 285-296. doi: 10.1016/S1535-6108(03)00050-3.

Dong, L.-H., Huang, J.-J., Zu, P., Liu, J., Gao, X., Du, J.-W., et al. 2021. CircKDM4C upregulates P53 by sponging hsa-let-7b-5p to induce ferroptosis in acute myeloid leukemia. *Environmental Toxicology,* 36**,** 1288-1302. doi: 10.1002/tox.23126.

Drummen, G. P. C., Van Liebergen, L. C. M., Op Den Kamp, J. a. F. & Post, J. A. 2002. C11-BODIPY581/591, an oxidation-sensitive fluorescent lipid peroxidation probe: (micro)spectroscopic characterization and validation of methodology. *Free Radical Biology and Medicine,* 33**,** 473-490. doi: 10.1016/S0891-5849(02)00848-1.

Du, J., Wang, T., Li, Y., Zhou, Y., Wang, X., Yu, X., et al. 2019. DHA inhibits proliferation and induces ferroptosis of leukemia cells through autophagy dependent degradation of ferritin. *Free Radic Biol Med,* 131**,** 356-369. doi: 10.1016/j.freeradbiomed.2018.12.011.

Du, Y., Bao, J., Zhang, M.-J., Li, L.-L., Xu, X.-L., Chen, H., et al. 2020. Targeting ferroptosis contributes to ATPR-induced AML differentiation via ROS-autophagy-lysosomal pathway. *Gene,* 755**,** 144889. doi: 10.1016/j.gene.2020.144889.

Eaton, J. K., Furst, L., Ruberto, R. A., Moosmayer, D., Hilpmann, A., Ryan, M. J., et al. 2020. Selective covalent targeting of GPX4 using masked nitrile-oxide electrophiles. *Nature Chemical Biology,* 16**,** 497-506. doi: 10.1038/s41589-020-0501-5.

Ebert, L. M., Vandyke, K., Johan, M. Z., Denichilo, M., Tan, L. Y., Myo Min, K. K., et al. 2022. Desmoglein-2 expression is an independent predictor of poor prognosis patients with multiple myeloma. *Molecular Oncology,* 16**,** 1221-1240. doi: 10.1002/1878-0261.13055.

Else, P. L. 2020. The highly unnatural fatty acid profile of cells in culture. *Progress in Lipid Research,* 77**,** 101017. doi: 10.1016/j.plipres.2019.101017.

Epstein, M. M., Divine, G., Chao, C. R., Wells, K. E., Feigelson, H. S., Scholes, D., et al. 2017. Statin use and risk of multiple myeloma: An analysis from the cancer research network. *Int J Cancer,* 141**,** 480-487. doi: 10.1002/ijc.30745.

Federico, C., Alhallak, K., Sun, J., Duncan, K., Azab, F., Sudlow, G. P., et al. 2020. Tumor microenvironment-targeted nanoparticles loaded with bortezomib and ROCK inhibitor improve efficacy in multiple myeloma. *Nature Communications,* 11**,** 6037. doi: 10.1038/s41467-020-19932-1.

Fellmann, C., Hoffmann, T., Sridhar, V., Hopfgartner, B., Muhar, M., Roth, M., et al. 2013. An Optimized microRNA Backbone for Effective Single-Copy RNAi. *Cell Reports,* 5**,** 1704-1713. doi: 10.1016/j.celrep.2013.11.020.

Feng, H. & Stockwell, B. R. 2018. Unsolved mysteries: How does lipid peroxidation cause ferroptosis? *PLOS Biology,* 16**,** e2006203. doi: 10.1371/journal.pbio.2006203.

Friedmann Angeli, J. P., Schneider, M., Proneth, B., Tyurina, Y. Y., Tyurin, V. A., Hammond, V. J., et al. 2014. Inactivation of the ferroptosis regulator Gpx4 triggers acute renal failure in mice. *Nature Cell Biology,* 16**,** 1180-1191. doi: 10.1038/ncb3064.

Fu, B., Shao, R., Wang, H., Chen, G., Bai, S. & Wang, H. 2022. Integrated assessment of the clinical and biological value of ferroptosis-related genes in multiple myeloma. *Cancer Cell International,* 22**,** 326. doi: 10.1186/s12935-022-02742-4.

Fujita, H., Tanaka, Y. K., Ogata, S., Suzuki, N., Kuno, S., Barayeu, U., et al. 2024. PRDX6 augments selenium utilization to limit iron toxicity and ferroptosis. *Nat Struct Mol Biol,* 31**,** 1277-1285. doi: 10.1038/s41594-024-01329-z.

Gan, B. 2021. Mitochondrial regulation of ferroptosis. *J Cell Biol,* 220. doi: 10.1083/jcb.202105043.

Gao, D., Liu, R., Lv, Y., Feng, Y., Hong, F., Xu, X., et al. 2023. A novel ferroptosis-related gene signature for predicting prognosis in multiple myeloma. *Frontiers in Oncology,* 13. doi: 10.3389/fonc.2023.999688.

Gao, D., Lv, Y., Hong, F., Wu, D., Wang, T., Gao, G., et al. 2025. Peroxiredoxin 6 maintains mitochondrial homeostasis and promotes tumor progression through ROS/JNK/p38 MAPK signaling pathway in multiple myeloma. *Sci Rep,* 15**,** 70. doi: 10.1038/s41598-024-84021-y.

Gao, M., Monian, P., Pan, Q., Zhang, W., Xiang, J. & Jiang, X. 2016. Ferroptosis is an autophagic cell death process. *Cell Research,* 26**,** 1021-1032. doi: 10.1038/cr.2016.95.

García-Sánchez, D., González-González, A., Alfonso-Fernández, A., Del Dujo-Gutiérrez, M. & Pérez-Campo, F. M. 2023. Communication between bone marrow mesenchymal stem cells and multiple myeloma cells: Impact on disease progression. *World J Stem Cells,* 15**,** 421-437. doi: 10.4252/wjsc.v15.i5.421.

Gaschler, M. M. & Stockwell, B. R. 2017. Lipid peroxidation in cell death. *Biochem Biophys Res Commun,* 482**,** 419-425. doi: 10.1016/j.bbrc.2016.10.086.

Gentile, M., Martino, M., Recchia, A. G., Vigna, E., Morabito, L. & Morabito, F. 2016. Sorafenib for the treatment of multiple myeloma. *Expert Opinion on Investigational Drugs,* 25**,** 743-749. doi: 10.1517/13543784.2016.1169272.

Ghandi, M., Huang, F. W., Jané-Valbuena, J., Kryukov, G. V., Lo, C. C., Mcdonald, E. R., et al. 2019. Next-generation characterization of the Cancer Cell Line Encyclopedia. *Nature,* 569**,** 503-508. doi: 10.1038/s41586-019-1186-3.

Golara, A., Kozłowski, M., Guzik, P., Kwiatkowski, S. & Cymbaluk-Płoska, A. 2023. The Role of Selenium and Manganese in the Formation, Diagnosis and Treatment of Cervical, Endometrial and Ovarian Cancer. *International Journal of Molecular Sciences* [Online], 24.

Gong, H., Li, H., Yang, Q., Zhang, G., Liu, H., Ma, Z., et al. 2022. A Ferroptosis Molecular Subtype-Related Signature for Predicting Prognosis and Response to Chemotherapy in Patients with Chronic Lymphocytic Leukemia. *BioMed Research International,* 2022**,** 5646275. doi: 10.1155/2022/5646275.

Gou, Z., Tang, K., Zeng, C., Yuan, H., Zhang, C., Huang, Y., et al. 2024. Photothermal therapy of xenografted tumor by carbon nanoparticles-Fe(II) complex. *Colloids and Surfaces B: Biointerfaces,* 240**,** 113968. doi: 10.1016/j.colsurfb.2024.113968.

Granatowicz, A., Piatek, C. I., Moschiano, E., El-Hemaidi, I., Armitage, J. D. & Akhtari, M. 2015. An Overview and Update of Chronic Myeloid Leukemia for Primary Care Physicians. *Korean J Fam Med,* 36**,** 197-202. doi: 10.4082/kjfm.2015.36.5.197.

Grignano, E., Cantero-Aguilar, L., Tuerdi, Z., Chabane, T., Vazquez, R., Johnson, N., et al. 2023. Dihydroartemisinin-induced ferroptosis in acute myeloid leukemia: links to iron metabolism and metallothionein. *Cell Death Discovery,* 9**,** 97. doi: 10.1038/s41420-023-01371-8.

Gryzik, M., Asperti, M., Denardo, A., Arosio, P. & Poli, M. 2021. NCOA4-mediated ferritinophagy promotes ferroptosis induced by erastin, but not by RSL3 in HeLa cells. *Biochimica et Biophysica Acta (BBA) - Molecular Cell Research,* 1868**,** 118913. doi: 10.1016/j.bbamcr.2020.118913.

Gu, Z., Wang, H., Xia, J., Yang, Y., Jin, Z., Xu, H., et al. 2015. Decreased ferroportin promotes myeloma cell growth and osteoclast differentiation. *Cancer Res,* 75**,** 2211-21. doi: 10.1158/0008-5472.Can-14-3804.

Guo, S., Zhang, D., Dong, Y., Shu, Y., Wu, X., Ni, Y., et al. 2024. Sulfiredoxin-1 accelerates erastin-induced ferroptosis in HT-22 hippocampal neurons by driving heme Oxygenase-1 activation. *Free Radic Biol Med,* 223**,** 430-442. doi: 10.1016/j.freeradbiomed.2024.08.008.

Guo, X. & Zhou, X. 2022. Risk stratification of acute myeloid leukemia: Assessment using a novel prediction model based on ferroptosis-immune related genes. *Mathematical Biosciences and Engineering,* 19**,** 11821-11839. doi: 10.3934/mbe.2022551.

Han, W., Duan, X., Ni, K., Li, Y., Chan, C. & Lin, W. 2022. Co-delivery of dihydroartemisinin and pyropheophorbide-iron elicits ferroptosis to potentiate cancer immunotherapy. *Biomaterials,* 280**,** 121315. doi: 10.1016/j.biomaterials.2021.121315.

Hangauer, M. J., Viswanathan, V. S., Ryan, M. J., Bole, D., Eaton, J. K., Matov, A., et al. 2017. Drug-tolerant persister cancer cells are vulnerable to GPX4 inhibition. *Nature,* 551**,** 247-250. doi: 10.1038/nature24297.

Hanspers, K., Willighagen, E., Slenter, D., Hu, F., Lupascu, D. & Weitz, E. 2024. *Ferroptosis (WP4313)* [Online]. Available: https://www.wikipathways.org/instance/WP4313 [Accessed November 2024].

Hassannia, B., Vandenabeele, P. & Vanden Berghe, T. 2019. Targeting Ferroptosis to Iron Out Cancer. *Cancer Cell,* 35**,** 830-849. doi: 10.1016/j.ccell.2019.04.002.

Hassannia, B., Wiernicki, B., Ingold, I., Qu, F., Van Herck, S., Tyurina, Y. Y., et al. 2018. Nano-targeted induction of dual ferroptotic mechanisms eradicates high-risk neuroblastoma. *J Clin Invest,* 128**,** 3341-3355. doi: 10.1172/jci99032.

Hayes, J. D., Dinkova-Kostova, A. T. & Tew, K. D. 2020. Oxidative Stress in Cancer. *Cancer Cell,* 38**,** 167-197. doi: 10.1016/j.ccell.2020.06.001.

He, C., Wang, C., Liu, H. & Shan, B. 2022. Kayadiol exerted anticancer effects through p53-mediated ferroptosis in NKTCL cells. *BMC Cancer,* 22**,** 724. doi: 10.1186/s12885-022-09825-5.

Ho, M., Patel, A., Hanley, C., Murphy, A., Mcsweeney, T., Zhang, L., et al. 2019. Exploiting autophagy in multiple myeloma. *Journal of Cancer Metastasis and Treatment,* 5**,** 70. doi: 10.20517/2394-4722.2019.25.

Hoang, B., Benavides, A., Shi, Y., Frost, P. & Lichtenstein, A. 2009. Effect of autophagy on multiple myeloma cell viability. *Molecular Cancer Therapeutics,* 8**,** 1974-1984. doi: 10.1158/1535-7163.Mct-08-1177.

Hong, Y., Ren, T., Wang, X., Liu, X., Fei, Y., Meng, S., et al. 2022. APR-246 triggers ferritinophagy and ferroptosis of diffuse large B-cell lymphoma cells with distinct TP53 mutations. *Leukemia,* 36**,** 2269-2280. doi: 10.1038/s41375-022-01634-w.

Hsieh, M. S., Ling, H. H., Setiawan, S. A., Hardianti, M. S., Fong, I. H., Yeh, C. T., et al. 2024. Therapeutic targeting of thioredoxin reductase 1 causes ferroptosis while potentiating anti-PD-1 efficacy in head and neck cancer. *Chem Biol Interact,* 395**,** 111004. doi: 10.1016/j.cbi.2024.111004.

Hu, K., Qiu, J., Hu, Y., Wang, Y., Yu, C. & Wu, Y. 2024. Efficacy of FERscore in predicting sensitivity to ferroptosis inducers in breast cancer. *npj Breast Cancer,* 10**,** 74. doi: 10.1038/s41523-024-00685-9.

Huan, H., Lyamzaev, K. G., Panteleeva, A. A. & Chernyak, B. V. 2024. Mitochondrial lipid peroxidation is necessary but not sufficient for induction of ferroptosis. *Front Cell Dev Biol,* 12**,** 1452824. doi: 10.3389/fcell.2024.1452824.

Huang, C., Ma, W., Luo, Q., Shi, L., Xia, Y., Lao, C., et al. 2019. Iron overload resulting from the chronic oral administration of ferric citrate induces parkinsonism phenotypes in middle-aged mice. *Aging (Albany NY),* 11**,** 9846-9861. doi: 10.18632/aging.102433.

Huang, Q. T., Hu, Q. Q., Wen, Z. F. & Li, Y. L. 2023. Iron oxide nanoparticles inhibit tumor growth by ferroptosis in diffuse large B-cell lymphoma. *Am J Cancer Res,* 13**,** 498-508.

Huang, X., Zhou, D., Ye, X. & Jin, J. 2022. A novel ferroptosis-related gene signature can predict prognosis and influence immune microenvironment in acute myeloid leukemia. *Bosnian Journal of Basic Medical Sciences,* 22**,** 608-628. doi: 10.17305/bjbms.2021.6274.

Hurt, E. M., Thomas, S. B., Peng, B. & Farrar, W. L. 2006. Reversal of p53 epigenetic silencing in multiple myeloma permits apoptosis by a p53 activator. *Cancer Biology & Therapy,* 5**,** 1154-1160. doi: 10.4161/cbt.5.9.3001.

Ingold, I., Berndt, C., Schmitt, S., Doll, S., Poschmann, G., Buday, K., et al. 2018. Selenium Utilization by GPX4 Is Required to Prevent Hydroperoxide-Induced Ferroptosis. *Cell,* 172**,** 409-422.e21. doi: 10.1016/j.cell.2017.11.048.

Ingold, I. & Conrad, M. 2018. Selenium and iron, two elemental rivals in the ferroptotic death process. *Oncotarget,* 9**,** 22241-22242. doi: 10.18632/oncotarget.25295.

Ishikawa, C., Senba, M. & Mori, N. 2020. Evaluation of artesunate for the treatment of adult T-cell leukemia/lymphoma. *European Journal of Pharmacology,* 872**,** 172953. doi: 10.1016/j.ejphar.2020.172953.

Ito, J., Nakamura, T., Toyama, T., Chen, D., Berndt, C., Poschmann, G., et al. 2024. PRDX6 dictates ferroptosis sensitivity by directing cellular selenium utilization. *Mol Cell,* 84**,** 4629-4644.e9. doi: 10.1016/j.molcel.2024.10.028.

Jenke, R., Oliinyk, D., Zenz, T., Körfer, J., Schäker-Hübner, L., Hansen, F. K., et al. 2024. HDAC inhibitors activate lipid peroxidation and ferroptosis in gastric cancer. *Biochemical Pharmacology,* 225**,** 116257. doi: 10.1016/j.bcp.2024.116257.

Ji, P., Wang, X., Yin, J., Yao, Y. & Du, W. 2022. Amplification of ferroptosis with a liposomal nanoreactor cooperates with low-toxicity doxorubicin apoptosis for enhanced tumor chemotherapy. *Biomaterials Science,* 10**,** 1544-1553. doi: 10.1039/D2BM00079B.

Jiang, H., Li, Q., Yang, X., Jia, L., Cheng, H., Wang, J., et al. 2024a. Bone marrow stromal cells protect myeloma cells from ferroptosis through GPX4 deSUMOylation. *Cancer Lett,* 611**,** 217388. doi: 10.1016/j.canlet.2024.217388.

Jiang, H., Wang, L., Zhang, Q., Wang, S., Jia, L., Cheng, H., et al. 2024b. Bone marrow stromal cells dictate lanosterol biosynthesis and ferroptosis of multiple myeloma. *Oncogene,* 43**,** 1644-1653. doi: 10.1038/s41388-024-03020-5.

Jiang, X., Stockwell, B. R. & Conrad, M. 2021. Ferroptosis: mechanisms, biology and role in disease. *Nat Rev Mol Cell Biol,* 22**,** 266-282. doi: 10.1038/s41580-020-00324-8.

Jiang, Y., Mao, C., Yang, R., Yan, B., Shi, Y., Liu, X., et al. 2017. EGLN1/c-Myc Induced Lymphoid-Specific Helicase Inhibits Ferroptosis through Lipid Metabolic Gene Expression Changes. *Theranostics,* 7**,** 3293-3305. doi: 10.7150/thno.19988.

Jiang, Z., Wang, H., Qi, G., Jiang, C., Chen, K. & Yan, Z. 2022. Iron overload-induced ferroptosis of osteoblasts inhibits osteogenesis and promotes osteoporosis: An in vitro and in vivo study. *IUBMB Life,* 74**,** 1052-1069. doi: 10.1002/iub.2656.

Jog, E., Jainarayanan, A. K., La Ferlita, A., Chakraborty, A., Dalwai, A., Yahya, S., et al. 2025. Inhibiting de novo lipogenesis identifies a therapeutic vulnerability in therapy-resistant colorectal cancer. *Redox Biology,* 79**,** 103458. doi: 10.1016/j.redox.2024.103458.

Jurczyszyn, A., Czepiel, J., Gdula-Argasińska, J., Paśko, P., Czapkiewicz, A., Librowski, T., et al. 2015. Plasma fatty acid profile in multiple myeloma patients. *Leukemia Research,* 39**,** 400-405. doi: 10.1016/j.leukres.2014.12.010.

Kagan, V. E., Mao, G., Qu, F., Angeli, J. P., Doll, S., Croix, C. S., et al. 2017. Oxidized arachidonic and adrenic PEs navigate cells to ferroptosis. *Nat Chem Biol,* 13**,** 81-90. doi: 10.1038/nchembio.2238.

Kazandjian, D. & Landgren, O. 2021. A new era of novel immunotherapies for multiple myeloma. *The Lancet (British edition),* 398**,** 642-643. doi: 10.1016/S0140-6736(21)01602-0.

Ke, P., Bao, X., Liu, C., Zhou, B., Huo, M., Chen, Y., et al. 2022. LPCAT3 is a potential prognostic biomarker and may be correlated with immune infiltration and ferroptosis in acute myeloid leukemia: a pan-cancer analysis. *Translational Cancer Research,* 11**,** 3491-3505.

Khokhlatchev, A. V., Sharma, A., Deering, T. G., Shaw, J. J. P., Costa-Pinheiro, P., Golla, U., et al. 2022. Ceramide nanoliposomes augment the efficacy of venetoclax and cytarabine in models of acute myeloid leukemia. *Faseb j,* 36**,** e22514. doi: 10.1096/fj.202200765R.

Kim, H., Kim, H. J. & Kim, S. H. 2020. Diagnostic Approach for Double-Hit and Triple-Hit Lymphoma Based on Immunophenotypic and Cytogenetic Characteristics of Bone Marrow Specimens. *Ann Lab Med,* 40**,** 361-369. doi: 10.3343/alm.2020.40.5.361.

Kim, J.-W., Min, D. W., Kim, D., Kim, J., Kim, M. J., Lim, H., et al. 2023. GPX4 overexpressed non-small cell lung cancer cells are sensitive to RSL3-induced ferroptosis. *Scientific Reports,* 13**,** 8872. doi: 10.1038/s41598-023-35978-9.

Kinowaki, Y., Kurata, M., Ishibashi, S., Ikeda, M., Tatsuzawa, A., Yamamoto, M., et al. 2018. Glutathione peroxidase 4 overexpression inhibits ROS-induced cell death in diffuse large B-cell lymphoma. *Laboratory Investigation,* 98**,** 609-619. doi: 10.1038/s41374-017-0008-1.

Kirshner, J., Thulien, K. J., Martin, L. D., Debes Marun, C., Reiman, T., Belch, A. R., et al. 2008. A unique three-dimensional model for evaluating the impact of therapy on multiple myeloma. *Blood,* 112**,** 2935-2945. doi: 10.1182/blood-2008-02-142430.

Klett, E. L., Chen, S., Yechoor, A., Lih, F. B. & Coleman, R. A. 2017. Long-chain acyl-CoA synthetase isoforms differ in preferences for eicosanoid species and long-chain fatty acids. *J Lipid Res,* 58**,** 884-894. doi: 10.1194/jlr.M072512.

Konstorum, A., Tesfay, L., Paul, B. T., Torti, F. M., Laubenbacher, R. C. & Torti, S. V. 2020. Systems biology of ferroptosis: A modeling approach. *J Theor Biol,* 493**,** 110222. doi: 10.1016/j.jtbi.2020.110222.

Koppula, P., Zhang, Y., Zhuang, L. & Gan, B. 2018. Amino acid transporter SLC7A11/xCT at the crossroads of regulating redox homeostasis and nutrient dependency of cancer. *Cancer communications (London, England),* 38**,** 12-12. doi: 10.1186/s40880-018-0288-x.

Kothari, A., Hittelman, W. N. & Chambers, T. C. 2016. Cell Cycle-Dependent Mechanisms Underlie Vincristine-Induced Death of Primary Acute Lymphoblastic Leukemia Cells. *Cancer Res,* 76**,** 3553-61. doi: 10.1158/0008-5472.Can-15-2104.

Kraft, V. a. N., Bezjian, C. T., Pfeiffer, S., Ringelstetter, L., Müller, C., Zandkarimi, F., et al. 2020. GTP Cyclohydrolase 1/Tetrahydrobiopterin Counteract Ferroptosis through Lipid Remodeling. *ACS Central Science,* 6**,** 41-53. doi: 10.1021/acscentsci.9b01063.

Kuang, F., Liu, J., Tang, D. & Kang, R. 2020. Oxidative Damage and Antioxidant Defense in Ferroptosis. *Frontiers in Cell and Developmental Biology,* 8. doi: 10.3389/fcell.2020.586578.

Kuang, F., Liu, J., Xie, Y., Tang, D. & Kang, R. 2021. MGST1 is a redox-sensitive repressor of ferroptosis in pancreatic cancer cells. *Cell Chem Biol,* 28**,** 765-775.e5. doi: 10.1016/j.chembiol.2021.01.006.

Kumar, S. K., Harrison, S. J., Cavo, M., De La Rubia, J., Popat, R., Gasparetto, C., et al. 2020. Venetoclax or placebo in combination with bortezomib and dexamethasone in patients with relapsed or refractory multiple myeloma (BELLINI): a randomised, double-blind, multicentre, phase 3 trial. *Lancet Oncol,* 21**,** 1630-1642. doi: 10.1016/s1470-2045(20)30525-8.

Kumar, S. K., Rajkumar, S. V., Dispenzieri, A., Lacy, M. Q., Hayman, S. R., Buadi, F. K., et al. 2008. Improved survival in multiple myeloma and the impact of novel therapies. *Blood,* 111**,** 2516-2520. doi: 10.1182/blood-2007-10-116129.

Kwon, M. Y., Park, E., Lee, S. J. & Chung, S. W. 2015. Heme oxygenase-1 accelerates erastin-induced ferroptotic cell death. *Oncotarget,* 6**,** 24393-403. doi: 10.18632/oncotarget.5162.

Labunskyy, V. M., Hatfield, D. L. & Gladyshev, V. N. 2014. Selenoproteins: Molecular Pathways and Physiological Roles. *Physiological Reviews,* 94**,** 739-777. doi: 10.1152/physrev.00039.2013.

Lagal, D. J., Montes-Osuna, A. M., Ortiz-Olivencia, A., Arribas-Parejas, C., Ortiz-Alcántara, Á., Pescuezo-Castillo, C., et al. 2024a. Tumoral Malignancy Decreases Coupled with Higher ROS and Lipid Peroxidation in HCT116 Colon Cancer Cells upon Loss of PRDX6. *Antioxidants (Basel),* 13. doi: 10.3390/antiox13070881.

Lagal, D. J., Ortiz-Alcántara, Á., Pedrajas, J. R., Mcdonagh, B., Bárcena, J. A., Requejo-Aguilar, R., et al. 2024b. Loss of peroxiredoxin 6 alters lipid composition and distribution resulting in increased sensitivity to ferroptosis. *Biochemical Journal,* 481**,** 1997-2015. doi: 10.1042/bcj20240445.

Lee, J.-Y., Nam, M., Son, H. Y., Hyun, K., Jang, S. Y., Kim, J. W., et al. 2020. Polyunsaturated fatty acid biosynthesis pathway determines ferroptosis sensitivity in gastric cancer. *Proceedings of the National Academy of Sciences,* 117**,** 32433-32442. doi: 10.1073/pnas.2006828117.

Lee, J. & Roh, J.-L. 2024. Cholesterol-ferroptosis nexus: Unveiling novel cancer therapeutic avenues. *Cancer Letters,* 597**,** 217046. doi: 10.1016/j.canlet.2024.217046.

Lei, F. J., Chiang, J. Y., Chang, H. J., Chen, D. C., Wang, H. L., Yang, H. A., et al. 2023. Cellular and exosomal GPx1 are essential for controlling hydrogen peroxide balance and alleviating oxidative stress in hypoxic glioblastoma. *Redox Biol,* 65**,** 102831. doi: 10.1016/j.redox.2023.102831.

Lei, G., Zhuang, L. & Gan, B. 2022. Targeting ferroptosis as a vulnerability in cancer. *Nature Reviews Cancer,* 22**,** 381-396. doi: 10.1038/s41568-022-00459-0.

Leukaemia Foundation 2023. State of The Nation: Blood Cancers in Australia. Australia: Leukaemia Foundation.

Lewis, W. D., Lilly, S. & Jones, K. L. 2020. Lymphoma: Diagnosis and Treatment. *Am Fam Physician,* 101**,** 34-41.

Li, D., Zhang, M. & Chao, H. 2021. Significance of glutathione peroxidase 4 and intracellular iron level in ovarian cancer cells—"utilization" of ferroptosis mechanism. *Inflammation Research,* 70**,** 1177-1189. doi: 10.1007/s00011-021-01495-6.

Li, L., Gao, Y., Zhang, W. & Zheng, Y. 2022a. Antitumor Potential of Selenium Nanoparticles (SeNPs) Against Multiple Myeloma Model in RPMI8226 Cells. *Journal of Cluster Science,* 33**,** 2771-2780. doi: 10.1007/s10876-021-02191-5.

Li, M., Zhang, C. L., Zhou, D. S., Chan, S. H., Liu, X. Q., Chen, S. N., et al. 2024a. Identification of COQ2 as a regulator of proliferation and lipid peroxidation through genome-scale CRISPR-Cas9 screening in myeloma cells. *Br J Haematol,* 204**,** 1307-1324. doi: 10.1111/bjh.19375.

Li, S., Young, K. H. & Medeiros, L. J. 2018. Diffuse large B-cell lymphoma. *Pathology,* 50**,** 74-87. doi: 10.1016/j.pathol.2017.09.006.

Li, W., Fu, H., Fang, L., Chai, H., Ding, B. & Qian, S. 2023a. Andrographolide induced ferroptosis in multiple myeloma cells by regulating the P38/Nrf2/HO-1 pathway. *Arch Biochem Biophys,* 742**,** 109622. doi: 10.1016/j.abb.2023.109622.

Li, W., Fu, H., Fang, L., Chai, H., Gao, T., Chen, Z., et al. 2022b. Shikonin induces ferroptosis in multiple myeloma via GOT1-mediated ferritinophagy. *Frontiers in Oncology,* 12. doi: 10.3389/fonc.2022.1025067.

Li, W., Yin, X., Fu, H., Liu, J., Weng, Z., Mao, Q., et al. 2024b. Ethanol extract of Eclipta prostrata induces multiple myeloma ferroptosis via Keap1/Nrf2/HO-1 axis. *Phytomedicine,* 128**,** 155401. doi: 10.1016/j.phymed.2024.155401.

Li, Y., Xu, X., Wang, X., Zhang, C., Hu, A. & Li, Y. 2023b. MGST1 Expression Is Associated with Poor Prognosis, Enhancing the Wnt/β-Catenin Pathway via Regulating AKT and Inhibiting Ferroptosis in Gastric Cancer. *ACS Omega,* 8**,** 23683-23694. doi: 10.1021/acsomega.3c01782.

Liang, L., Liu, Y., Wu, X. & Chen, Y. 2023. Artesunate induces ferroptosis by inhibiting the nuclear localization of SREBP2 in myeloma cells. *International Journal of Medical Sciences,* 20**,** 1535-1550. doi: 10.7150/ijms.86409.

Liang, X., Chen, M., Bhattarai, P., Hameed, S., Tang, Y. & Dai, Z. 2021. Complementing Cancer Photodynamic Therapy with Ferroptosis through Iron Oxide Loaded Porphyrin-Grafted Lipid Nanoparticles. *ACS Nano,* 15**,** 20164-20180. doi: 10.1021/acsnano.1c08108.

Liao, A., Hu, R., Zhao, Q., Li, J., Li, Y., Yao, K., et al. 2012. Autophagy induced by FTY720 promotes apoptosis in U266 cells. *European Journal of Pharmaceutical Sciences,* 45**,** 600-605. doi: 10.1016/j.ejps.2011.12.014.

Liao, P., Wang, W., Wang, W., Kryczek, I., Li, X., Bian, Y., et al. 2022. CD8+ T cells and fatty acids orchestrate tumor ferroptosis and immunity via ACSL4. *Cancer Cell,* 40**,** 365-378.e6. doi: 10.1016/j.ccell.2022.02.003.

Linkermann, A. & Green, D. R. 2014. Necroptosis. *N Engl J Med,* 370**,** 455-65. doi: 10.1056/NEJMra1310050.

Lipchick, B. C., Fink, E. E. & Nikiforov, M. A. 2016. Oxidative stress and proteasome inhibitors in multiple myeloma. *Pharmacological Research,* 105**,** 210-215. doi: 10.1016/j.phrs.2016.01.029.

Liu, C., Wang, Y., Xia, H., Liu, Y., Yang, X., Yuan, X., et al. 2025. High Concentration of Iron Ions Contributes to Ferroptosis-Mediated Testis Injury. *Biological Trace Element Research,* 203**,** 891-902. doi: 10.1007/s12011-024-04192-7.

Liu, J., Zhang, C., Wang, J., Hu, W. & Feng, Z. 2020. The Regulation of Ferroptosis by Tumor Suppressor p53 and its Pathway. *Int J Mol Sci,* 21. doi: 10.3390/ijms21218387.

Liu, L., Yang, C., Zhu, L., Wang, Y., Zheng, F., Liang, L., et al. 2024. RSL3 enhances ROS-mediated cell apoptosis of myelodysplastic syndrome cells through MYB/Bcl-2 signaling pathway. *Cell Death & Disease,* 15**,** 465. doi: 10.1038/s41419-024-06866-5.

Liu, Q., Zhao, Y., Zhou, H. & Chen, C. 2023a. Ferroptosis: challenges and opportunities for nanomaterials in cancer therapy. *Regenerative Biomaterials,* 10**,** rbad004. doi: 10.1093/rb/rbad004.

Liu, R., Rong, G., Liu, Y., Huang, W., He, D. & Lu, R. 2021a. Delivery of apigenin-loaded magnetic Fe2O3/Fe3O4@mSiO2 nanocomposites to A549 cells and their antitumor mechanism. *Materials Science and Engineering: C,* 120**,** 111719. doi: 10.1016/j.msec.2020.111719.

Liu, S., Wu, W., Chen, Q., Zheng, Z., Jiang, X., Xue, Y., et al. 2021b. TXNRD1: A Key Regulator Involved in the Ferroptosis of CML Cells Induced by Cysteine Depletion In Vitro. *Oxid Med Cell Longev,* 2021**,** 7674565. doi: 10.1155/2021/7674565.

Liu, S., Yan, S., Zhu, J., Lu, R., Kang, C., Tang, K., et al. 2022. Combination RSL3 Treatment Sensitizes Ferroptosis- and EGFR-Inhibition-Resistant HNSCCs to Cetuximab. *Int J Mol Sci,* 23. doi: 10.3390/ijms23169014.

Liu, X., Tian, Y., Yang, A., Zhang, C., Miao, X. & Yang, W. 2023b. Antitumor Effects of Poplar Propolis on DLBCL SU-DHL-2 Cells. *Foods,* 12**,** 283.

Logie, E., Van Puyvelde, B., Cuypers, B., Schepers, A., Berghmans, H., Verdonck, J., et al. 2021. Ferroptosis Induction in Multiple Myeloma Cells Triggers DNA Methylation and Histone Modification Changes Associated with Cellular Senescence. *Int J Mol Sci,* 22. doi: 10.3390/ijms222212234.

Long, F., Lin, Z., Long, Q., Lu, Z., Zhu, K., Zhao, M., et al. 2023. CircZBTB46 Protects Acute Myeloid Leukemia Cells from Ferroptotic Cell Death by Upregulating SCD. *Cancers* [Online], 15.

Lou, S., Hong, H., Maihesuti, L., Gao, H., Zhu, Z., Xu, L., et al. 2021. Inhibitory effect of hydnocarpin D on T-cell acute lymphoblastic leukemia via induction of autophagy-dependent ferroptosis. *Experimental Biology and Medicine,* 246**,** 1541-1553. doi: 10.1177/15353702211004870.

Lourenço, D., Lopes, R., Pestana, C., Queirós, A. C., João, C. & Carneiro, E. A. 2022. Patient-Derived Multiple Myeloma 3D Models for Personalized Medicine—Are We There Yet? *International Journal of Molecular Sciences* [Online], 23.

Love, M. I., Huber, W. & Anders, S. 2014. Moderated estimation of fold change and dispersion for RNA-seq data with DESeq2. *Genome Biology,* 15**,** 550. doi: 10.1186/s13059-014-0550-8.

Lu, B., Chen, X.-B., Hong, Y.-C., Zhu, H., He, Q.-J., Yang, B., et al. 2019. Identification of PRDX6 as a regulator of ferroptosis. *Acta Pharmacologica Sinica,* 40**,** 1334-1342. doi: 10.1038/s41401-019-0233-9.

Luo, P., Liu, D., Zhang, Q., Yang, F., Wong, Y.-K., Xia, F., et al. 2022. Celastrol induces ferroptosis in activated HSCs to ameliorate hepatic fibrosis via targeting peroxiredoxins and HO-1. *Acta Pharmaceutica Sinica B,* 12**,** 2300-2314. doi: 10.1016/j.apsb.2021.12.007.

Luo, Y., Li, L., Hu, Q., Zhang, Z., Liu, F., Peng, Y., et al. 2024. Iron overload increases the sensitivity of endometriosis stromal cells to ferroptosis via a PRC2-independent function of EZH2. *Int J Biochem Cell Biol,* 169**,** 106553. doi: 10.1016/j.biocel.2024.106553.

Lyamzaev, K. G., Huan, H., Panteleeva, A. A., Simonyan, R. A., Avetisyan, A. V. & Chernyak, B. V. 2024. Exogenous Iron Induces Mitochondrial Lipid Peroxidation, Lipofuscin Accumulation, and Ferroptosis in H9c2 Cardiomyocytes. *Biomolecules* [Online], 14.

Maccarinelli, F., Coltrini, D., Mussi, S., Bugatti, M., Turati, M., Chiodelli, P., et al. 2023. Iron supplementation enhances RSL3-induced ferroptosis to treat naïve and prevent castration-resistant prostate cancer. *Cell Death Discovery,* 9**,** 81. doi: 10.1038/s41420-023-01383-4.

Mackenzie, E. L., Iwasaki, K. & Tsuji, Y. 2008. Intracellular iron transport and storage: from molecular mechanisms to health implications. *Antioxid Redox Signal,* 10**,** 997-1030. doi: 10.1089/ars.2007.1893.

Magtanong, L., Ko, P. J., To, M., Cao, J. Y., Forcina, G. C., Tarangelo, A., et al. 2019. Exogenous Monounsaturated Fatty Acids Promote a Ferroptosis-Resistant Cell State. *Cell Chem Biol,* 26**,** 420-432 e9. doi: 10.1016/j.chembiol.2018.11.016.

Magtanong, L., Mueller, G. D., Williams, K. J., Billmann, M., Chan, K., Armenta, D. A., et al. 2022. Context-dependent regulation of ferroptosis sensitivity. *Cell Chemical Biology,* 29**,** 1409-1418.e6. doi: 10.1016/j.chembiol.2022.06.004.

Maher, K. R., Shafer, D., Schaar, D., Bandyopadhyay, D., Deng, X., Wright, J., et al. 2025. A phase I study of MLN4924 and belinostat in relapsed/refractory acute myeloid leukemia or myelodysplastic syndrome. *Cancer Chemotherapy and Pharmacology,* 95**,** 24. doi: 10.1007/s00280-024-04742-9.

Mai, T. T., Hamai, A., Hienzsch, A., Caneque, T., Muller, S., Wicinski, J., et al. 2017. Salinomycin kills cancer stem cells by sequestering iron in lysosomes. *Nat Chem,* 9**,** 1025-1033. doi: 10.1038/nchem.2778.

Mancuso, R. I., Foglio, M. A. & Olalla Saad, S. T. 2021. Artemisinin-type drugs for the treatment of hematological malignancies. *Cancer Chemotherapy and Pharmacology,* 87**,** 1-22. doi: 10.1007/s00280-020-04170-5.

Mao, C., Liu, X., Zhang, Y., Lei, G., Yan, Y., Lee, H., et al. 2021. DHODH-mediated ferroptosis defence is a targetable vulnerability in cancer. *Nature,* 593**,** 586-590. doi: 10.1038/s41586-021-03539-7.

Markovina, S., Callander, N. S., O'connor, S. L., Xu, G., Shi, Y., Leith, C. P., et al. 2010. Bone marrow stromal cells from multiple myeloma patients uniquely induce bortezomib resistant NF-kappaB activity in myeloma cells. *Mol Cancer,* 9**,** 176. doi: 10.1186/1476-4598-9-176.

Mbaveng, A. T., Fotso, G. W., Ngnintedo, D., Kuete, V., Ngadjui, B. T., Keumedjio, F., et al. 2018a. Cytotoxicity of epunctanone and four other phytochemicals isolated from the medicinal plants Garcinia epunctata and Ptycholobium contortum towards multi-factorial drug resistant cancer cells. *Phytomedicine,* 48**,** 112-119. doi: 10.1016/j.phymed.2017.12.016.

Mbaveng, A. T., Ndontsa, B. L., Kuete, V., Nguekeu, Y. M. M., Çelik, İ., Mbouangouere, R., et al. 2018b. A naturally occuring triterpene saponin ardisiacrispin B displayed cytotoxic effects in multi-factorial drug resistant cancer cells via ferroptotic and apoptotic cell death. *Phytomedicine,* 43**,** 78-85. doi: 10.1016/j.phymed.2018.03.035.

Mcbrayer, S. K., Cheng, J. C., Singhal, S., Krett, N. L., Rosen, S. T. & Shanmugam, M. 2012. Multiple myeloma exhibits novel dependence on GLUT4, GLUT8, and GLUT11: implications for glucose transporter-directed therapy. *Blood,* 119**,** 4686-4697. doi: 10.1182/blood-2011-09-377846.

Meng, Z., Liang, H., Zhao, J., Gao, J., Liu, C., Ma, X., et al. 2021. HMOX1 upregulation promotes ferroptosis in diabetic atherosclerosis. *Life Sci,* 284**,** 119935. doi: 10.1016/j.lfs.2021.119935.

Merollini, K. M. D., Gordon, L. G., Ho, Y. M., Aitken, J. F. & Kimlin, M. G. 2022. Cancer Survivors' Long-Term Health Service Costs in Queensland, Australia: Results of a Population-Level Data Linkage Study (Cos-Q). *International Journal of Environmental Research and Public Health,* 19**,** 9473.

Metsalu, T. & Vilo, J. 2015. ClustVis: a web tool for visualizing clustering of multivariate data using Principal Component Analysis and heatmap. *Nucleic Acids Res,* 43**,** W566-70. doi: 10.1093/nar/gkv468.

Miao, H., Meng, H., Zhang, Y., Chen, T., Zhang, L. & Cheng, W. 2024. FSP1 inhibition enhances olaparib sensitivity in BRCA-proficient ovarian cancer patients via a nonferroptosis mechanism. *Cell Death & Differentiation,* 31**,** 497-510. doi: 10.1038/s41418-024-01263-z.

Mishima, E., Nakamura, T., Zheng, J., Zhang, W., Mourão, A. S. D., Sennhenn, P., et al. 2023. DHODH inhibitors sensitize to ferroptosis by FSP1 inhibition. *Nature,* 619**,** E9-E18. doi: 10.1038/s41586-023-06269-0.

Mishra, A., Tamari, R., Dezern, A. E., Byrne, M. T., Gooptu, M., Chen, Y. B., et al. 2022. Eprenetapopt Plus Azacitidine After Allogeneic Hematopoietic Stem-Cell Transplantation for TP53-Mutant Acute Myeloid Leukemia and Myelodysplastic Syndromes. *J Clin Oncol***,** Jco2200181. doi: 10.1200/jco.22.00181.

Miyamoto, K., Watanabe, M., Boku, S., Sukeno, M., Morita, M., Kondo, H., et al. 2020. xCT Inhibition Increases Sensitivity to Vorinostat in a ROS-Dependent Manner. *Cancers* [Online], 12.

Mizushima, N. & Yoshimori, T. 2007. How to Interpret LC3 Immunoblotting. *Autophagy,* 3**,** 542-545. doi: 10.4161/auto.4600.

Mo, M., Pan, L., Deng, L., Liang, M., Xia, N. & Liang, Y. 2024. Iron Overload Induces Hepatic Ferroptosis and Insulin Resistance by Inhibiting the Jak2/stat3/slc7a11 Signaling Pathway. *Cell Biochemistry and Biophysics,* 82**,** 2079-2094. doi: 10.1007/s12013-024-01315-8.

Moosmayer, D., Hilpmann, A., Hoffmann, J., Schnirch, L., Zimmermann, K., Badock, V., et al. 2021. Crystal structures of the selenoprotein glutathione peroxidase 4 in its apo form and in complex with the covalently bound inhibitor ML162. *Acta Crystallogr D Struct Biol,* 77**,** 237-248. doi: 10.1107/s2059798320016125.

Morgan, M. J. & Kim, Y.-S. 2022. Roles of RIPK3 in necroptosis, cell signaling, and disease. *Experimental & Molecular Medicine,* 54**,** 1695-1704. doi: 10.1038/s12276-022-00868-z.

Moriya, S., Che, X.-F., Komatsu, S., Abe, A., Kawaguchi, T., Gotoh, A., et al. 2013. Macrolide antibiotics block autophagy flux and sensitize to bortezomib via endoplasmic reticulum stress-mediated CHOP induction in myeloma cells. *Int J Oncol,* 42**,** 1541-1550. doi: 10.3892/ijo.2013.1870.

Mynott, R. L. & Wallington-Beddoe, C. T. 2021. Drug and Solute Transporters in Mediating Resistance to Novel Therapeutics in Multiple Myeloma. *ACS Pharmacol Transl Sci,* 4**,** 1050-1065. doi: 10.1021/acsptsci.1c00074.

N. Adham, A., F. Hegazy, M. E., Naqishbandi, A. M. & Efferth, T. 2020. Induction of Apoptosis, Autophagy and Ferroptosis by Thymus vulgaris and Arctium lappa Extract in Leukemia and Multiple Myeloma Cell Lines. *Molecules,* 25**,** 5016.

Nakamura, T., Mishima, E., Yamada, N., Mourão, A. S. D., Trümbach, D., Doll, S., et al. 2023. Integrated chemical and genetic screens unveil FSP1 mechanisms of ferroptosis regulation. *Nature Structural & Molecular Biology,* 30**,** 1806-1815. doi: 10.1038/s41594-023-01136-y.

Nerini-Molteni, S., Ferrarini, M., Cozza, S., Caligaris-Cappio, F. & Sitia, R. 2008. Redox homeostasis modulates the sensitivity of myeloma cells to bortezomib. *British Journal of Haematology,* 141**,** 494-503. doi: 10.1111/j.1365-2141.2008.07066.x.

Nishizawa, H., Matsumoto, M., Shindo, T., Saigusa, D., Kato, H., Suzuki, K., et al. 2020. Ferroptosis is controlled by the coordinated transcriptional regulation of glutathione and labile iron metabolism by the transcription factor BACH1. *J Biol Chem,* 295**,** 69-82. doi: 10.1074/jbc.RA119.009548.

O'donnell, E. K., Shapiro, Y. N., Yee, A. J., Nadeem, O., Hu, B. Y., Laubach, J. P., et al. 2022. Quality of life, psychological distress, and prognostic perceptions in patients with multiple myeloma. *Cancer,* 128**,** 1996-2004. doi: 10.1002/cncr.34134.

Oh, S.-J., Ikeda, M., Ide, T., Hur, K. Y. & Lee, M.-S. 2022. Mitochondrial event as an ultimate step in ferroptosis. *Cell Death Discovery,* 8**,** 414. doi: 10.1038/s41420-022-01199-8.

Onoue, S., Yamada, S. & Chan, H. K. 2014. Nanodrugs: pharmacokinetics and safety. *Int J Nanomedicine,* 9**,** 1025-37. doi: 10.2147/IJN.S38378.

Pai, A. B. & Garba, A. O. 2012. Ferumoxytol: a silver lining in the treatment of anemia of chronic kidney disease or another dark cloud? *J Blood Med,* 3**,** 77-85. doi: 10.2147/JBM.S29204.

Palumbo, A., Chanan-Khan, A., Weisel, K., Nooka, A. K., Masszi, T., Beksac, M., et al. 2016. Daratumumab, Bortezomib, and Dexamethasone for Multiple Myeloma. *New England Journal of Medicine,* 375**,** 754-766. doi: 10.1056/NEJMoa1606038.

Pan, B., Li, Y., Xu, Z., Miao, Y., Yin, H., Kong, Y., et al. 2022. Identifying a novel ferroptosis-related prognostic score for predicting prognosis in chronic lymphocytic leukemia. *Frontiers in Immunology,* 13. doi: 10.3389/fimmu.2022.962000.

Panaroni, C., Fulzele, K., Mori, T., Siu, K. T., Onyewadume, C., Maebius, A., et al. 2022. Multiple myeloma cells induce lipolysis in adipocytes and uptake fatty acids through fatty acid transporter proteins. *Blood,* 139**,** 876-888. doi: 10.1182/blood.2021013832.

Panaroni, C., Fulzele, K., Soucy, R., Huang, C., Mukaihara, K., Chattopadhyay, S., et al. 2019. Polyunsaturated Fatty Acid (PUFA) Signaling Induces Ferroptosis-Mediated Cell-Death in Multiple Myeloma. *Blood,* 134**,** 3108-3108. doi: 10.1182/blood-2019-131906.

Panaroni, C., Fulzele, K., Soucy, R., Siu, K. T., Mukaihara, K., Huang, C., et al. 2018. Arachidonic Acid Induces Ferroptosis-Mediated Cell-Death in Multiple Myeloma. *Blood,* 132**,** 4498-4498. doi: 10.1182/blood-2018-99-118482.

Pedrera, L., Espiritu, R. A., Ros, U., Weber, J., Schmitt, A., Stroh, J., et al. 2021. Ferroptotic pores induce Ca(2+) fluxes and ESCRT-III activation to modulate cell death kinetics. *Cell Death Differ,* 28**,** 1644-1657. doi: 10.1038/s41418-020-00691-x.

Pei, Z., Liu, Y., Liu, S., Jin, W., Luo, Y., Sun, M., et al. 2021. FUNDC1 insufficiency sensitizes high fat diet intake-induced cardiac remodeling and contractile anomaly through ACSL4-mediated ferroptosis. *Metabolism,* 122**,** 154840. doi: 10.1016/j.metabol.2021.154840.

Peng, Z. & Peng, N. 2023. Microsomal glutathione S-transferase 1 targets the autophagy signaling pathway to suppress ferroptosis in gastric carcinoma cells. *Human & Experimental Toxicology,* 42**,** 09603271231172915. doi: 10.1177/09603271231172915.

Perillo, B., Di Donato, M., Pezone, A., Di Zazzo, E., Giovannelli, P., Galasso, G., et al. 2020. ROS in cancer therapy: the bright side of the moon. *Experimental & Molecular Medicine,* 52**,** 192-203. doi: 10.1038/s12276-020-0384-2.

Petrich, A. M., Gandhi, M., Jovanovic, B., Castillo, J. J., Rajguru, S., Yang, D. T., et al. 2014. Impact of induction regimen and stem cell transplantation on outcomes in double-hit lymphoma: a multicenter retrospective analysis. *Blood,* 124**,** 2354-61. doi: 10.1182/blood-2014-05-578963.

Pino, L. K., Searle, B. C., Bollinger, J. G., Nunn, B., Maclean, B. & Maccoss, M. J. 2020. The Skyline ecosystem: Informatics for quantitative mass spectrometry proteomics. *Mass Spectrom Rev,* 39**,** 229-244. doi: 10.1002/mas.21540.

Pontel, L. B., Bueno-Costa, A., Morellato, A. E., Carvalho Santos, J., Roue, G. & Esteller, M. 2022. Acute lymphoblastic leukemia necessitates GSH-dependent ferroptosis defenses to overcome FSP1-epigenetic silencing. *Redox Biol,* 55**,** 102408. doi: 10.1016/j.redox.2022.102408.

Powell, J. A., Lewis, A. C., Zhu, W., Toubia, J., Pitman, M. R., Wallington-Beddoe, C. T., et al. 2017. Targeting sphingosine kinase 1 induces MCL1-dependent cell death in acute myeloid leukemia. *Blood,* 129**,** 771-782. doi: 10.1182/blood-2016-06-720433.

Probst, L., Dächert, J., Schenk, B. & Fulda, S. 2017. Lipoxygenase inhibitors protect acute lymphoblastic leukemia cells from ferroptotic cell death. *Biochemical Pharmacology,* 140**,** 41-52. doi: 10.1016/j.bcp.2017.06.112.

Pyun, J., Mcinnes, L. E., Donnelly, P. S., Mawal, C., Bush, A. I., Short, J. L., et al. 2022. Copper bis(thiosemicarbazone) complexes modulate P-glycoprotein expression and function in human brain microvascular endothelial cells. *Journal of Neurochemistry,* 162**,** 226-244. doi: 10.1111/jnc.15609.

Qin, J., Sharma, A., Wang, Y., Tobar-Tosse, F., Dakal, T. C., Liu, H., et al. 2022. Systematic discrimination of the repetitive genome in proximity of ferroptosis genes and a novel prognostic signature correlating with the oncogenic lncRNA CRNDE in multiple myeloma. *Frontiers in Oncology,* 12. doi: 10.3389/fonc.2022.1026153.

Quan, J., Bode, A. M. & Luo, X. 2021. ACSL family: The regulatory mechanisms and therapeutic implications in cancer. *European Journal of Pharmacology,* 909**,** 174397. doi: 10.1016/j.ejphar.2021.174397.

Rajkumar, S. V. & Kumar, S. 2016. Multiple Myeloma: Diagnosis and Treatment. *Mayo Clinic Proceedings,* 91**,** 101-119. doi: 10.1016/j.mayocp.2015.11.007.

Raninga, P. V., Di Trapani, G., Vuckovic, S. & Tonissen, K. F. 2016. Cross-talk between two antioxidants, thioredoxin reductase and heme oxygenase-1, and therapeutic implications for multiple myeloma. *Redox biology,* 8**,** 175-185. doi: 10.1016/j.redox.2016.01.007.

Raninga, P. V., Trapani, G. D., Vuckovic, S., Bhatia, M. & Tonissen, K. F. 2015. Inhibition of thioredoxin 1 leads to apoptosis in drug-resistant multiple myeloma. *Oncotarget,* 6.

Rees, M. G., Seashore-Ludlow, B., Cheah, J. H., Adams, D. J., Price, E. V., Gill, S., et al. 2016. Correlating chemical sensitivity and basal gene expression reveals mechanism of action. *Nat Chem Biol,* 12**,** 109-16. doi: 10.1038/nchembio.1986.

Riedell, P. A. & Smith, S. M. 2018. Double hit and double expressors in lymphoma: Definition and treatment. *Cancer,* 124**,** 4622-4632. doi: 10.1002/cncr.31646.

Riegman, M., Sagie, L., Galed, C., Levin, T., Steinberg, N., Dixon, S. J., et al. 2020. Ferroptosis occurs through an osmotic mechanism and propagates independently of cell rupture. *Nat Cell Biol,* 22**,** 1042-1048. doi: 10.1038/s41556-020-0565-1.

Rink, J. S., Lin, A. Y., Mcmahon, K. M., Calvert, A. E., Yang, S., Taxter, T., et al. 2021. Targeted reduction of cholesterol uptake in cholesterol-addicted lymphoma cells blocks turnover of oxidized lipids to cause ferroptosis. *J Biol Chem,* 296**,** 100100. doi: 10.1074/jbc.RA120.014888.

Saini, R. 2011. Coenzyme Q10: The essential nutrient. *J Pharm Bioallied Sci,* 3**,** 466-7. doi: 10.4103/0975-7406.84471.

Sallman, D. A., Dezern, A. E., Garcia-Manero, G., Steensma, D. P., Roboz, G. J., Sekeres, M. A., et al. 2021. Eprenetapopt (APR-246) and Azacitidine in TP53-Mutant Myelodysplastic Syndromes. *J Clin Oncol,* 39**,** 1584-1594. doi: 10.1200/jco.20.02341.

Sato, M., Kusumi, R., Hamashima, S., Kobayashi, S., Sasaki, S., Komiyama, Y., et al. 2018. The ferroptosis inducer erastin irreversibly inhibits system xc− and synergizes with cisplatin to increase cisplatin's cytotoxicity in cancer cells. *Scientific Reports,* 8**,** 968. doi: 10.1038/s41598-018-19213-4.

Schmitt, A., Xu, W., Bucher, P., Grimm, M., Konantz, M., Horn, H., et al. 2021. Dimethyl fumarate induces ferroptosis and impairs NF-kappaB/STAT3 signaling in DLBCL. *Blood,* 138**,** 871-884. doi: 10.1182/blood.2020009404.

Seashore-Ludlow, B., Rees, M. G., Cheah, J. H., Cokol, M., Price, E. V., Coletti, M. E., et al. 2015. Harnessing Connectivity in a Large-Scale Small-Molecule Sensitivity Dataset. *Cancer Discov,* 5**,** 1210-23. doi: 10.1158/2159-8290.Cd-15-0235.

Sehn, L. H. & Salles, G. 2021. Diffuse Large B-Cell Lymphoma. *N Engl J Med,* 384**,** 842-858. doi: 10.1056/NEJMra2027612.

Seibt, T. M., Proneth, B. & Conrad, M. 2019. Role of GPX4 in ferroptosis and its pharmacological implication. *Free Radic Biol Med,* 133**,** 144-152. doi: 10.1016/j.freeradbiomed.2018.09.014.

Seiler, A., Schneider, M., Förster, H., Roth, S., Wirth, E. K., Culmsee, C., et al. 2008. Glutathione Peroxidase 4 Senses and Translates Oxidative Stress into 12/15-Lipoxygenase Dependent- and AIF-Mediated Cell Death. *Cell Metabolism,* 8**,** 237-248. doi: 10.1016/j.cmet.2008.07.005.

Shan, X., Li, J., Liu, J., Feng, B., Zhang, T., Liu, Q., et al. 2023. Targeting ferroptosis by poly(acrylic) acid coated Mn3O4 nanoparticles alleviates acute liver injury. *Nature Communications,* 14**,** 7598. doi: 10.1038/s41467-023-43308-w.

Shanbhag, S. & Ambinder, R. F. 2018. Hodgkin lymphoma: A review and update on recent progress. *CA Cancer J Clin,* 68**,** 116-132. doi: 10.3322/caac.21438.

Shao, R., Wang, H., Liu, W., Wang, J., Lu, S., Tang, H., et al. 2021. Establishment of a prognostic ferroptosis-related gene profile in acute myeloid leukaemia. *Journal of Cellular and Molecular Medicine,* 25**,** 10950-10960. doi: 10.1111/jcmm.17013.

Shin, D., Kim, E. H., Lee, J. & Roh, J.-L. 2018. Nrf2 inhibition reverses resistance to GPX4 inhibitor-induced ferroptosis in head and neck cancer. *Free Radical Biology and Medicine,* 129**,** 454-462. doi: 10.1016/j.freeradbiomed.2018.10.426.

Shintoku, R., Takigawa, Y., Yamada, K., Kubota, C., Yoshimoto, Y., Takeuchi, T., et al. 2017. Lipoxygenase-mediated generation of lipid peroxides enhances ferroptosis induced by erastin and RSL3. *Cancer Sci,* 108**,** 2187-2194. doi: 10.1111/cas.13380.

Silva, A., Silva, M. C., Sudalagunta, P., Distler, A., Jacobson, T., Collins, A., et al. 2017. An Ex Vivo Platform for the Prediction of Clinical Response in Multiple Myeloma. *Cancer Res,* 77**,** 3336-3351. doi: 10.1158/0008-5472.Can-17-0502.

Sneddon, A. A., Wu, H.-C., Farquharson, A., Grant, I., Arthur, J. R., Rotondo, D., et al. 2003. Regulation of selenoprotein GPx4 expression and activity in human endothelial cells by fatty acids, cytokines and antioxidants. *Atherosclerosis,* 171**,** 57-65. doi: 10.1016/j.atherosclerosis.2003.08.008.

Stockwell, B. R., Friedmann Angeli, J. P., Bayir, H., Bush, A. I., Conrad, M., Dixon, S. J., et al. 2017. Ferroptosis: A Regulated Cell Death Nexus Linking Metabolism, Redox Biology, and Disease. *Cell,* 171**,** 273-285. doi: 10.1016/j.cell.2017.09.021.

Stringer, B. W., Day, B. W., D'souza, R. C. J., Jamieson, P. R., Ensbey, K. S., Bruce, Z. C., et al. 2019. A reference collection of patient-derived cell line and xenograft models of proneural, classical and mesenchymal glioblastoma. *Scientific Reports,* 9**,** 4902. doi: 10.1038/s41598-019-41277-z.

Su, Q., Li, Q., Zhang, W., Li, B. & Zhuang, W. 2022. Integrative analysis of enrichment and prognostic value of ferroptosis-related genes and pathways in multiple myeloma. *Carcinogenesis*. doi: 10.1093/carcin/bgac080.

Subburayan, K., Thayyullathil, F., Pallichankandy, S., Cheratta, A. R., Alakkal, A., Sultana, M., et al. 2024. Tumor suppressor Par-4 activates autophagy-dependent ferroptosis. *Communications Biology,* 7**,** 732. doi: 10.1038/s42003-024-06430-z.

Subramanian, A., Tamayo, P., Mootha, V. K., Mukherjee, S., Ebert, B. L., Gillette, M. A., et al. 2005. Gene set enrichment analysis: A knowledge-based approach for interpreting genome-wide expression profiles. *Proceedings of the National Academy of Sciences,* 102**,** 15545-15550. doi: 10.1073/pnas.0506580102.

Sun, Q., Liu, D., Cui, W., Cheng, H., Huang, L., Zhang, R., et al. 2023. Cholesterol mediated ferroptosis suppression reveals essential roles of Coenzyme Q and squalene. *Communications Biology,* 6**,** 1108. doi: 10.1038/s42003-023-05477-8.

Sun, X., Ou, Z., Chen, R., Niu, X., Chen, D., Kang, R., et al. 2016. Activation of the p62-Keap1-NRF2 pathway protects against ferroptosis in hepatocellular carcinoma cells. *Hepatology,* 63**,** 173-184. doi: 10.1002/hep.28251.

Sun, Y., Berleth, N., Wu, W., Schlütermann, D., Deitersen, J., Stuhldreier, F., et al. 2021. Fin56-induced ferroptosis is supported by autophagy-mediated GPX4 degradation and functions synergistically with mTOR inhibition to kill bladder cancer cells. *Cell Death & Disease,* 12**,** 1028. doi: 10.1038/s41419-021-04306-2.

Tang, D., Chen, X., Kang, R. & Kroemer, G. 2021a. Ferroptosis: molecular mechanisms and health implications. *Cell Research,* 31**,** 107-125. doi: 10.1038/s41422-020-00441-1.

Tang, H. M. & Tang, H. L. 2019. Cell recovery by reversal of ferroptosis. *Biology Open,* 8**,** bio043182. doi: 10.1242/bio.043182.

Tang, Z., Ju, Y., Dai, X., Ni, N., Liu, Y., Zhang, D., et al. 2021b. HO-1-mediated ferroptosis as a target for protection against retinal pigment epithelium degeneration. *Redox Biology,* 43**,** 101971. doi: 10.1016/j.redox.2021.101971.

Thayyullathil, F., Cheratta, A. R., Alakkal, A., Subburayan, K., Pallichankandy, S., Hannun, Y. A., et al. 2021. Acid sphingomyelinase-dependent autophagic degradation of GPX4 is critical for the execution of ferroptosis. *Cell Death & Disease,* 12**,** 26. doi: 10.1038/s41419-020-03297-w.

The Human Protein Atlas. 2023a. *Acyl-CoA synthetase long chain family member 3* [Online]. Available: https://www.proteinatlas.org/ENSG00000123983-ACSL3 [Accessed 15th August 2024].
The Human Protein Atlas. 2023b. *Acyl-CoA synthetase long chain family member 4* [Online]. Available: https://www.proteinatlas.org/ENSG00000068366-ACSL4 [Accessed 15th August 2024].
The Human Protein Atlas. 2023c. *Arachidonate 15-lipoxygenase* [Online]. Available: https://www.proteinatlas.org/ENSG00000161905-ALOX15 [Accessed 15th August 2024].
The Human Protein Atlas. 2023d. *Ferritin heavy chain 1* [Online]. Available: https://www.proteinatlas.org/ENSG00000167996-FTH1/cell+line [Accessed 15th August 2024].
The Human Protein Atlas. 2023e. *Ferritin light chain* [Online]. Available: https://www.proteinatlas.org/ENSG00000087086-FTL [Accessed 15th August 2024].
The Human Protein Atlas. 2023f. *Glutathione peroxidase 4* [Online]. Available: https://www.proteinatlas.org/ENSG00000167468-GPX4 [Accessed 15th August 2024].
The Human Protein Atlas. 2023g. *Lysophosphatidylcholine acyltransferase 3* [Online]. Available: https://www.proteinatlas.org/ENSG00000111684-LPCAT3 [Accessed 15th August 2024].
The Human Protein Atlas. 2023h. *Nuclear receptor coactivator 4* [Online]. Available: https://www.proteinatlas.org/ENSG00000266412-NCOA4 [Accessed 15th August 2024].
The Human Protein Atlas. 2023i. *Receptor interacting serine/threonine kinase 3* [Online]. Available: https://www.proteinatlas.org/ENSG00000129465-RIPK3 [Accessed 15th August 2024].
The Human Protein Atlas. 2023j. *Solute carrier family 7 member 11* [Online]. Available: https://www.proteinatlas.org/ENSG00000151012-SLC7A11 [Accessed 15th August 2024].
The Human Protein Atlas. 2023k. *Solute carrier family 40 member 1* [Online]. Available: https://www.proteinatlas.org/ENSG00000138449-SLC40A1 [Accessed 15th August 2024].
The Human Protein Atlas. 2023l. *Transferrin receptor* [Online]. Available: https://www.proteinatlas.org/ENSG00000072274-TFRC [Accessed 15th August 2024].
The Human Protein Atlas. 2023m. *Tumor protein p53* [Online]. Available: https://www.proteinatlas.org/ENSG00000141510-TP53 [Accessed 15th August 2024].
Tonelli, C., Chio, I. I. C. & Tuveson, D. A. 2017. Transcriptional Regulation by Nrf2. *Antioxidants & Redox Signaling,* 29**,** 1727-1745. doi: 10.1089/ars.2017.7342.
Tong, J., Li, D., Meng, H., Sun, D., Lan, X., Ni, M., et al. 2022. Targeting a novel inducible GPX4 alternative isoform to alleviate ferroptosis and treat metabolic-associated fatty liver disease. *Acta Pharmaceutica Sinica B,* 12**,** 3650-3666. doi: 10.1016/j.apsb.2022.02.003.
Trujillo-Alonso, V., Pratt, E. C., Zong, H., Lara-Martinez, A., Kaittanis, C., Rabie, M. O., et al. 2019. FDA-approved ferumoxytol displays anti-leukaemia efficacy against cells with low ferroportin levels. *Nature Nanotechnology,* 14**,** 616-622. doi: 10.1038/s41565-019-0406-1.
Turunen, M., Olsson, J. & Dallner, G. 2004. Metabolism and function of coenzyme Q. *Biochim Biophys Acta,* 1660**,** 171-99. doi: 10.1016/j.bbamem.2003.11.012.
Ung, J., Tan, S.-F., Fox, T. E., Shaw, J. J. P., Taori, M., Horton, B. J., et al. 2023. Acid Ceramidase Inhibitor LCL-805 Antagonizes Akt Signaling and Promotes Iron-Dependent Cell Death in Acute Myeloid Leukemia. *Cancers* [Online], 15.
Vande Voorde, J., Ackermann, T., Pfetzer, N., Sumpton, D., Mackay, G., Kalna, G., et al. 2019. Improving the metabolic fidelity of cancer models with a physiological cell culture medium. *Science Advances,* 5**,** eaau7314. doi: 10.1126/sciadv.aau7314.
Viswanathan, V. S., Ryan, M. J., Dhruv, H. D., Gill, S., Eichhoff, O. M., Seashore-Ludlow, B., et al. 2017. Dependency of a therapy-resistant state of cancer cells on a lipid peroxidase pathway. *Nature,* 547**,** 453-457. doi: 10.1038/nature23007.
Vučković, A.-M., Bosello Travain, V., Bordin, L., Cozza, G., Miotto, G., Rossetto, M., et al. 2020. Inactivation of the glutathione peroxidase GPx4 by the ferroptosis-inducing molecule RSL3 requires the adaptor protein 14-3-3ε. *FEBS Letters,* 594**,** 611-624. doi: 10.1002/1873-3468.13631.
Wallington-Beddoe, C. T., Hewson, J., Bradstock, K. F. & Bendall, L. J. 2011. FTY720 produces caspase-independent cell death of acute lymphoblastic leukemia cells. *Autophagy,* 7**,** 707-715. doi: 10.4161/auto.7.7.15154.
Wallington-Beddoe, C. T. & Mynott, R. L. 2021. Prognostic and predictive biomarker developments in multiple myeloma. *Journal of Hematology & Oncology,* 14**,** 151. doi: 10.1186/s13045-021-01162-7.

Wang, F., Oudaert, I., Tu, C., Maes, A., Van Der Vreken, A., Vlummens, P., et al. 2022a. System Xc− inhibition blocks bone marrow-multiple myeloma exosomal crosstalk, thereby countering bortezomib resistance. *Cancer Letters,* 535**,** 215649. doi: 10.1016/j.canlet.2022.215649.

Wang, N., Zeng, G.-Z., Yin, J.-L. & Bian, Z.-X. 2019a. Artesunate activates the ATF4-CHOP-CHAC1 pathway and affects ferroptosis in Burkitt's Lymphoma. *Biochemical and Biophysical Research Communications,* 519**,** 533-539. doi: 10.1016/j.bbrc.2019.09.023.

Wang, X., Chen, Y., Yang, X., Cheng, L., He, Z., Xin, Y., et al. 2022b. Activation of ALOX12 by a multi-organelle-orienting photosensitizer drives ACSL4-independent cell ferroptosis. *Cell Death Dis,* 13**,** 1040. doi: 10.1038/s41419-022-05462-9.

Wang, X., Lu, S., He, C., Wang, C., Wang, L., Piao, M., et al. 2019b. RSL3 induced autophagic death in glioma cells via causing glycolysis dysfunction. *Biochemical and Biophysical Research Communications,* 518**,** 590-597. doi: 10.1016/j.bbrc.2019.08.096.

Wang, Y., Qiu, J., Yan, H., Zhang, N., Gao, S., Xu, N., et al. 2024. The Bach1/HO-1 pathway regulates oxidative stress and contributes to ferroptosis in doxorubicin-induced cardiomyopathy in H9c2 cells and mice. *Arch Toxicol,* 98**,** 1781-1794. doi: 10.1007/s00204-024-03697-3.

Wang, Z., Hu, H., Heitink, L., Rogers, K., You, Y., Tan, T., et al. 2023. The anti-cancer agent APR-246 can activate several programmed cell death processes to kill malignant cells. *Cell Death & Differentiation*. doi: 10.1038/s41418-023-01122-3.

Warner, G. J., Berry, M. J., Moustafa, M. E., Carlson, B. A., Hatfield, D. L. & Faust, J. R. 2000. Inhibition of selenoprotein synthesis by selenocysteine tRNA[Ser]Sec lacking isopentenyladenosine. *J Biol Chem,* 275**,** 28110-9. doi: 10.1074/jbc.M001280200.

Weaver, K. & Skouta, R. 2022. The Selenoprotein Glutathione Peroxidase 4: From Molecular Mechanisms to Novel Therapeutic Opportunities. *Biomedicines,* 10**,** 891.

Webb, J. 1963. *Enzyme and metabolic inhibitors. Volume 1. General principles of inhibition*, Academic Press, Inc., New York:London.

Wei, J., Nai, G. Y., Dai, Y., Huang, X. J., Xiong, M. Y., Yao, X. Y., et al. 2021. Dipetidyl peptidase-4 and transferrin receptor serve as prognostic biomarkers for acute myeloid leukemia. *Annals of Translational Medicine,* 9**,** 1381.

Wei, J., Xie, Q., Liu, X., Wan, C., Wu, W., Fang, K., et al. 2020. Identification the prognostic value of glutathione peroxidases expression levels in acute myeloid leukemia. *Ann Transl Med,* 8**,** 678. doi: 10.21037/atm-20-3296.

Wei, X., Deng, W., Dong, Z., Xie, Z., Zhang, J., Wang, R., et al. 2022. Identification of Subtypes and a Delayed Graft Function Predictive Signature Based on Ferroptosis in Renal Ischemia-Reperfusion Injury. *Frontiers in Cell and Developmental Biology,* 10. doi: 10.3389/fcell.2022.800650.

Weng, J., Chen, L., Liu, H., Yang, X.-P. & Huang, L. 2022. Ferroptosis Markers Predict the Survival, Immune Infiltration, and Ibrutinib Resistance of Diffuse Large B cell Lymphoma. *Inflammation,* 45**,** 1146-1161. doi: 10.1007/s10753-021-01609-6.

White, J. B., Trim, P. J., Salagaras, T., Long, A., Psaltis, P. J., Verjans, J. W., et al. 2022. Equivalent Carbon Number and Interclass Retention Time Conversion Enhance Lipid Identification in Untargeted Clinical Lipidomics. *Anal Chem,* 94**,** 3476-3484. doi: 10.1021/acs.analchem.1c03770.

Williams, M. 2015. Selenoamino acid metabolism. February 2015 ed.: Reactome.

Woo, J. H., Shimoni, Y., Yang, W. S., Subramaniam, P., Iyer, A., Nicoletti, P., et al. 2015. Elucidating Compound Mechanism of Action by Network Perturbation Analysis. *Cell,* 162**,** 441-451. doi: 10.1016/j.cell.2015.05.056.

Wu, F., Du, Y., Yang, J., Shao, B., Mi, Z., Yao, Y., et al. 2022a. Peroxidase-like Active Nanomedicine with Dual Glutathione Depletion Property to Restore Oxaliplatin Chemosensitivity and Promote Programmed Cell Death. *ACS Nano,* 16**,** 3647-3663. doi: 10.1021/acsnano.1c06777.

Wu, H., Zhang, J., Fu, L., Wu, R., Gu, Z., Yin, C., et al. 2023a. Identification and Development of a 4-Gene Ferroptosis Signature Predicting Overall Survival for Diffuse Large B-Cell Lymphoma. *Technol Cancer Res Treat,* 22**,** 15330338221147772. doi: 10.1177/15330338221147772.

Wu, S., Mao, C., Kondiparthi, L., Poyurovsky, M. V., Olszewski, K. & Gan, B. 2022b. A ferroptosis defense mechanism mediated by glycerol-3-phosphate dehydrogenase 2 in mitochondria. *Proceedings of the National Academy of Sciences,* 119**,** e2121987119. doi: 10.1073/pnas.2121987119.

Wu, X., Chen, S., Huang, K. & Lin, G. 2023b. Triptolide promotes ferroptosis by suppressing Nrf2 to overcome leukemia cell resistance to doxorubicin. *Mol Med Rep,* 27**,** 17. doi: 10.3892/mmr.2022.12904.

Wu, Y. C., Huang, C. S., Hsieh, M. S., Huang, C. M., Setiawan, S. A., Yeh, C. T., et al. 2024. Targeting of FSP1 regulates iron homeostasis in drug-tolerant persister head and neck cancer cells via lipid-metabolism-driven ferroptosis. *Aging (Albany NY),* 16**,** 627-647. doi: 10.18632/aging.205409.

Xian, M., Wang, Q., Xiao, L., Zhong, L., Xiong, W., Ye, L., et al. 2024. Leukocyte immunoglobulin-like receptor B1 (LILRB1) protects human multiple myeloma cells from ferroptosis by maintaining cholesterol homeostasis. *Nature Communications,* 15**,** 5767. doi: 10.1038/s41467-024-50073-x.

Xie, P., Huang, Y., Tang, K., Wu, X., Zeng, C., Yang, S.-T., et al. 2023. Carbon nanoparticles-Fe(II) complex for efficient theranostics of xenografted colonic tumor. *Cancer Nanotechnology,* 14**,** 38. doi: 10.1186/s12645-023-00196-5.

Xu, X. H., Gan, Y. C., Xu, G. B., Chen, T., Zhou, H., Tang, J. F., et al. 2012. Tetrandrine citrate eliminates imatinib-resistant chronic myeloid leukemia cells in vitro and in vivo by inhibiting Bcr-Abl/β-catenin axis. *J Zhejiang Univ Sci B,* 13**,** 867-74. doi: 10.1631/jzus.B1200021.

Yagoda, N., Von Rechenberg, M., Zaganjor, E., Bauer, A. J., Yang, W. S., Fridman, D. J., et al. 2007. RAS-RAF-MEK-dependent oxidative cell death involving voltage-dependent anion channels. *Nature,* 447**,** 864-8. doi: 10.1038/nature05859.

Yang, R., Li, Y., Wang, X., Yan, J., Pan, D., Xu, Y., et al. 2019. Doxorubicin loaded ferritin nanoparticles for ferroptosis enhanced targeted killing of cancer cells. *RSC Advances,* 9**,** 28548-28553. doi: 10.1039/C9RA04478G.

Yang, W. S., Kim, K. J., Gaschler, M. M., Patel, M., Shchepinov, M. S. & Stockwell, B. R. 2016. Peroxidation of polyunsaturated fatty acids by lipoxygenases drives ferroptosis. *Proceedings of the National Academy of Sciences,* 113**,** E4966. doi: 10.1073/pnas.1603244113.

Yang, W. S., Sriramaratnam, R., Welsch, M. E., Shimada, K., Skouta, R., Viswanathan, V. S., et al. 2014. Regulation of ferroptotic cancer cell death by GPX4. *Cell,* 156**,** 317-331. doi: 10.1016/j.cell.2013.12.010.

Yang, W. S. & Stockwell, B. R. 2008. Synthetic lethal screening identifies compounds activating iron-dependent, nonapoptotic cell death in oncogenic-RAS-harboring cancer cells. *Chem Biol,* 15**,** 234-45. doi: 10.1016/j.chembiol.2008.02.010.

Yang, W. S. & Stockwell, B. R. 2016. Ferroptosis: Death by Lipid Peroxidation. *Trends Cell Biol,* 26**,** 165-176. doi: 10.1016/j.tcb.2015.10.014.

Ye, P., Mimura, J., Okada, T., Sato, H., Liu, T., Maruyama, A., et al. 2014. Nrf2- and ATF4-dependent upregulation of xCT modulates the sensitivity of T24 bladder carcinoma cells to proteasome inhibition. *Molecular and cellular biology,* 34**,** 3421-3434. doi: 10.1128/MCB.00221-14.

Yin, J., Lin, Y., Fang, W., Zhang, X., Wei, J., Hu, G., et al. 2022. Tetrandrine Citrate Suppresses Breast Cancer via Depletion of Glutathione Peroxidase 4 and Activation of Nuclear Receptor Coactivator 4-Mediated Ferritinophagy. *Front Pharmacol,* 13**,** 820593. doi: 10.3389/fphar.2022.820593.

Yin, Z., Lv, Y., Deng, L., Li, G., Ou, R., Chen, L., et al. 2023. Targeting ABCB6 with nitidine chloride inhibits PI3K/AKT signaling pathway to promote ferroptosis in multiple myeloma. *Free Radical Biology and Medicine,* 203**,** 86-101. doi: 10.1016/j.freeradbiomed.2023.04.003.

Ying, Q., Lou, J. & Zheng, D. 2023. Ginsenoside Rh4 inhibits the malignant progression of multiple myeloma and induces ferroptosis by regulating SIRT2. *Clinical and Experimental Pharmacology and Physiology,* 50**,** 757-765. doi: 10.1111/1440-1681.13805.

Yu, H., Guo, P., Xie, X., Wang, Y. & Chen, G. 2017. Ferroptosis, a new form of cell death, and its relationships with tumourous diseases. *Journal of cellular and molecular medicine,* 21**,** 648-657. doi: 10.1111/jcmm.13008.

Yu, M., Yu, J., Yi, Y., Chen, T., Yu, L., Zeng, W., et al. 2022. Oxidative stress-amplified nanomedicine for intensified ferroptosis-apoptosis combined tumor therapy. *Journal of Controlled Release,* 347**,** 104-114. doi: 10.1016/j.jconrel.2022.04.047.

Yu, Y., Meng, Y., Xu, X., Tong, T., He, C., Wang, L., et al. 2023. A Ferroptosis-Inducing and Leukemic Cell-Targeting Drug Nanocarrier Formed by Redox-Responsive Cysteine Polymer for Acute Myeloid Leukemia Therapy. *ACS Nano,* 17**,** 3334-3345. doi: 10.1021/acsnano.2c06313.

Yu, Y., Xie, Y., Cao, L., Yang, L., Yang, M., Lotze, M. T., et al. 2015. The ferroptosis inducer erastin enhances sensitivity of acute myeloid leukemia cells to chemotherapeutic agents. *Molecular & Cellular Oncology,* 2**,** e1054549. doi: 10.1080/23723556.2015.1054549.

Yuan, H., Li, X., Zhang, X., Kang, R. & Tang, D. 2016. Identification of ACSL4 as a biomarker and contributor of ferroptosis. *Biochemical and Biophysical Research Communications,* 478**,** 1338-1343. doi: 10.1016/j.bbrc.2016.08.124.

Yun, Z., Zhichao, J., Hao, Y., Ou, J., Ran, Y., Wen, D., et al. 2017. Targeting autophagy in multiple myeloma. *Leukemia Research,* 59**,** 97-104. doi: 10.1016/j.leukres.2017.06.002.

Yusuf, R., Saez, B., Sharda, A., Van Gastel, N., Yu, V. W. C., Baryawno, N., et al. 2020. Aldehyde dehydrogenase 3a2 protects AML cells from oxidative death and the synthetic lethality of ferroptosis inducers. *Blood,* 136. doi: 10.1182/blood.2019001808.

Zhang, J., Liu, L., Wei, J., Wu, X., Luo, J., Wei, H., et al. 2023a. High expression level of the FTH1 gene is associated with poor prognosis in children with non-M3 acute myeloid leukemia. *Frontiers in Oncology,* 12. doi: 10.3389/fonc.2022.1068094.

Zhang, J., Liu, Y., Li, Q., Zuo, L., Zhang, B., Zhao, F., et al. 2023b. ACSL4: a double-edged sword target in multiple myeloma, promotes cell proliferation and sensitizes cell to ferroptosis. *Carcinogenesis,* 44**,** 242-251. doi: 10.1093/carcin/bgad015.

Zhang, J., Liu, Y., Zuo, L., Fan, F., Yan, H., Zhao, F., et al. 2024a. Class Ⅱ ferroptosis inducers are a novel therapeutic approach for t(4;14)-positive multiple myeloma. *Blood Advances*. doi: 10.1182/bloodadvances.2023010335.

Zhang, J., Qiao, P., Yao, G., Zhao, H., Wu, Y. & Wu, S. 2020. Ionizing Radiation Exacerbates the Bone Loss Induced by Iron Overload in Mice. *Biological Trace Element Research,* 196**,** 502-511. doi: 10.1007/s12011-019-01929-7.

Zhang, J., Yang, J., Zuo, T., Ma, S., Xokrat, N., Hu, Z., et al. 2021a. Heparanase-driven sequential released nanoparticles for ferroptosis and tumor microenvironment modulations synergism in breast cancer therapy. *Biomaterials,* 266**,** 120429. doi: 10.1016/j.biomaterials.2020.120429.

Zhang, J., Ye, Z. W., Chakraborty, P., Luo, Z., Culpepper, J., Aslam, M., et al. 2023c. Microsomal glutathione transferase 1 controls metastasis and therapeutic response in melanoma. *Pharmacol Res,* 196**,** 106899. doi: 10.1016/j.phrs.2023.106899.

Zhang, K., Ma, Z., Li, S., Wu, Y., Zhang, J., Zhang, W., et al. 2022a. Disruption of dual homeostasis by a metal-organic framework nanoreactor for ferroptosis-based immunotherapy of tumor. *Biomaterials,* 284**,** 121502. doi: 10.1016/j.biomaterials.2022.121502.

Zhang, L., Liu, X., Liu, Y., Yan, F., Zeng, Y., Song, Y., et al. 2023d. Lysophosphatidylcholine inhibits lung cancer cell proliferation by regulating fatty acid metabolism enzyme long-chain acyl-coenzyme A synthase 5. *Clinical and Translational Medicine,* 13**,** e1180. doi: 10.1002/ctm2.1180.

Zhang, Q., Li, N., Deng, L., Jiang, X., Zhang, Y., Lee, L. T. O., et al. 2023e. ACSL1-induced ferroptosis and platinum resistance in ovarian cancer by increasing FSP1 N-myristylation and stability. *Cell Death Discovery,* 9**,** 83. doi: 10.1038/s41420-023-01385-2.

Zhang, Q., Xiong, L., Wei, T., Liu, Q., Yan, L., Chen, J., et al. 2023f. Hypoxia-responsive PPARGC1A/BAMBI/ACSL5 axis promotes progression and resistance to lenvatinib in hepatocellular carcinoma. *Oncogene,* 42**,** 1509-1523. doi: 10.1038/s41388-023-02665-y.

Zhang, S., Kang, L., Dai, X., Chen, J., Chen, Z., Wang, M., et al. 2022b. Manganese induces tumor cell ferroptosis through type-I IFN dependent inhibition of mitochondrial dihydroorotate dehydrogenase. *Free Radical Biology and Medicine,* 193**,** 202-212. doi: 10.1016/j.freeradbiomed.2022.10.004.

Zhang, T., Sun, B., Zhong, C., Xu, K., Wang, Z., Hofman, P., et al. 2021b. Targeting histone deacetylase enhances the therapeutic effect of Erastin-induced ferroptosis in EGFR-activating mutant lung adenocarcinoma. *Translational Lung Cancer Research,* 10**,** 1857-1872.

Zhang, T., Wang, Y., Inuzuka, H. & Wei, W. 2022c. Necroptosis pathways in tumorigenesis. *Semin Cancer Biol,* 86**,** 32-40. doi: 10.1016/j.semcancer.2022.07.007.

Zhang, W., Li, Q., Zhang, Y., Wang, Z., Yuan, S., Zhang, X., et al. 2024b. Multiple myeloma with high expression of SLC7A11 is sensitive to erastin-induced ferroptosis. *Apoptosis,* 29**,** 412-423. doi: 10.1007/s10495-023-01909-2.

Zhang, W., Trachootham, D., Liu, J., Chen, G., Pelicano, H., Garcia-Prieto, C., et al. 2012. Stromal control of cystine metabolism promotes cancer cell survival in chronic lymphocytic leukaemia. *Nature Cell Biology,* 14**,** 276-286. doi: 10.1038/ncb2432.

Zhang, Y., He, F., Hu, W., Sun, J., Zhao, H., Cheng, Y., et al. 2024c. Bortezomib elevates intracellular free Fe2+ by enhancing NCOA4-mediated ferritinophagy and synergizes with RSL-3 to inhibit multiple myeloma cells. *Annals of Hematology,* 103**,** 3627-3637. doi: 10.1007/s00277-024-05762-4.

Zhang, Y., Su, W., Yang, Z., Zhao, D., Guan, Q., Liao, T., et al. 2025. iPLAβ regulates the dual effects of arachidonic acid in thyroid cancer. *Head & Neck,* 47**,** 504-516. doi: 10.1002/hed.27937.

Zhang, Y., Tan, H., Daniels, J. D., Zandkarimi, F., Liu, H., Brown, L. M., et al. 2019. Imidazole Ketone Erastin Induces Ferroptosis and Slows Tumor Growth in a Mouse Lymphoma Model. *Cell Chem Biol,* 26**,** 623-633 e9. doi: 10.1016/j.chembiol.2019.01.008.

Zhang, Y., Wang, X., Li, X., Xiong, X., Xue, R., Zang, L., et al. 2024d. Novel methyltransferase G9a inhibitor induces ferroptosis in multiple myeloma through Nrf2/HO-1 pathway. *Ann Hematol,* 103**,** 2405-2417. doi: 10.1007/s00277-024-05728-6.

Zhao, J., Ma, W., Wang, S., Zhang, K., Xiong, Q., Li, Y., et al. 2024. Differentiation of intestinal stem cells toward goblet cells under systemic iron overload stress are associated with inhibition of Notch signaling pathway and ferroptosis. *Redox Biology,* 72**,** 103160. doi: 10.1016/j.redox.2024.103160.

Zhao, Y., Li, Y., Zhang, R., Wang, F., Wang, T. & Jiao, Y. 2020. The Role of Erastin in Ferroptosis and Its Prospects in Cancer Therapy. *Onco Targets Ther,* 13**,** 5429-5441. doi: 10.2147/OTT.S254995.

Zheng, X., Liang, Y. & Zhang, C. 2023. Ferroptosis Regulated by Hypoxia in Cells. *Cells,* 12. doi: 10.3390/cells12071050.

Zhong, F.-M., Yao, F.-Y., Liu, J., Zhang, H.-B., Zhang, J., Zhang, N., et al. 2022. Ferroptosis-related molecular patterns reveal immune escape, inflammatory development and lipid metabolism characteristics of the tumor microenvironment in acute myeloid leukemia. *Frontiers in Oncology,* 12. doi: 10.3389/fonc.2022.888570.

Zhong, Y., Tian, F., Ma, H., Wang, H., Yang, W., Liu, Z., et al. 2020. FTY720 induces ferroptosis and autophagy via PP2A/AMPK pathway in multiple myeloma cells. *Life Sciences,* 260**,** 118077. doi: 10.1016/j.lfs.2020.118077.

Zhou, F. & Chen, B. 2021. Prognostic significance of ferroptosis-related genes and their methylation in AML. *Hematology,* 26**,** 919-930. doi: 10.1080/16078454.2021.1996055.

Zhou, N., Yuan, X., Du, Q., Zhang, Z., Shi, X., Bao, J., et al. 2023. FerrDb V2: update of the manually curated database of ferroptosis regulators and ferroptosis-disease associations. *Nucleic Acids Research,* 51**,** D571-D582. doi: 10.1093/nar/gkac935.

Zhou, Y., Shen, Y., Chen, C., Sui, X., Yang, J., Wang, L., et al. 2019. The crosstalk between autophagy and ferroptosis: what can we learn to target drug resistance in cancer? *Cancer Biol Med,* 16**,** 630-646. doi: 10.20892/j.issn.2095-3941.2019.0158.

Zhu, H. Y., Huang, Z. X., Chen, G. Q., Sheng, F. & Zheng, Y. S. 2019. Typhaneoside prevents acute myeloid leukemia (AML) through suppressing proliferation and inducing ferroptosis associated with autophagy. *Biochem Biophys Res Commun,* 516**,** 1265-1271. doi: 10.1016/j.bbrc.2019.06.070.

Zhu, K., Lang, Z., Zhan, Y., Tao, Q., Yu, Z., Chen, L., et al. 2022. A novel 10-gene ferroptosis-related prognostic signature in acute myeloid leukemia. *Frontiers in Oncology,* 12. doi: 10.3389/fonc.2022.1023040.

Zhu, K., Liang, W., Ma, Z., Xu, D., Cao, S., Lu, X., et al. 2018. Necroptosis promotes cell-autonomous activation of proinflammatory cytokine gene expression. *Cell Death & Disease,* 9**,** 500. doi: 10.1038/s41419-018-0524-y.

Zhu, K., Zhu, X., Sun, S., Yang, W., Liu, S., Tang, Z., et al. 2021. Inhibition of TLR4 prevents hippocampal hypoxic-ischemic injury by regulating ferroptosis in neonatal rats. *Experimental Neurology,* 345**,** 113828. doi: 10.1016/j.expneurol.2021.113828.

Zhu, L. & Du, Y. 2024. A promising new approach to cancer therapy: Manipulate ferroptosis by hijacking endogenous iron. *International Journal of Pharmaceutics,* 662**,** 124517. doi: 10.1016/j.ijpharm.2024.124517.

Zou, Y., Palte, M. J., Deik, A. A., Li, H., Eaton, J. K., Wang, W., et al. 2019. A GPX4-dependent cancer cell state underlies the clear-cell morphology and confers sensitivity to ferroptosis. *Nature Communications,* 10**,** 1617. doi: 10.1038/s41467-019-09277-9.